Technische Universität München
Fakultät für Elektrotechnik und Informationstechnik
Lehrstuhl für Energiewirtschaft und Anwendungstechnik

Modeling and Optimization of Energy Generation and Storage Systems for Thermal Conditioning of Buildings Targeting Conceptual Building Design

Milica Grahovac

Vollständiger Abdruck der von der Fakultät für Elektrotechnik und Informationstechnik der Technischen Universität München zur Erlangung des akademischen Grades eines

Doktor-Ingenieurs

genehmigten Dissertation.

Vorsitzender: Univ.-Prof. Dr.-Ing., Dr.-Ing. habil. Erwin Biebl

Prüfer der Dissertation:

1. Univ.-Prof. Dr. rer. nat. Thomas Hamacher
2. Univ.-Prof. Dr.-Ing. Gerhard Hausladen
3. Univ.-Prof. Dr.-Ing. Ulrich Wagner

Die Dissertation wurde am 25. 04. 2012 bei der Technischen Universität München eingereicht und durch die Fakultät für Elektrotechnik und Informationstechnik am 29. 11. 2012 angenommen.

Acknowledgments

I have been given the chance to prepare and write this thesis at the Institute for Energy Economy and Application Technology of Technische Universität München between April 2008 and April 2012. During this time, I have found many reasons to be thankful. I owe a great deal to all those who have supported, encouraged and challenged me during this time.

I would especially like to thank IGSSE for providing a great scientific and social environment and for funding my research.

My sincere thanks go to my mentor, Prof. Thomas Hamacher, for his motivating suggestions, support, understanding and patience. This thesis would not have been possible without Prof. Ulrich Wagner, whom I thank for providing me with the opportunity to work at the Institute, for mentoring my work during the first two years and for reviewing my thesis. I am also grateful to Prof. Gerhard Hausladen for kindly agreeing to review the thesis and Prof. Erwin Biebl for kindly accepting to chair the exam.

I owe a great deal to the project team leader, Dr. Peter Tzscheutschler, for his support and perceptive advice and for making my life easier. I would like to thank Prof. Christoph van Treeck, who led our project team during the first year, for introducing me to the field of building simulation.

I benefited greatly from working with Craig Wray, who reminded me what it means to be a “real engineer”. I am grateful to him for inviting me to spend time working at LBNL.

I thank all the colleagues from the Institute and the team members for cooperation, sharing ideas, and for the fun. I would also like to acknowledge the students for their help, interest and challenges, for I have learned a lot from them.

Special thanks go to the colleagues, friends, and family members who invested their time to help me review the thesis.

I thank my mother Slavenka Grahovac for her continuous love, support, and inspiration.

Abstract

The thermal conditioning systems are responsible for almost half of the energy consumption by commercial buildings. In many European countries and in the USA, buildings account for around 40% of primary energy consumption and it is therefore vital to explore further ways to reduce the HVAC (Heating, Ventilation and Air Conditioning) system energy consumption. This thesis investigates the relationship between the energy generation and storage systems for thermal conditioning of buildings (shorter: primary HVAC systems) and the conceptual building design.

Certain building design decisions irreversibly influence a building's energy performance and, conversely, many generation and storage components impose restrictions on building design and, by their nature, cannot be introduced at a later design stage. The objective is, firstly, to develop a method to quantify this influence, in terms of primary HVAC system dimensions, its cost, emissions and energy consumption and, secondly, to enable the use of the developed method by architects during the conceptual design.

In order to account for the non-stationary effects of the intermittent renewable energy sources (RES), thermal storage and for the component part load efficiencies, a time domain system simulation is required. An abstract system simulation method is proposed based on seven pre-configured primary HVAC system models, including components such as boilers, chillers and cooling towers, thermal storage, solar thermal collectors, and photovoltaic modules. A control strategy is developed for each of the models and their annual quasi-stationary simulation is performed. The performance profiles obtained are then used to calculate the energy consumption, carbon emissions and costs. The annuity method has been employed to calculate the cost.

Optimization is used to automatically size the HVAC systems, based on their simulation performance. Its purpose is to identify the system component dimensions that provide minimal costs, emissions or consumption, while maintaining the quality of the supply and, where specified, achieving the targeted annual solar ratio. Two optimization algorithms, the global bounded Nelder Mead and the Exhaustive search are implemented.

Simulation and optimization performance has been evaluated using building and weather data for four cities situated in four different climates.

Finally a tool, entitled PROBA, has been proposed by adding a user interface to the models. The major characteristic of the interface is its suitability for non-expert users. This is achieved by, firstly, reducing amount of input data by implementing preset values and, secondly, providing information support. Making this tool available to the architects represents an effective way to consider the primary HVAC during the preliminary design, without causing additional cost. Although such a tool can never replace an HVAC engineer, its use can heighten the awareness of architects regarding the significance of building energy consumption and inspire further education in this field.

Kurzfassung

Knapp die Hälfte des Energieverbrauchs von Bürogebäuden entsteht durch die Gebäudekonditionierung. In vielen Europäischen Ländern und in den USA werden 40 % des Primärenergieverbrauchs von Gebäuden verursacht. Es ist deshalb entscheidend, weitere Wege der Verbrauchsreduzierung von Heizungs-, Lüftungs- und Klima-Anlagen (HLK) zu finden und zu untersuchen. In dieser Arbeit wird der Zusammenhang zwischen der Anlage für Wärme- und Kälteerzeugung und Speicherung – kurz der thermischen Anlage – und der Entwurfsgebäudeplanung analysiert.

Durch manche Entwurfsentscheidungen wird der Gebäudeenergieverbrauch weitestgehend unveränderbar vorbestimmt. Viele Erzeugungs- und Speicheranlagen wiederum verlangen bestimmte Bauarten und können in einer späteren Entwurfsphase nicht mehr eingeplant werden. Ziel dieser Arbeit ist es den Einfluss des Gebäudeentwurfs auf die Anlagengrößen, die Kosten, die Emissionen und den Energieverbrauch zu untersuchen, sowie, in einem zweiten Schritt, Architekten die Nutzung der entwickelten Methode in der Entwurfsphase zu ermöglichen.

Um die dynamischen Effekte der fluktuierenden Erneuerbaren Energiequellen (EE), die thermischen Speicher und die Teillastwirkungsgrade der Komponenten abzubilden, ist eine zeitlich hochaufgelöste Simulation notwendig. Eine abstrakte Simulationsmethode für sieben vordefinierte Anlagenmodelle wird vorgestellt. Die Anlagenmodelle bilden die Systemkomponenten wie Boiler, Kühler und Kühltürme, solarthermische Kollektoren und Photovoltaikmodule ab. Für jedes Modell wird eine Regelstrategie entwickelt und eine quasi-stationäre Simulation der Fahrweise im Jahresverlauf wird durchgeführt. Aus den so erhaltenen Leistungsprofilen werden der Gesamtenergieverbrauch, die Emissionen und die Kosten bestimmt. Zur Berechnung der Kosten wird die Annuitätenmethode angewandt.

Um die Dimensionierung der thermischen Anlage automatisch zu bestimmen, wird eine Optimierung eingesetzt, die die Größe der einzelnen Komponenten anhand der Simulationsergebnisse bestimmt, indem die Gesamtkosten, Emissionen oder der Verbrauch minimiert werden. Hierbei muss die Versorgungssicherheit gewährleistet und gegebenenfalls der angestrebte Solaranteil erreicht werden. Zwei Optimierungsalgorithmen, der Global Bounded Nelder Mead (GBNM) und die erschöpfende Gittersuche wurden implementiert.

Die Simulations- und Optimierungsmethode wurde anhand von Gebäude- und Klimadaten von vier verschiedenen Städten in vier Klimazonen evaluiert.

Durch Hinzufügen einer Benutzeroberfläche wurde das Werkzeug PROBA geschaffen. Dieses zeichnet sich vor allem durch seine Eignung für die Nutzung durch Laien aus. So wurde die Anzahl der Eingabeparameter durch die Einführung von Standardwerten stark reduziert, und erläuternde Informationen wurden hinzugefügt. Durch die Nutzung des PROBA-Werkzeugs von Architekten kann die thermische Anlage bereits in frühen Entwurfsphasen berücksichtigt werden, ohne zusätzliche Kosten zu verursachen. Auch wenn das Werkzeug keinen Ingenieur ersetzen kann, kann es zur Bewusstseinsschaffung bezüglich des Gebäudeenergieverbrauchs beitragen und weitere Aufklärung in diesem Bereich anregen.

Contents

List of Symbols

Component Models

β_{pv}	PV temperature coefficient, 1/°C
ΔT	Temperature difference, °C
η_b	Boiler efficiency
η_o	Optical solar collector efficiency (Conversion factor)
ρ	Water density, kg/m3
$\eta_{ref,pv}$	PV efficiency at reference conditions
$a_1,\ldots,a_6$	Coefficients of FCOP
a_{c1}, a_{c2}	Solar collector linear and quadratic loss coefficients
A_{pv}	Vector of photovoltaic surfaces [Horizontal Optimal North South East West]
$b_1,\ldots,b_6$	Coefficients of FCAP
c_1, c_2, c_3	Coefficients of FPLR
CAP	Chiller capacity at both current temperature conditions and current load **
CAP_{full}	Chiller capacity at current temperature conditions and full load **
CAP_{ref}	Chiller capacity at reference temperature conditions and full load **
COP	Chiller coef. of performance at current temp. conditions and current load **
COP_{full}	Chiller coef. of performance at current temp. conditions and full load **
COP_{ref}	Chiller coef. of performance at reference temp. conditions and full load **
c_p	Specific heat capacity, kJ/(kgK)
$E_{el,pv,out}$	Annual PV generated electrical energy, Wh/a
E_{sol}	Annual solar radiation energy, Wh/a
FC	Fuel consumption (all fuel types utilized), kW **
$FCAP$	Capacity chiller model performance function
$FCOP$	COP chiller model performance function
f_{perf}	PV performance factor
$FPLR$	PLR chiller model performance function
f_{sys}	PV system factor
f_{temp}	PV temperature factor
HR	Heat of rejection, kW *
I	Total solar radiation on collector or PV module surface, W/ m2 *

After annual simulation with a timestep of 1h, the variable is a:

* A column vector representing a yearly profile. [8760 x 1]

** An array formed by annual profiles of all components. [8760 x no. of components]

*** A row vector of annual cumulative values for all components. [1 x no. of components]

(Valid throughout the List of Symbols)

IAM	Incidence angle modifier
I_{ref}	Reference solar radiation on PV module surface, W/ m2
$k_{el,aircool}$	Air cooled condenser electricity consumption coefficient
$k_{el,ct}$	Cooling tower sizing coefficient
k_T	PV ventilation factor, °C/(W/m2)
k_{wc}	Ratio between cooling tower and condenser cooling water flow
P	Boiler design power, kW
$p_{ct,wloss}$	Cooling tower blowdown percentage
P_{el}	Power consumption, kW *
$P_{el,airc}$	Power consumption of an air cooled condenser, kW
$P_{el,ch}$	Chiller electricity consumption at current temp. conditions and current load, kW **
$P_{el,ch,ref}$	Chiller electricity consumption at ref. temp. conditions and full load, kW **
$P_{el,ct}$	Cooling tower electricity cons. at current temp. conditions and current load, kW **
$P_{el,ct,d}$	Cooling tower design capacity, kW
PLR	Part load ratio **
PLR_{1st}	First stage part load ratio of a two staged boiler **
PLR_{min}	Condensing boiler or VC chiller minimal PLR **
$PLR_{min,ct}$	Cooling tower fan turn off limit (fraction of full HR load requiring fan oper.)
P_{pk}	PV peak power, W
P_{pv}	PV power generation, W *
Q_o	Optical collector gain *
Q_{tl}	Collector thermal loss *
Q_u	Useful collector gain *
SC_{max}	Maximal storage capacity, kWh
SP_{max}	Maximal hourly storage discharge, kW
T_{amb}	Ambient temperature, °C *
$T_{chil,out}$	Chilled water supply temperature (exiting the evaporator) , °C *
$T_{cool,in}$	Cooling water inlet temperature (entering the condenser) , °C *
T_m	Average collector fluid temperature, °C *
T_{pv}	PV module temperature, °C *
V	Storage volume, m3
WC	Water consumption, m3/h *

System Model Simulation

BSD	Load delivered by the storage tank which is fed by an on-off boiler *
C_b	Boiler control signal, 0 or 1 *
CBD	Load delivered by the auxiliary condensing boilers **
CBL	Load demanded from the auxiliary condensing boilers **

$CP1$	Condensing boiler 1 power, kW *
$CP2$	Condensing boiler 2 power, kW *
D	Load delivered to the thermal distribution system, kW *
DR	Maximal storage discharge rate, referred to full capacity
f_{RL}	Remaining load factor
GA	Gross collector area, m2
I_{SCh}	Incidence matrix mapping the chiller combinations to the corresponding SCh value
I_{SP}	Incidence matrix mapping the boiler combinations to the corresponding SP value
L	Load imposed to the primary HVAC system (primary load), kW *
LD	Annual load duration profile
q	SP index indicating optimal cond. boiler combination to cover the load
r	SMP index ind. the boiler comb. with the largest SMP smaller than the load
RA	Roof area under collectors, m2
RL	Remaining load, kW *
S, M, B	Small building, medium building, big building
SC	Storage state of charge, kWh *
SCh	Sorted sums of full capacity chiller combinations
SC_{max}	Maximal storage capacity
SG	Solar gain, kW *
SMP	Sorted sums of condensing boiler minimal powers
SMP_P	SMP sorted by increasing SP
SP	Sorted sums of full power condensing boiler combinations
SSD	Load delivered by the storage tank fed by a solar thermal collector *
t	Time, hourly resolution

Costs and Emissions

β_m	Maintenance cost factor
β_x; β_e	Dynamic present value factor; Same factor for the energy consumption ***
a	Annuity factor
AC_i	Annuity of investment costs, €/a
AC_r	Average (over T) annual running costs, €/a
AC_t	Total annual costs, €
C_0	Investment cost at the beginning of the calculation period, €
CE	Energy consumption (all utilized energy carriers), kWh/a ***
C_e	Cost of consumed energy, €/a
C_{ip}	Initial component purchase price, €
C_i	Investment cost, €
C_m	Maintenance costs, €/a

C_r	Replacement cost, €
E_{CO2}	CO2 emissions, kg/a
EP	Energy prices (all utilized energy carriers), €/kWh ***
f_{inst}	Installation factor
R	Market interest rate
R_i	Inflation rate
R_p	Price development rate
R_R	Real interest rate
SE	Specific emissions (all utilized energy carriers), kg/kWh ***
T	Cost calculation period, years
T_{life}	Component life duration, years
V_{future}	Future value, €
$V_{present}$	Present value, €

Optimization

C	Counter of undersupply timesteps
CE_{sum}	Sum of all annual energy consumptions of all consumed energy carriers, kWh
C_{SuP}	Permitted number of undersupply timesteps
OF	Objective function
P_{feedIn}	PV generated power fed to the grid, kW
p_{SoP}	Solar penalty coefficient
p_{SuP}	Supply penalty coefficient
R_{SuP}	Delivered vs. set load ratio
SoP	Solar penalty function
SR	Solar ratio
SR_{target}	Target solar ratio
SuP	Supply penalty function

1 Introduction

Commercial building is a complex product planned, designed, constructed, owned, and operated by professionals from diverse backgrounds over a certain period of time. In spite of its rather complex multivariate nature, a building's primary function is to host people and processes by providing a space where visual, acoustic and thermal comforts are satisfied. Another function of a building is its esthetic appeal; it is a work of applied art. During design process a high interaction occurs between these two building functions, a visual appearance and the utilization. The third, and for the design process increasingly important, function is the building energy performance (BEP). It is not to be separated from the previous two. In fact, each building represents a dynamic object on the energy map of a municipality, a country or a region. This new role is expected to transform all buildings from being mere energy consumers into entities that also produce energy in order to maintain its sustainability. The synchronization of dynamic demand and power generation profiles will play an important role in both the supply of electricity and the stability of the power grid. Electrical energy together with the rest of primary energy sources, such as gas, oil or biomass, used to achieve comfort in buildings, contributes to increased carbon emissions. Luckily with the maturing of building simulation tools, BEP is cutting its way into the very base of the building design process, where it rightfully belongs.

The motivation to put the BEP under the magnifying glass can easily be found in the impact of buildings sector on the global energy consumption. Based on [1] in 2008 buildings consumed 40% of total primary energy in the USA, with commercial buildings holding a share of 18.4%. It has to be considered that the USA is the consumer of approximately one fifth of global energy [2]. Around 40% of primary energy consumed in buildings is used for HVAC (Heating, Ventilation and Air Conditioning), [3]. In Germany, a country holding 2.8% of global primary energy consumption, a different technology is dominant in HVAC domain. Nevertheless, similarly to USA, around 17% of total primary energy is consumed by buildings in commercial sector, [4]. According to [5], in the European Union buildings also account for 40% of total energy consumption. Furthermore, [6] predicts a 5% delivered energy consumption increase in building sector by 2035 if technology from 2009 is used.

It is therefore no wonder that a whole set of regulations and national policies are being defined to reduce building energy consumption. They usually set targets of energy consumption reduction (with regard to a year in the past and by the year in the future) or prescribe efficiency increase for relevant components, such as building envelope elements, HVAC systems and equipment, lightning equipment etc. during the life cycle of a building. For example, directive 2010/31/EU of the European parliament (EPBD) [5] imposes a set of minimal requirements for new and existing buildings, with an objective to reach nearly-

zero energy consumption buildings by 2020. Additional action in consumption and carbon emission reduction is taken by using building certification and rating systems, such as LEED (USA), DGNB (Germany), and EPC and DEC (UK).

To reach these targets and obey the regulations, the way buildings are designed is changing. At the beginning of [8] Clarke suggests that "The better design of new buildings would result in a 50-75% reduction in their energy consumption relative to 2000 levels, and that appropriate intervention in the existing stock would readily yield a 30% reduction". Let us remember the building functions defined at the beginning of the chapter. Depending on a planning and design process structure, one or the other of those functions might be dominant during the design while the others are treated as a slave. For example, to compensate for the poor thermal insulation property of an esthetically valuable façade in answering the utilization demands such as thermal comfort, the BEP is suffering. This is a consequence of sequential design and low interoperability between the professionals involved in a project. The building industry is realizing that in order to improve the BEP, building design process has to host a high level of interoperability between architects, engineers and constructors. A holistic approach to design and operation can be achieved if building information model (BIM) is utilized. In [9] Bazjanac defines BIM as "An instance of populated data model of buildings that contains multidisciplinary data specific to a particular building which they describe unambiguously". In such a way all the disciplines involved in design rely on the same data model. This enables fast communication of changes and progress in the design, instant cost assessment, interdisciplinary consistency, easier alternative design considerations, to name just a few of the advantages. It is realistic to expect the future benefits of BIM to be beyond predictable due to interdisciplinary knowledge each of the practitioners will gain.

The energy performance of a building is a dynamic process due to the transient nature of heat transfer, energy storage, control systems operation, fluctuating weather conditions, occupancy etc. To anticipate the BEP of a proposed design, a model of a building containing data relevant to energy performance needs to be simulated over a given period of time. Only by accounting for the transient effects can the realistic energy demand profiles be accessed and the energy supply systems tailored to fit the demand whilst maintaining high energy efficiency and indoor comfort. During the 70's the first dynamic building simulation software tools were developed. In December 2011, the Building Energy Software Tools Directory, [10], lists over 400 software tools, ranging from whole-building energy performance simulation tools, to specific topic related tools, such as e.g. HVAC plant and system simulation, daylight performance, economic calculations, and simplified qualitative design tools. The simulation tools are becoming more robust, reliable and interconnected. Utilization of HVAC system simulation provides detailed assessment of energy consumption, operational costs and emissions. Simulation enables both operation and design optimization, in an ideal case followed by interdisciplinary design iterations.

The advent of all these simulation tools has put the BEP at the forefront of building design process. Therefore, in the following sections, a contribution to the emerging field of simulation aided building design is presented. This thesis is a part of the efforts to improve the BEP position in the early design from the primary system point of view, which is often not given the necessary attention.

1.1 Problem Statement and Main Contributions

This thesis investigates the interplay between the initial architectural design decisions and the choice of the primary HVAC configuration. An HVAC system consists of a primary and secondary system. According to [11], “The primary system converts energy from fuel or electricity into a heating and/or cooling medium”, while “The secondary system delivers heating, ventilation, and/or cooling to the occupied space”. In the literature, the primary system, or at least a large part of it, is sometimes referred to as the equipment or the plant. Implementing various measures of improving the building envelope (e.g. shading, orientation, and insulation) decreases the demand but occasionally completely removes it (Step 1 at Figure 1.1). The next step towards lower primary energy consumption consists in reducing the distribution losses and parasitic consumption of the thermal distribution network (Step 2 at Figure 1.1). Finally and where this thesis makes a contribution, the efficiency of the primary HVAC system, the energy generation plant, needs to be improved (Step 3 at Figure 1.1).

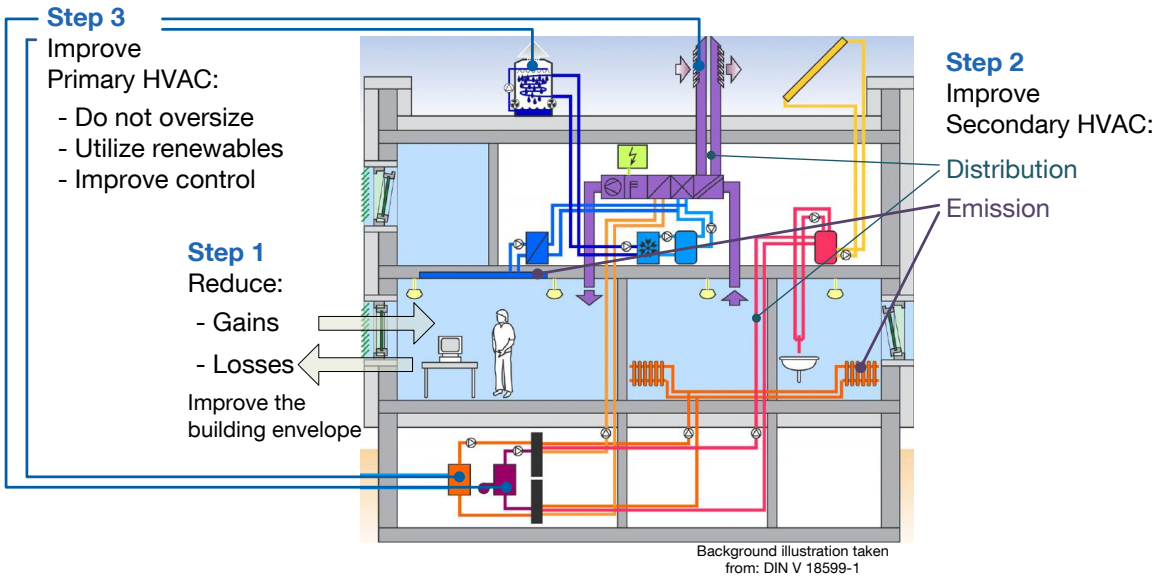

Figure 1.1 Steps in order to reduce HVAC energy consumption. This thesis develops a method of primary HVAC (Step 3) simulation and optimization for the conceptual building design stage.

The BEP can benefit greatly from the architect having the outline concept regarding the energy sources and conversion devices appropriate for the specific climate and coarse building geometry. Many generation and storage components impose restrictions on building design and these cannot be introduced at a later stage. The components, such as solar thermal collectors, photovoltaic (PV) panels, biomass boilers and large thermal storage tanks, impose significant building surface and floor area requirements. Therefore, the quantification of the influence, which early architectural decisions have on the primary system configuration, needs to be provided. This quantification consists of cost, emission and consumption assessment of the primary system. As a prerequisite for this, the system

configuration and dimensions need to be determined. In the thesis, a methodology of the primary HVAC simulation and optimization is developed, that includes the cost, consumption and carbon emission assessment, applicable during the conceptual building design.

The major challenge for optimizing the space heating and cooling energy source during conceptual building design is the lack of information about the distribution system (the secondary HVAC) and working fluid parameters, such as flow rates and temperatures. However, there are several common mistakes, which can be avoided if the primary system simulation is performed at the earliest possible design stage. Namely, the primary system is often expected to perfectly match the demand and supply of heating and cooling energy, with a production profile that synchronizes to the building demand profile. The simplest way to achieve this simultaneity is to utilize boilers for heating and chillers for cooling, while sizing them according to peak demand. For the sake of supply security, components are often oversized, or redundant components (especially in case of chillers) implemented. The efficiency of conventional HVAC system components has significantly increased during recent decades. However, further savings can be achieved if utilizing intermittent renewable energy sources (RES) and relying more on thermal storage. The reasons such systems have not yet become standard equipment are the higher investment costs and the system design and control complexity.

Utilizing a conventional steady-state component dimensioning often leads to unsatisfactory overall system performance efficiency. Time domain system simulation considers part load performance, thermal storage dynamics, the fluctuating renewable energy availability and system controls operation. Most reliable simulation results are achieved by parallel coupling of system and building simulation. However, the level of detail of such a simulation is high compared to data available at the time the early design decisions are made. That is why modelers often resort to a sequential approach, where the previously calculated building demand serves as a set load for the system simulation.

Having this in mind, the following set of features needs to be incorporated in a primary HVAC design and optimization tool targeting conceptual building design:

- Implementation of: intermittent RES and thermal storage;
- Optimal boiler and chiller staging considering part load efficiency;
- Cost, fuel/power consumption and carbon emission assessment;
- Design optimization;
- Simple user interface suitable for non-experts; and
- Reduced user input data demand suitable for conceptual design.

In an answer to these requirements, the following major contributions described in this thesis are:

- A series of representative primary HVAC models (system models - SMs) are preconfigured to present a method of considering the thermal storage, RES, and part load performance during conceptual design;
- The developed SMs are energy balance based and deal only with loads. The inertia of thermal systems is taken into account by allowing short term load shifting. Model simulation is quasi-stationary and yearly, with an hourly resolution. The SM performance is governed by a dedicated load allocation control;

- Each simulation yields SM performance profiles, costs, emissions and fuel consumption;
- The design optimization procedure performs system dimensioning, based on the following goals: total and investment cost, energy consumption or carbon emission minimization. Each of the goals can be combined with a minimal required percentage of the demand to come from a solar source; and
- Both simulation and optimization models are available to the user through a proposed graphical user interface. After following a clear set of steps, the user is provided with dimensions, costs, energy consumption and emissions of the optimized system.

Sequentially coupled with the FassadenTool developed by Liedl, [12], the developed tool allows a rapid means to access the influence of a change in façade design based on the cost, emissions, and dimensions of the primary HVAC components. In the case of a simple system, the tool utilization is equivalent to receiving recommendations from an experienced HVAC engineer, available to the architect anytime he uses the tool. Further benefits are gained with the increased utilization of complex hybrid systems, due to the difficulty in experience-based initial dimensioning. The results obtained are to be considered with care, as they are not design values but recommendation and orientation values.

1.2 Previous and Related Work

The research was conducted within the scope of an interdisciplinary project of the International Graduate School of Science and Engineering (IGSSE). The project was entitled “Interplay between a building, its users, the climate, and energy efficiency: principles for planning buildings in different climate zones bearing thermal comfort, room climate, energy requirements and technical aspects in mind”. The topic arose from the fact that early conceptual design (predesign) decisions have a strong impact on the energy performance of commercial buildings. Three institutes were involved, each belonging to a different department of the Technische Universität München:

- Civil Engineering - Lehrstuhl für Computation in Engineering;
- Architecture - Lehrstuhl für Bauklimatik und Haustechnik;
- Electrical Engineering - Lehrstuhl für Energiewirtschaft und Anwendungstechnik.

Regarding stated project, these institutes focused on, respectively:

- Indoor comfort analyses;
- Interaction between building envelope, user and climate in forming the heating and cooling demand;
- Generation of heating and cooling energy (primary HVAC plant) to satisfy the remaining demand.

The overall goal was to provide guidelines concerning building envelope and heating/cooling energy sources in order to increase energy efficiency of buildings by including the subject of energy consumption in the conceptual building design stage, [13]. As an answer to this, Liedl in [12] provided detailed analyses on how the climate conditions (including solar radiation, temp and humidity) influence the user comfort, the heating and/or cooling demand. The climate analysis is provided to the user through an interactive ClimateTool. Furthermore, Liedl conducted a parameter study on façade concepts including the orientation, window area ratio, shadings and thermal characteristics of construction materials for four cities. With the fast economic growth in countries like China, India, Russia and Arabic countries, the commercial building planning schedules are getting ever tighter. For this reason, the cities of Bangalore, Dubai, Moscow and Shanghai have been selected. In [12] these cities are considered as typical representatives of their climates. The results of the study are available through the FassadenTool. Using the specific ideal heating and cooling demand profiles provided by the FassadenTool, the set load for the models developed within this thesis can be formed. In such a way the interplay between the climate, façade and the primary HVAC can be observed and analyzed.

Before deciding to create a new tool capable of satisfying the set of features listed in the problem statement, the existing ones were considered and tested. In [14] a categorization of simulation tools according to the problems they address has been provided. Following this categorization, the simulation tool suitable for addressing the problem presented in the previous section is both:

1) A tool for primary HVAC energy performance analyses; and
2) A tool for system optimization.

The requirement allowing the usage of the externally created ideal load:

3) Compatibility with the externally generated hourly load profile.

Additional requirements stemming from the problem statement are:

4) A tool capable of cost and carbon emission assessment;
5) A tool suitable for usage in conceptual design; and
6) A tool targeting non-expert users.

The number of available commercial and educational tools is increasing. This short review focuses on primary HVAC simulation tools that satisfy most of the criteria listed above.

Several approaches have been identified in the existing primary system design tools. Their complexity ranges from quantitative, such as CIBSE RESET tool [7], which is a descriptive Microsoft Excel based tool providing evaluation of renewable energy potential depending on the location, to sophisticated dynamic simulation tools that will be mentioned at the end of the review.

The majority of HVAC practitioners rely on simple spreadsheet based tools, the 1st generation tools [8], relying on procedures prescribed by national standards (e.g. DIN EN DIN V 18599 [15], DIN EN 15316 [53]). Several manufacturers have taken this approach a level higher and offer complete load, system and economic analysis. Examples are Carrier's HAP [16] and TRACE 700 [17] developed by Trane, which sequentially simulate building loads and the plant in hourly steps. Both tools comply with ASHRAE Standard 90.1 [18]

and require engineering knowledge to compare alternative designs. A tool based on the ASHRAE temperature bin method, RETScreen [19], analyses not only heating and cooling systems for buildings, but also district heating and power systems. The tool has the capability to size the heating and cooling energy generators based on base/peak load and perform economic analysis. However, it is not a simulation tool and cannot be coupled with any externally generated load profile. Sakurai et al. in [20] have developed a tool to assist the early choice of a heating system. After choosing a system, components have default sizes based on a calculated load profile and thus not based on system performance optimization.

Optimization and price comparison of hybrid power systems, including RES and power storage using time series data, is possible with the energy modeling software HOMER [21]. When it comes to optimization, it can perform parametric runs and exhaustive search optimization after the user has defined the discrete component sizes. At each timestep, it meets the power demand using a predefined dispatch strategy, which is a common method in the optimization of power generation on a regional scale. The lack of working fluid parameters, due to the unknown distribution system type and configuration, inspired the utilization of such an approach in the building sector. In [22] Fabrizio developed a multi-energy modeling and optimization framework, which is able to optimize the configuration of the energy (cooling, heating and electrical power) sources and their sizes based on cost and emission minimization. In his thesis he adopted the energy-hub model, which is a generic framework for the steady-state modeling and optimization of energy systems, including multiple energy carriers presented in [23]. Two approaches are offered by [22]: optimization based on the seasonal energy amount; and optimization for hour to hour demand profile satisfaction. Unfortunately, this framework includes neither the energy storage and the solar energy converters, nor the control strategies necessary to include such components.

A freeware building energy use analysis tool based on DOE-2.2 [24], eQuest [25], offers comprehensive support for BEP design. The user can choose from two levels of detail and is further led through the building and system definition by the wizard. Up to two boilers and chillers are offered if using the simpler procedure, which is more suitable for the early design. Chillers and boilers are sized automatically, taking base and peak load into consideration. The program performs cost calculations and displays monthly result analyses. Parametric runs are available for alternative comparisons. Although this sophisticated tool can provide great support and reliable results during design, the following two drawbacks were noticed. Firstly, the thermal storage is considered not as a part of heating system, but only as a hot water supply component, and secondly, it does not model solar collectors. As stated in [26], architects find that eQuest requires detailed and technical data input.

The level of detail and input demand, in terms of both data and user expertise, limits the usability of highly sophisticated tools like TRNSYS [27] and EnergyPlus [28] during conceptual design. EnergyPlus is a comprehensive, freely distributed, whole building energy simulation program. Apart from several commercial graphical user interfaces (GUI) currently available, such as DesignBuilder [29], a dedicated GUI enhancing the usability and interoperability with i.a. BIM tools is under development by the creators of EnergyPlus. TRNSYS is a simulation environment for transient energy simulation, encompassing multi-zone building, primary and secondary systems, economic analyses, etc. Its

modular structure ensures a high level of flexibility. It offers GUIs for component drag and drop and building definition, as well as plug-ins to other relevant tools, such as 3D building definition and optimization programs. Both tools cover a broad range of primary HVAC system component models and controls, enabling detailed system configuration and performance analyses. The optimization and parameter runs are possible by coupling these tools with the optimization program GenOpt [30], which offers a broad range of optimization algorithms.

Since the satisfaction of all the criteria listed would require a combination of several existing software packages and approaches, the decision was made to develop a new tool in Matlab environment, [31]. Such an approach enabled high flexibility and control in terms of both tool development and distribution.

1.3 Thesis Outline

The thesis is organized into seven chapters and two appendices. The topics of chapters 3, 4 and 5 are put in order according to the overall model dataflow, as in Figure 2.1, and thus cover its complete configuration. Each of the chapters provides a dedicated summary and discussion section. These sections start with a short summary of the chapter content, followed with a critical discussion of the implemented method. They continue with the proposed further work and finally provide a transition to the next chapter.

Chapter 2 (Method and Approach) introduces concepts and methodologies applied to model, simulate and optimize primary HVAC components and systems. It explains the structure and introduces the usability of the tool created.

Chapter 3 (System Models) begins by introducing the configuration of the featured system models (primary HVAC plants). It continues with mathematical models of implemented generation and storage components. Most importantly, it describes the simulation performance of the system models, which includes presenting the control and load allocation strategies. The performance of each of the system models is illustrated through examples.

Chapter 4 (Costs and Emissions) describes the implemented annuity cost calculation method. The method allows total investment cost to be expressed in annual portions. The results of system simulation are transformed into annual energy cost and carbon emission values. It considers the inflation and market rate, as well as the price developments. The chapter provides references to component specific investment and maintenance cost, as well as to fuel, power, feed-in and water tariffs.

Chapter 5 (Optimization) establishes the primary HVAC (system model) design optimization problem. The values calculated in chapter 4 are set as optimization goals. The mathematical description of the problem includes defining the objectives and the constraints. The constraints are reformulated as penalty functions. After that, suitable optimization

algorithms are identified and described. The final sections show an optimization example for each of the system models.

Chapter 6 (PROBA Tool Prototype) proposes a user interface, build upon the developed models, yielding a tool entitled PROBA. The chapter describes the functionality and the usage of the tool in steps. It provides an example of how the tool implementation influences the building design and BEP.

Chapter 7 (Conclusion and Outlook) provides a concise summary of the thesis. It outlines the tasks, the challenges and the contributions. The outlook discusses further applications of the main developments, as well as the potential improvements. It ends with a critical discussion regarding the overall topic of the thesis.

Appendix A verifies the method of using single office simulation to approximate building ideal heating and cooling load and explains its transformation into a primary HVAC set load. It illustrates the load and weather data utilized in the examples throughout the thesis.

Appendix B consists of tables and figures holding all utilized cost and performance data.

2 Method and Approach

As mentioned in the previous chapter, the objective is to identify the optimal dimensions of energy generation and storage components of a primary system. To achieve this, a system equipped with appropriate controls is optimized to minimize one of the following: investment or total cost, CO_2 emissions or fuel consumption.

Low level of user expertise in primary HVAC design and the scarcity of information about the building that the proposed system is intended to condition pose major challenges for model development. However, it is worth facing those challenges to allow early primary HVAC system consideration and thus improve the BEP. One of the benefits can be illustrated on an example of a primary system containing a solar thermal collector. The user wishes to reduce the fuel consumption, thus the primary system design is subjected to fuel consumption minimization. Its result provides the information on just how large the area to place solar collectors should be in order to achieve the targeted fuel consumption reduction. Obviously, this directly influences the building design. Additionally, the user could explore the influence of the increase in collector dedicated area on the annual solar ratio.

To include transient effects of thermal storage, the intermittent nature of RES, boiler or chiller part load efficiency and their optimal staging, component dimensions need to be identified based on simulated system performance, rather than on one stationary peak load condition. Since non-expert users are not expected to know how to configure a primary system and its control, a set of preconfigured systems is developed. The configuration of models presented is chosen so that each of these systems, further referred to as system models (SMs), illustrates one or more of the mentioned effects. Using these representative SMs the properties and development of the optimization tool is demonstrated. Based on the methodology to be described herein, further SMs could easily be added to the tool. The advantage of having the SM preconfigured is its simple usage, while the low user flexibility is a drawback.

This chapter provides basic principles used for modeling, simulation and optimization. It shows the embedding of the system model into the optimization process. Additionally, it explains how the tool, comprising of all mentioned components and processes, is made available to the user.

2.1 General Structure

The general structure of an optimization process is shown in Figure 2.1. The optimizer passes the set of component dimensions (optimization parameters) to the simulator. The simulator evaluates the SM performance based on the given set of data, determines the relevant system performance profiles in order to calculate costs and emissions, and defines the objective function. It returns the objective function value to the optimizer, which either defines a new set of component dimensions to be evaluated by the simulator in case the minimum has not been reached, or returns the optimal result. The result data contain:

- Optimal component sizes;
- Total, investment and running cost of such a system;
- CO_2 emissions;
- Reached solar ratio; and
- Information on satisfying the demand.

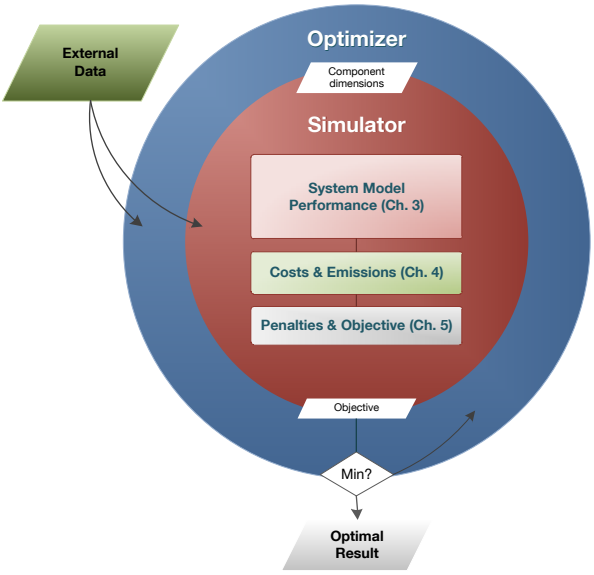

Figure 2.1 General structure of a system model (SM) performance based design optimization.

A detailed representation of the same process is provided in Figure 2.2.

2.1.1 Data Input

The upper part of Figure 2.2 gives a short overview of the input data. From the user perspective, the complete external data can be classified as following:

- Obligatory user input, i.e. ideal building load, weather data, and (SM specific) available area to harvest solar energy;
- Optional user input (preset technical and cost data in Figure 2.2); and

- Fixed parameters: e.g. penalty function parameters, simplified secondary system loss coefficients.

The weather data are required by the models directly depending on ambient conditions. These data consist of the solar radiation and ambient dry and wet bulb temperature profiles.

An ideal building load is used to approximate the primary system set load. The coupling between building and primary HVAC system simulation is sequential. A method to "imitate" the interaction of the primary system with the building despite this coupling method is developed and described later in this chapter. This could be omitted in the case of parallel building and system simulation, where the building sends the demand signal step by step in response to the supply. However, before becoming an initial set load profile to be processed within the SM performance simulation, the unrealistic peaks of every ideal building load are shaved (see Appendix A) and load is increased for the assumed losses in the distribution and emission system. Although not insignificant, currently the secondary system losses are modeled only very roughly, while the focus remains on the primary system modeling.

2.1.2 Modeling and Simulation

Similar to those featured by the majority of the currently available tools, all the involved models are deterministic. The simulator hosts the complete process of transforming the input parameters into the objective function value. This process deals with the following three topics, which are differentiated by red, green and gray color in the Figure 2.2:

- Determination of annual SM performance profiles;
- Assessment of investment, running and total cost, and CO_2 emission based on performance profiles; and
- Penalizations of a given set of component dimensions if a calculated supply profile or solar ratio has failed to reach the set values, and calculation of the objective.

The core process is the hourly simulation of the system model performance, which yields yearly performance profiles for all the SM components at an hourly resolution. The performance profiles are e.g. PLR or efficiency profiles for boilers, COP profiles for chillers, utilized solar gains, storage charge and discharge profiles. Each of the components of the system is assigned an appropriate equation or set of equations to describe its performance with sufficient precision. The implemented models are:

- Empirical, obtained by manufacturer data regression and modified empirical models taken from the literature (used for e.g. boilers, chillers);
- Semi-empirical (used for e.g. solar thermal collectors); and
- Simplified theoretical (used for e.g. thermal storage).

The complexity level of system components is low due to the lack of detailed data in the early design. Rather than defining the components by inlet and outlet mass and heat flows,

the energy-balance approach has been adopted. In other words, the load allocation strategy based on known values is prescribed for each SM. Solar thermal collectors and PV useful energy gain profiles are modeled as time-step independent, so that the complete hourly profile can be generated within the same calculation step by applying appropriate transformations to the weather data time series. It should be noted that the defined collector heat gain time series, if that component is included in the SM, is fed into the system model performance simulation step by step, where each of these values represent the available solar energy for that hour.

The previously mentioned SM performance simulation is a quasi-stationary forward simulation. In each timestep the control, which will be described in more detail further down, regulates the energy flows from and to (i.e. thermal storage) each of the components. Even though the SM level of detail is relatively low, two important benefits of implementing a time-domain simulation are:

- The plant simulation models are energy balance based and deal only with loads, but the inertia of thermal systems is taken into account by allowing limited short term load shifting. If within one timestep a certain percentage of the set load has not been satisfied, that amount is shifted to the following timestep and added to the previously calculated initial set load. Further in the thesis this amount is called the remaining load. In terms of achieved system efficiency and energy balance, a system where such a load shift is allowed, under defined limitations, performs similarly to the well-controlled real system. Namely, the real control system in case of, for instance, a very cold night would turn the heating generation on some hours before the actual schedule. Thus the peak, which, if occurred, would subject to load shifting in the SM performance, would simply not occur due to the preheating. Since the simulation used to generate the ideal load profile, usually does not include changes in the heating time schedule, the mentioned peak occurs. If direct coupling of a system and building simulation is implemented, the actual building response would influence the set load and this artificial load shifting would not be necessary.
- Thermal storage consideration.

Additional measures are applied in order to overcome the problems that come as a consequence of load based modeling of thermal systems. The simulated heat flow direction is made thermodynamically possible due to temperature limitations imposed to component performance, depending on the configuration. Related to that, the temperature also influences the efficiencies of affected components. These temperatures are either the weather data time series or the assumed return or supply temperatures. The example of this is the higher solar collector thermal loss in case of utilizing the radiator emissions system, compared to the floor heating utilization. The reason for this is the higher supply temperature, which implies higher solar collector to thermal storage inlet temperature, thus increasing the thermal losses of the collector and reduces the available collector gains.

SMs account only for the generation and storage components. The only primary system distribution components considered are those that are not common for all of the SMs, such as simplified consideration of solar collector distribution system losses. The assumption

adopted considering the precision required in the early design phase is that if comparing systems, they will all have distribution components with similar consumption and losses.

The control assigns the tasks to each of the components in each timestep. Two kinds of control can be found within the models. The first is the hysteresis control, used to control the storage charge by the two or one stage boiler, in order to improve the storage utilization and reduce the number of boiler start-ups. The second is the sequential controller in the case of utilizing a number of chillers or condensing boilers. This controller relies on the component specific operational optimization algorithm to increase the overall efficiency of the components. The control is idealized and assumes the implementation of a competent control and regulation system.

The costs are quantified as annuities for the chosen or preset lifetime duration. In terms of calculation flow, the investment costs can be assessed as soon as the component dimensions are known and do not need to wait for the SM performance profiles, which are needed to assess the energy consumption and thus the running costs.

The most important constraint imposed on the optimization is the supply task satisfaction. Where user insists on a specific solar ratio, the solar ratio constraint is activated. Both constraints are implemented as a penalty function, increasing the value of the objective in case the constraint is breached.

2.1.3 Optimization

The optimization objective is a simulation based non-linear and non-convex function. Two algorithms, robust enough to identify the global minimum, are implemented in the optimizer:

- Global Bounded Nelder-Mead (GBNM), since it only evaluates the value of the function, and not its derivatives; and
- Exhaustive search, since the components are only manufactured in certain sizes. It is modified to exclude the sets of optimization parameters already known not to be able to yield the optimum.

Apart from the optimization algorithm loop, in Figure 2.2 an additional process within the optimizer can be seen. This process exempts a potential user from defining the optimization parameter bounds. The bounds are defined automatically based on the load imposed on the SM, as well as the discrete optimization parameter sets used in exhaustive search. Another usage of the exhaustive search is to verify the global minimum found by the GBNM algorithm.

To enable the analysis of the optimization process, the algorithm for automatic two- and three-dimensional parameter visualization has been developed. It visualizes the influence of chosen parameters after the exhaustive search algorithm has formed a map of results.

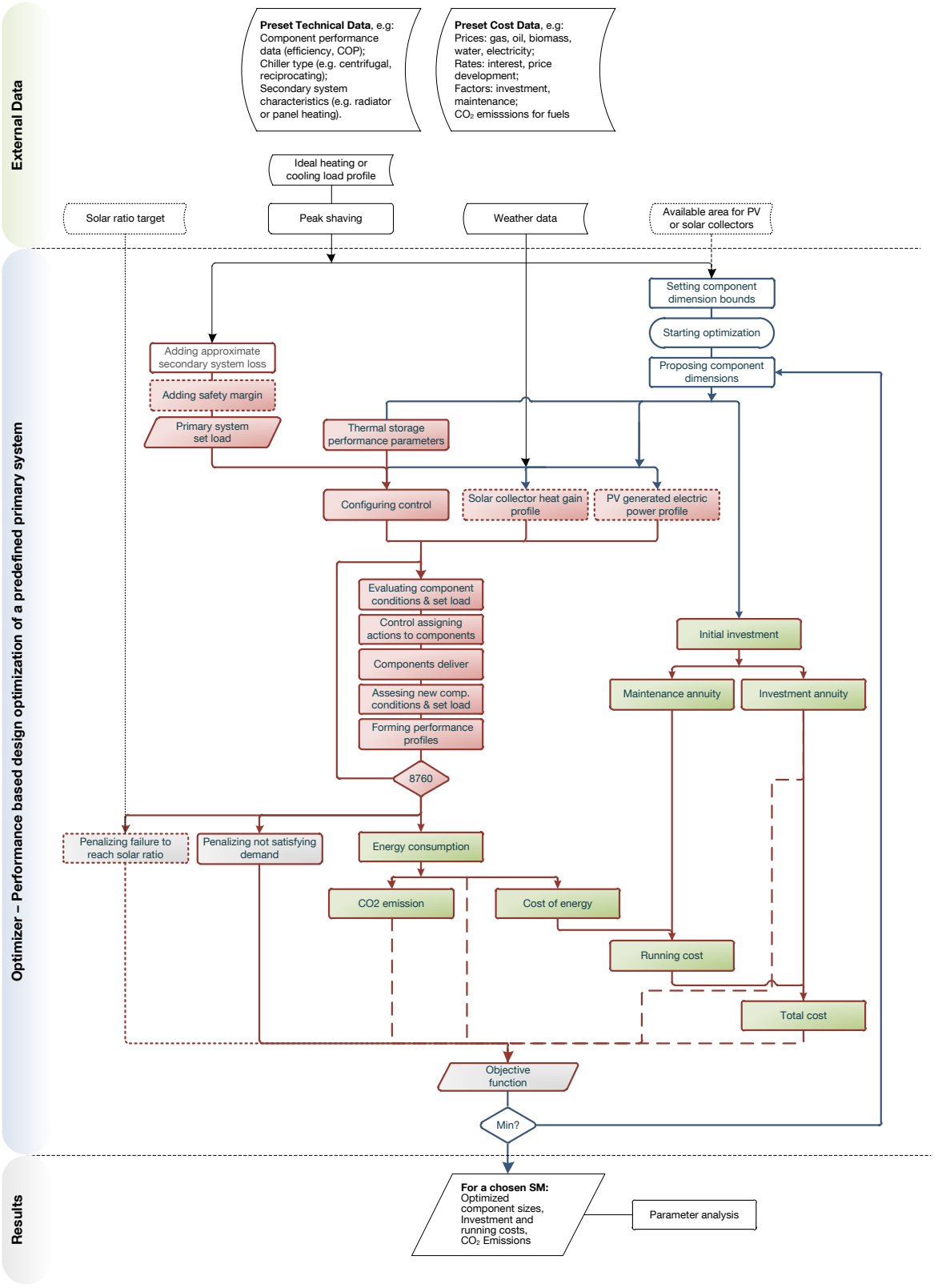

Figure 2.2 Overall process flow: external data flow into the optimizer which runs the simulator to yield the result. Blue connection lines belong to the optimizer, red to the simulator, which consists of pink SM performance processes, green cost and emission calculation processes and grey objective definition processes. Dotted lines represent SM specific inputs and processes. Each of the dashed lines connects a value that added to the penalties defines one objective function.

2.2 User Interface

To enable the practical implementation of the presented modeling, simulation and optimization environment by a user who is not an HVAC engineer, a graphical user interface (GUI) is proposed. It is structured as a wizard guiding the user step by step. The GUI will automatically disable usage of SMs that cannot supply the necessary energy profile in the chosen climate, as well as provide first information on how environmentally friendly the SM is. The purpose of this is to simplify the choice of SM for the user. There are two degrees of difficulty in the process of entering obligatory input; the easy one enabled through the connection with FassadenTool, [12].

As already mentioned, the tool developed serves to examine the proposed methodology and has not been verified in practice and thus the results currently have an educational value. The complete tool is developed in MATLAB environment. Several open source tools and TRNSYS have been used to perform simulation comparisons.

3 System Models

System models form the basis for the introduced concept of preliminary primary HVAC optimization. The SMs consist of energy generation and storage components. The chapter explains how the SMs are configured and provides mathematical models of each considered component. Later it describes the fundamental element of the overall model, which are the implemented control strategies and the simulation performance for each of the SMs.

3.1 System Model Configuration

Many different primary HVAC plants configurations are possible with current technologies. Even the same combination of generation and storage components can perform differently depending on the hydraulic scheme, the control system and secondary HVAC configuration. This additionally increases the number of combinations. More importantly, it shows that in order to evaluate the system it needs to be simulated throughout a heating or a cooling season. The simulation defines the hourly performance of each component and component interactions. Only such an approach to primary system modeling can capture the transient effects of thermal storage, evaluate the possibilities of intermittent solar energy utilization, and account for the component part load performance. However, a user who requires a simple tool usually lacks either the knowledge or the time necessary to configure such a system in order to perform the simulation. Therefore, seven systems are preconfigured into system models (SM1 to SM7). These configured systems demonstrate the effects mentioned previously. Despite the lack of system information during conceptual design, a method to perform a quasi-stationary system simulation is developed.

The components implemented, see Table 3.1, can be separated into energy converters and energy storage. They include conventional building heating and cooling generators, such as boilers and chillers. The renewable source featured is the solar energy. The cost and energy consumption differences can be observed by comparing conventional and more advanced configurations with or without thermal storage, solar collectors and photovoltaics. Namely, the decision to include more RES is surely made easier if the consequent effect on the cost is visible.

The right columns of the same table indicate to which of the SMs a component belongs. Each SM has an inbuilt control governing the load allocation during each simulation timestep. Thus it directly influences the energy consumption profile of the system. De-

pending on the characteristics of components included, the control strategy ensures that the system operates in a realistic and an energy efficient manner. The purpose of the implemented system specific control is to maximize the efficiency during operation. The quality of the proposed component dimensions is evaluated through the load allocation process. In this way the control strategy influences the investment cost of the components. Energy consumption is a direct consequence of load allocation governed by the control strategy.

Table 3.1 Components and relevant system effects. System model configuration.

Component	Effects relevant for the system performance and design	System Model						
		1	2	3	4	5	6	7
Vacuum Compression Chiller	Optimal staging (load allocation) Part load performance Dependence on ambient conditions Power consumption					+	+	+
Cooling Tower	Part load performance, dependence on ambient conditions Water and power consumption Reserving space on the roof						+	+
On-off or staged boiler	Optimal operation to reduce number of start-ups: coupling with storage, base load coverage Fuel (biomass) consumption Biomass fuel storage requires larger space	+			+	+		
Condensing boiler	Optimal staging (load allocation) Part load performance Low temperature heating desired Gas/oil consumption		+	+	+	+		
Thermal storage tank	Thermal storage – short term generation/demand decoupling Improves performance of: boiler, solar collector, (chiller) Space requirement – placing, mounting Thermal loss to environment	+		+	+			
Solar thermal collector	Intermittent production – energy storage desired Low temperature heating desired Space requirement: roof and façade surfaces	+		+				
Photovoltaic	Intermittent production Local consumption and grid feed-in Space requirement: roof and façade surfaces; orientation.							+

SM1 consists of an on-off boiler (represented by a biomass boiler), thermal storage and solar thermal collectors. Biomass fuels are considered to have zero net carbon emissions. The efficiency of boilers burning biomass in its solid state (opposed to biomass gasification) is increased by decreasing the number of start-ups and prolonging full load operation. This is achieved by implementing a thermal storage, which provides a buffer between demand and production. The most simple renewable energy converters in HVAC are solar collectors and these additionally reduce the environmental impact of the system. Optimal SM1 configuration strongly depends on the intentions of the user. As an illustration, without the storage and solar collectors the only remaining component, an on-off boiler, overproduces and has an increased number of start-ups. Disregarding the higher investment cost and allowing maximal collector area and a suitable storage tank leads to significant

carbon reduction. Such a configuration will also have a significant influence on the architectural design. In particular, apart from the obvious question of placing the solar collectors and mounting the storage tank, a building needs to accommodate a relatively big boiler and more significantly the storage for the biomass fuel.

SM2 is a system containing an arbitrary number of condensing boilers. Condensing boilers represent the most efficient technology to provide heat by burning fossil fuels (gas or oil). Furthermore, boiler burners are highly modulating and have a fast response, making condensing boilers a good peak load source. SM2 focuses on developing an optimal load allocation strategy relying on boiler efficiency in part load operation. The shape of the load profiles can thus influence the optimal design of multiple boilers, even in the case of identical peak loads. Condensing boilers perform better with low temperature heating. A suitable heating emission system could be planned, such as thermally activated building systems (TABS). Condensing boilers do not demand a lot of space, but the dimensions of a mechanical room accommodating a gas installation are strictly regulated by standards.

SM3 combines the thermal storage, solar collectors and condensing boilers. The storage is charged using the solar energy. If the storage state of charge allows it, the demand is covered by discharging the storage. The rest of the demand is supplied by condensing boilers, which are able to respond fast in meeting the load. The cost of such a system is relatively high. On the other hand, it is reliable and more flexible than SM1, but still with a high ratio of renewables. A low temperature space heat emissions system makes an excellent combination with SM3. Thus TABS or any other design of large surface emission system (floor heating) would be suitable.

SM4 is a conventional system of on-off boiler and thermal storage in combination with the flexible condensing boiler/s as an auxiliary source. It demonstrates a system utilizing two energy carriers: biomass and gas in the examples. The model is suitable for demonstrating how strongly both investment and fuel cost influence the optimal system configuration.

SM5 is a typical base load – peak load system without any thermal storage. A load allocation strategy directs the two-stage conventional boiler to cover the appropriate base load and avoids short cycling. The rest of the load is assigned to the condensing boiler/s. The space and investment for a storage tank can be saved and the flexibility is provided by condensing boilers. The control prohibits boiler short cycling.

SM6 consists of an arbitrary number of vacuum compression chillers with the appropriate cooling tower. It is the mostly utilized cooling source in HVAC. The model incorporates an optimal chiller load allocation strategy, which influences the optimal design and running costs. The optimization model avoids excessive chiller oversize, while maintaining a certain safety margin. A wet cooling tower is implemented. Its performance depends on ambience conditions and consequently so does the performance of chillers. SM6 represents a reference cooling system.

SM7 consists of vacuum compression chillers and photovoltaic panels. The intermittent PV power usually coincides with the cooling demand. The architect decides to place a defined area of PV panels to any of the building surfaces. The model calculates its effect on both the power consumed from, as well as the power fed to the grid. The investment and the space available pose the limitations.

The SMs are used to perform a design optimization based on the system operation rather than to choose the component dimensions based on an isolated peak load condition. The simulation goal was to obtain the intermittent data for the cost calculation and design optimization. The method is applicable to further primary plant system configurations. For instance, SM4 can easily be transformed in the small CHP unit featuring thermal storage and a peak load boiler. A heat pump model would be similar to the chiller models, SM6 and SM7. The heat for absorption chillers can be produced by SM1 or SM2, etc. Mathematical formulation of both component and system models is provided in the rest of the chapter.

3.2 Generation and Storage Component Models

The models of all featured components that are used to form the SMs are described in the following sections. After describing the general functionality of a component, a short overview of available component models is given, followed by the mathematical description of the adopted model and, if that is the case, its modifications. The limited availability of system parameters plays the crucial role in the model selection. The sections dealing with solar collectors and photovoltaics include the collector tilt optimization for targeted locations.

3.2.1 Vacuum Compression Chillers

To maintain the interior building temperature and humidity at the comfortable level below the outside conditions, the heat needs to be extracted from the building space. Figure 3.1 sketches basic heat flow circuits of the most common cooling energy generation system implemented in large commercial buildings, the vacuum compression chillers. The air is conditioned in one or more AHUs (Air Handler Units). The chilled water flowing through the AHU cooling coil absorbs the excess heat from the air stream. The air is directed to the conditioned space, while the water exiting the coil unloads the heat from the space by evaporating the chiller refrigerant. The refrigerant vapor is compressed to exceed the cooling water temperature, which is at least marginally higher than the ambient wet bulb temperature. Now the heat can be unloaded from the compressed refrigerant to the cooling water. The amount of this heat equals the heat extracted from the space plus the process heat. The cooling water ejects the heat to the environment through a cooling tower, which reduces the temperature of the cooling water in preparation for the next cycle. The condensed refrigerant passes through a relieve valve which reduces its pressure in preparation for evaporation, which chills the water heading to the AHU coil. This closes the circuit.

Apart from using air as a cooling medium, the chilled water can be taken directly to the conditioned space similar to the most common heating systems. Radiation cooling emission system, such as chilled ceilings or fan coils, allows higher chilled water temperature

utilization, which increases the COP (coefficient of performance) of the chiller. In this case, one heat exchange circuit less than in the sketch is implemented. The top circuit can be omitted if using condenser fans, but that is not effective for large buildings and hot climates. More information about cooling towers is given in 3.2.2.

Either way, the main process is a vapor compression refrigeration cycle that raises the excess space heat to a higher temperature level in order to enable its rejection to the environment. As mentioned, the excess space heat evaporates the refrigerant. The nominal value of this heat flow defines the chiller capacity. To achieve this capacity, the compressor consumes electrical energy. COP is a ratio between the energy extracted from the space to the electrical energy consumed for this extraction during a chosen period of time. For reference conditions COP is:

$$COP_{ref} = \frac{CAP_{ref}}{P_{el,ch,ref}} \tag{3.1}$$

where COP_{ref} represents the coefficient of performance, CAP_{ref} the capacity and $P_{el,ch,ref}$ the compressor power, all at reference conditions. The type of a compressor has a big influence on the chiller performance. Those usually utilized in refrigeration cycles are reciprocating, rotary (screw, scroll) and centrifugal compressor.

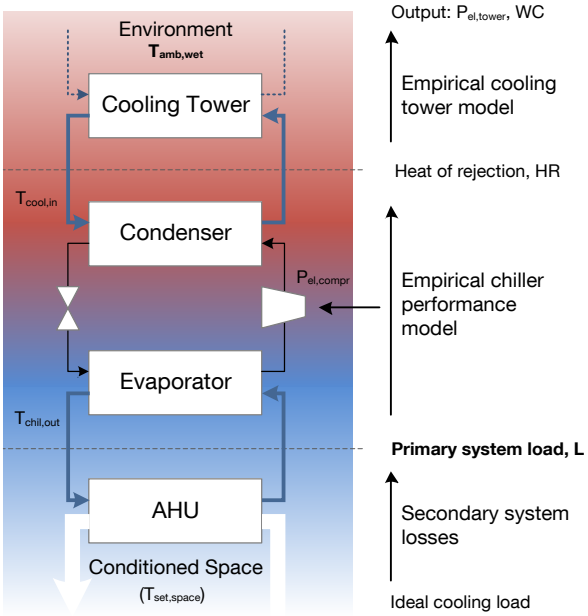

Figure 3.1 Heat transfer circuits to condition a space by providing conditioned air using a vapour compression chiller and a cooling tower as a heat rejection device. Input variables are given in bold.

Detailed models including physical descriptions related to all four thermodynamical processes of the refrigeration cycle do exist, but for the purpose of modeling space conditioning water chillers more simple approaches have shown good results. Various empirical and semi-empirical models based on measurements on the water side (indicated by blue thicker arrows in Figure 3.1 on the condenser and evaporator side) have been developed. They have been evaluated by Lee et Lu in [32]. A similar data fitting approach is seen in

TRNSYS and TESS models. EnergyPlus implements the DOE-2 chiller model described in [33] and [34], as well as a slightly modified version of that same model, which is described in [35].

Here the DOE-2 chiller model described in [34] is adopted and implemented in the SMs containing the vapour compression chiller. It is an empirical model that determines the chiller power consumption based on condenser cooling water inlet ($T_{cool,in}$) and evaporator chilled water return ($T_{chil,out}$) temperature. Three performance curves model the chiller performance. The first is the capacity function, *FCAP*, whose value multiplied with the reference capacity (CAP_{ref}) yields the chiller full load capacity at current temperature conditions (CAP_{full}):

$$FCAP = a_1 + a_2 T_{chil,out} + a_3 T_{chil,out}^2 + a_4 T_{cool,in} + a_5 T_{cool,in}^2 + a_6 T_{chil,out} T_{cool,in} = \frac{CAP_{full}}{CAP_{ref}} \quad (3.2)$$

where a_1 to a_6 are the empirical coefficients, as well as all the further coefficients used in this model. Reference COP (COP_{ref}) divided by the second performance function, *FCOP*, defines the full load COP (COP_{full}) at current conditions:

$$FCOP = b_1 + b_2 T_{chil,out} + b_3 T_{chil,out}^2 + b_4 T_{cool,in} + b_5 T_{cool,in}^2 + b_6 T_{chil,out} T_{cool,in} = \frac{COP_{ref}}{COP_{full}} \quad (3.3)$$

With these two performance functions the full load capabilities at current conditions are determined. However, the chiller power does not change linearly with the part load ratio (PLR):

$$PLR = \frac{L}{CAP_{full}} \quad (3.4)$$

Here L represents the load delivered by the chiller. So the third function is introduced, *FPLR*, which multiplied with the current condition full load power ($P_{el,ch,full}$) yields the actual power consumed by the chiller ($P_{el,ch}$) under the given L load and current temperature conditions:

$$FPLR = c_1 + c_2 PLR + c_3 PLR^2 = \frac{P_{el,ch}}{P_{el,ch,full}} \quad (3.5)$$

Equations (3.1), (3.2), (3.3) and (3.5) model the chiller performance at current part load and temperature conditions and yield the chiller power as:

$$P_{el,ch} = P_{el,ch,ref} \cdot FCAP \cdot FCOP \cdot FPLR \quad (3.6)$$

Implemented values of performance coefficients, minimal PLR and reference condition performance are given in Table B 5 although the user could enter custom parameters if available.

The question of which temperatures are actually passed to the model, since the system models (SMs) are load based, is answered in sections describing the SMs containing this

component, 3.3.6 and 3.3.7. The basic approach is to use the outdoor wet bulb temperature, provided in the weather data set, to approximate condenser inlet and assume the chilled water supply temperature.

3.2.2 Cooling Towers

The heat exchanger at the top in Figure 3.1 represents a cooling tower. This is a heat and mass exchanger that rejects the heat extracted from the building space, increased for the compressor heat, to the environment. This heat is taken from the cooling water by evaporating the cooling tower water splashed on the surfaces of the cooling tower fill (other constructions are also available) with the aim of increasing the air-water contact area and thus the evaporation area. This latent heat transfer is possible until the air reaches the wet bulb temperature. [11] provides the following basic classification of cooling towers: the direct contact (open cooling tower) and indirect contact (closed circuit cooling tower). The water that was in contact with the air in the open cooling towers is the same cooling water flowing through the condenser. Closed circuit cooling towers have a heat exchanger in addition to the fill, so the water that evaporates in the tower circulates only within the cooling tower. Both kinds can have natural or mechanical draft (fans are used to increase the air velocity) depending on the construction.

Several modeling approaches can be found in the literature. [11] provides performance curves showing how the “range” depends on various cooling water flow rates, inlet and outlet temperature, and air wet bulb temperature. The range is the cooling water temperature change within the cooling tower. Another important parameter in cooling tower engineering is the “approach”, determining the difference between the wet bulb and the cooling water exiting temperature. The level of detail depends on the heat exchange modeling approach. For example, Zweifel et al. [36] modeled the closed circuit cooling tower implemented in TESS libraries [37] assuming the overall heat transfer coefficient depends only on cooling water mass flow. Similar to modeling heating and cooling coils, models implementing NTU-effectiveness are found in EnergyPlus [33].

Since the cooling tower power consumption is small compared to the chiller consumption, the following simple model is implemented in the SMs. It approximates the electricity and water consumption of a cooling tower. The cooling tower design capacity, $P_{el,ct,d}$, is proportional to the maximal chiller heat of rejection (HR):

$$P_{el,ct,d} = k_{el,ct} \cdot max\left(HR\right) \tag{3.7}$$

The equation is adopted from EnergyPlus [33]

To determine the part load performance of the cooling tower, a linear approximation for single stage fans from [38] is assumed, as well as the fan shut off for PLR under 15%. As a result, the power consumption, $P_{el,ct}$, in each timestep is determined using:

$$P_{el,ct} = \begin{cases} 0, & HR < PLR_{min,ct} \cdot max\ (HR) \\ k_{el,ct} \cdot HR, & HR \geq PLR_{min,ct} \cdot max\ (HR) \end{cases} \tag{3.8}$$

where $PLR_{min,ct}$ is the cooling tower fan turn off limit and $k_{el,ct}$ is the cooling tower sizing coefficient. The tower water flow rate is modeled as a linear function of the heat of rejection using the rule of a thumb from [33]. Adopting the claim found in [39], that 0.1% of that flow is lost to the environment; the water consumption is calculated as:

$$WC = p_{ct,wloss} \cdot k_{wc} \cdot HR \tag{3.9}$$

with $p_{ct,wloss}$ being the cooling tower blowdown percentage and k_{wc} the ratio between the cooling tower water flow rate and its load.

Section 3.3.6 holds more information to understand the cooling tower connection to the chiller model and their control, including the description of how the wet bulb temperature is taken into account.

Other devices to reject the condenser heat are the air and evaporative condenser. Air cooled condensers consist of a heat exchanger providing contact between the fan driven flow of outside air and the condensing water or even directly the refrigerant, e.g. small split systems. Although they are simple in construction and consume no water, they require condenser temperatures significantly above air dry bulb one. This causes a decrease in the chiller COP and an increase in the fans power consumption. The situation is somewhat better with the evaporative condenser where, before coming to the condenser coil, the air is precooled by evaporative cooling, which makes it somewhat similar to closed circuit towers. In the SMs these kinds of cooling are not presented, but the preparation for the air-cooling is done with a simple model adopted from [40]:

$$P_{el,airc} = k_{el,aircool} \cdot HR \tag{3.10}$$

which determines the power consumption of the air condenser cooling, $P_{el,airc}$. $k_{el,aircool}$ is the related consumption coefficient. Of all four climates taken into account, the commercial buildings in Moscow could be conditioned with this kind of heat rejection.

All mentioned coefficients are given in Table B 6.

3.2.3 Boilers

A purpose of a boiler is to transfer heat to a fluid. In general, there are many boiler types, constructions, sizes and utilizations, from the small electrical hot water boilers, to large steam generators used in thermal power plants. Their classification is provided in [11]. In this thesis only the combustion boilers, used to provide hot water for space heating, are of interest. Their sizes can range from 10 kW to several MW.

In a combustion chamber of a heating boiler, the heat obtained by fuel combustion is used to increase the temperature of a water stream. This water transfers the energy to emitters in the conditioned space or to the AHU heating coil. Numerous available constructions of the combustion chamber and flue gas to water heat exchanger will not be further discussed.

To provide a precise description of the boiler performance, the combustion and heat transfer processes are to be described. However, such a model would be unnecessarily compli-

cated for preliminary fuel consumption assessment. Several physical and empirical boiler models can be found in the literature. A physical model of a boiler, suitable for oil, gas, pellet or wood chip combustion, has been developed and validated by Haller et al. in [41]. In [42] a physical model applicable to condensing boilers has been presented. In TRNSYS, [27], a simple overall efficiency model is available, while TESS models, [37], provide a similar model with an additional parameter – the efficiency of the consumption. The latter assumes constant or efficiency that varies with the part load ratio (PLR). Such empiric models are still a standard in the majority of the simulation tools. Since detailed enough, this data regression approach has been adopted within the SMs. Furthermore, manufacturer data regression models are applicable to both condensing and non-condensing boilers. They provide the boiler efficiency depending on the PLR, which is defined as a ratio of the boiler load to the nominal boiler power:

$$PLR = \frac{L}{P} \tag{3.11}$$

where PLR is the part load ratio, L is the boiler load and P is its design power. Which boiler types to implement in the SMs is selected upon several simple criteria. The first is that these boilers are a part of conventionally installed heating systems. The second is the fuel – the goal was to enable the utilization of, apart from gas and oil, the biomass. The last criteria, which yielded two boiler models, is a differentiation between a fully modulating burner control and an on/off or on/low/off burner control. Even though fully modulating non-condensing boilers do exist, the decision is made to model this boiler type as an on/off or on/low/off boiler. This model is suitable for boilers burning solid biomass. In addition, such non-modulating boilers benefit the most from coupling with the thermal storage, which is consequently investigated later, in the SM analysis. The modulating boilers are modeled as condensing boilers. However, it is possible to assign any of the mentioned three fuel types to both of the boiler types. It should be noted the cycling losses are disregarded, considering that the implemented control reduces boiler cycling. Additionally, [43] suggests the condensing boilers are not much influenced by cycling.

3.2.3.1 On/Off and On/Low/Off Boiler Model

Contemporary non-condensing (also conventional, traditional) boilers achieve high overall efficiencies of over 85%. In the SMs, this category of boilers is represented by single (on/off) and two-stage (on/low/off) boilers. In each boiler operation timestep, the part load ratio of the boiler can take one of the following two values: full load (PRL=1) or low load (first stage, PLR_{1st}, a value between 0 and 1). On-off boilers operate only at full load. Thus this simplified boiler model can be written as:

$$\eta_b = \begin{cases} \eta_{b,design}, & PLR = 1 \\ \eta_{b,PLR\,1st}, & PLR = PLR_{1st} \end{cases} \tag{3.12}$$

where η_b is the boiler efficiency, which either takes the value of the first stage efficiency, $\eta_{b,design}$, or of the second stage efficiency, $\eta_{b,PLR1st}$. The default coefficients are illustrated in Figure B 2. All the boiler losses are embodied in the boiler efficiency coefficient. On/off

boilers are included in SM1 and SM4, while the SM5 contains a two-staged boiler. It is usual for solid biomass boilers to have one or two stages due to the nature of the combustion process. Biomass boilers are considered to be neutral in terms of carbon emission. Thus in the SM simulation examples, wood pellet boilers are assumed. Such boilers can benefit from coupling with a storage tank to follow the intermittent demand profile while maintaining low cycling. Later in sections describing each of the SMs, the control governing the boiler - storage interaction is explained.

3.2.3.2 Condensing (Modulating) Boiler Model

Condensing boilers can recover the latent heat of vapor consisted in the flue gases, by cooling them down below the dew point. Almost all condensing boilers are modulating. Modulation ranges from a minimal part load ratio (PLR), usually not less than 20% of design power, to PLR=1, which is 100% of design power. The minimum boiler power is thus the product of the design power and minimal PLR.

A polynomial, based on manufacturer data fitting, models the boiler performance:

$$\eta_b = aPLR^3 + bPLR^2 + cPLR + d \tag{3.13}$$

Boiler efficiency η_b depends on the part load ratio and the regression coefficients a, b, c and d. Two different polynomials are utilized in order to differentiate between the emissions systems. A cubic function for radiator heating (high temperature return) and a square function (a=0) in case of panel heating (low temperature return). Default implemented coefficients are provided in Figure B 1. Boiler performance benefits from lower return temperatures, since it improves the flue gas condensation. The condensation can also be intensified by increasing the flue gas heat exchanger area. However, this increases the investment significantly, since expensive corrosion resistant materials have to be used.

Condensing boilers use gas or oil as a fuel. Usually, for larger buildings several condensing boilers are implemented. For each boiler in the system the fuel type, minimal part load ratio (minimal boiler power) and the emission system type can be selected. Otherwise a default setting is provided. Later in section 3.3.2 it is explained how an internal operational optimization controls the load allocation between condensing boilers.

The previous two equations define boiler efficiencies within each timestep. Using these values, the fuel consumption of both implemented boiler models is determined as, in kWh:

$$FC = \frac{P \cdot PLR}{\eta_b} \tag{3.14}$$

where fuel consumption FC, boiler design power P, part load ratio PLR and efficiency η_b are vectors of length equal to the number of boilers implemented in the model.

A mechanical room accommodating combustion boilers needs to satisfy a list of requirements, including the sufficient combustion air supply, flue extraction, standards for gas installations and pressure vessels, etc., which can all influence its size and position in a building.

3.2.4 Thermal Storage

There are many types of thermal storage. Within the SMs only the sensible water thermal storage is considered. The purpose of thermal storage is to allow decoupling of the time of energy production from the time of energy utilization. Thus, some of the benefits of using water thermal storage are:

- Boiler or chiller design size can be even smaller than the peak load – lower investment and longer full load operation;
- Boiler or chiller staging can be reduced – increased efficiency, improved combustion;
- The load can be matched more closely compared to, for instance, staged boiler operation – a potential to reduce overproduction;
- The energy gained by the intermittent sources, such as solar energy, can be stored when available and used later when demanded – increased RES utilization; and
- Increased CHP unit operation hours by shifting the thermal to meet the electrical energy demand, [44].

To make sure these benefits become realized, the thermal storage size and its charge and discharge control need to be optimized to suit the utilization purpose. Evidently a lot can be achieved by storage utilization so many thermal storage models have been developed, each suiting a certain level of detail. Both TRNSYS [27] and EnergyPlus [28] provide a range of fully mixed and stratified water storage tank models.

A simplified sensible water thermal storage model is implemented in the tool in order to enable the short term decoupling of the primary HVAC energy production and building heating or cooling demand. The storage is represented by its volume and discharge rate. Its maximal energy capacity, SC_{max}, is defined by the storage volume V and the installed/planned heat emission systems:

$$SC_{max} = \begin{cases} \rho V c_p \Delta T_{high}, & \text{e.g. radiator heating} \\ \rho V c_p \Delta T_{low}, & \text{e.g. panel heating} \end{cases} \tag{3.15}$$

where ρ is the water density. The model differentiates between the high and the low temperature heating using two separate temperature differences, ΔT_{high} and ΔT_{low}.

The term panel is used for e.g. floor heating, which requires lower supply temperatures compared to radiator heating. Thus such a system yields lower temperature difference within the storage tank. This is, for instance, suitable for the solar or ground storage supported heating. Apart from solar collectors, boilers are used to feed the storage. In that case the control system might demand maintaining higher water temperature in the storage, despite utilizing the low temperature heating, and then mixing the return and supply stream to lower the temperature. This process, although common in the practice, causes exegetical losses and diminishes the advantages of low temperature heating. In the systems that include the storage model, the storage charge and discharge are regulated by the control strategy, which will be described in section 3.3.1. As it can be concluded from the equa-

tion, the model has no intelligence to recognize if the temperature level of the energy flow charging the storage exceeds its current level. Thus the second law of thermodynamic could be disobeyed. To overcome this problem and prohibit a false storage energy increase, the energy flows that charge the storage are assumed to have a temperature higher than the one at the middle of the tank. To accomplish this, the solar collector return temperature control set point depends on the heating type. For example, this temperature is higher if radiator heating is implemented.

The second parameter of the storage performance is the storage discharge rate. It defines which fraction of the maximum capacity can be delivered to the load within one timestep (if the current storage state of charge allows it). This value takes the physical limitations of the distribution system into account. The product of the discharge rate and maximal storage capacity defines a value designated as storage power, SP_{max} (maximal hourly storage discharge):

$$SP_{\max} = SC_{max} \cdot DR \tag{3.16}$$

Another idealization is the definition of the storage tank thermal loss to the environment. This loss is approximated as a small constant energy flow linearly proportional to the storage volume. The implemented thermal losses data are based on the equation provided in [40]. This and other storage related data implemented in the tool are given in Table B 4.

In the process of SM design optimization, which is presented in chapter 5, the storage tank optimization parameters are the volume and the discharge rate.

3.2.5 Solar Thermal Collectors

Solar thermal collectors convert solar energy into heat. The surface of the collector absorbs solar radiation to increase the temperature of the fluid flowing through the collector. Two collector types commonly used for heating purposes are flat plate collector and evacuated tube collector.

The objective here was to create a collector model which can simulate a solar collector energy gain profile. The profile corresponds to the user or optimization algorithm specified horizontal area available for solar collectors (e.g. roof area) and determines the available solar energy at each timestep. The model needs to be relatively simple and flexible in terms of further incorporation with other energy converters within the plant simulation.

As is the case with many others models, the solar collector model implemented here is based on the quadratic efficiency model originating from theoretical equations developed by Duffie and Beckman [45]. First the utilized model equations are presented. The parameters and coefficients appearing in the equations are explained, as well as their sources provided, later in this section. The collector efficiency is modeled as a quadratic function of temperature difference between the ambient air and average collector fluid temperature:

$$\eta = \eta_0 \cdot IAM - \frac{a_{c1}\left(T_m - T_{amb}\right)}{I} - \frac{a_{c2}\left(T_m - T_{amb}\right)^2}{I} \tag{3.17}$$

where η_0 represents the optical collector efficiency (conversion factor), a_1 and a_2 are the linear and quadratic loss coefficients, T_m the average collector fluid temperature, T_{amb} the ambient temperature, and I is the solar radiation on the collector surface. Analyzing the previous equation, optical collector gains, Q_o, are:

$$Q_o = \eta_0 \cdot IAM \cdot I \cdot GA \tag{3.18}$$

where IAM is the incidence angle modifier and GA is the gross collector area. The incidence angle modifier is used to correct the measured optical efficiency in the parts of the day when solar radiation is not perpendicular to the collector surface. The necessity for its utilization originates form the fact that, the collector parameters are obtained by testing the collector performance using perpendicular radiation. More details about IAM can be found in [45].

The second type of losses encountered is the thermal loss, Q_{tl}, which is a consequence of the temperature difference between the collector fluid and the ambient air:

$$Q_{tl} = \left(a_{c1}\left(T_m - T_{amb}\right) - a_{c2}\left(T_m - T_{amb}\right)^2\right) \cdot GA \tag{3.19}$$

In the model implementation in the SMs the user provides available horizontal roof area, while the GA is calculated using the collector tilt angle. Thermal losses are lower for evacuated tube collectors, but still significant, as illustrated in Figure 3.2. For this reason the evacuated tube collectors are more suitable for colder climates.

Depending on the ambient conditions, the thermal loss can occasionally be greater than the product of optical efficiency and current solar radiation. Obviously only the positive energy gains are considered useful. Therefore, useful solar gains, Q_u, are the positive difference between optical gains, Q_o, and thermal losses, Q_{tl}:

$$Q_u = \begin{cases} Q_o - Q_{tl}, Q_o > Q_{tl} \\ 0, Q_o \leq Q_{tl} \end{cases} \tag{3.20}$$

This useful gain value is calculated for each timestep to form the yearly solar gain profile. An example solar gain profile for the Shanghai climate and flat plate collector with the latitude tilt is shown in Figure 3.3. Solar gains reach its peak during the late summer, after the air has dried out during the warm summer months. Within the SM simulation such hourly profiles define the amount of energy that can be fed to the storage from the solar collectors in each simulation timestep. To account for the thermal losses in the solar collector thermal distribution network, a constant loss coefficient of 5% has been implemented.

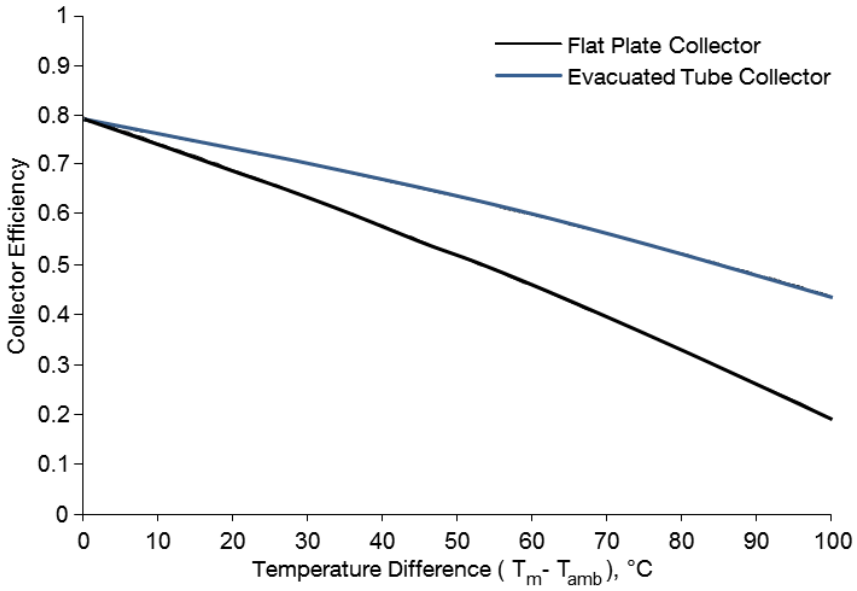

Figure 3.2. Collector efficiency drops with the increased temperature difference between collector fluid and the ambience. Evacuated tube collectors are well isolated and perform better than flat plate. Data from Table B 1 used.

The average fluid temperature inside the collector, as well as the incidence angle modifier, IAM, is assumed constant over time. The SM simulation sets this temperature depending on the application of the collector generated heat. For instance, for a floor heating system collector outlet temperatures lower than 40°C are high enough, but to run an absorption chiller collector outlet temperature should be at least two times higher.

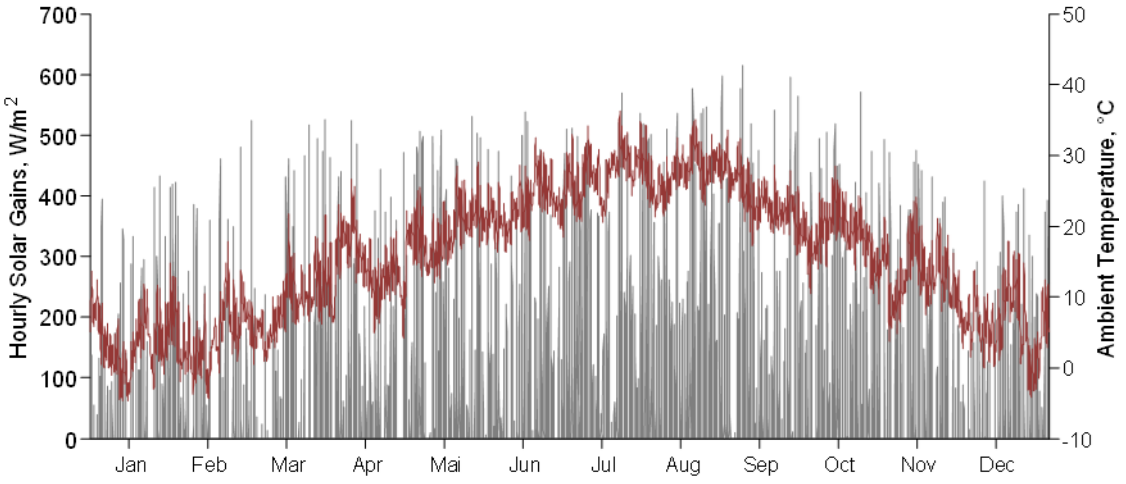

Figure 3.3. Hourly flat plate collector solar gain and ambient temperature profile for Shanghai. Latitude tilt.

Data necessary to utilize the model are collector test parameters and weather data. [46] and [47] prescribe test procedures for obtaining collector test parameters. The sources differ in

defining the collector to ambient temperature difference: [46] uses outlet and [47] average collector fluid temperature. It is important to notice to which area collector parameters are referenced: gross, aperture or absorber. Collector parameters implemented in the tool for both flat plate and evacuated tube collectors are the averaged data for a number of collectors of different manufacturers tested by SPF, [48]. TRNSYS radiation processor, [27], was utilized to obtain the solar radiation profiles on tilted surface for four targeted cities. These data are available within the tool and enable easy tool usage for planning at those locations. The review of methods to calculate the radiation on tilted surface is given in [49]. Weather data for any location can be prepared using the ClimateTool [12].

Solar collector performance is largely influenced by its correct positioning. Here are some of the recommendations concerning the collector inclination. The collectors should face south if located in the Northern Hemisphere and vice versa. Good performance can be achieved by setting the collector tilt – the angle between collector surface and horizontal – to equal the latitude angle. To reach the seasonal maximum, the tilt should be increased by 15° (max +20°) during the winter and decreased by 10° during the summer, since the zenith angle changes during the year. In thermal applications the goal is to maximize the energy output, while some photovoltaic (PV) applications may benefit from maximizing the power. The optimal tilt can be achieved with the objective to maximize the integral of hourly solar gains. This will maximize the annual solar fraction of the plant. Another advantage of considering the primary HVAC in conceptual design is the possibility to optimize building design to suit the optimal collector tilt. Optimizations of collector tilt angles on yearly and seasonal bases were performed in TRNSYS [27] coupled with GenOpt [30], using Hooke-Jeeves optimization algorithm. Table 3.2 shows the results of tilt angle optimizations for Shanghai, Dubai, Bangalore and Moscow. Winter and summer optima for flat plate collectors agree with the mentioned recommendations. As expected, due to the geometry of evacuated tube collectors, seasonal tilt deviations from latitude are not as high as those of flat plate collectors. The decision on the suitable tilt angle has to be made based on the utilization. For instance, if used for solar cooling, the collector tilt angle should be closer to summer optimum.

Table 3.2. Optimal tilt angles (annual and seasonal optima) and latitudes.

		Flat Plate			Evacuated Tube		
	Location Latitude, °N	Annual Optimum, °	Seasonal Optimum, °		Annual Optimum, °	Seasonal Optimum, °	
			Winter	Summer		Winter	Summer
Shanghai	31	26	46	11.5	26	43	13
Dubai	25	24	44	8	25	45	9
Bangalore	13	18	34	-2	20	36	-1
Moscow	56	44	68	34	41	66	30

Figure 3.4 shows flat plate collector monthly solar gains calculated by the simplified model. In this case collector tilt is equal to the latitude. The largest gains, which at the same time are rather equally distributed throughout the year, are noticeable for Dubai. Bangalore

has lower gains during summer months due to the high air humidity preventing the direct solar radiation. For the same reason, solar gains during June and July in Shanghai are lower than in Moscow, whilst just the opposite is expected and also true for the rest of the year.

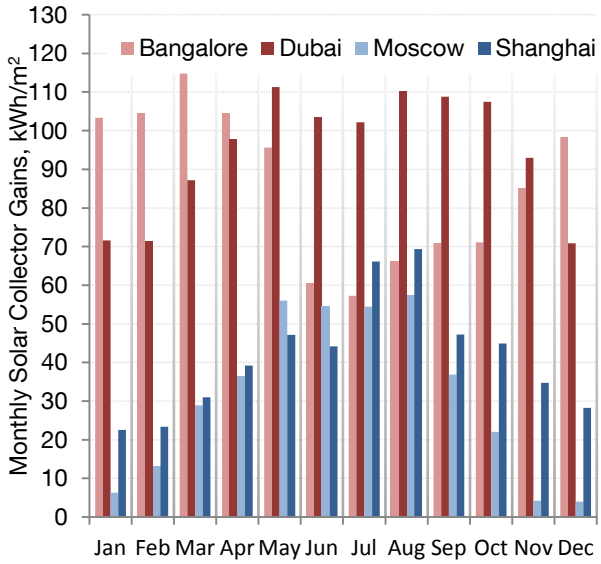

Figure 3.4. Flat plate collector monthly solar gains simulated for project locations using the simplified model. Latitude tilt.

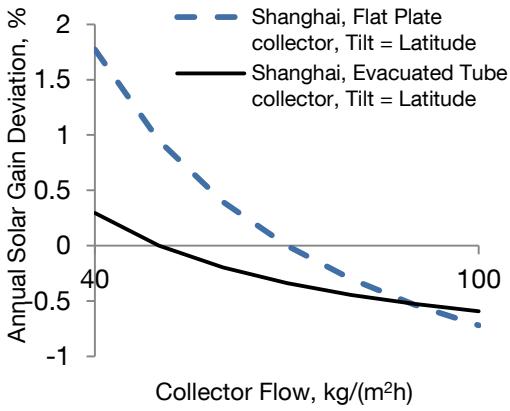

Figure 3.5. Collector flow rates other than test flow rate and their influence on annual solar gain. The deviation can be neglected for the demanded model precision.

To verify the performance of the model, it is compared to a more detailed model simulated in TRNSYS. A constant collector inlet temperature was assumed and the influence of using flow rates other than the test flow disregarded. The sensitivity to the change in collector flow is shown in Figure 3.5. The deviation in the annual solar gain value remains less than 2% for flows from 40 to 100 kg/(m^2h).

Both TRNSYS and the simplified model performed an annual hourly simulation. To compare the models, annual gains per square meter flat plate collector are presented in Figure 3.6. The two simulation models perform similarly.

The same comparison is given in Figure 3.7 for evacuated tube collectors. The data refer to 1 m^2 gross collector area. The absorber to gross area ratio for these collectors is smaller, see Table B 1. For that reason the two graphs are not to be compared directly. Even so, it is obvious the annual gains in colder climates are higher than those obtained with the flat plate collector. The comparison again yields a satisfying result.

The simplified collector model to assess solar collector gains is developed. The user can specify the type (flat plate or evacuated tube). The collector utilization, such as floor or radiator heating, absorption cooling, etc. defines the collector fluid temperature level. Since currently solar collectors are only used for heating SMs, the minimal average collector temperature has different preset values in case of radiator and panel heating. The rea-

sons have already been mentioned in section 3.2.4. The developed collector model has a very short calculation time and can easily be integrated into the plant system model and its optimization. The model is integrated in SM1 and SM3, sections 3.3.1 and 3.3.3.

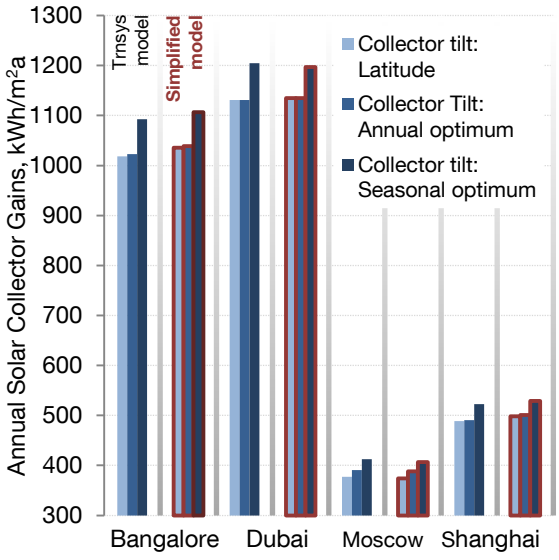

Figure 3.6. Flat plate collector annual gains comparison for four locations and three collector tilt configurations. TRNSYS and simplified model yield similar result.

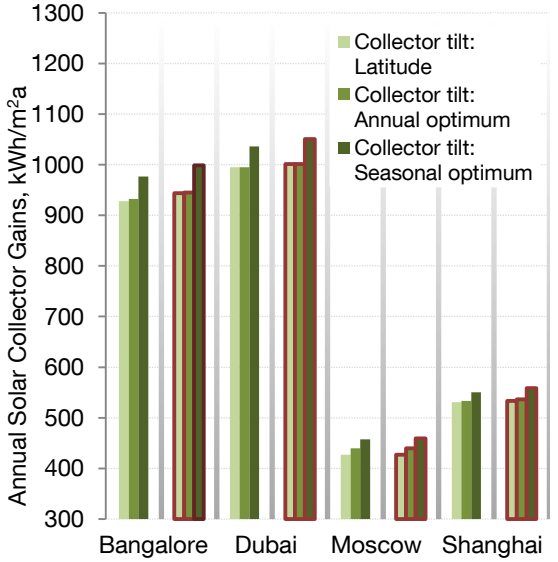

Figure 3.7. Evacuated tube collector annual gains comparison for four locations and three collector tilt configurations. TRNSYS and simplified model yield similar result. Referred to gross collector area.

3.2.6 Photovoltaics Modules

Photovoltaics (PV) exhibit direct conversion of solar radiation into electric power. In the form of photovoltaic modules they can be mounted on or, even better, integrated (BIPV-Building Integrated Photovoltaics) into the building façade or the roof. The direct electrical current produced by photovoltaics is inverted into an alternating current to be either utilized within the building or sold to the grid. The objective here is to configure a model which estimates the yearly hour to hour power profile generated by the PV covering the area or areas defined by the user.

Several models of PV performance have been identified in the literature, starting from very detailed theoretical models founded on physical behaviour of a solar cell, to semi-empirical ones focusing on overall thermal and electrical performance of a PV module, to very coarse empirical models for annual electrical energy production assessment. PVsyst [50] is a software tool offering help in preliminary or project design of PV components. PVGIS [51] is a web-based PV performance estimator for locations in Europe and Africa. Both tools mentioned can provide an optimal module tilt. TRNSYS and EnergyPlus offer a variety of models to suit the necessary level of detail or modeling focus. RETScreen also

has the capability to model PV modules. Several of the models listed rely on [45]. In [52] a PV performance estimation tool for initial building design has been developed based on a parameter study performed in TRNSYS. DIN EN 15316 4-6 [53] provides simple recommendations and factors related to PV power estimation and tilts. These are only several of the existing models available in the literature.

From the architect's point of view, the areas covered with PVs and their positions on the building are the relevant design parameters. Hence, the area and its orientation are obtained as an input to the model and an hourly power generation profile is the result. With this in mind, the following model is developed to make an estimate suitable for the preliminary building design. The factors accounted for within the model are:

- System efficiency (e.g. cable and inverter losses);
- The change of reference efficiency with the collector temperature; and
- The building integration (the quality of module ventilation).

DIN EN 15316 4-6 [53] suggests following equation to calculate annual PV generated electrical energy, $E_{el,pv,out}$:

$$E_{el,pv,out} = \frac{E_{sol} P_{pk} f_{perf}}{I_{ref}} \tag{3.21}$$

where E_{sol} represents the annual solar radiation energy, P_{pk} is the peak PV power, f_{perf} is a system performance factor accounting for annual system and temperature losses and the art of building integration, while I_{ref} stands for the reference solar radiation on the PV module surface. In order to break this cumulative into hour-to-hour generated energy, the following needs to be considered. The annual solar energy E_{sol} is to be replaced with the relevant hourly solar radiation profile, which is calculated from the weather data set for the given PV tilt. Since ambient temperature fluctuates during the year, the PV temperature will also vary and thus the module efficiency. For that reason the factor f_{perf} is split into the static system factor, f_{sys}, and the dynamic temperature factor, f_{temp},:

$$f_{perf} = f_{sys} f_{temp} \tag{3.22}$$

In [54] it is mentioned that crystalline silicon cells lose 0.4% of measured reference efficiency with each degree increase of the PV temperature in comparison to the reference. This parameter is called the temperature coefficient. The temperature factor β_{pv} is thus linearly related to the temperature difference between the actual PV surface temperature, T_{pv}, and the reference temperature, T_{ref}:

$$f_{temp} = 1 + \beta_{pv} \left(T_{pv} - T_{ref} \right) \tag{3.23}$$

With the increase in module temperature the efficiency is dropping. If the precise definition of this temperature is required, an iteration method from [45] or further methods that are listed in [33] could be used. Suitable for the level of detail of this model, a linear approximation used in [51] is implemented:

$$T_{pv} = T_{amb} + k_T I \tag{3.24}$$

where k_T is the PV ventilation factor and I is the total solar radiation on the PV module surface. Although in most of the PV applications the peak power, P_{pk}, is the primary design variable, in this case the area dedicated to PV by the architect dictates the peak power:

$$P_{pk} = \eta_{ref,pv} A_{pv} I_{ref} \tag{3.25}$$

where $\eta_{ref,pv}$ stands for the PV reference efficiency, A_{pv} is the surface area of the PV panel. If the last four equations are introduced into the equation (3.21) modified to yield the hourly profile of photovoltaic energy generation, P_{pv}, the following equation is obtained:

$$P_{pv} = \eta_{ref,pv} f_{sys} \left(1 + \beta_{pv} \left(T_{amb} + k_T I - T_{ref}\right)\right) A_{pv} I \tag{3.26}$$

The model includes four parameters, each having a distinct physical meaning:

- The reference efficiency $\eta_{ref,pv}$ – it will increase in the years to follow as the PV technology advances;
- The system factor f_{sys} – primarily accounting for inverter and cable losses;
- The temperature coefficient β_{pv} – it accounts for the module performance sensitivity to module temperature; and
- The ventilation factor k_T – depends on the difference between the module and the ambient temperature.

In the model implemented in SM7, A_{pv} is an array of 6 values determining the areas available for the PV in the following order: optimal tilt, horizontal surface, surfaces facing north, south, west and east.

The model performance is compared with a TRNSYS model based on PV Type 562h, with an approximation of system losses of 14%. The same value can be found in [51]. Since the simplified model disregards several influences on PV performance, such as IAM, these influences are taken into consideration by imposing 8% higher system losses. Additionally, the static DIN EN 15316 method recommends a system performance factor of 70% - 75%, which also accounts for the temperature losses. Relying on the stated data, the actual implemented system performance factor equals 78%.

Figure 3.8 shows the results of this comparison for the four target cities and four different PV module orientations. The differences in annual cumulative energy production lie below 0.5%.

In [45] it is mentioned that the tilt angle should be 10°–15° higher than the angle of latitude during the winter and 10°–15° lower than the latitude during the summer. Nevertheless, for the cities Bangalore, Dubai, Moscow and Shanghai the optimal slope of PV surface is identified using TRNSYS optimization plug-in GenOpt [30], similarly to solar thermal collector tilt optimization. All the mentioned locations are on the Northern Hemisphere, thus the modules are facing south – the angle of azimuth is 0 degrees. The objective was to maximize the annual PV output using Type 562h and Hooke-Jeeves algorithm. The optimization results are shown in Table 3.3. These inclinations are confirmed using PVGIS [51]. Similar angles are obtained for both locations featured within the tool's database:

Moscow is 39, Dubai 24. For the other two locations the check is performed with PVsyst [50] and the results show good compliance.

Table 3.3. PV tilt angles: annual optima

	Location Latitude, °N	Annual Optimum, °
Shanghai	31	24
Dubai	25	24
Bangalore	13	16
Moscow	56	41

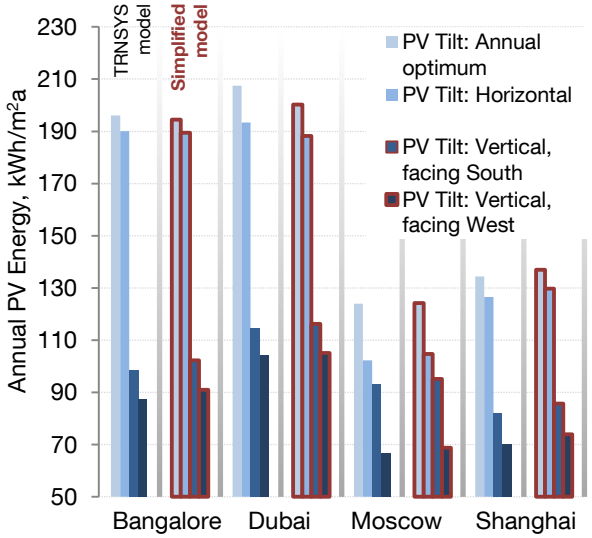

Figure 3.8 Comparison of the annual PV electrical energy estimate utilizing a TRNSYS Type 562h PV model and the simplified model utilized in the tool. 4 PV tilts for 4 cities.

A quick utilization of six PV orientations is enabled for the four target cities: optimal tilt, horizontal modules, and vertical modules facing each of the cardinal directions. The radiation profiles on tilted surfaces are generated using the TRNSYS weather data processor. To include the whole spectrum of orientations, a radiation calculation procedure within the tool should be implemented, which was previously mentioned in 3.2.1. Additionally, a simplified approach can be found in [53].

More about the utilization of this model within the tool can be found in section 3.3.7, where this fast and simple model forms a system model with any chosen number of vacuum compression chillers.

The implemented data values are given in Table B 3.

3.3 System Model Simulation

The following sections are dedicated to each of the preconfigured SMs. They describe the system control and simulation performance.

Before beginning these descriptions, it is important to provide the information on the utilized load and weather data. The weather data for four cities (Dubai, Shanghai, Bangalore and Moscow) originate from the Meteonorm database [55]. The load profiles used to demonstrate this performance originate from FassadenTool, [12]. Originally, they are given as the specific ideal load profiles (kW/m^2) for each of the four cardinal directions. Appendix A provides a complete description related to obtaining the primary HVAC load data utilized to demonstrate the SM performance. The concrete building load data utilized within the SM performance examples can be found in section A 1.3, Table A 3, while the short information on the weather data can be found in the section A 2.

3.3.1 SM1: On-Off Boiler, Thermal Storage and Solar Collector

This section explains the first preconfigured primary HVAC system. The system, schematically presented in Figure 3.9, consists of an on-off boiler, a thermal storage unit and a solar collector array. Based on the control strategy, the solar collector and the boiler feed the storage, which delivers the energy to the distribution system.

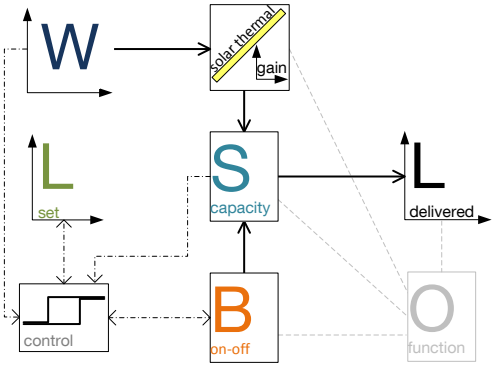

Figure 3.9 Schematic representation of the modeled system and component interaction. S – storage, B – boiler, L – loads, W – weather data, O – optimization objective.

3.3.1.1 System Performance Control

As already mentioned, the system runs under an idealized control. The goal of the control strategy is to approximate the thermal energy consumption of a real system. Although not imitating it, the control strategy in the model assumes a competent control of the real system. Hysteresis control, as illustrated in Figure 3.10, is used to avoid boiler short cycling and fully exploit the advantages of the thermal storage. During the process of charging the storage, the boiler stays on until one additional step of delivering the boiler full load to the

storage would overfill it. After the higher limit is reached, the boiler is turned off and the storage takes over supplying the load, until its capacity has reached the lower limit, which is proportional to the fraction of the maximal load.

If available, solar gains are fed to the storage regardless of the boiler on-off status, until the maximum capacity is reached:

$$SC(t) = \begin{cases} SC(t-dt) + SG(t), & SC_{max} \geq SC(t-dt) + SG(t) \\ SC_{max}, & SC_{max} < SC(t-dt) + SG(t) \end{cases} \tag{3.27}$$

where *t* represents the time, *dt* the timestep, *SC(t)* stands for the storage state of charge and *SG(t)* is the solar gain.

Additionally, the boiler can be turned off before the storage is fully charged if solar gains are available. To summarize, in each of the 8760 simulation steps the boiler control signal is determined based on control and storage charge values from the previous timestep and the solar gain value from the current timestep.

An amount of energy (power during one timestep) that is delivered by the system, *D(t)*, depends on the current status of the system variables and inputs:

$$D(t) = f(L(t), C_b(t), P, SC(t), SC_{max}, DR, SG(t)) \tag{3.28}$$

where $L(t)$ is the set load, $C_b(t)$ the boiler control signal, P the boiler design power, and DR is the storage discharge ratio.

To be more precise, the load is allocated as follows:

$$D(t) = \begin{cases} SP_{max}, & SP_{max} \leq min(L(t), SC(t)) \\ SC(t), & SC(t) \leq min(L(t), SP_{max}) \\ L(t), & L(t) \leq min(SP_{max}, SC(t)) \end{cases} \tag{3.29}$$

Each timestep the storage capacity decreases for the energy discharged and, where the boiler was on, increases for hourly boiler generated energy. Thus the storage capacity for the following timestep, *SC(t+dt)*, is defined as:

$$SC(t+dt) = SC(t) + P \cdot C_b(t)dt - D(t)dt \tag{3.30}$$

At this stage the remaining load, *RL(t)*, can be introduced. It is quantified as a difference between the set and the delivered load:

$$RL(t) = L(t) - D(t) \tag{3.31}$$

The remaining load has two basic functions. Firstly, it is used in defining the optimization constraint concerning the supply task, which is later explained in detail in section 5.2.1. Secondly, it introduces a certain dynamics between the primary HVAC and the building simulation despite those being decoupled, allowing the active change of the set load for the following hour based on the delivery satisfaction of the current hour:

$$L(t+dt) = L(t) + RL(t) \tag{3.32}$$

In previous explanation a timestep of one hour is assumed.

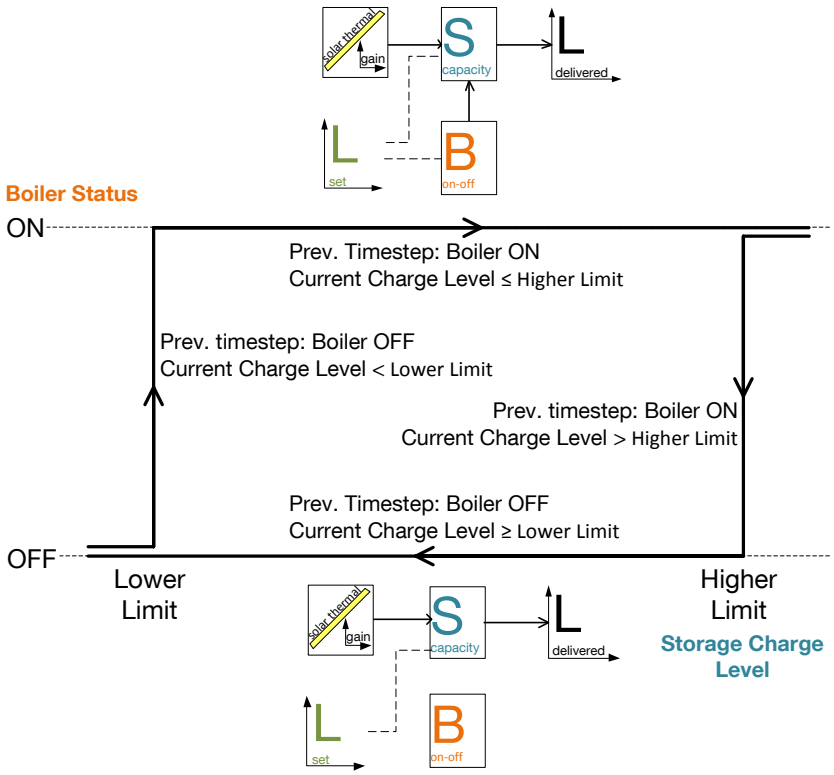

Figure 3.10 Boiler on-off status depends on the storage state of charge and its own previous status. This minimizes short cycling and takes advantage of the storage utilization.

The similarity between the model utilizing the remaining load and the real system lies in the possibility of the real system to pre-condition the building. Occasional shifting of a certain amount of energy to supply it before or after it was originally due will not cause a significant change in the annual fuel consumption, since the energy balance remains satisfied. Remaining load is illustrated by the arrow in Figure 3.11, with further explanation in the next section analyzing the simulation performance of the SM.

3.3.1.2 Simulation Performance

The duration of one annual simulation is approximately 55 ms[i]. That implies 11000 function evaluations within 10 minutes, which is significant for the optimization process described later in chapter 5. Here the model performance and control strategy is explained and illustrated.

[i] Calculation performed at: Intel Core i7-960 CPU, 3.20GHz; 12GB RAM.

Figure 3.11 shows a week of SM performance. Obviously, in creating the ideal load profile, the heating system was scheduled to operate only during working hours. The demonstrational component sizes are given in Table 3.4. Based on component models, additional information on such an SM1 are:

- A fully charged storage tank of 2 m^3 stores 120 kWh assuming radiator heating;
- Thus the storage discharge rate of 0.2 can cover the maximal load of 24 kW per timestep, which is close to the peak load imposed to the primary system of the building "S" ("small building", see Table A 3) in Shanghai; and
- The boiler power of 20 kW lies beneath the peak load.

Considering the yearly demand profile, the highest heating demand occurs during the presented week, while low solar gains are available. During the Monday morning peak, the storage is nearly empty and the boiler needs to supply the load. Since the full load cannot be met, the remaining load is postponed for the following timestep, and the process is continued until the full load can be supplied. The shifted load is indicated by the arrow in Figure 3.11. The real system would charge the storage prior to scheduled office hours in case of low outside temperatures to avoid the lack of power, so the similarity with the real systems in terms of energy balance is achieved. The boiler stays on until the storage is fully charged and can take over the supply. Thanks to the storage, the boiler cycles only four times during the analyzed week.

Table 3.4 Component sizes utilized in system demonstrated. Boilers supply "S" building in Shanghai.

Boiler Power, kW	Storage Volume, m^3	Storage discharge rate, %	Heating type	Solar collector gross area, m^2
20 kW	2	20	Radiator	20

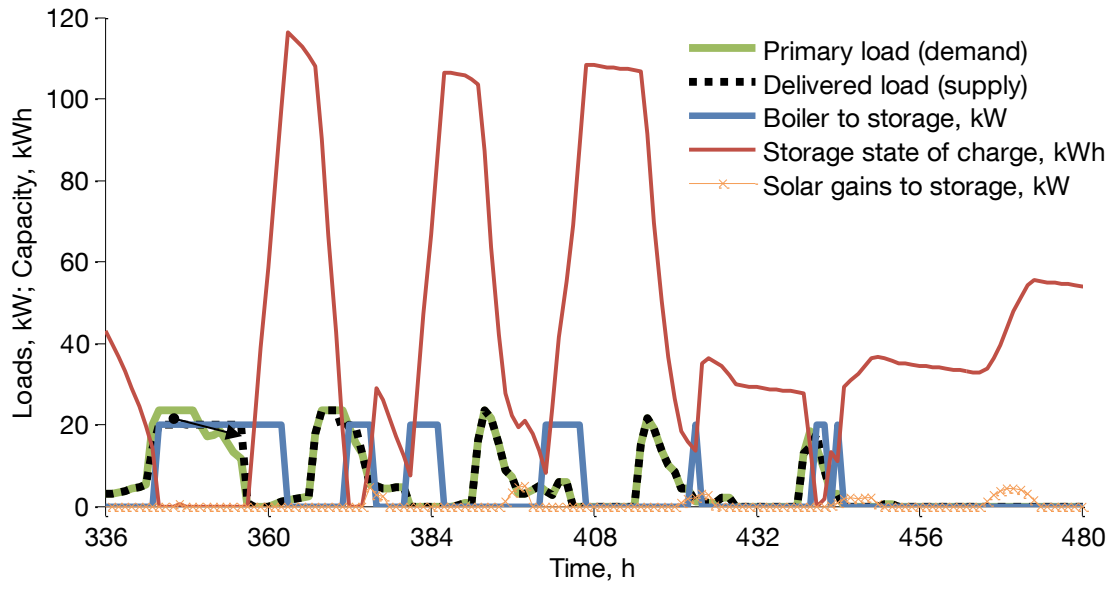

Figure 3.11 Simulation performance of SM1, with dimensions given in Table 3.4 during the third January week. The system provides heating for an "S" building in Shanghai.

Although highly simplified, this SM1 is quick and yields a good estimate of the suitability, cost and performance of system configurations. Simulation results for the peak heating season week show good model performance. The postponed unsatisfied load is, if the component size allows it, covered within the following lower load hours. Chapter 5 on optimization will explain the role of the remaining load values in ensuring the satisfactory demand coverage.

3.3.2 SM2: Condensing Boilers

The SM2 accounts for an arbitrary number of condensing boilers. Nevertheless, to provide help in comprehending the more complex model, the main characteristics of supplying the load utilizing condensing boilers are initially addressed by modeling only one boiler. Obviously, the more complex model is also able to account for a single condensing boiler.

3.3.2.1 One Condensing Boiler

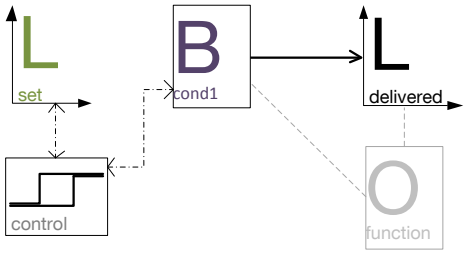

Figure 3.12 Schematic representation of the modeled system containing one condensing boiler (Bcond1).

Figure 3.12 represents an SM2 consisting of a single heat generating component – a condensing boiler. Just as a reminder, the annual simulation of the system yields the results necessary to calculate cost and emissions used to define the optimization objective.

In each timestep, the condensing boiler modulates between its minimal and maximal power (as introduced in section 3.2.3.2) to meet the load imposed to the system. This is illustrated in Figure 3.13. In the periods during which the load lies between the boiler minimum ($PLR_{min} \cdot P$) and maximum power ($PLR_{max} \cdot P$), the exact demanded load is supplied. If the demand does not reach the minimal power, that minimal power still has to be delivered, which results in slight overproduction. On the other hand, if the demand is higher than the maximum power, the load cannot be met – the maximum power is supplied. An equation describing these three cases, and an additional one in case the set load equals zero, defines the delivery task assigned to the boiler:

$$D(t) = \begin{cases} 0, & L(t) = 0 \\ PLR_{min} P, & 0 \le L(t) \le PLR_{min} P \\ L(t), & PLR_{min} P \le L(t) \le P \\ P, & L(t) \ge P \end{cases} \tag{3.33}$$

where PLR_{min} is the minimal part load ratio the boiler can achieve.

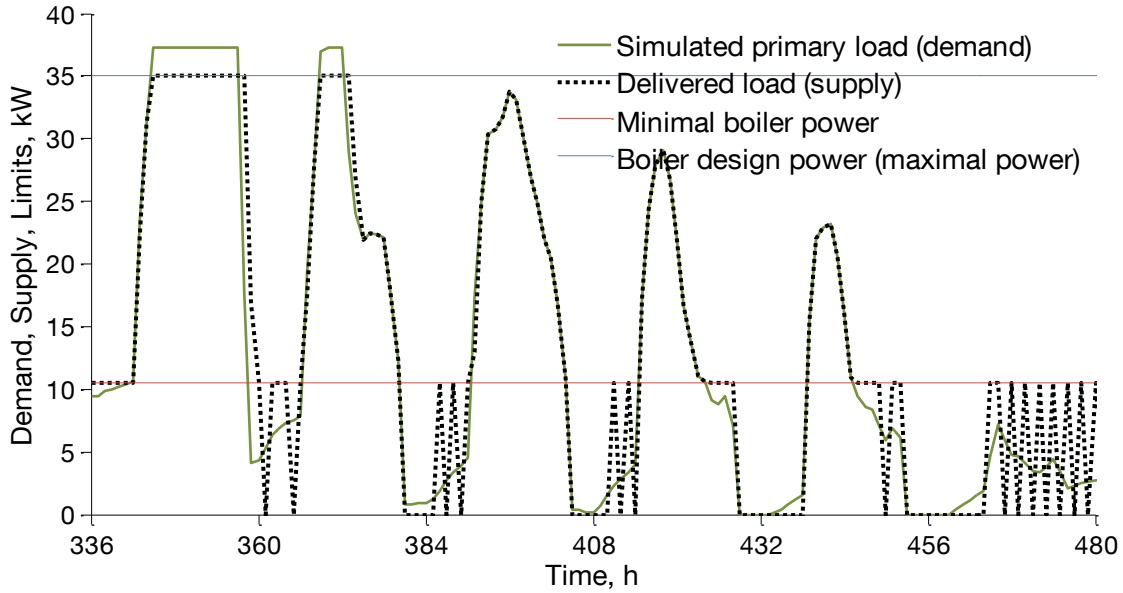

Figure 3.13 One condensing boiler (35 kW) model performance during the third January week for Moscow weather data and "S" building. Loads between the limits are met exactly, while those breaching the limits cause: in the case of exceeding the design power – prolonged operation of the boiler, or in the case of loads lower than minimum – boiler short cycling.

The remaining load, which will influence the demand in the following timestep, is introduced:

$$RL(t) = (L(t) - D(t)) \cdot f_{RL} \tag{3.34}$$

while f_{RL} is a factor that allows different weighting for the production deficiency and overproduction:

$$f_{RL} = \begin{cases} 1, & L(t) > P \\ 0.75, & L(t) < PLR_{min} P \end{cases} \tag{3.35}$$

The remaining load changes the set load for the following hour, thus introducing the active system performance influence on the simulated primary load:

$$L(t + dt) = L(t) + RL(t) \tag{3.36}$$

Boiler does not react to set loads lower than 5% of the annual maximum, but these loads are still added to the remaining load. Another function of the remaining load is its role in defining the objective function penalty, as explained in chapter 5.

A further value determined by the simulation is the PLR profile:

$$PLR\left(t\right)=\frac{D\left(t\right)}{P} \tag{3.37}$$

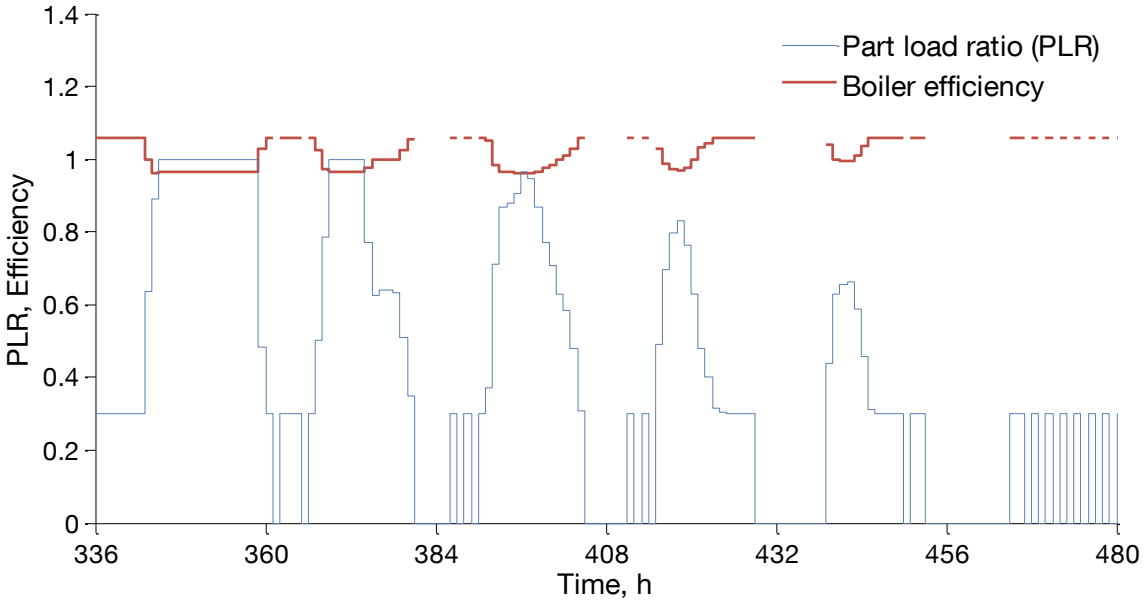

Figure 3.14 Simulated part load ratio and boiler efficiency during the third January week for Moscow weather data and "S" building. Minimal PLR is 30%. A decrease in PLR increases the efficiency.

Once the yearly PLR profile is known, the efficiency profile is defined by (3.13). Efficiency is needed to determine the energy consumption, which is addressed in section 4.3.2 on SM energy cost.

3.3.2.2 An Array of Condensing Boilers - System Performance Control

If utilizing more than one condensing boiler, each of these boilers can provide powers lying between its minimal and maximal power. This increases the overall modulation span. The theoretical system utilizing an integer number n of condensing boilers is presented in Figure 3.15.

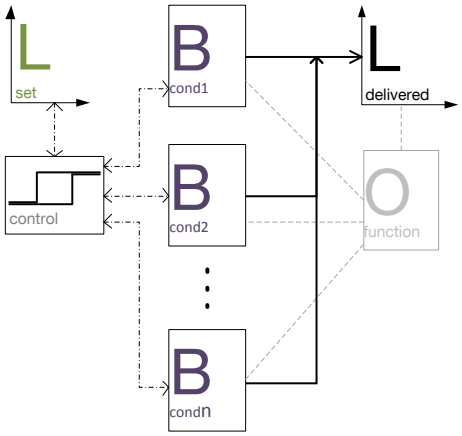

Figure 3.15 Schematic representation of the modeled system containing n heat generating components (n condensing boilers). Control makes sure the set load is efficiently met. The differences in set and delivered loads are tracked since this will be used in the optimization process.

Along with satisfying the demand, the following goals were targeted while developing the optimal load allocation strategy (optimal dispatch):

- Overproduction minimization;
- Efficiency maximization; and
- Decrease of boiler "wear and tear".

To fulfil these goals, the boiler utilization control strategy is developed. Due to the tendency of boiler efficiency to increase as the PLR reduces, the overall annual efficiency will increase if boilers perform in part load the majority of the operation time. This is true assuming that, as the demand rises, the delivery adapts to it primarily by increasing the water flow, rather than its temperature. Therefore the goal for the control strategy is to maintain boiler performance as far below their full capacity as possible, as illustrated in Figure 3.16. One could consider, since the efficiency rises as the PLR drops, that the bigger the boiler, the better the overall efficiency would be. Could the optimization yield unusually big boilers? Firstly, this is limited by minimizing objective including investment costs and by limiting the maximal boiler size in the optimization procedure. Secondly, even without this limitation smaller boilers should be implemented in combination with bigger ones to avoid overproduction. This is due to their ability to meet the exact load, even for very low loads. Chapter 5 on optimization will show that these characteristics cause the optimization to yield boilers of considerable sizes.

In order to address the mentioned goals, combinatorial optimization is implemented to ensure good load allocation. It controls the performance of a system containing any number of condensing boilers. The user (in the case of simulation) or the optimizer (in the case of optimization) provides this input. Vector *SP*, containing sums of design powers of all possible boiler combinations, is generated and sorted in an ascending order. An accompanying incidence matrix, I_{SP}, is generated to allow identification of boiler combinations responsible for each row of these sums. The equivalent is done for the sums of minimal powers, forming vector *SMP*. In addition, the sums of minimal powers are sorted by the

increasing sums of design powers, SMP_P, in order to determine the minimal power of boiler combinations responsible for each design power sum.

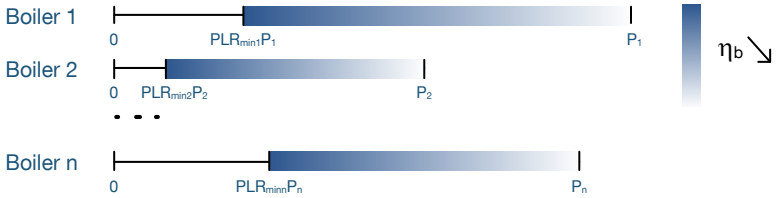

Figure 3.16 Operational powers of condensing boilers 1 to n. Efficiency decrease is approximated by the color fading, as well as PLR increase starting from the minimal PLR. Minimal PLR can be different for each boiler. Maximal PLR equals 1 (full design power). The control has a goal to keep boilers performing at the darkest possible area of sketched PLR values.

At each timestep the model determines a boiler combination whose minimal power lies slightly under the demand. However, it is not certain if this boiler combination can actually satisfy the demand – the demand could lie above the sum of its design powers. This is the consequence of the fact that each of the boilers can have different powers and minimal PLRs. Figure 3.17 illustrates this problem using an example of two condensing boilers. The figure shows the minimal power of the second boiler exceeding the design (maximum) power of the first one. So, for loads lying between these two values, indicated by a set load ribbon, the first smaller minimal power combination is solely Boiler 2, but its full power is not high enough to satisfy the load. The model is forced to overproduce. Minimal overproduction is achieved by utilizing Boiler 1 at its minimal power.

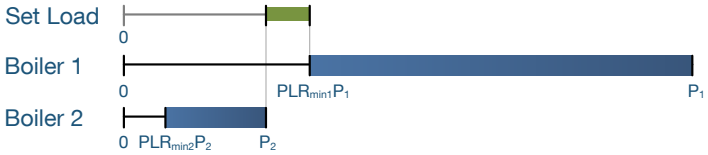

Figure 3.17 Minimal power achievable by Boiler 1 is higher than the design power of Boiler 2. If the set load lies between these two values (green ribbon), the exact load cannot be met. To cover such loads the boiler 1 is on and generating its minimal power, thereby overproducing.

Extended to any number of boilers, the boiler combination yielding the first bigger minimal load (compared to the set load) is chosen to deliver. It delivers slightly more than demanded.

Although the control goal is to maximize the efficiency, the overproduction minimization has higher priority. To conclude, two conditions for load allocation strategy are formulated out of the mentioned two goals:

- Difference between the load and cumulative minimal power of the active boiler combination is minimal, but positive – otherwise there is overproduction;
- The combination with the biggest sum of powers for which the previous condition holds is utilized – it insures maximal efficiency.

Based on this, the load allocation strategy is developed. If a boiler combination for which both of the conditions hold exists at a certain timestep, an exact demanded load is supplied:

$$D(t) = L(t), \quad RL(t) = 0 \tag{3.38}$$

The load is shared by the boilers in such a way to yield an equally distributed increase in PLR:

$$PLR(t) = PLR_{min} + \frac{D(t) - SMP_P(q)}{(SP(q) - SMP_P(q))\ (\mathbf{1} - PLR_{min})} \tag{3.39}$$

where $SMP_p(q)$ represents a single row of the vector obtained by sorting the SMP by increasing SP, and the row is indicated by the SP index indicating optimal cond. boiler combination to cover the load. $SP(q)$ is a single row of the sorted sums of full power condensing boiler combinations, indicated by the same index q.

If the first condition cannot be satisfied, for example in case of the loads falling on the green ribbon in the Figure 3.17, the system is forced to overproduce. For arbitrary number of boilers this case is easy to identify. Namely, it happens if the first bigger SP boiler combination contains a boiler whose minimal power has not been exceeded by the current set load. The smallest overproduction is achieved by the boiler combination which has the minimal but positive difference between its *SMP* and set load. The identified boiler combination is operated at their minimal PLRs:

$$D(t) = SMP\ (r+1) \tag{3.40}$$

where SMP represents the sorted sums of condensing boiler minimal powers and the index r identifies the boiler combination with the biggest sum of minimal powers, but still smaller than the load. Remaining load (in this case negative) and its influence on the set load is the same as defined by equations (3.31), (3.35) and (3.32). As expected, in the situation described the vector of PLRs takes minimal values for boilers defined in the $SMP(r+1)$ combination:

$$PLR(t) = PLR_{min} \tag{3.41}$$

For loads exceeding the sum of all design powers, the maximum possible power is provided by running all boilers at full load and the rest of the load is postponed for the next hour, as remaining load, equations (3.31), (3.35) and (3.32). If this happens too often or the remaining load value is too big, the supply penalty will increase indicating the simulated set of boilers cannot satisfy the demand. PLR equals 1 for all the boilers:

$$PLR(t) = \mathbf{1} \tag{3.42}$$

Equations (3.39), (3.41) and (3.42) summarize the optimal load allocation strategy in case any chosen number of condensing boilers is utilized. Depending on the boiler configuration and the set load at the timestep, one of these equations is chosen to define the PLR of all utilized boilers. After performing the whole year simulation a *PLR* matrix containing 8760 values for each of the boilers is formed. PLR values are used to assess the efficiency profiles for each boiler and thus their energy consumption.

3.3.2.3 Simulation Performance

This section presents system performance using an example SM2 utilizing two condensing boilers, schematically given in Figure 3.18. If not stated differently by the user, the model assumes a PLR of 30% for each boiler, gas as a fuel, and radiators as heating emitters. Performance curves from Figure B 1 have been used.

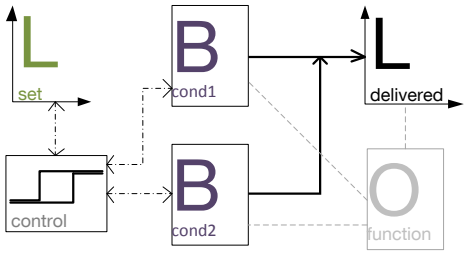

Figure 3.18 Schematic representation of the modeled system and component interaction. Two gas condensing boilers (cond. boiler 1 and cond. boiler 2) serve as heating energy sources.

Performance of such a system with boiler design powers of 25 and 15 kW, see Table 3.5, is observed for the Moscow climate and "S" building. One simulation (function evaluation) takes around 150 ms, which is about 4000 evaluations within 10 min. According to Figure 3.19, during the first shown day (hours 336 to 360) the sum of design powers is lower than the set load (demand). This causes the remaining load procrastination by adding it to the set load of the following timesteps. From the third day on (hour 384) the demand is lower than the sum of boiler design powers. As a result the exact meeting of the load is possible, with occasional overproduction in case the load is lower than minimal power of the smaller boiler.

Table 3.5 System parameters for simulation results in Figure 3.19

Cond. Boiler 1	Cond. Boiler 2	PLR, %	Fuel Type	Heating Type
25 kW	15 kW	30	Gas	Panel

The curves representing PLRs illustrate the calculation explained in section 3.3.2.1. If the demand is lower than the minimal power of the bigger boiler, the smaller boiler delivers the total demanded load. As soon as the load exceeds the sum of minimal powers, both boilers are turned on. For that and larger loads boilers operate with the same PLR in order to approach the maximal efficiency.

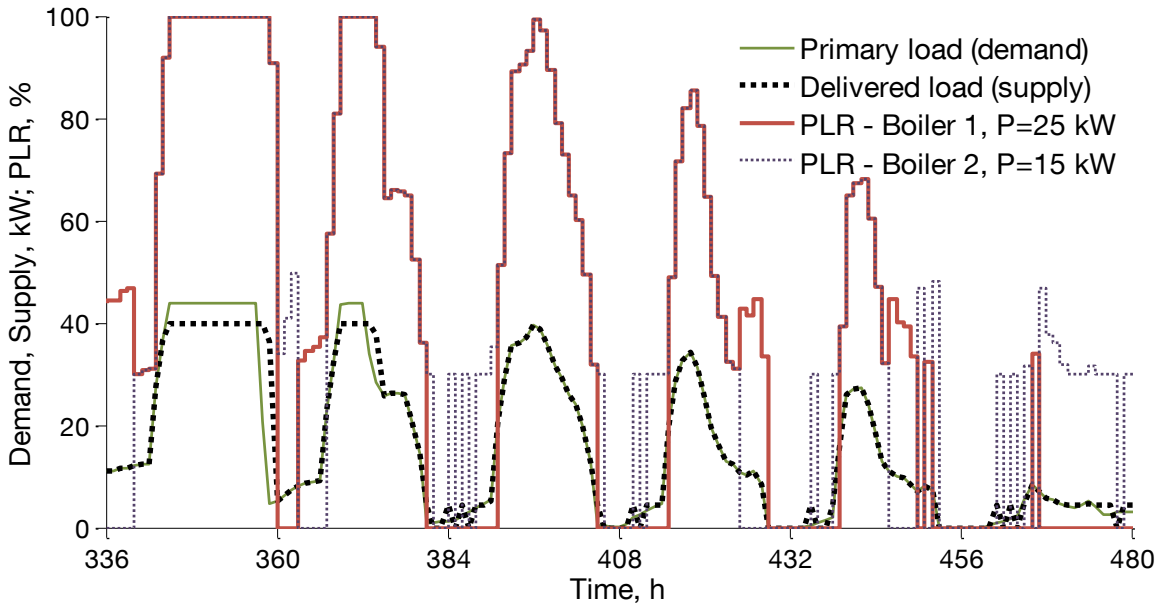

Figure 3.19 Two condensing boilers with design powers of 25 and 15 kW cover the heating load in an "S" building in Moscow during the third January week. Loads above 40 kW cannot be met – the remaining load shifting occurs. Most of the time PLRs are equal for both boilers, except for e.g. loads lower than 30% of 25 kW boiler (its minimal PLR), which are taken over by the smaller 15 kW boiler solely.

3.3.3 SM3: Thermal Storage, Solar Collectors and Condensing Boilers

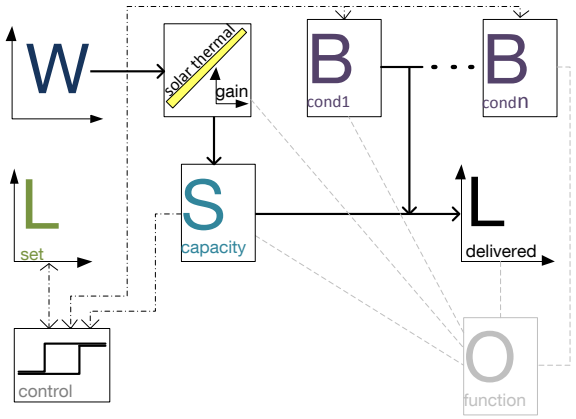

Figure 3.20 Schematic representation of the modeled system and of the component interaction. Heating energy is produced by solar collectors and n condensing boilers (Bcond1 to Bcondn) and stored for later use by the storage tank. Control ensures the system satisfies the demand while maximizing the solar energy utilization.

A third preconfigured heating system comprises solar thermal collector, thermal storage and either one or several condensing boilers. It is especially suitable for warmer climates with lower heating loads and higher solar radiation during the heating season. Boilers are utilized as an auxiliary in case the stored solar collector gained heat is not sufficient. Due

to their fast start-up and modulation response, condensing boilers are a good auxiliary heating source.

As well as the previously presented SMs, this configuration is simulated in hourly steps to obtain one average meteorological year of system performance. All the components of this system have already been mentioned in SM1 and SM2. Component interaction and the control strategy followed by system performance analyses are explained in following sections.

3.3.3.1 System Performance Control

The energy gained hourly by solar collectors is fed to the storage, which delivers the demanded or maximal available amount to the building space through the secondary HVAC. This delivered load (*SSD(t)*) is calculated according to equation (3.29). In case of unsatisfactory storage performance in a given timestep, the auxiliary heating source, in this case condensing boiler/s, is turned on. Such performance is caused by the fact that energy storage has a limitation in the form of a maximal discharge rate or the mere fact that the amount of stored energy is too low. In case the demand exceeds the sum of this storage limitation and current solar gain, which would be able to provide the energy in the last moment, the auxiliary is activated and needs to deliver the remaining demand. Thus the load imposed on the auxiliary condensing boilers, *CBL(t)*, is:

$$CBL\,(t) = L(t) - SSD\,(t) \tag{3.43}$$

Equations describing the performance of condensing boilers, given in section 3.3.2, can be used here. The only change is in the notation. Namely, here the set load *L(t)* is replaced by the auxiliary condensing boiler set load, *CBL*(*t*), and the resulting delivered load *D(t)* by the load delivered by the condensing boilers *CBD*(*t*).

The final load delivered by the system is the sum of loads delivered by the storage and auxiliary condensing boilers:

$$D(t) = SSD\,(t) + CBD\,(t) \tag{3.44}$$

The model allows utilization of an arbitrary number of auxiliary condensing boilers. The PLR profiles are defined within the model. Again the remaining load utilization, eq. (3.31), assures a degree of flexibility in satisfying the load.

3.3.3.2 Simulation Performance

In order to observe the behavior of the system, the model has been simulated to supply the “S” building located in Shanghai. One simulation (function evaluation) for condensing boilers model takes around 430 ms, which is about 1400 evaluations within 10 min.

The system is sized according to Table 3.6. The second January week performance illustrated in Figure 3.21 confirms the load has been satisfied by the system. During the hours of increased solar radiation the demand drops and the building can be supplied by solar collectors, while the excess energy is stored, e.g. Friday afternoon (hours 276 - 288). The

stored excess energy provides the heating energy until the storage is discharged and the supply task is taken over by condensing boilers, e.g. Monday morning (hours 176 - 192).

Table 3.6 Component sizes utilized in the demonstration. Boilers supply an "S" building in Shanghai. Radiator heating assumed.

Storage Volume, m^3	Storage discharge rate, %	Solar collector gross area, m^2	Conden. Boilers CBo1 (Table 5.1)	
			Power 1, kW	Power 2, kW
2	20	40	15	10

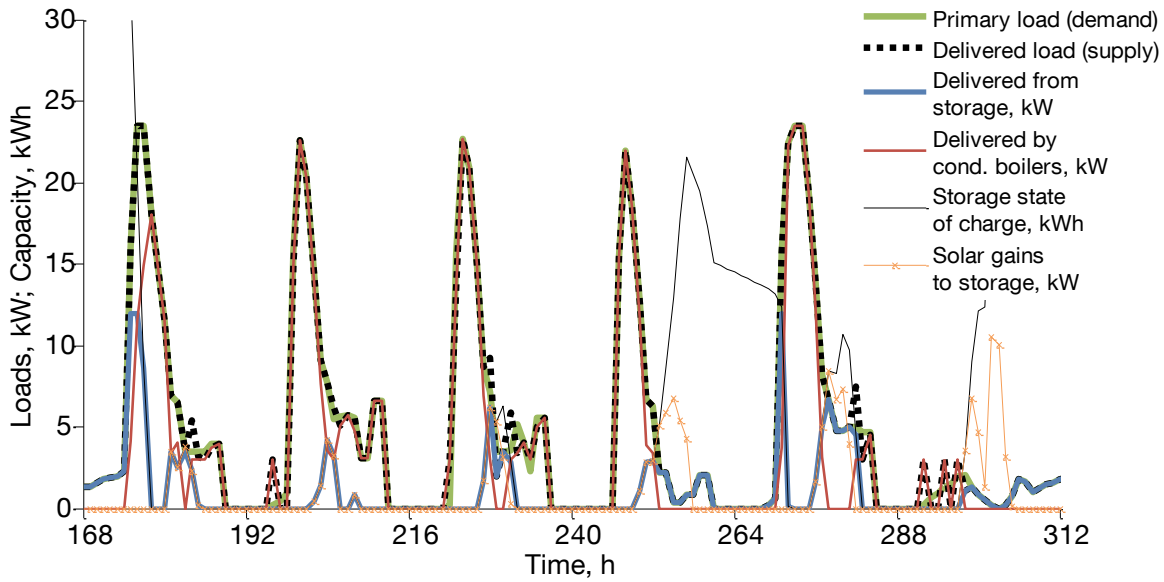

Figure 3.21 Solar thermal collector, thermal storage and two condensing auxiliary boilers supply an "S" building in Shanghai during the second January week. If possible, the load is satisfied from the storage charged by solar collectors, otherwise condensing boilers deliver the auxiliary energy.

3.3.4 SM4: On-Off Boiler, Thermal Storage and Condensing Boilers

This SM represents a conservative system consisting of a base load and peak load heating source. An on-off boiler (e.g. biomass boiler) charging the storage covers the base load, while occasional peaks are supplied from the auxiliary condensing boiler/s. An advantage of implementing a peak boiler is the possibility to reduce boiler and storage sizes, thus storage losses. On the other hand, additional investment for the auxiliary increases the costs. The storage utilization reduces the number of on-off boiler start-ups.

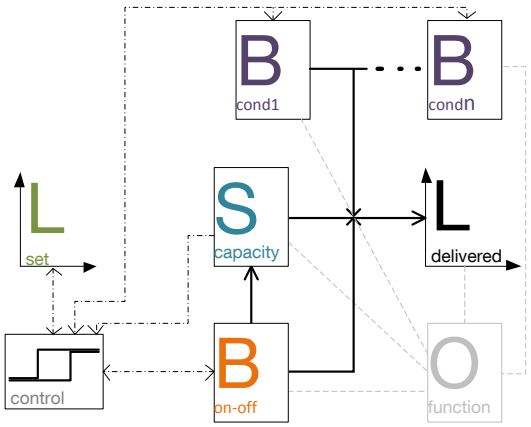

Figure 3.22 Schematic representation of the system model comprising an on-off boiler, thermal storage and an arbitrary number of condensing boilers. Hysteresis control and optimal load allocation are implemented. Occasional lack of stored energy is compensated by condensing boilers.

3.3.4.1 System Performance Control

The storage is charged using the boiler control strategy based on hysteresis, as described in 3.3.1.1. Auxiliary condensing boiler operation is identical to that in the previous model, where the storage is charged from solar collectors. The storage discharge (*BSD*) is calculated using equation (3.29). Thus the whole system delivers the load defined as:

$$D(t) = \begin{cases} BSD\ (t), & L(t) > min\ (SC\ (t), SP\ max\ ) \\ BSD\ (t) + CBD\ (t), & L(t) \le min\ (SC\ (t), SP\ max\ ) \end{cases} \tag{3.45}$$

3.3.4.2 Simulation Performance

For a demonstration of system performance, again the heating load of an “S” building located in Moscow has been used. The performance during the second January week illustrated in Figure 3.23 confirms load partition into a base and peak load, each covered by the respective boiler type. System sizes utilized are given in Table 3.7. Since winters in Moscow are cold, the night set point temperature needs to be maintained. This forces the system to be on during the night. Nevertheless, the load is low during these hours enabling charging of the storage. Discharge follows during early office hours. For most of the office hours during the presented week the load is higher than the biomass boiler power. The difference is supplied by condensing boilers.

Table 3.7 Component sizes utilized for simulation results presented in Figure 3.23.

Biomass Boiler Power, kW	Storage Volume, m^3	Storage discharge rate, %	Condensing Boilers, minPLR=30%	
			Power 1, kW	Power 2, kW
20	1	20	15	10

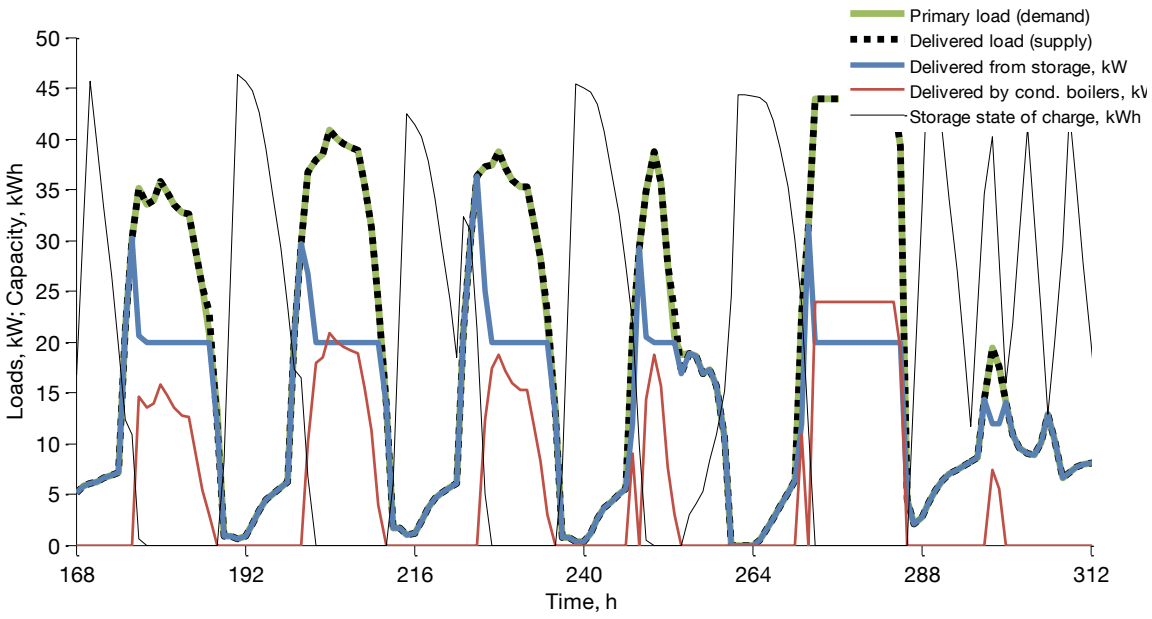

Figure 3.23 Biomass boiler, thermal storage and two condensing auxiliary boilers supply an "S" building in Moscow during the second January week. If possible, the load is satisfied from the storage charged by the biomass boiler, otherwise condensing boilers deliver the auxiliary energy.

3.3.5 SM5: Two Stage Boiler and Condensing Boilers

This SM is derived from the previous system, SM4, with two crucial differences. Namely, the boiler covering the base load operates in two stages and it has different control in comparison with the already described on-off boiler. For systems without the thermal storage, this control strategy is more reasonable from the fuel consumption and emission point of view.

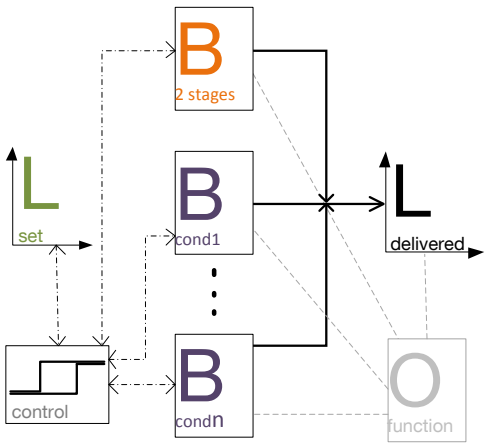

Figure 3.24 Schematic representation of the system model comprising a two-stage boiler covering all the loads larger than its first or second stage power and an arbitrary number of condensing boilers, which cover the rest of the load.

3.3.5.1 System Performance Control

The first and second (full power) stage of the two staged boiler is turned on only if the set load exceeds its first and second stage power, respectively. The difference between the supply and demand is provided by condensing boilers. The load delivered by the system can thus be written as:

$$D(t) = \begin{cases} CBD\ (t), & L(t) < PLR_{\ 1} P \\ PL\ R_{1st}\ P + CBD\ (t), & PL\ R_{1st}\ P \le L(t) \le P \\ P + CBD\ (t), & L(t) > \mathrm{P} \end{cases} \tag{3.46}$$

Cycling degrades the boiler performance. The simple operation strategy described reduces the number of boiler cycles, despite the lack of thermal storage. It compels auxiliary boiler utilization to cover low loads and loads between the boiler stages. If the boiler has only one stage ($PLR_{1st}=1$), one might assume the model performance identical to the SM4 described in section 3.3.4, if the thermal storage is excluded. However, the boiler from this SM will turn on only if the load is higher or equal to its full performance power, whereas the boiler in SM4 operates whenever there is a load.

3.3.5.2 Simulation Performance

In this example to illustrate the SM performance the system needs to satisfy the heating load of an "S" building located in Moscow.

Observed system size combination (Table 3.8) can satisfy the set load. In Figure 3.25 simulation results from the third January week are presented. Low loads, such as those during the night set back are covered solely by condensing boilers, since the part load of the two stage boiler has not been reached. Higher loads are satisfied by summing up the loads delivered by both boiler types.

Table 3.8 Component sizes utilized for simulation results presented in Figure 3.25.

Two stage boiler power, kW	Condensing Boilers CBo1 (Table 5.1)		Heating Type
	Power 1, kW	Power 2, kW	
20 (1st stage: 10)	15	5	Radiator

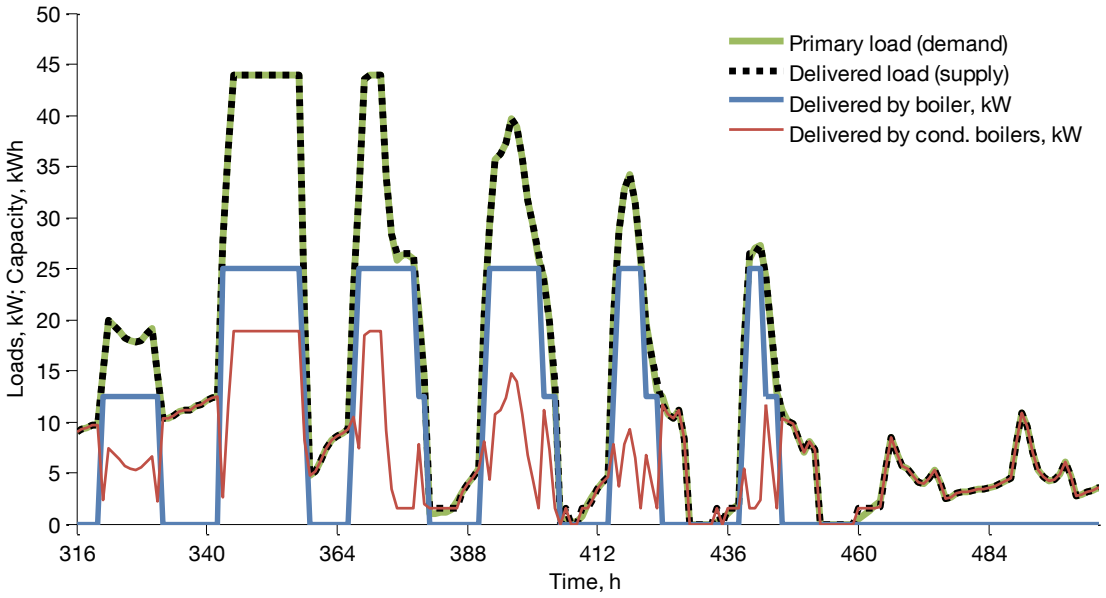

Figure 3.25 Two-stage boiler and two condensing boilers supply "S" building in Moscow during the third January week. Radiator heating assumed.

3.3.6 SM6: Vacuum Compression Chillers

The component most widely utilized to provide space cooling energy in commercial buildings is a vacuum compression chiller. Usually a number of chillers supply the distribution system to cool the building space. This SM comprises any chosen number of chillers and an autosized cooling tower. The control integrates the chiller (3.2.1) and cooling tower (3.2.2) models into a system simulation model. Later, in the optimization, the number of chillers will be automatically selected depending on the load imposed. For this reason, the simulation of any number of chillers is enabled. The SM itself performs a combinatorial operational optimization to increase the overall COP of the chiller system (chiller load allocation).

Similar to the approach described in 3.3.2, first the operation of an SM featuring one chiller is presented including detailed description of input data and parameters used. Thereupon the simulation model containing an arbitrary number of chillers is introduced, focusing on the explanation of the inbuilt optimal chiller load allocation algorithm.

In practice, various measures to increase the chiller plant reliability can be found, such as utilization of a redundant chiller or oversizing the chillers to meet the calculated design load increased in 10 to 20% [11], called a safety margin. Often the safety measures are compounded, which is only justifiable if providing air conditioning for processes that require a high degree of reliability (e.g. industry, server cooling etc.). Considering the peak load only occurs for a short period of time, it is obvious that any safety margin will prolong the part load chiller operation. This is why [11] refrains from using a safety margin if accurate load calculation is available. In [56] the authors analyze a practice of adding the

safety margin or a redundant chiller to the air-cooled chiller plant. It provides useful information on current design practice and concludes i.a. that assuming good maintenance the redundant chiller can be omitted.

3.3.6.1 One Vacuum Compression Chiller

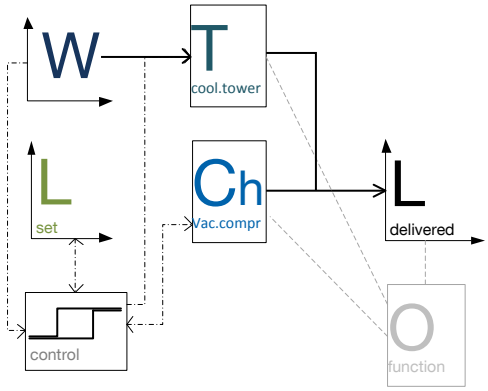

Figure 3.26 Schematic representation of a cooling energy generation SM containing a vacuum compression chiller and a cooling tower. Component performance depends on the imposed load and weather conditions for every timestep. Yearly performance profiles are used to define the objective function which will be evaluated in the optimization (5.4.6).

In Figure 3.26 the SM containing one vacuum compression chiller and a cooling tower is presented. In order to perform system simulation, the load profile and weather data are to be supplied. As already familiar from the presented heating SMs, the ideal building load provided by the user is increased for the assumed secondary system losses, which is approximated using a simple efficiency factor (more details in A 1.3). Additionally, a safety margin of 10% is added to the calculated secondary load to form the initial set load profile for the chiller plant. If required, the safety margin can easily be removed.

To determine the chiller performance based on the model presented in 3.2.1 the chiller performance parameters need to be defined, as well as the condenser cooling water inlet and evaporator chilled water return temperature. The chiller performance parameters for two generic chiller types, DOE-2 reciprocating and centrifugal chiller, are implemented as default. These performance parameters are given in Table B 5. If not chosen differently, a chiller with a design capacity smaller than 400 kW is simulated as a reciprocating one, while a larger chiller is considered to be a centrifugal chiller. Each of the chillers modulates between its minimal and maximal PLR, which also belong to the set of component parameters. The user can impose the chiller type definition or even input custom performance parameters. A wet closed circuit cooling tower is assumed and modeled as described in 3.2.2.

The control assumes condenser water and chilled water temperature reset. The outside air wet bulb temperature, $T_{amb,wb}$, from the weather data set, minimal ($T_{cool,in,min}$) and maximal ($T_{cool,in,max}$) cooling water inlet temperature from the chiller performance data, and the "approach" of 3°C (a value originating from [11]) define the condenser cooling water inlet temperature ($T_{cool,in}$). This temperature is thus equal to either the wet bulb (increased for

the value of the approach) or the minimal cooling water inlet temperature, whichever is higher. If such a temperature exceeds the maximal cooling water temperature for more than 1°C, the warning message is displayed stating that safe chiller operation cannot be granted. Practically, the cooling water temperature is a linear function of wet bulb temperature between its limits. It is defined as:

$$T_{cool,in} = min\left(max\left(\left(T_{amb,wb} + \Delta T_{approach}\right), T_{cool,in,min}\right), T_{cool,in,max}\right) \tag{3.47}$$

The wet bulb temperatures within the weather data used in demonstration examples performed without returning a warning. The chilled water return temperature ($T_{chill,out}$) is a linear function of the load between its limits ($T_{chill,out,min}$ and $T_{chill,out,max}$ - defined within the chiller model data set):

$$T_{chill,out} = \left(max\left(L\right) - L(t)\right)\frac{max\left(L\right) - min\left(L\right)}{T_{chill,out,max} - T_{chill,out,min}} \tag{3.48}$$

Once the set load and the temperatures are defined, the chiller full load performance can be determined using (3.2) to (3.6). In each timestep the chiller is able to deliver any load between its minimum PLR multiplied by the full load capacity under current temperature conditions and that full load capacity (assuming the full load PLR equals 1). Hence the load imposing strategy is almost identical to the one first introduced with (3.33):

$$D(t) = \begin{cases} PLR_{min} CAP_{full}, & L(t) \le PLR_{min} CAP_{full} \\ L(t), & PLR_{min} CAP_{full} \le L(t) \le CAP_{full} \\ P, & L(t) \ge CAP_{full} \end{cases}. \tag{3.49}$$

Obviously the timestep independent boiler design power is replaced by a full load chiller capacity defined for current timestep conditions. Considering this, the three equations following the (3.33) can also be adopted here to define the remaining load and its influence on the following timestep's set load. Once the chiller is assigned the load to deliver, the part load ratio is defined and (3.5) can be used to assess the COP and thus the power consumption. Another value readily available at this stage is the heat of rejection (HR), which is the cooling capacity delivered (the heat taken from the space cooling medium) added to the compressor power. After all 8760 timesteps (assuming hourly steps) have completed, a complete HR profile is defined. The peak of the HR profile is used to autosize the cooling tower according to (3.7). The COP profile, chiller power profile, heat of rejection and thus the cooling tower power and water consumption profile, as well as all the sizes of mentioned components provide a base for the cost calculation. This issue is addressed in detail in 4.3.2.

In order to illustrate the proposed system model performance, it has been simulated using a chiller of 135 kW design capacity for an "S" building located in Dubai. This chiller size is chosen by the optimizer while minimizing total costs, which will be explained in detail in section 5.4.6. Upper left corner of Figure 3.27 shows a January day of SM performance during mild weather conditions, which resulted in low cooling loads. Cooling water temperature is at its minimal limit due to the low wet bulb temperature and the chilled water temperature only slightly beneath its maximum, which causes only a minor decrease in full

load capacity during operation hours. Outside the scheduled operation, the load equals 0 yielding maximal chilled water temperatures, see (3.48). If, in addition, the cooling water temperature equals its minimal limit, the maximal full load capacity is achieved, which is almost 160 kW if observing the red curve at the figure. Next to that graph, on the right, the same red line is already significantly lower, since the SM operates during a hot day in August, where only the “approach” separates the wet bulb from the cooling water supply temperature. As the demand is rising, the chilled water temperature set point is decreasing. Both effects degrade the chiller performance, so the full load capacity drops all the way to 120 kW. In both days the remaining load was active with the difference that, during the January day the minimal PLR limitation caused overproduction, while the peak August day caused demand higher than the full load capacity – the underproduction. The overproduction is followed by the resulting load reduction in the subsequent hour. On the upper right (Figure 3.27), the underproduction accumulated during the day is produced after the demand drops under the peak capacity of the system. In practice, the building could have been precooled before the peak demand hours, which would yield approximately the same energy consumption. The same peak day can also be seen at the lower half of the same figure, which shows the SM performance during the two peak load weeks in August. Wet bulb temperature remains high causing the cooling water temperature to follow with the $\Delta T_{approach}$ offset. The heat of rejection is shown in all three figures using a black curve, showing the sum of the delivered load and the power used, which is rejected through the cooling tower.

Figure 3.28 shows the part load ratio profile for the presented two weeks, as well as the coefficient of performance, which, for the reciprocating chiller under such severe weather conditions, lies below 3.5.

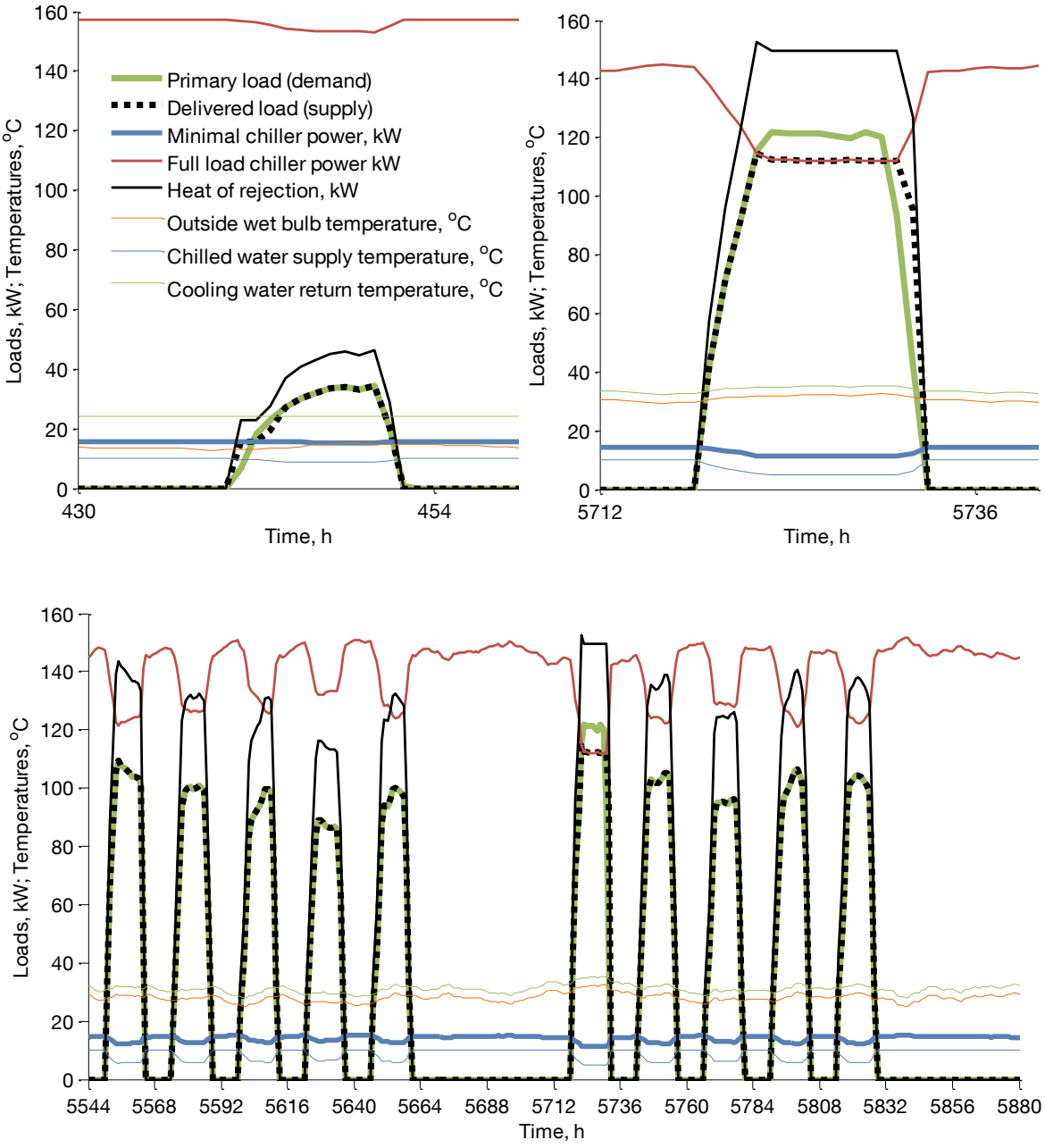

Figure 3.27 Simulation performance of SM6 with one 135 kW chiller to satisfy the cooling demand of an "S" building located in Dubai. *Upper left:* A January low load day, *Upper right:* Peak load Monday in August, *Below*: During two August weeks, including mentioned Monday.

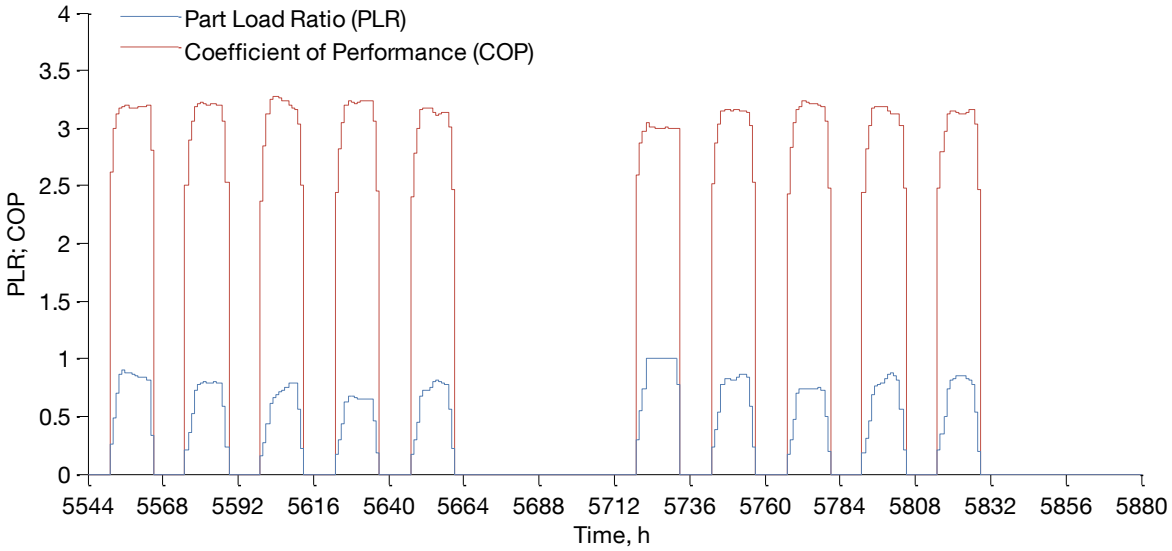

Figure 3.28 An "S" building located in Dubai served by SM6 with one 135 kW chiller. Part load ratio during two August weeks is high, reaching one at the beginning of the second week, while severe outside air conditions cause decrease in COP.

Figure 3.29 presents a complete year of system performance, from which the two weeks were extracted. The drop in chiller full load capacity due to weather conditions is obvious.

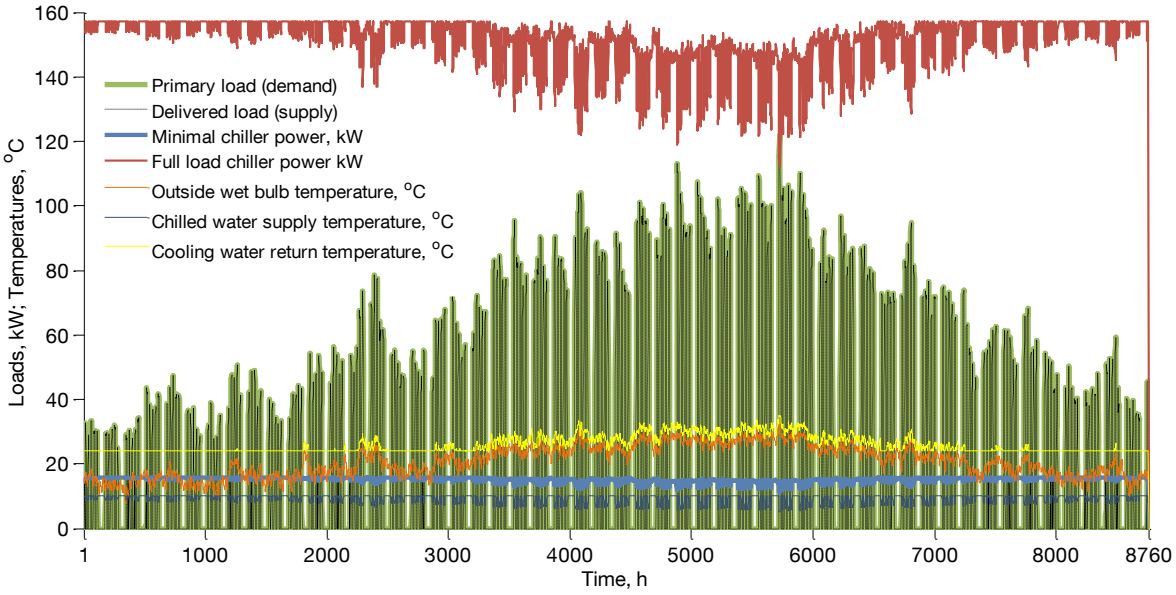

Figure 3.29 Yearly performance of SM6 with one 135 kW chiller supplying an "S" building located in Dubai.

3.3.6.2 An Array of Chillers - System Performance Control

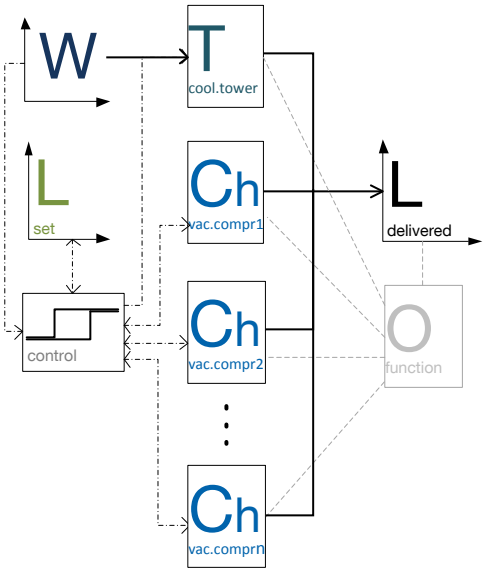

Figure 3.30 Schematic representation of a cooling generation SM containing any integer number of vacuum compression chiller and a cooling tower that serves all the chillers. Control distributes the load among chillers using combinatorial optimization algorithm with a goal to reduce the power consumption.

With regard to obligatory input data necessary for the model operation, the SM shown in Figure 3.30 is identical to the model containing only one chiller described in the previous section. However, this model can contain any given number of chillers in charge of covering the demand. The important difference compared to the previous model is the load allocation strategy. If required, the user can specify the chiller type for each of the chillers or even enter custom chiller performance parameters. Of course, if this model is assigned with only one chiller, it will yield a result identical to the previously described.

A good chiller load allocation strategy has a goal to reduce the part load operation and frequent chiller on-off operation. Many contributions in this field can be found in the literature. For example, in [57] the branch and bound algorithm was used to identify the optimal load allocation, while [58] utilizes the differential evolution algorithm. Keeping in mind the purpose of evaluating the model performance within this thesis, which is to assess the operational costs of a system capable of satisfying the demand, a rather simple algorithm for optimal load allocation is developed. It assumes the chiller COP increases with the PLR. The justification for this assumption can be found in the literature. The experimental results used to verify models compared in [59] confirm the COP rises with the PLR. The same tendency is shown in [60] for air-cooled chillers. The same authors in [61] have found that although the maximum of COP does not occur at full load, it is still reasonable to sequence the chillers to the full load.

One should not be misled by Figure 3.28, where seemingly the PLR decrease causes the COP increase. Low PLRs coincide with low loads caused by mild weather conditions, so both cooling and chilled water temperature are in favour of increasing the COP of a chiller. To isolate the PLR influence on the chiller performance in Figure 3.31, the temperatures

are kept constant at their reference values. Even though this cannot be generalized for any chiller, for both generic chiller types and reference conditions the increase in PLR was in favour of the chiller COP.

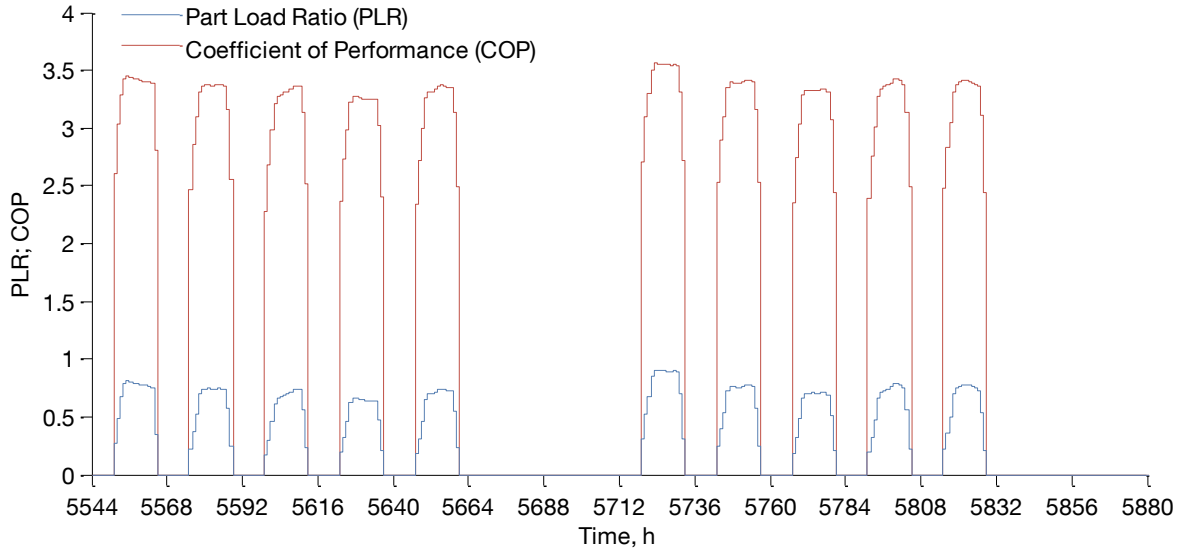

Figure 3.31 The system and the timeframe are the same as in Figure 3.28. Reference temperature conditions are adopted as constant chilled and cooling water temperatures in order to isolate the influence of PLR onto COP. Decrease in PLR causes lower COPs. Performance data for the reciprocating chiller used.

Supported by the mentioned references and the analyses in Figure 3.31, which yielded the same tendency in the case of centrifugal chillers, an assumption that the COP rises with the rise in PLR illustrated in Figure 3.32 was adopted. This assumption plays an important role in the optimal chiller load allocation algorithm responsible for step by step optimal chiller loading. It simplifies the optimization algorithm. Namely, instead of minimizing the chiller power the average PLR is maximized before the power is even calculated.

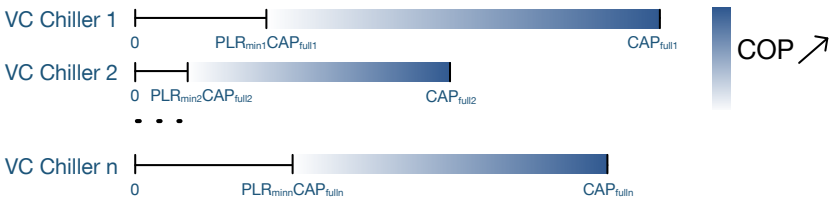

Figure 3.32 Assumed COP increase with the PLR. If the load is allocated in such a way to increase the PLR, the COP is also increased.

There are two basic differences between the optimal chiller load allocation and the condensing boiler load allocation presented in 3.3.2. The first and obvious one is that in the case of chillers, the goal is to maximize the PLR. The second difference is the sequence loading of the chillers, where the additional chiller is loaded once the demand exceeds the previously active chiller's/chillers' full load. Conversely, the multiple condensing boilers are loaded to have equal PLR whenever possible.

Let an SM comprising of n chillers be assumed. Vector *SCh* holding full load capacities of all chiller combinations (2^n) is formed and sorted in an ascending order. Accompanying incidence matrix, I_{SCh}, identifies the chillers responsible for each of the *SCh* values. In each timestep the demand is compared to the *SCh* values until the first bigger capacity is found. This value is mapped to the I_{SCh} to indicate which chillers are utilized to cover the current timestep's load. The demand is then distributed so that all chillers from the smallest to the second biggest active chillers operate in full load, while the biggest covers the rest of the load. If m of n chillers supply the load in the current timestep, the load is allocated in the following way:

$$
\begin{aligned}
&D(t)_{1,\dots,m-1} = CAP_{full}(t)_{1,\dots,m-1} \\
&PLR(t)_{1,\dots,m-1} = \mathbf{1} \\
&D(t)_m = \begin{cases} PLR_{min} CAP_{full}(t)_m, & L(t) \le PLR_{min} CAP_{full}(t)_m \\ L(t) - \sum_{i=1}^{m-1} D(t)_i, & PLR_{min} CAP_{full} \le L(t) \le CAP_{full} \end{cases} \\
&PLR(t)_m = \frac{D(t)_m}{CAP_{full}(t)_m}
\end{aligned}
\tag{3.50}
$$

Where the demand exceeds the sum of current chiller capacities, all the chillers are fully loaded, while the uncovered load is moved to the next step, as in the previous models (remaining load, see (3.31)).

Although in practice the loading is more likely to start from the biggest towards the smallest, the utilized approach has proven to be appropriate for the given purpose.

3.3.6.3 Three Chillers SM6 Performance

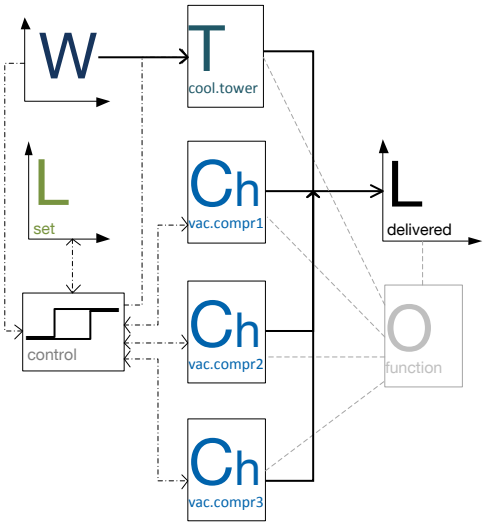

Figure 3.33 Schematic representation of a cooling generation SM containing three vacuum compression chillers and a cooling tower that serves all the chillers.

The SM in Figure 3.33 is used to present the described operation strategy. The model consists of three chillers and a cooling tower. Chiller sizes are given in Table 3.9. The system supplies a "B" ("big building", Table A 4) building located in Bangalore. In Figure 3.34 the first April week of chiller performance is magnified showing good demand coverage. Each day, immediately after starting the building cooling operation, the Chiller 2 (400 kW) covers the load. After the load has increased above the range of the Chiller 2, it is turned off to let the larger chiller, the "Chiller 3" (Table 3.9), cover the load. Shortly after, the operation of both mentioned chillers is required due to the increase in demand load. They keep operating for the most of the day, while the "Chiller 3" is turned on once the demand load exceeds the sum of full load capacities of chillers "1" and "2". The black curve shows the total heat of rejection for all chillers, which represents the cooling tower load.

Table 3.9 Component sizes utilized for simulation results presented in Figure 3.34. SM supplies a "B" building in Bangalore.

VC chiller reference capacity, kW and type			Space cooling medium	Cooling tower
Chiller 1	Chiller 2	Chiller 3		
670, centrifugal	400, centrifugal	50, reciprocating	Air	Indirect wet

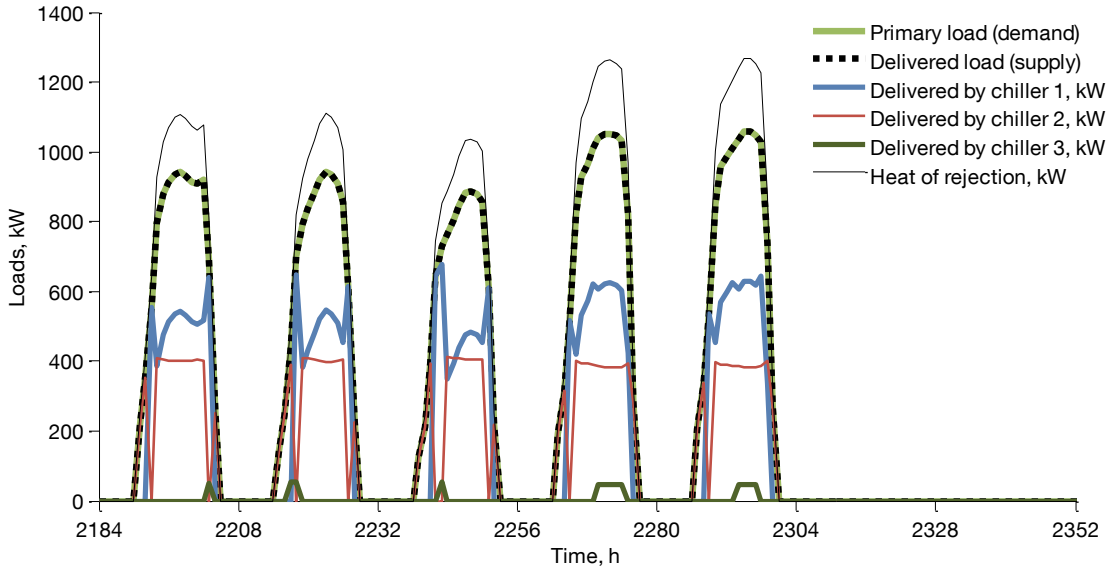

Figure 3.34 Three chillers (670 kW, 400 kW, 50 kW) supply a "B" building in Bangalore during the first April week. The load is satisfied.

In Figure 3.35 one can observe the effects of the explained load allocation strategy. Chillers "2" and "3" operate in full load most of their operation hours. Chiller 1 operates in part load, but its PLR also remains rather high yielding an annual average of 5.95. The curves representing COPs confirm good operation, with the overall annual COP of 5.1. One should keep in mind the reciprocating chillers have lower reference COP. The chiller loading algorithm is fast and appropriate for considering PLR and weather condition influ-

ence on plant performance for the purpose of plant sizing. One yearly simulation run including three chillers takes around 0.9 s.

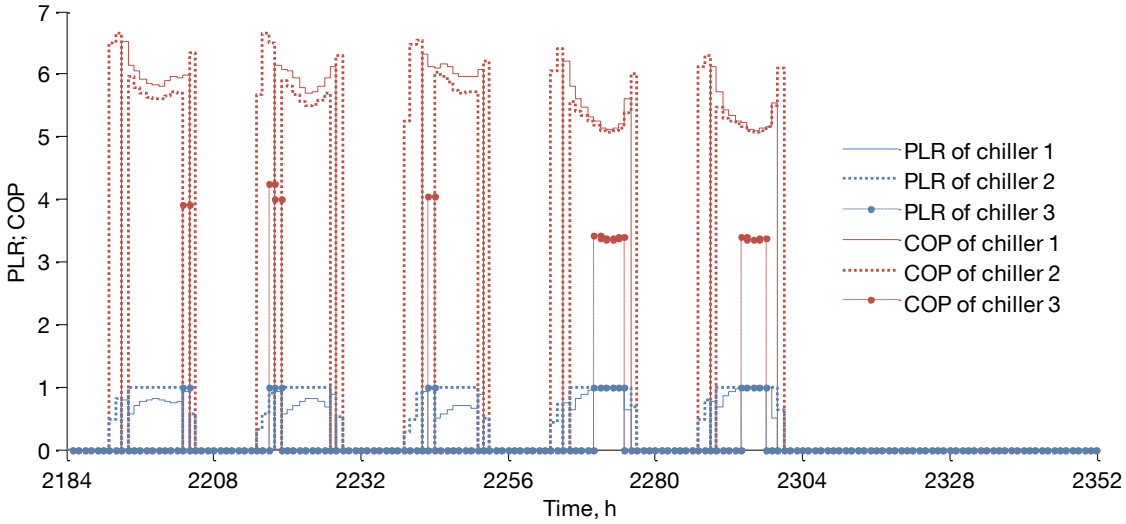

Figure 3.35 Chiller part load ratios and coefficients of performance during the same operation shown in the previous figure.

The implemented chiller performance data assume the chilled water supplies the AHU coils in order to cool the supply air. The preparation for using water as a distribution medium to serve emission systems such as chiller beams or fan coils is implemented. Additionally, in the case of low cooling loads the condenser can also be air-cooled, reducing the investment cost. Another issue to be considered in order to improve the SM would be to include the free cooling operation (water-side economizer) and the economizer (increase in outside air fraction once the outside air enthalpy is lower than the return air enthalpy). These issues should be considered while generating the ideal load used as input to the SM. The best result would be obtained if simulating the building and the plant in parallel, as already mentioned in chapter 2.

3.3.7 SM7: Vacuum Compression Chillers and Photovoltaics

The photovoltaic (PV) panel generated yearly electrical power production profile is as intermittent as the solar radiation profile at the location. Since none of power storage technologies on the building scale (e.g. batteries, electric vehicles) is accounted for in this thesis, the generated power needs to be either consumed or fed to the power grid simultaneously as it is produced. Depending on the nature of regulations existing in different countries, the most profitable PV power utilization strategy might vary. The strategy currently implemented in the tool is quite simple. The chiller power demand occurring simultaneously with the production will be covered by the available PV power. If the demand is higher than production, the power will be bought from the grid. If more PV power is produced than demanded, the surplus will be sold to the grid. Country specific feed-in tariffs

are accounted for if available. The relevant prices are given in Table B 9 and Table B 10. Custom regulations could easily be integrated in the model.

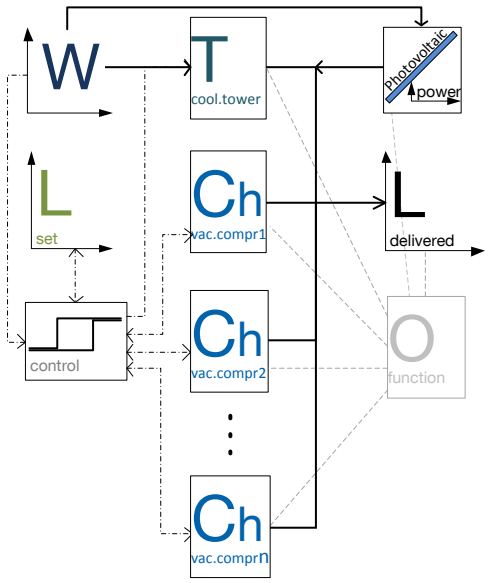

Figure 3.36 Schematic representation of a cooling energy generation SM comprising any number of vacuum compression chillers and photovoltaic (PV) panels. PV power coincident with the demand is used to power the SM. If needed, additional power is bought from the grid. If PV power exceeds the SM demand, it is sold to the grid.

In terms of chiller and cooling tower operation, this model is essentially identical to SM6. The only difference is the presence of PV panels in this model. The PV model from 3.2.2 is integrated in the way that the user can place the PVs on any of four vertical walls (by default facing north, south, east and west), on the horizontal, and on an optimally inclined surface. This enables the user to examine the influence of covering certain parts of building façade or roof with PV. Consequently, after identifying the advantages of covering certain areas with PV panels, this can be carried through the further design process. Another benefit of allowing PV distribution at different orientations is the possibility to influence the shape of the daily PV power profile and increase the simultaneity with the cooling demand. Figure 3.37 shows PV profiles during the same April week in Bangalore shown in Figure 3.34 and Figure 3.35 gained from 1 m^2 of PV placed in each of the 6 possible positions. Average PV power representing the mean PV power profile per 1 m^2 indicates how the profile is broadened by using the early morning east side or late afternoon west side gains. Depending on the climate and the demand the PV panel distribution can cause better demand coverage and relieve the grid in the peak load period. PV power generated during the non-office hours, such as weekends or holidays can cover the still existing building electrical loads (exceeds the scope of this thesis) or it can be sold to the grid.

To illustrate the benefits of PV power generation in supporting vacuum compression chiller power supply, the example model presented in the previous section (see Figure 3.34 and Table 3.9) is equipped with PV panels according to Table 3.10. To simplify the comparison, the result, shown in Figure 3.38, features the same week as in previously presented performance figures.

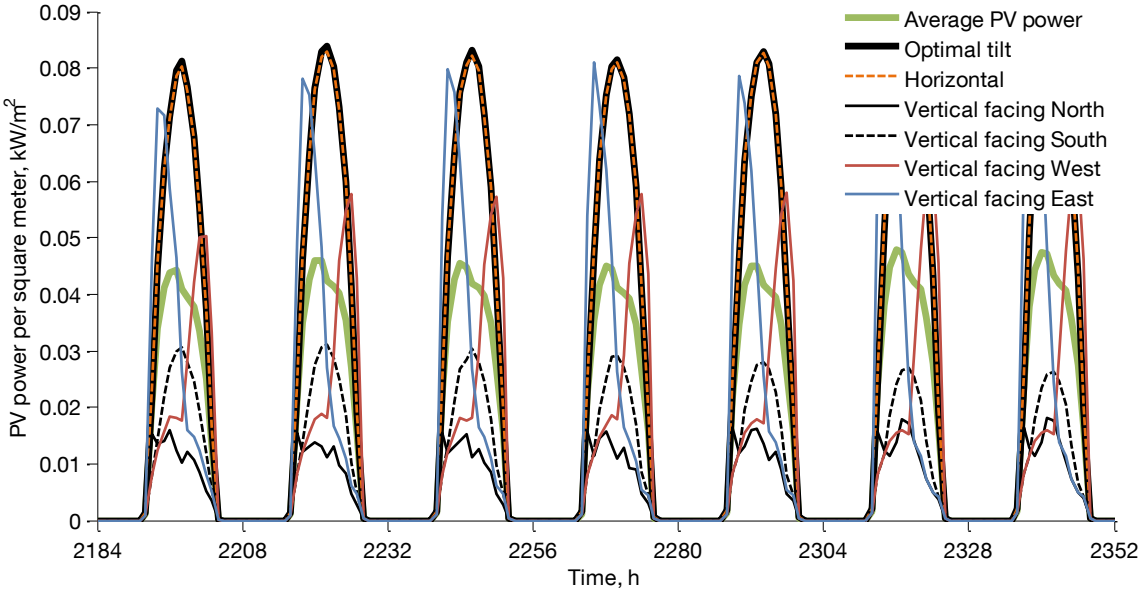

Figure 3.37 PV gain profiles per square meter of PV for 6 stated orientations and their average. Bangalore climate, first April week. Panels facing east produce during the morning and those facing west during the afternoon. Due to low latitude, optimal and horizontal panels have almost identical production, which is around 3 times bigger than production of vertical panels facing south.

Table 3.10 PV panel areas at the "B" building in Bangalore

Optimal tilt	Horizontal	Facing north	Facing south	Facing west	Facing east
100	200	0	200	200	200

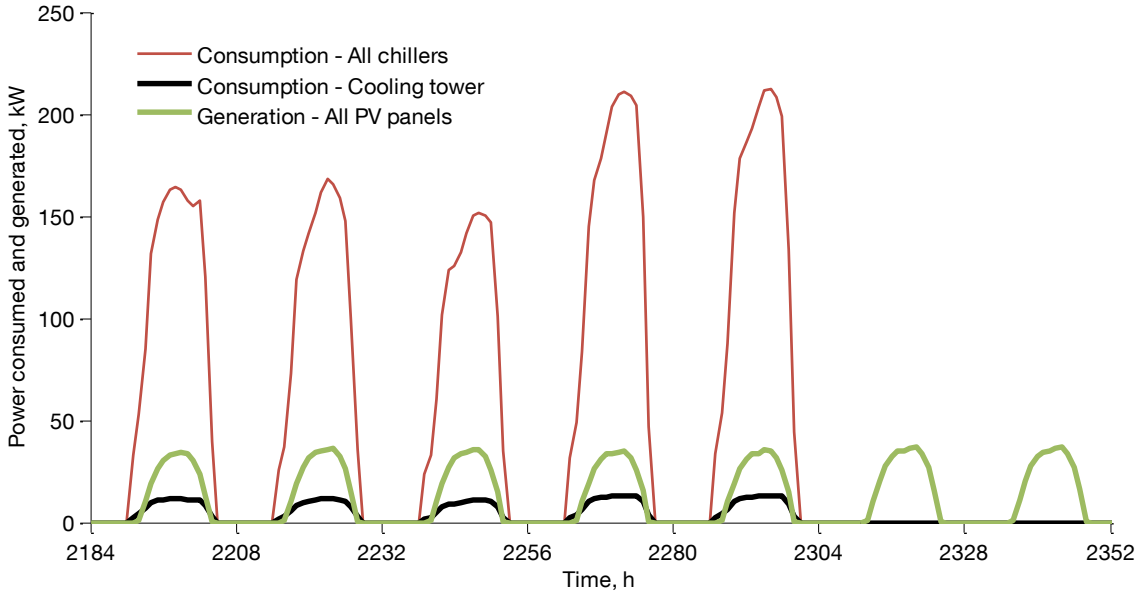

Figure 3.38 Three chillers from Table 3.9 are air-conditioning the "B" building in Bangalore. Cumulative PV power production of PV panels given in Table 3.10 is shown in green. The shape of production is coincident with the consumption.

Figure 3.38 shows the produced PV power can instantly be consumed by the cooling system. The solar ratio achieved in the example is 32%, which is also visible in the next figure showing the annual power demand and generation of the same system.

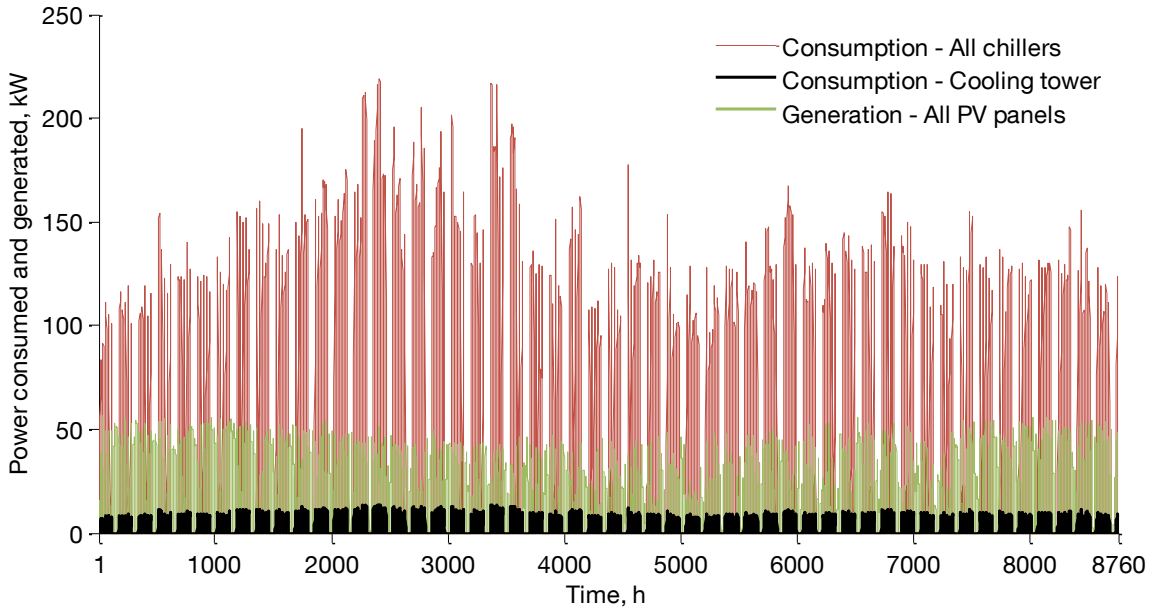

Figure 3.39 Whole year performance of three chillers from Table 3.9 and PVs from Table 3.10. 32% of total power consumed by chillers and cooling towers is covered by PV power.

3.4 Summary and Discussion

This chapter described the component and system models (SMs) of seven primary HVAC systems. To help with the orientation within the thesis, Figure 2.1 may be recalled. It shows that, with this chapter, the first major task of the simulator has been explained. The SMs were configured to develop a method of primary HVAC simulation for preliminary building design. Despite the large amount of undetermined system characteristics, the annual hourly performance was defined in order to account for the part load performance, energy storage and utilization of intermittent energy sources. The mathematical models of the featured generation and storage components were presented. This served as an introduction to the section handling the system simulation, which described the load allocation and control strategies. As a result the annual hourly performance profiles for the SMs were generated.

For further development and exploitation of the developed system models, validation and testing are required. The proposed methodology has been demonstrated and theoretically investigated using these seven system models. With this knowledge, further generation and storage components can easily be incorporated and new system models configured. Components such as ground, seasonal, and PCM (Phase Change Material) storage, heat pumps, absorption chiller and wind turbines are recommended as the additional generation and

storage components. In terms of system control, the strategies for all these components have been introduced through the currently featured ones and would require only minor modifications. In addition to that, and having the overall goal of system design optimization in mind, it would be interesting to develop one generic system model or a just a couple of them. This system would include all the generation and storage components, with the major challenge being the development of a suitable control strategy. Such a control needs to maintain the resemblance to a well-controlled realistic system, independent of the obtained system configuration. The illustration of this can be given based on the existing systems. For example, if solar collectors are added to the SM4, a new system would feature all components from both SM1 and SM2, as well as their control strategies. As a consequence, the optimizer, which will be described in chapter 5, could configure this new system to resemble any of its subsystems (e.g. SM1, SM2), depending on the imposed optimization goal imposed. Thus the major benefit of having a generic system model would be the automation of the system component selection, enabled by the developed optimization procedure.

The SMs can be simulated in parallel with the building simulation. In that case, the role of the remaining load is slightly changed. Its value should still be recorded to quantify the load satisfaction, but it should not influence the set load in the following timestep. The latter is due to the new set load coming directly from the building simulation iteration.

The results of the annual SM simulation are its performance profiles, which form a base for the further calculation. Firstly, these profiles enable the fuel consumption, running cost and RES utilization calculation to be made, and secondly, the quantification of the supply quality. Power, water, and fuel consumption define a significant fraction of the running costs. The transformation of the performance profiles, generated in the SM simulation, into costs and emission is shown in the following chapter.

4 Costs and Emissions

The economical aspect is the most important decision-making factor in the building sector. Costs and prices are a part of our everyday lives. We almost instinctively compare prices and consider alternatives. Due to the complexity of parameters that comprise the costs, the estimation and comparison of the heating and cooling equipment cost requires clearly defined calculation methodology.

Similar to other engineering applications, the basic purpose of the cost calculation method presented in this chapter is to compare alternative plant designs. In [62] the following engineering economy definition has been proposed: “Fundamentally, engineering economy involves formulating, estimating, and evaluating the economic outcomes when alternatives to accomplish a defined purpose are available. Another way to define engineering economy is as a collection of mathematical techniques that simplify economic comparison.” Hence, the calculation method must provide equivalence among costs calculated for systems consisting of different components, allowing the differences in component lifetime duration, energy consumption, maintenance requirements, etc.

Carbon emission reduction is one of the main requirements of government regulations and building certification systems. Therefore it is of interest to calculate how much of this greenhouse gas each of the systems emits during one year of operation.

This chapter begins with the description of the utilized cost calculation method. This is followed by defining the calculation of carbon emissions. Finally, the specifics of applying the presented calculation methods to system models are shown. The calculation of cost and emission values defined in this chapter is a preparation for their minimization, which will be presented in chapter 5.

4.1 Costs Calculation

There are a vast amount of references dealing with cost calculation methods, starting from generic methods, described in economy textbooks, to engineering oriented sources. The latter are based on the engineering experiences in cost calculation, which resulted in the adaptation of cost calculation methods for engineering problems. Several references offer identical methods but use different terminology, which is probably due to the country of origin and/or translation issues.

In [62] several models, techniques and tools from the field of engineering economy have been presented. Also highlighted in [63], a couple of these methods are suitable for comparing alternative designs:

- Present worth analyses: The costs are represented as their present moment equivalent. To perform the comparison the time frame for all compared systems needs to be identical. Intuitively, the investment cost is represented more clearly in such a method, since the running costs for the calculation duration have to be compounded;
- Annual costs: Also suitable for comparing alternative designs. The only difference to the previous method is that the due values are compared on an annual basis. Consequently, in this method the running cost is represented in a more natural way. The investment is partitioned in equal portions, which represents a case of paying of a loan.

Another method considered was the in the [64] described revenue requirement method. However, this method is suitable for detailed whole building cost estimation and it includes everything from the cost of purchased equipment, their installation, supervision, start-up, etc., to costs of research and development. Thus it cannot be used for preliminary design.

Similar cost calculation approaches can be encountered in the German national standards. For instance, the guideline VDI 6025 [65] provides comprehensive methods for economic calculations in heating system design. The guideline distinguishes between capital-linked payments, comprising the initial investment and annual maintenance costs, consumption-linked payments, such as energy and operating material consumption, operation-linked payments, covering everything from operation to insurance costs, and other payments not covered by the previously listed ones. The standard explains several methods: capital value, annuity, interest rates and amortisation methods. Another VDI guideline, VDI 2067 [66], uses the mentioned VDI 6025 as a base and addresses the fundamentals of economic efficiency for building installations. It provides useful data including component life duration and installation and maintenance costs. In addition, DIN EN 15459 [67] provides a standard economic evaluation procedure for energy systems in buildings.

For comparing alternatives, DIN EN 15459 provides two methods of cost calculation:

- Global cost, where all the costs are brought to a present value; and
- Annuity cost, where all the costs are represented by a uniform annual value.

These methods are, in fact, identical to those mentioned at the beginning of this section bearing somewhat different names. To avoid confusion, the terms and definitions adopted in the following sections are taken from this standard, DIN EN 15459.

Although, in fact, both the global and the annuity cost calculation methods are based on the same calculation method, the decision is made to use the annuity cost calculation in the rest of the thesis. The reason for this is the importance of energy consumption minimization. The amount of consumed energy seems more declarative if expressing the running cost as an annual value. It does not depend on the calculation period, apart from accounting for the assumed change in fuel price during that period, which can also be significant.

The adopted annuity method and, together with the utilized equations, is based on DIN EN 15459 [67] and VDI 2067 [66]. To summarize, the goal is to obtain an annual value, which accounts for all the considered costs, allowing the comparison of alternative designs over the same calculation period. It has been adopted that the total costs consist of:

- Investment costs (initial cost of equipment, its installation, and possible replacements depending on a life span of a component), and
- Running costs (maintenance and energy costs).

In order to define the annuity of these costs, the time value is introduced.

The implemented values for all the factors that are encountered in this chapter are given in Table B 7.

4.1.1 Time Value of Money

The same amount of money has different values at various points in time. Primary HVAC design considers observing the time spans in the range of a couple of decades. Consequently, the value of the payment made or due needs to be corrected taking the timeframe into consideration. Thus the terms present and future value are introduced.

The interest rates that rule the dynamics of the cost are inflation rate R_i, market interest rate R, and price development rate R_p, which takes the component price evolution into account. We use compound interest rates. This means that after each interest period (in this case one year), the interest amount is added to the principal to form the new principal for the next period. Inflation rates and market interest rates define the real interest rate R_R:

$$R_R = \frac{R - R_i}{1 + R_i} \tag{4.1}$$

Based on the point in time, an amount can be projected to any moment before or after that point using the following factors. The present value of a payment due in the future is obtained by multiplying the payment amount by the present value factor, $V_{present}$:

$$V_{present} = \left(1 + R_R\right)^{-T} \tag{4.2}$$

where T represents the number of years in the calculation period. Its inverse is the future value factor, V_{future}:

$$V_{future} = \left(1 + R_R\right)^{T} \tag{4.3}$$

which is used to multiply an amount in order to define its future value.

The annuity factor enables the distribution of costs that do not occur annually, such as investment costs, into equal annual portions over the calculation period. In such a way, a series of amounts due is formed, which can be presented either as a future or as a present value. In this thesis its present value is used. The annuity factor, a, is defined as:

$$a(T) = \frac{R_R}{1 - (1 + R_R)^{-T}} \tag{4.4}$$

It is the sum of the present value factors for each of the amounts from the series.

4.1.2 Investment Cost

Initial investment, C_i, is the price paid for the component itself at the moment of purchase, at the beginning of the calculation period. Initial investment price charts for relevant components can be found in Appendix B.

Installation costs can be assessed using the installation factor, f_{inst}, provided in [66], which represents installation costs as a percentage of initial investment. Therewith the investment cost at the beginning of the calculation period, C_0, is defined as:

$$C_0 = C_{ip}(1 + f_{inst}) \tag{4.5}$$

where C_{ip} represents the initial component purchase price.

If the calculation period goes beyond the component life duration, the component will be replaced. The component price at that time will differ from the initial one. This change is expressed through the price development rate, R_p, which enables the estimation of the component purchase price in the future. The new price is then brought back to the present moment using the real interested rate factor, R_R. Thus, the replacement costs C_r are the sum of all the necessary component replacements during the calculation period:

$$C_r = \sum_{j=1}^{\left\lfloor \frac{T}{T_{life}} \right\rfloor} C_{ip}(1 + R_p)^{T_{life} j}(1 + R_R)^{-T_{life} j} \tag{4.6}$$

where T_{life} is the component life duration and T is the calculation period.

If the end of the calculation period is not coincident with the end of the last installed component life duration, that component still has a certain value at the end of the calculation period. This is a final value of the component and it needs to be subtracted from the previously calculated costs in order to assess the actual investment costs relevant for the imposed calculation period. A final value is determined using linear depreciation of the price for the last replacement, taking the price development into account, indicated with the dotted line in Figure 4.1. The value obtained at the end of the calculation period is then discounted to yield its present value. It represents the present value of the final value, V_{final}:

$$V_{final} = C_{ip}(1 + R_p)^{T_{life} \cdot \left\lfloor \frac{T}{T_{life}} \right\rfloor} \cdot \frac{T_{life} - T}{T_{life}}(1 + R_R)^{-T} \tag{4.7}$$

The resulting investment cost, C_i, is:

$$C_i = C_0 + C_r - V_{final} \tag{4.8}$$

4.1.2.1 Investment Cost Calculation Example

In support to the previous explanation, a graphical example of the investment cost calculation is provided in Figure 4.1. The example deals with purchasing a single component and using it for the time period T. The objective is to calculate the present value of the investment cost.

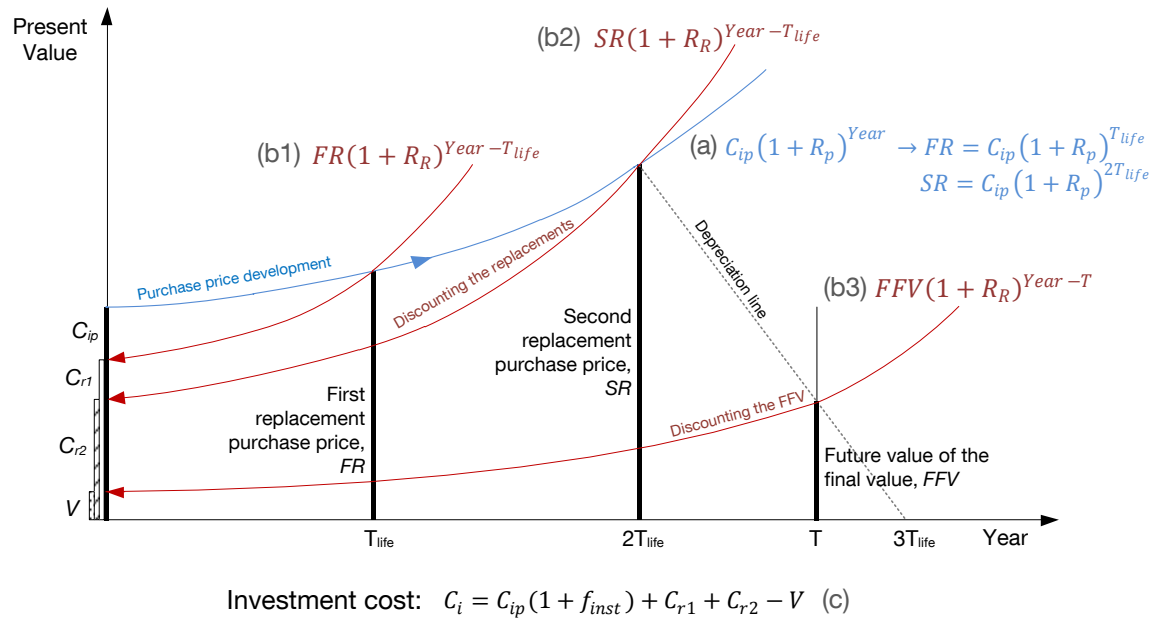

Investment cost: $C_i = C_{ip}(1+f_{inst}) + C_{r1} + C_{r2} - V$ (c)

Figure 4.1 Example of assessing the present value of the total investment in the case of purchasing a component with an initial investment cost C_{ip}, that requires two component replacements during the calculation period T. The life duration (T_{life}) of the second replacement exceeds the period T, yielding a final value that needs to be discounted.

The cost of the initial purchase is known, C_{ip}. Using the installation factor f_{inst}, the investment cost of the component at the beginning of the calculation period can be calculated, as shown in equation (4.5). Since the required component operation period is more than two, and less than three times longer than the life duration of the component, in addition to the first purchase, two replacements are needed. Knowing the current purchase price, C_{ip}, and the price development rate, R_p, the purchase prices of these replacements can be calculated following the blue "Purchase development" curve and using equation (a). These values are named FR for the first and SR for the second replacement. The resemblance of the equation (a) with the first two factors from the equation (4.6) can be noticed.

The FR and SR represent the purchase prices in the future and thereby need to be discounted in order to determine their present value. The illustrated red curves, entitled "Discounting the replacements", need to be followed to the present moment, where "Year" equals zero, in order to define the present value. Mathematical formulation of this is provided by equations (b1) and (b2). If setting Year=0, the equations (b1) and (b2) become identical as the third and the last factor in (4.6). Now the present values of the replacement costs, C_{r1} and C_{r2} are known.

The last value that needs to be calculated is the final value. Namely, after the period T is over, the second replacement still carries a certain value. The “Depreciation line” illustrates how the future value of the final value is obtained using linear depreciation. As with the replacement costs, this value is discounted to the present time using (b3).

The sum of the first component investment, together with its installation cost, and the present values of the costs for the two replacements, needs to be reduced for the present value of the final value to finally yield the investment cost. This is expressed by the equation (c), which is equivalent to the equation (4.8).

4.1.3 Investment Cost Annuity

Using the annuity factor *a*, equation (4.4), the investment costs are partitioned into annually due amounts, expressed as their present value ([66], page 9):

$$AC_i = a(T)C_i \tag{4.9}$$

4.1.4 Running Cost Annuity

Running costs include energy, C_e, and maintenance costs, C_m. The energy cost C_e is a sum of products of the consumed energy amounts, CE, and their prices, EP, for all utilized energy carriers.

$$C_e = \sum (CE \cdot EP) \tag{4.10}$$

The calculation implemented in the tool enables conversion of energy prices given in units other than €/kWh into that unit.

Since it cannot be expected for the fuel and electrical energy prices to stay constant over the calculation period, the dynamic present value factor β_x is introduced:

$$\beta_x = \frac{1 - \left(\frac{1 + R_{px}}{1 + R}\right)^T}{1 - \left(\frac{1 + R_i}{1 + R}\right)^T} \cdot \frac{\frac{R - R_i}{1 + R_i}}{\frac{R - R_{px}}{1 + R_{px}}} \tag{4.11}$$

where R_{px} is a price development rate for a given good. Annual maintenance costs are approximated as a small fraction (β_m) of the initial component purchase price. Thus the average annual running costs during the given calculation time can be expressed as:

$$AC_r = C_e \beta_e + C_{ip} \beta_m \tag{4.12}$$

where β_e is the dynamic present value factor for each of the utilized energy carriers.

4.1.5 Total Cost Annuity

The total costs due in yearly intervals, AC_t, equal the sum of the investment annuity and the running costs:

$$AC_t = AC_i + AC_r \tag{4.13}$$

The annual cost defined in this way is the average annual cost in the year 0, as in [67].

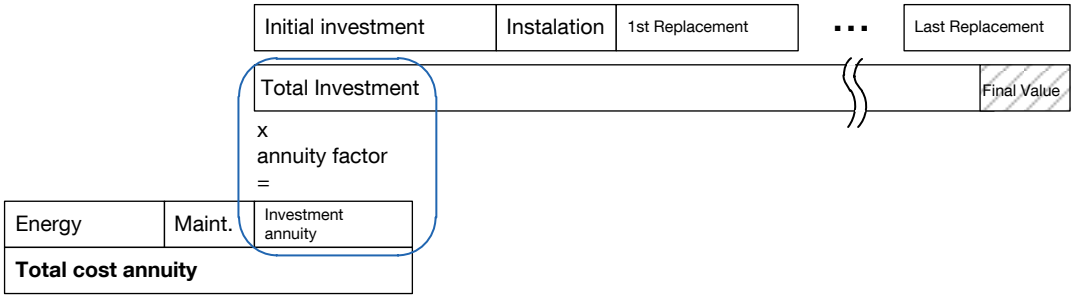

Figure 4.2 A summary of the cost calculation method through a schematic representation of the cost classification.

4.1.6 Assumptions and Simplifications

Interest rates and other dynamic cost calculation parameters are considered to stay constant during the calculation period. Risks and uncertainties related to the future costs are neglected. Since the system models presented in the previous chapter consist of components for energy production, conversion and storage, only these components are taken into account while calculating investment, installation and maintenance costs. The costs for piping, valves and other armatures, pumps etc. are assumed to be equal for all the alternatives and thus do not play a role in the comparisons. Taxes and insurance have also been neglected.

4.2 Carbon Emission Calculation

Of all considered components, those that generate carbon emissions during operation are boilers, chillers and, in small amounts, cooling towers. How much carbon is emitted by a boiler depends on the chemical composition of a fuel burned, the amount of consumed fuel and the quality of the combustion process. In the empirical models, presented in 3.2.3, the latter influence is accounted for within the boiler efficiency. The chillers and cooling towers cause carbon emissions through the consumed electric power. Annual carbon emission equals the sum of emissions obtained from all utilized energy carriers:

$$E_{CO\,2} = \sum (CE \cdot SE) \tag{4.14}$$

where *SE* is the vector of specific emissions in kg/kWh. Fuel specific emission units are converted to kg/kWh.

Fuels currently featured in the tool are wood pellets, gas and oil. Their emission data is given in Table B 8. The environmental benefits of burning pellets with their 0.04 kg CO_2 per kWh compared to fossil fuels are obvious. However, the efficiency of condensing boilers advances significantly compared to biomass burning boilers. Moreover, the gas combustion in modern boilers is a very efficient combustion process. This is due to the optimal fuel to air ratio, their good mixing and the chemical composition of the gaseous fuel. This puts gas, the most common condensing boiler fuel, with its emissions of 0.277 kg/kWh, in front of all other fossil fuels in terms of the quality of combustion products. Oil consumption is the least ecological of the three, not only due to the highest specific CO_2 emissions of 0.33 kg/kWh, but also due to its sulphur content and NO_x emission.

Electric power related emissions for four demonstration cities are given in Table B 9. Their value depends on the power plant portfolio of the related country.

Further emissions such as carbon monoxide, particles or NO_x are not accounted for within the implemented boiler models, since the analyses of these values has little meaning for the conceptual design phase. The level of detail of the models implemented could only provide their coarse approximation.

4.3 Application to System Models

This section begins with the explanation of the initial investment (C_{ip}) for the components utilized within system models and references the utilized price curves. Afterwards, it clarifies how the fuel and utility costs are assessed.

4.3.1 Component Price Assessment

The most reliable way to obtain valid price information is to request a quotation from the vendor. However, this is not necessarily something a designer intends to do in the conceptual phase. At that point one just needs a quick comparison for alternative solutions. Consequently, the price curves of the components from section 3.2 can be defined by:

- Regressing the vendor provided data; or
- Using regression curves identified in literature.

An example of obtaining the price function by vendor data regression is shown in Figure 4.3.

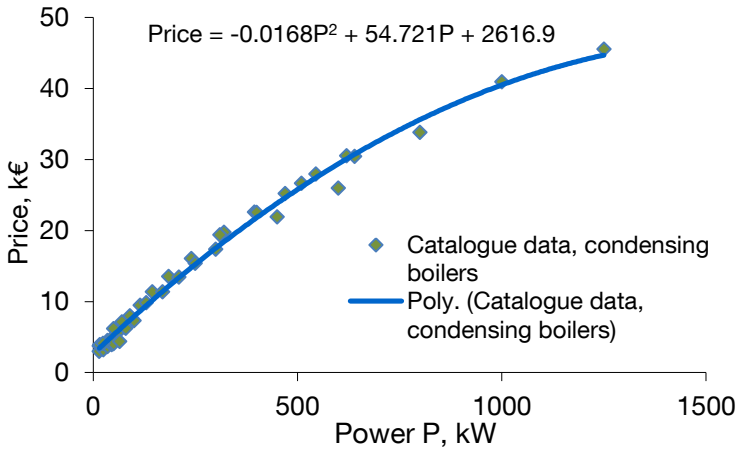

Figure 4.3 Price function obtained using vendor price data for gas fired condensing boilers.

Appendix B provides the obtained initial investment curves in analytical and graphical form and references the data sources.

Solar Collector price is a linear function of the gross collector area, Figure B 3. The price increase is steeper for evacuated tube than for flat plate collectors.

Photovoltaic modules are priced per installed peak power. Implemented value is given in Table B 11. Boiler prices are a function of component design power.

Biomass boilers are represented by a pellet boiler. The price function is a linear regression of the vendor data, see Figure B 5. Same figure shows a quadratic function representing the price of **condensing boilers**.

Figure B 4 provides a cost function for two **thermal storage** types. The first is the combination storage tank used in models containing solar thermal collectors. The cost function is logarithmical. The second type is a simple buffer storage tank. The cost determining variable is the tank volume.

The price functions of **vacuum compression chillers** and **cooling towers** are both given in Figure B 6. Chiller prices are a function of component design capacity.

The mentioned and referenced curves represent the preset values implemented in the tool. Nevertheless, there are cases where a price curve customization might be demanded. It would enable investigation of the sensitivity of the optimal design to the change in initial component prices. A customized price might be demanded if the component performs a special task or in case a user simply decides to improve the solution by using location adjusted and up-to-date data. If difficulties with the component price search exist and the price for one component size is known (C_{known}), [64] suggests using the following price estimation for the unknown sizes ($C_{unknown}$):

$$C_{unknown} = C_{known} \left(\frac{Size_{unknown}}{Size_{known}} \right)^{m} \tag{4.15}$$

and provides a number of m values. If m is unknown, a value of 0.6 may be used (six-tenths rule).

4.3.2 SM Fuel Consumption and Utilities

After determining the energy consumption of the system, the annual cost of energy can be calculated according to (4.10). Energy consumption is defined as fuel and electrical energy consumed by SM components. The values of these consumptions are available after performing the annual SM simulation. The amount of consumed energy depends on the efficiency of the utilized conversion devices, SM configuration and the implemented control, building location and load imposed. Consumed energy, *CE*, is a vector holding the annual consumption of each component. The same value is used to calculate the total annual carbon emissions, see (4.14). Currently implemented fuel and power consuming components include gas, pellet and oil boilers, vacuum compression chillers and cooling towers. Additionally, systems incorporating the last two components consume significant amounts of water, whose cost is also included in the annual running cost of the SM.

4.3.2.1 Fuel Consumed

The fuel consumed by boilers is relevant for energy cost and emission assessment of systems SM1 to SM4.

At each simulation timestep the boiler model is assigned a control signal, which determines the PLR within that step. That value is passed to equation (3.14) to calculate the fuel consumption of all implemented boilers at each timestep (*FC*). Consequently, at the end of the annual hourly simulation the profiles containing 8760 fuel consumption values are formed. A vector of annual energy consumptions *CE* is thus a sum of those hourly values for each of the boilers:

$$CE = \sum_{t=1}^{8760} FC(t),\ kWh \tag{4.16}$$

As a reminder, the vector form of *CE* is needed, since different fuel can be used by each of the boilers.

4.3.2.2 Power and Water Consumed

Electric power is consumed by VC chillers and cooling towers and produced by PV panels. Wet cooling towers are also water consumers. Thus power and water consumption need to be accounted for in SM6 and SM7.

At each timestep, equations (3.6), (3.10) and (3.26) define chiller and cooling tower power consumption and PV power generation, respectively. Similar to fuel consumption assessment, appropriate SM simulation defines hourly profiles of power consumption and generation. In return, the profile that needs to be bought from the grid, P_{el}, is:

$$P_{el} = \left| P_{el,ch} + P_{el,ct} - P_{pv} \right| \tag{4.17}$$

while its negative part can be sold to the grid in case the needed infrastructure and feed in tariffs exist at the location, see Table B 9.

To assess power related carbon emissions the annual power consumption obtained by summing up all the hourly values of the power consumption profile is used. In the case where feed-in tariffs exist, the annual electrical energy sold to the grid is deducted from the annual power consumption obtained. The result is multiplied with the specific emissions for the location, Table B 9, to obtain the annual electric power related carbon emission. Somewhat more complex is the utility cost assessment, due to the power and water tariffs. Table B 10 shows how those prices depend on the monthly consumed amounts. Thus the annual price of power and water consumed is calculated by multiplying the monthly consumption with the appropriate price and adding all resulting monthly costs together.

4.4 Summary and Discussion

This chapter described the method utilized to calculate the SM related costs and emissions, thereby covering the second task of the simulator, as illustrated in Figure 2.1. The annuity cost calculation method has been selected. In this method, the investment related costs are represented as the present value of the series of annually due values, according to a given time frame. Apart from the cost of the energy consumed, running costs include the maintenance expenses. Finally, these two cost categories, the investment and the running cost annuity, formed the total cost annuity. The component-specific investment price functions for all the utilized components were obtained using data regression. The annual energy consumption does not only relate to costs, but also to carbon emissions. They were calculated depending on the utilized energy carrier and related specific emissions.

The annuity method was selected since it is suitable for comparing alternatives, where both investment and running costs are relevant. It is interesting to observe the relationship between the annual consumption related cost and the annualized investment. While comparing alternatives, the difference in annual running cost is available on an annual level, providing information on potential savings. Nevertheless, once the basics of the cost calculation have been implemented, the method could easily be converted into, for instance, the global cost method. Such a calculation would yield the present value of the investment, while the running costs would be summed for a given timeframe. In principle, these two calculation methods are the same. The decision as to which method is more practical depends on the type of financing of a concrete project.

The limitations of the cost calculation method are as follows. Until all the details regarding the plant design have been defined, it is only possible to make cost estimations. Only after all the assumptions of such estimations are known, can the quality of the cost calculation result be judged. How detailed this estimation should be depends upon the purpose of the calculation. The cost calculation implemented in the SM simulator only accounts for the generation and storage component investment and replacement costs, and energy and water consumption cost. The models could be extended to comprehend more detailed cost categories, if the utilization for other than preliminary building design would be intended. The

cost functions, fuel prices and rates should be maintained in order to remain up to date, and new cost data amended in case of adding further models to the tool.

If recalling the Figure 2.2, a scalar value is assigned to consumption, emissions and costs after each SM simulation described in the previous chapter. Following the flowchart, the further purpose of these values is to define the objective functions for the optimization. The next step toward design optimization is to form the penalties and optimization objectives.

5 Optimization

Design optimization is a process of identifying system component sizes, which lead to a decrease in cost, emission or fuel consumption, while maintaining satisfactory system performance. This section begins with the explanation of the optimization problem. It continues with the mathematical formulation of the introduced problem, which is followed by the description of the optimization methods used to solve it. These methods are then evaluated by showing optimization examples for each of the SMs. The examples represent the complete model functionality introduced in chapter 2.

5.1 Optimization Problem

The performance of the primary system is evaluated in chapter 3. SM performance profiles resulting from the simulation provide states and efficiencies of components for each of the simulation timesteps. Energy consumption and emissions are determined using these profiles and form a basis to calculate the costs, as described in chapter 4. Thus the annual fuel consumption, emissions, and costs are defined after each simulation run. These values are used to form the goals for design optimization. The optimizer is set to identify the most, or most closely suitable combination of system component dimensions to minimize any of the following:

- Total costs;
- Investment costs;
- Energy consumption (fuel and electricity); and
- CO_2 emissions.

Total cost minimization has the goal to achieve the smallest possible cost annuity, defined in (4.13). Total cost is defined as a sum of running (4.12) and investment (4.9) cost, so its minimization provides a trade-off between these two goals. It can be seen as a multi objective optimization with running and investment cost as its two goals. Here is a descriptive representation of the total cost, AC_t:

$$AC_t = f(\text{prices, rates, lifetime, performance}) \tag{5. 1a}$$

In most cases, systems with lower investment will have higher running costs. Some of the causes are that solar energy converters are still expensive, or that cheaper boilers and chill-

ers have lower efficiency and thus higher fuel consumption and emissions. With any change in investment or running costs the optimum is shifted to the corresponding direction. Significant changes in fuel price or maintenance factors will usually lead to investing in better equipment. If the initial cost or the rates of the equipment investment increase, the optimizer will allow the higher annual running costs caused by lower equipment quality.

Completely disregarding the negative environmental impact, the investors often simply target the lowest investment cost. This is not helped by the running costs usually being the responsibility of the third party tenant rather than the investor. It should be noted that the investment cost used by the optimizer equals the annuity containing the replacement cost and the final value. The investment cost, AC_i, is here described as:

$$AC_i = f(\text{prices, rates, lifetime}) \tag{5. 1b}$$

Energy consumption could be an interesting goal for a building operator. The total energy consumed, CE_{sum}, can also be minimized:

$$CE_{sum} = f(\text{energy carrier, performance}) \tag{5. 1c}$$

In order to achieve this, the values of all the consumed energy carriers are calculated in kWh.

If the cost is disregarded in order to identify a design with minimal environmental impact, emissions (eq. (4.14)) will be minimized:

$$E_{CO2} = f(CE_{sum}) \tag{5. 1d}$$

Energy consumption minimization will yield the same result as the CO_2 emission minimization where only one energy carrier is used. Both goals lead to maximized utilization of renewables.

If returning to Figure 2.2 one can notice these four goals at the bottom part of the optimizer, each value being connected to the objective function by a dashed line.

No matter which of these goals is imposed on the design optimization, the primary task of the SM must be fulfilled. The optimal design needs to provide sufficient coverage of the building heating or cooling loads in order to maintain user comfort. The quality of the supply depends upon how well the system performs in each of the timesteps. This is an essential constraint for the design optimization. Another interesting goal, apart from satisfying the demand, is to achieve an imposed solar ratio, defined as the fraction of solar generated in the total delivered/consumed energy. The user can input a target solar ratio which constrains the possible designs to those satisfying this target. This constraint applies exclusively to SMs utilizing solar energy.

Primary HVAC component dimensions can significantly influence building architecture. The most obvious examples are PV panels and solar collectors, which need to be planned very early in order to achieve both satisfactory BEP and building esthetics. For example, by deciding on the maximum allowable area reserved for harvesting solar energy, the architect defines the upper bound for the dimensions of PV panels or solar collectors. Another limitation in dimensioning is posed by technological limitations, e.g. centrifugal chillers are usually not manufactured in capacities lower than 350 kW. Where the evaluat-

ed SM contains such a chiller, this number becomes the lower bound for the feasible set of component dimensions. Component dimensions clearly too big or too small for the given load are also dismissed, which forms additional bounds. All the previously mentioned bounds are overlapped to yield a final set of bounds.

The sections below provide a more precise mathematical definition of the stated optimization problem and describe algorithms implemented to resolve it.

5.2 Mathematical Formulation of the Problem

In general, a continuous optimization problem can be written as:

$$\text{minimize } f(x),\ x \in \mathbf{R}^n \quad \text{subject to} \quad \begin{cases} g_k(x) \le 0, & k = 1, \dots, p \\ h_j(x) = 0, & j = 1, \dots, q \\ \underline{x}_i \le x_i \le \overline{x}_i, & i = 1, \dots, n \end{cases} \tag{5.1}$$

where x is a vector of optimization variables and $f(x)$ is the objective function. $g(x)$ and $h(x)$ respectively stand for inequality and equality constraints, while $\underline{x}$ and $\overline{x}$ are vectors of the lower and the upper bound. Together, they define the feasible domain of optimization variables.

In the given design optimization problem, the optimization variables are: the boiler and chiller capacities, storage volume and maximal discharge rate, and solar thermal collector and PV panel areas. The exact set of optimization variables is SM specific. Each of the four mentioned goals defines an objective function subjected to optimization. The set of optimization variables that minimizes the chosen objective function under the given constraints, characterizes the corresponding optimal design.

5.2.1 Handling Constraints

In engineering the majority of optimization problems are subject to problem-specific technical or physical constraints. In dealing with the stated optimization problem, the optimization constraints are reformulated into penalty functions, which are added to the objective function, transforming the constrained into an unconstrained optimization problem. By using penalty functions, the objective is assigned with values across the optimization parameter domain, as opposed to having no values at those parts of the domain where the constraint is breached. Consequently, by observing the values of a single function, the quality of all relevant optimization parameter combinations can be evaluated. Moreover, problem-specific penalty definitions give physical meaning to the penalty coefficients used. It provides two degrees of objective function evaluation. Firstly, its activation signals constraint violation and, secondly, its value shows how severe this violation is.

As mentioned, all SMs are intended to supply enough energy during each timestep to satisfy the demand. If minimizing any of the objective functions without stating a supply satisfaction constraint, all the component dimensions would simply become zero and yield zero costs, emissions and fuel consumption. In order to ensure good system performance, a supply task constraint is introduced. It is based on comparing each timestep's demand and delivery. The constraint limits the number of instances where the system is permitted to deliver less than a certain percentage of the timestep's set load. To simplify the explanation, the timestep is set to one hour. The supply constraint can be written as:

$$\sum_{t=1}^{8760} C(t) \le C_{SuP}, \quad \text{where} \quad C(t) = \begin{cases} 1, & \frac{D(t)}{L(t)} < R_{SuP} \\ 0, & \text{otherwise} \end{cases} \tag{5.2}$$

where $C(t)$ is a counter of undersupply timesteps, C_{SuP} is their maximal allowed number, and R_{SuP} is the ratio of the delivered to the set load. Counter $C(t)$ is counting the instances of supply shortcomings. If for example C_{SuP}=8 and R_{SuP}=0.9, the equation can be interpreted as: a maximum of 8 hours a year is a system allowed to deliver less than 90% of its set load. Otherwise, the given configuration is proclaimed as inadequate. The functioning of this constraint is closely connected to the remaining load, first introduced at eq. (3.31). Although 90% is significantly less than 100%, by the definition of the model performance, a constant consecutive underproduction is not possible. Namely, the remaining load will keep accumulating and thus increasing the set load, (3.32), where the system cannot satisfy the load in consecutive timesteps. This will eventually cause counter activation, even if the initial set load for the timestep was not too high. Due to the shape of a realistic building heating or cooling demand profile, if there is an instance during the day where the demand is slightly higher than the system capacity, the sum of the remaining and next hour's set load often remains well inside the feasible delivery. Such an instance will not activate the counter unless the deficit was higher than 10% (same example). This is justified by the fact that, in an actual building, a competent control system could increase the delivery in the previous hour and thus yield the same energy consumption and avoid impairing the comfort. So where the constraint has not been breached in the example given, it means there were less than 8 occasional peaks that were not completely satisfied, causing not more than 8 hours a year of slightly impaired comfort. To summarize, the two parameters C_{SuP} and R_{SuP} have the following physical meanings:

- Permitted number of undersupply timesteps, C_{SuP} – shows how many hours a year is the user of the building space allowed to feel some discomfort;
- Delivered vs. set load ratio, R_{SuP} – the higher this ratio is set, the lower the user discomfort is during the counted hours. Its basic purpose is to avoid dimensioning based on the rare demand peaks.

The penalty function to be added to the objective if the supply task constraint is violated is defined as:

$$SuP = \begin{cases} p_{SuP} \sum_{t=1}^{8760} RL(t), & \sum_{t=1}^{8760} C(t) > C_{SuP} \\ 0, & \text{otherwise} \end{cases} \tag{5.3}$$

where *SuP* represents the value of the supply penalty, p_{SuP} is a supply penalty coefficient and *RL* the remaining load. The supply penalty is proportional to the sum of remaining loads representing a measure of constraint violation. Consequently, such a definition allows comparison of a supply quality for systems that have breached the constraint, since the sum of remaining loads increases with the decrease in the supply quality. The stiffness of the penalty can be influenced by changing the following value:

- Supply penalty coefficient, p_{SuP} – defines the severity of the penalty. This value is selected with regard to the order of magnitude of the remaining load and the goal function should be considered.

Figure 5.1 illustrates the activation of a supply penalty formed during the first two weeks of SM2 yearly performance. Due to the capacity shortage the remaining loads start to accumulate. Already at the beginning of the second week the set C_{SuP} is reached, which activates the penalty. The supply penalty parameter in the example is 0.5. The scalar value added to the objective functions is the penalty value at the end of the year.

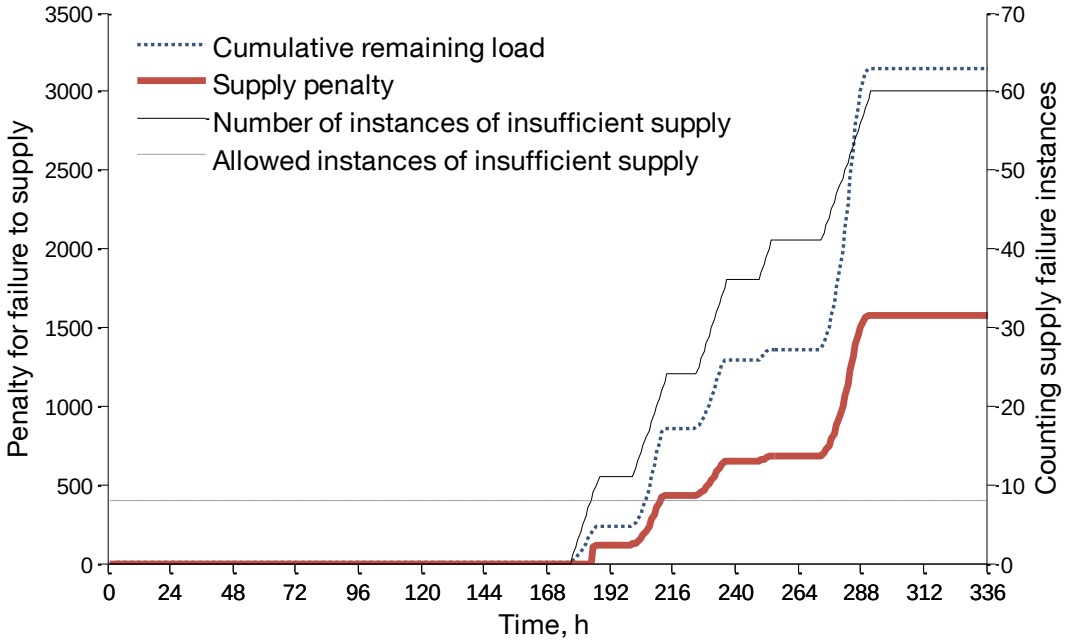

Figure 5.1 SM2 with 10 kW and 20 kW condensing boilers supplies an "S" building in Moscow. Since these design powers are insufficient, the constraint is violated and the value of the penalty function keeps increasing.

Another constraint exists in SM comprising a solar thermal collector or PV panels. It limits the component dimension combinations to those yielding a desired solar ratio.

$$SR \geq SR_{\text{target}} \tag{5.4}$$

where the solar ratio *SR* is defined as follows:

- In the case of solar collector utilization as:

$$SR = \frac{\sum_{t=1}^{8760} SG(t)}{\sum_{t=1}^{8760} D(t)} \tag{5.5}$$

- In the case of PV power generation as:

$$SR = \frac{\sum_{t=1}^{8760} \left(P_{pv}(t) - k_{noFeedIn} \cdot P_{feedIn}(t)\right)}{\sum_{t=1}^{8760} \left(P_{el}(t) + P_{el,ct}(t)\right)} \tag{5.6}$$

where, SG is the annual solar gain profile, D is the SM delivery profile, P_{pv}, P_{el}, $P_{el,ct}$ and P_{feedIn} are the power generation and consumption profiles. Only the own consumption of PV generated power is taken into account in case the grid feed-in is not possible ($k_{noFeedIn}$=1, otherwise 0).

The solar constraint is redefined in the form of a solar penalty function, which is activated when the solar ratio is lower than its set value and scaled by the inverse of the solar ratio:

$$SoP = \begin{cases} \frac{p_{SoP}}{SR}, & SR < SR_{target} \\ 0, & \text{otherwise} \end{cases} \tag{5.7}$$

where SoP is the solar penalty and p_{SoP} is the solar penalty coefficient.

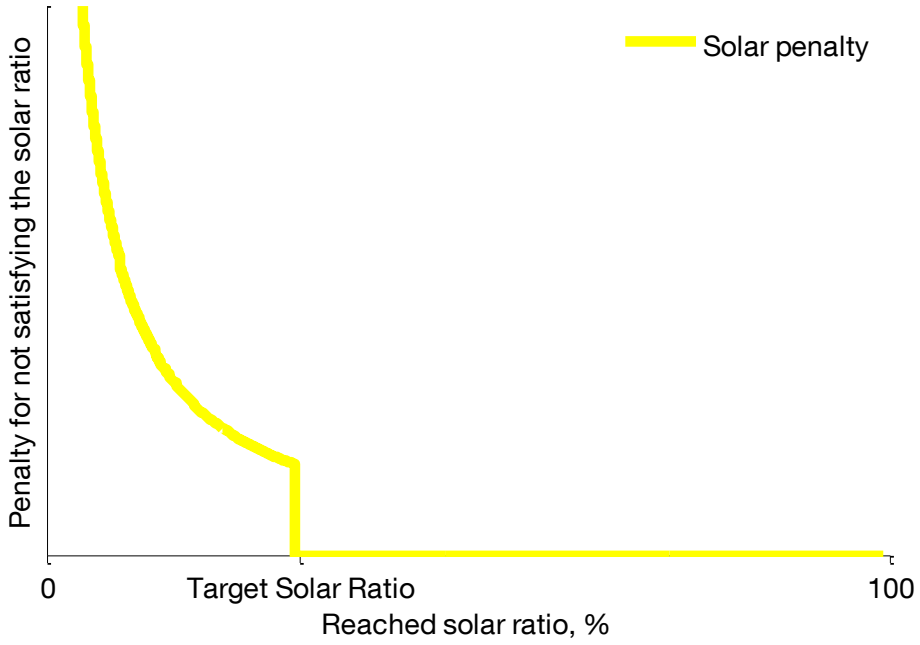

Figure 5.2 Solar penalty function is an inverse of the actually reached solar ratio. Its value equals 0 if the target solar ratio is reached.

Figure 5.2 shows how the value of the solar penalty depends on the solar ratio reached by the SM simulation. If activated, the penalty forms a barrier whose height depends on the

solar penalty coefficient p_{SoP}. The value of p_{SoP}, applied in the tool, ensures the penalty is much higher than the cost of PV or collector area increase. However, the firm limits (the user defined maximal available surfaces to place the mentioned components) can force the penalty activation.

The implemented supply and solar penalty parameters are heuristic values satisfying the given level of investigation. These parameters weight the penalty terms and define their strictness.

A special case of constraints are the optimization variable bounds. The bounds are set by the SM optimizer based on technical limitations and following user inputs:

- The choice of SM;
- The provided load profile;
- The areas available for solar thermal collector or PVs.

The process of setting the bounds (upper right part of Figure 2.2) is followed by starting optimization algorithm, which begins with proposing a combination of optimization variables within the bounds and evaluating the objective function based on simulation results.

5.2.2 Objective Function

Adding the penalties to each of the goal functions from section 5.1 yields final objective functions:

$$OF_1 = AC_t + SuP + SoP \tag{5.8a}$$

$$OF_2 = AC_i + SuP + SoP \tag{5.8b}$$

$$OF_3 = CE_{sum} + SuP + SoP \tag{5.8c}$$

$$OF_4 = E_{CO2} + SuP + SoP \tag{5.8d}$$

where OF_1 to OF_4 represent the objective functions. These functions subject only to variable bounds, while other constraints are represented by described penalties. In such a way, the problem is formulated as a bounded unconstrained optimization problem. Basic graphical representation of forming the objective function is given in Figure 5.3.

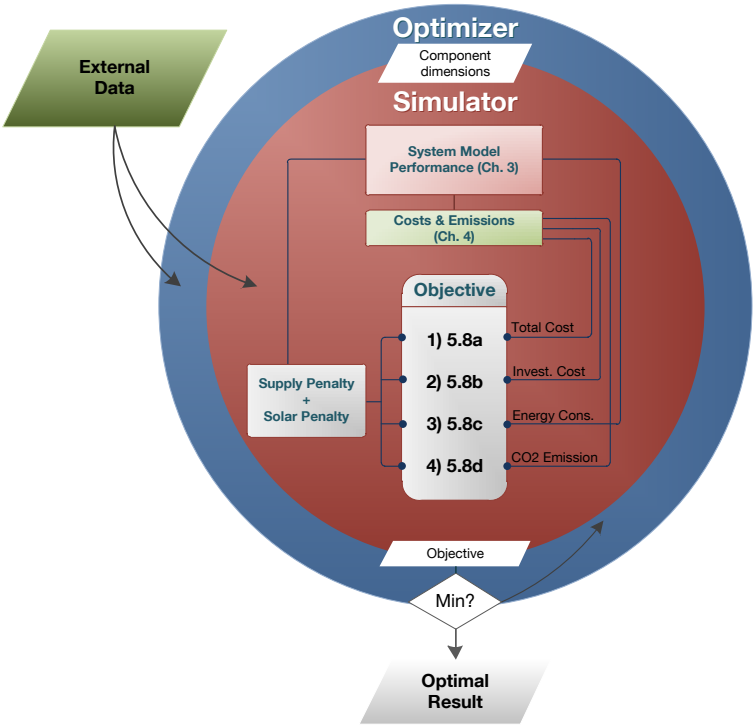

Figure 5.3 Schematic representation of defining objective functions by simulation.

5.3 Optimization Methods

The optimization method is selected based on the properties of the objective function and constraints. The presented objective functions are not analytical functions but the result of a simulation process. In general, the objectives are discontinuous, non-linear, non-differentiable and non-convex functions. Consequently, a problem solver is a zero order n-dimensional optimization method. In current SMs the number of optimization variables remains under 10. Even more complex SM configurations will maintain this order of magnitude.

A good introduction into optimization of energy related processes can be found in [68]. Several suitable algorithms are available in GenOpt, [30], which is a generic optimization program that can minimize a function evaluated by an external simulation program. As stated in [30] “Evaluating the cost function requires much more computation time than determining the values for the next iterate”. In the optimization process the simulation becomes a single iteration of the optimization algorithm. The objective here was to identify a method suitable for solving the introduced problem rather than to elaborate all possible methods. If approximating the solution using a simulation procedure, often a combination of methods or a significantly modified method is used. Nielsen in [69] provides an overview of previous studies in optimizing in the field of BEP simulation and implements direct search simulated annealing (DSA) to optimize the building design considering the

life cycle and energy costs. In his thesis Geidl, [23], uses commercial Matlab, Tomlab and Knitro solvers to deal with convex and non-convex mixed-integer linear programming problems in order to choose optimal layout and dispatch of a multi-energy system. The optimal upgrade of a power plant layout has been calculated in [70] using genetic algorithm. Kuhn, [71], has optimized the power plant and storage layout using linear programming.

Due to many simplifications introduced in the system performance, the simulation result represents only an approximation of the real system performance. The level of accuracy was kept in mind while deciding on the optimization method. Two methods were identified as robust enough to provide satisfactory solution of the introduced problem and allow complete freedom in further model development. The first algorithm is one of the sequential simplex methods, the globalized and bounded Nelder-Mead method (GBNM), as implemented in [72]. The second one is a simple exhaustive search method. Both evaluate only the function values and not its derivatives. The following sections describe these two methods and their successful implementation within the tool.

5.3.1 Globalized and Bounded Nelder-Mead Method

The Nelder-Mead algorithm belongs to direct search methods - it only evaluates the function value and not its derivatives. Consequently, this algorithm is popular for engineering applications and especially so for simulation defined objective functions sometimes referred to as “black-box” problems.

The original Nelder-Mead (NM) algorithm, as first presented in [73], performs unconstrained local optimization of a discontinuous, non-convex function by performing operations on an n-dimensional simplex. [74] describes sequential simplex methods and lists numerous applications in the field of chemistry. To extend its capabilities, several additions and modification to the original algorithm have been proposed. In [30], both O’Neill’s and additional stopping criterion modifications are implemented to improve algorithm performance in dealing with large objective function discontinuities, common in the building energy simulation field. Luersen et Le Riche [75] added modifications to account for optimization variable bounds and globalized the search using probabilistic restarts, forming a globalized and bounded Nelder-Mead method (GBNM). Due to its robustness concerning the properties of the objective function, GBNM is a suitable algorithm for the optimization problem presented here. It can be used for the design optimization of all SMs in their current formulation and it leaves space for the modification of existing and any additions to the components and systems.

The GBNM algorithm modification adopted here is almost identical to the one proposed in [75], as implemented and tested by Dorfner in [72]. The difference refers to convergence criteria, which are inherited from [72]. The constraints are already formed as penalty functions to enable the problem to be treated as unconstrained, as required by this method. The variable bounds are taken into account by projecting the variables on their bounds in case the variable tries to leave the domain. The Nelder–Mead local searches are repeated from different points distributed across the domain. These local searches end by detecting the

local minimum or simplex degeneration. Ending points and simplices are analyzed and saved, followed by a local search reinitialization, relying on probability density of the previously used starting points. A sufficiently high number of restarts will both enable the identification of the optimum near enough to the global one, and allow the analyses of the local optima.

The Nelder-Mead method is based on comparing values of the objective function f: $\mathbf{R}^n \rightarrow \mathbf{R}$ at each of the $n+1$ vertices of an n-dimensional simplex. It is practical to visualize the NM algorithm steps for a two-dimensional problem, since it yields a triangular simplex. Such an illustration is given in Figure 5.9.

Let us denote simplex vertices by $x_i, x \in \mathbf{R}^n$, where $i = 0, \ldots, n$ are the indices of $n+1$ vertices and the dimension of each vertex is equal to the number of optimization variables, n. Based on the given initial vertex, x_0, the remaining vertices of the initial simplex are calculated as:

$$x_i = x_0 + pe_i + q\frac{1}{n}\sum_{\substack{k=1 \\ k \neq i}}^{n} e_k, \quad i = 1, \ldots, n \tag{5.9}$$

where e_i are the unit coordinate vectors, while p and q depend on the size of the simplex, a:

$$\begin{aligned} p &= \frac{a}{n\sqrt{2}}\left(\sqrt{n+1} + n - 1\right) \\ q &= \frac{a}{n\sqrt{2}}\left(\sqrt{n+1} - 1\right) \end{aligned} \tag{5.10}$$

The recommended simplex size a is a random number lying within 2% to 10% of the smallest optimization variable range.

Once the simplex is initiated, the Nelder Mead algorithm can begin evaluating the objective function values at each vertex. Upon that evaluation, the vertex with the worst objective function value is replaced by its reflection, followed by an expansion or contraction. The vertex keeps stepping through the domain approaching a local minimum until the convergence criteria is satisfied. Where any of the vertex dimensions steps out of the domain, its value is projected on the bound:

$$x_i = \begin{cases} \underline{x}, & x_i < \underline{x} \\ \overline{x}, & x_i > \overline{x} \end{cases} \tag{5.11}$$

The steps of the NM algorithm are presented in detail in the following figure (in black). Projection on the bound (5.11) is performed at each reflection and expansion step.

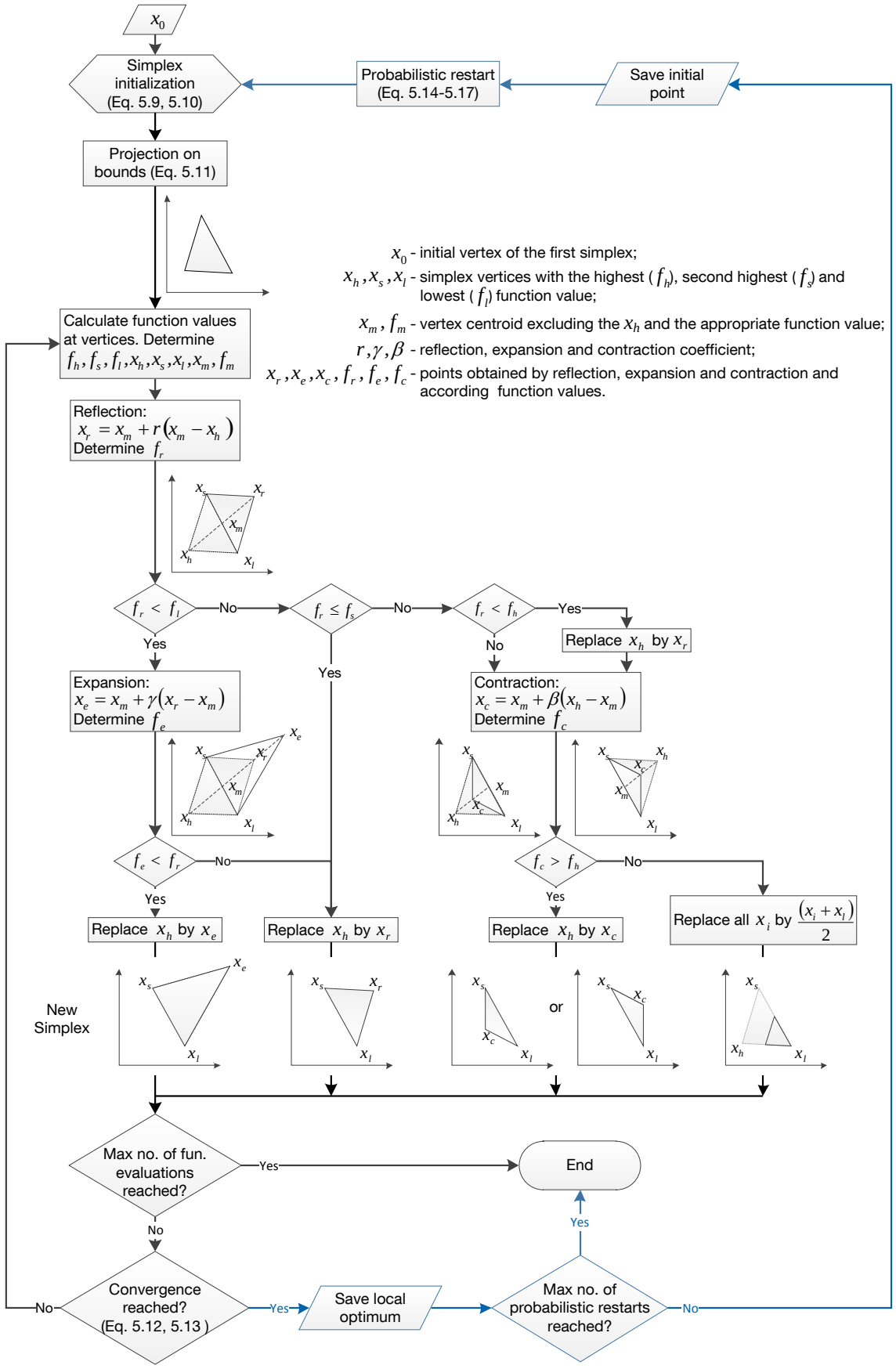
x_0
Simplex initialization (Eq. 5.9, 5.10)
Probabilistic restart (Eq. 5.14-5.17)
Save initial point
Projection on bounds (Eq. 5.11)
x_0 - initial vertex of the first simplex;
x_h, x_s, x_l - simplex vertices with the highest (f_h), second highest (f_s) and lowest (f_l) function value;
x_m, f_m - vertex centroid excluding the x_h and the appropriate function value;
r, γ, β - reflection, expansion and contraction coefficient;
$x_r, x_e, x_c, f_r, f_e, f_c$ - points obtained by reflection, expansion and contraction and according function values.
Calculate function values at vertices. Determine $f_h, f_s, f_l, x_h, x_s, x_l, x_m, f_m$
Reflection: $x_r = x_m + r(x_m - x_h)$ Determine f_r
$f_r < f_l$
No
$f_r \le f_s$
No
$f_r < f_h$
Yes
Replace x_h by x_r
Yes
No
Yes
Expansion: $x_e = x_m + \gamma(x_r - x_m)$ Determine f_e
Contraction: $x_c = x_m + \beta(x_h - x_m)$ Determine f_c
$f_e < f_r$
No
$f_c > f_h$
No
Yes
Yes
Replace x_h by x_e
Replace x_h by x_r
Replace x_h by x_c
Replace all x_i by $\frac{(x_i + x_l)}{2}$
New Simplex
or
Max no. of fun. evaluations reached?
Yes
End
No
Yes
Convergence reached? (Eq. 5.12, 5.13)
No
Yes
Save local optimum
Max no. of probabilistic restarts reached?
No

Figure 5.4 Bounded Nelder Mead local search algorithm (*black*) globalized by probabilistic restarts (*blue*).

After the appropriate simplex modification, two local convergence tests are performed. If any of the following inequalities is satisfied, the local search is terminated and the vertex with the lowest function value is saved as one of the local minima:

$$\frac{1}{n}\sum_{i=0}^{n}\left(f_i-\bar{f}\right)^2<\varepsilon,\quad \bar{f}=\frac{1}{n}\sum_{i=0}^{n}f_i \tag{5.12}$$

$$\max_k\ \frac{max_{\,i}\left(x_{i,k}\right)-min_{\,i}\left(x_{i,k}\right)}{\bar{x}-\underline{x}}<\sigma \tag{5.13}$$

where ε and σ are small positive scalars. (5.12) is satisfied if the function values are similar enough. Second inequality, (5.13) is satisfied if the simplex becomes too small, which is measured by comparing the biggest vertex dimension normalized by its range to the set value of σ.

The NM local search iteration process is embedded into a globalization procedure (blue part of Figure 5.9). After terminating one NM search, the identified local optimum is saved and the globalization of the algorithm is performed by restarting the local search. The initial point for the new simplex is chosen using probabilistic restart. The procedure relies on the previously sampled initial points, including the x_0, and the local minima identified, [72]. The goal is to initiate new simplices in regions where no search has yet been performed. This increases the probability of finding a good local or even the global minimum. If M is the total number of stored points, the probability $p(x)$ is:

$$p(x)=\frac{1}{M}\sum_{m=1}^{M}p_m(x) \tag{5.14}$$

where the normal multidimensional probability density p_m is calculated as:

$$p(m)=\frac{1}{\sqrt{(2\pi)^n\det\Sigma}}\exp\left(-\frac{1}{2}\left(x-x_m\right)^{\mathrm{T}}\Sigma^{-1}\left(x-x_m\right)\right) \tag{5.15}$$

using the covariance matrix Σ:

$$\Sigma=\begin{bmatrix}\sigma_1^2 & & 0\\ & \ddots & \\ 0 & & \sigma_n^2\end{bmatrix} \tag{5.16}$$

where the n variances are:

$$\sigma_k^2=\xi\left(\bar{x}_k-\underline{x}_k\right)^2 \tag{5.17}$$

and ξ is a positive scalar. The probability $p(x)$ is calculated for the chosen number of random points placed inside the domain. The point with the lowest probability is sampled to create the new initial simplex.

The algorithm terminates after the number of function evaluations or number of probabilistic restarts exceeds the defined maximum. The smallest reached local is considered to be the global minimum or sufficiently close to it. Several problems with convergence are stated in [75] and will not be evaluated here. Using a sufficiently high number of allowed restarts, the introduced algorithm has been able to approximate a global minimum for the problem described.

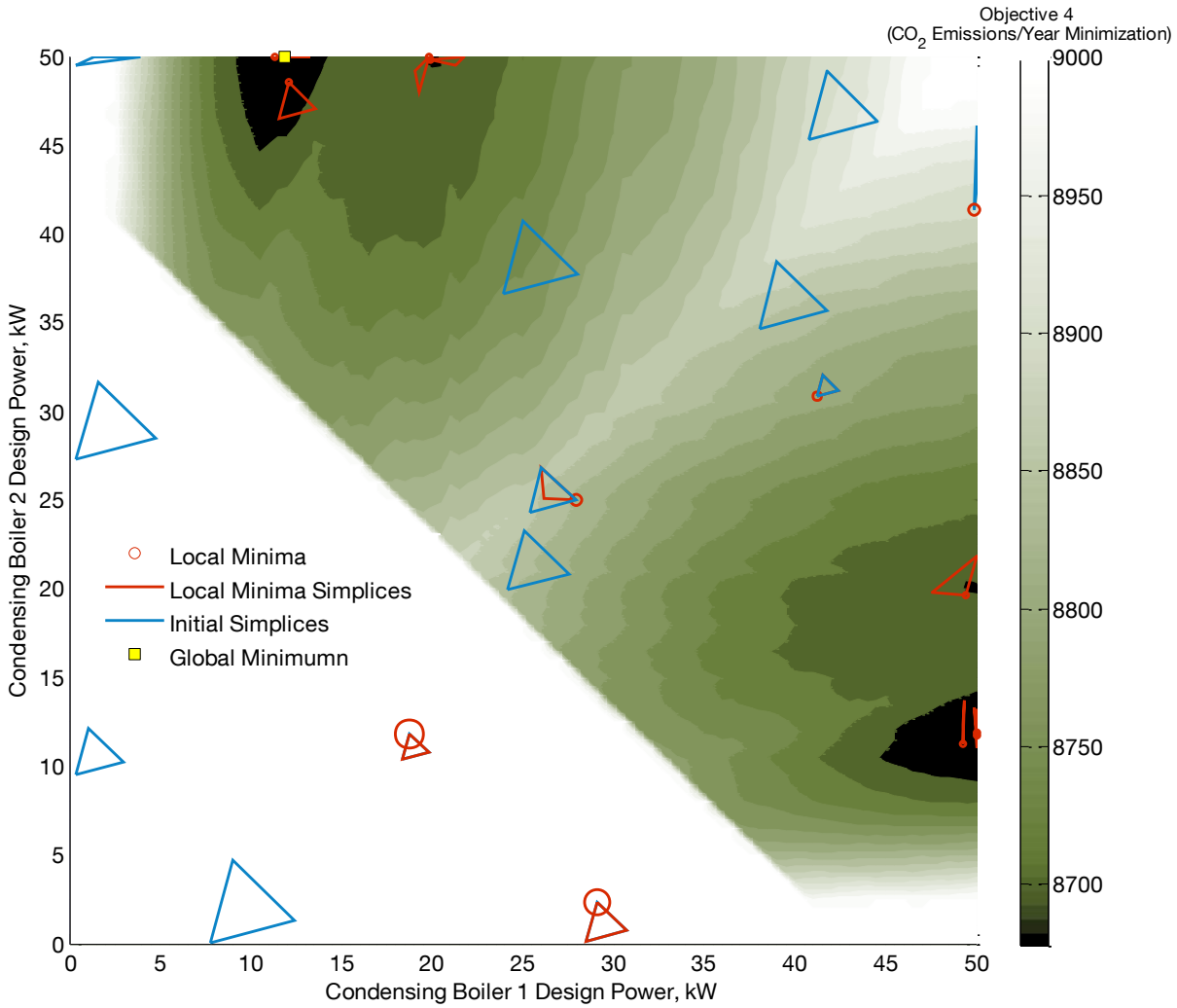

Figure 5.5 Searching a SM2 design that would yield minimal annual CO_2 emissions while supplying an "S" building in Moscow. Global minimum identified out of 1000 local minima at 11.89 kW and 50 kW, f=8677. Triangles: *blue* – initial simplices, *red* – convergence simplices. Red circuits are local minima, size increases with the equivalent function value.

In Figure 5.5, the application of the described optimization method is visualized on SM2 comprising two condensing boilers. The upper bound for the optimization variables was defined based on the yearly peak load and set to 50 kW. The contour approximates the shape of the emission minimization objective function. Its shape is symmetrical in relation to the line of identical boiler powers. The optimization variables assigned to the horizontal

and vertical axis are condensing boiler design powers. Large objective function values are obtained for insufficient cumulative boiler power due to the supply penalty activation, which is visible as a white area in the graph. Each triangle vertex presents a condensing boiler design size combination. Blue triangles represent some of the first simplices formed after probabilistic restarts and the global optimum initial simplex. The distribution of these simplices shows good domain coverage. The red triangles are the local search terminating simplices, whose one vertex, (denoted by the red circuit of size dependent on the function value), represents the identified local minimum. 1000 local searches were completed and the result of the 149th search yielded the lowest value, which has consequently been proclaimed as the global minimum. The minimum was obtained for boiler powers of 11.89kW and 50kW.

5.3.2 Exhaustive Search Method

Exhaustive search (brute-force search) is a trivial method of finding the global optimum by evaluating all points of the orthogonal grid placed in the optimization parameter domain. Since primary HVAC equipment is manufactured only in discrete standardized sizes, the actual component size is usually an approximation of the size calculated during design. For this reason, omitting certain component sizes will not influence the result if care is taken while forming the grid. To formulate the problem as a discrete optimization problem, dimension-specific steps are selected and each of the domain dimensions is replaced by a number of discrete values between and including the bounds. If $M_i, i = 1, \dots, n$ is a vector holding the number of discrete values in each dimension i, the number of function evaluations needed to complete the search is $\prod_1^n M_i$. Precision of the search is controlled by the step size. Clearly, by increasing the number of optimization variables, reducing the step size or enlarging the domain, an exhaustive search becomes very expensive in terms of calculation time. Nevertheless, where the number of optimization variables is small and the resolution is reasonable for the utilized components, it is a quicker and a safer way to identify the global optimum, compared to GBNM algorithm. Another advantage is the independence of function evaluations, enabling these to be performed in parallel.

Figure 5.6 shows the flow of the exhaustive search optimization procedure. The user provided load profile and additional technical limits are used to define the step and the domain size. Optionally, the objective can be subjected to additional constraints, which eliminate particular grid points. An example would be the elimination of component size combinations, whose sum of the design capacities significantly exceeds or comes short of the peak load. After the points are set, for each of them the SM Simulator runs to evaluate all four objective functions values. This is followed by saving the set of evaluated points, their SM specific system performance data and objective function values reached. Four optima corresponding to each of the objective functions are identified after a single optimization run. Practically, the objective function is a vector of four values:

$$OF = \begin{bmatrix} AC_t \\ AC_i \\ CF \\ E_{CO2} \end{bmatrix} + SuP + SoP \tag{5.18}$$

Now the objectives, penalties and performance values are mapped throughout the domain, it is possible to perform a parameter analysis. To visualize the data a code is developed to automate the generation of two and three dimensional data analyses graphs. These graphs are dealt with at section 5.4.

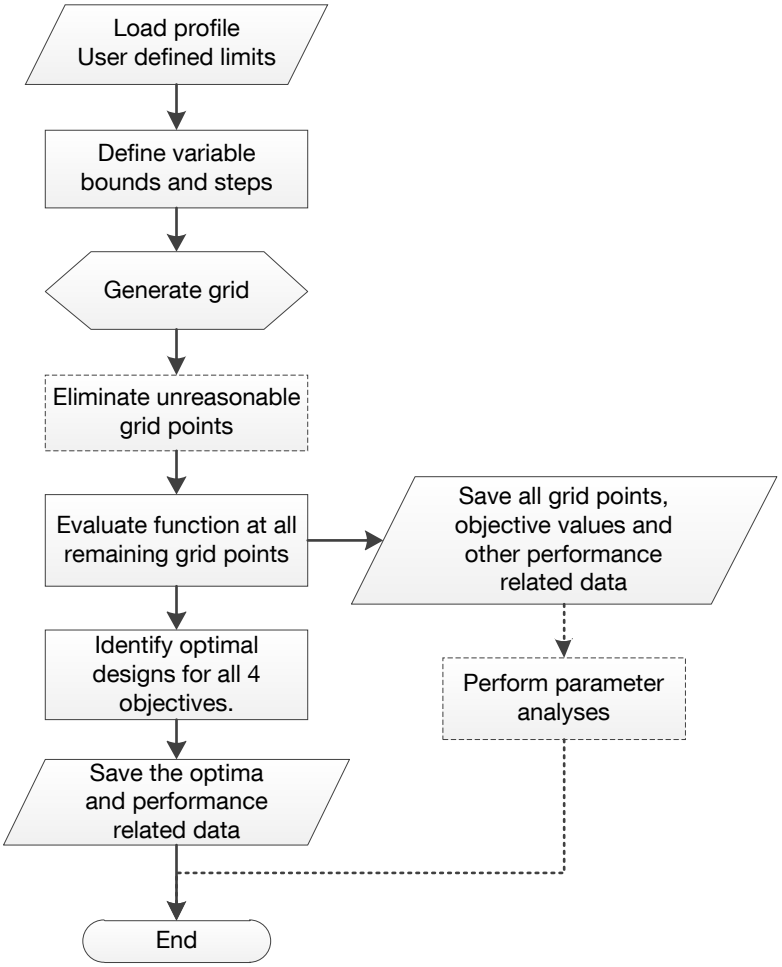

Figure 5.6 Preparing and performing exhaustive search optimization. Dotted lines represent optional processes.

The presented method was implemented to solve the same optimization problem shown in Figure 5.5. The optimization takes about 12.5s where the condensing boiler power step equals 5 kW. If the step is decreased to 2 kW, the optimization lasts 73 s using one and 23.4 s using 4 threads. In both cases, the domain is subjected to additional constraints on the sum of design powers, which reduces the number of simulation runs. The result is in accordance with the GBNM result, CP1 = 15kW (12 kW) and CP2 = 50 kW.

5.4 Application to System Models

Figure 2.2 summarizes the expected user input to the optimizer. The result of running the optimizer is the optimal system design determined by component sizes. Each SM is optimized separately. The user chooses the SM based on its individual goals and information on essential system characteristics provided in the user interface, as it will be shown in chapter 6. In short, this information guides the user to the suitable SM. For example, a system offering renewable energy utilization is more interesting to the building operator than to the investor, since it usually has lower running but higher investment costs. However, if the user desires to compare different SMs, the optimizer can run for each of the systems and the results can be compared. Several SMs could be optimized in parallel if there are sufficient calculation resources.

Finally, the optimization of a single SM will show how its component sizes change depending on the set goal and the desired solar ratio. If several SMs are optimized for the same utilization purpose, the optima between the SMs can be compared and evaluated.

The following sections provide an inside view of the optimization process in its application to each of the SMs. The examples demonstrate objective function characteristics and sensitivities and present the optimal component dimensions. The load and weather data utilized in chapter 3 are used again to perform example calculations. As a reminder, in Table A 3 and Table A 4 the loads are given for an “S” (small), “M” for (middle) and “B” (big) building. Figure A 19 shows basic meteorological data for building locations: Bangalore, Dubai, Moscow or Shanghai. Supply and solar penalty coefficients are heuristic values, satisfying the given level of investigation.

5.4.1 SM1: On-Off Boiler, Thermal Storage and Solar Collector

The SM1, performance of which was presented in section 3.3.1, optimization example compares the optimization results obtained using the GBNM and exhaustive search method. This was relevant to confirm the ability of the GBNM algorithm to identify the global or closely global minimum. The components to be dimensioned in this SM are an on-off boiler, a thermal storage tank and a solar thermal collector. Thus, the optimization variables are:

- The boiler design power;
- The storage tank volume;
- The storage tank discharge rate (fraction of its full capacity that can be discharged within one hour);
- The roof area[i] to be covered with solar collectors; and

[i] The user provides only the available horizontal area. However, the collector tilt is assumed to be optimal (3.2.5). The assessment of the maximal optimally tilted collector area, fitting the provided horizontal building (roof) area, is handled within the implemented collector model.

- The average solar collector temperature[i].

This section discusses the model optimization and introduces terms and values also relevant for the further subsections of 5.4.

At the beginning of this discussion, the three- and two-dimensional parameter sensitivity analyses are performed. Figure 5.7 visualizes the objective function, penalties and total costs, depending on the roof area and storage volume, while the rest of the optimization parameters remain constant (total cost optima are implemented). These constant values originate from total cost optimization for an "S" building in Moscow, with a required solar ratio of 30%. The boiler power equals 30 kW, storage discharge rate is 0.2 and the average collector fluid temperature is 60°C. The same values are encountered in the following section, in Figure 5.9 and represented by the light red colored columns.

In the upper left corner of Figure 5.7 the objective function dependence on the change in the storage volume and the available roof area is illustrated. The objective function value equals the sum of the remaining functions illustrated in the same figure. The supply penalty locally presents as highly non-convex, but on a larger scale it forms a wall to expel the systems incapable of satisfying the load. As expected, the total costs[ii] grow logarithmically with the storage volume and linearly with the roof area. The solar penalty, if activated, dominates the objective, posing a strict constraint that increases the collector size disregarding the costs, until the target solar ratio has been achieved. Another dimension is eliminated by slicing the three-dimensional graphs through the fixed storage volume and collector covered horizontal area, in order to investigate their influence on the objective function, costs, penalty and emissions[iii].

The left side of Figure 5.8 shows the increase in annuity of the investment and total cost as the collector area rises towards its limit, while the storage volume in kept to 23 m^3. In the calculated optimization example, at 155 m^2 the desired solar ratio is achieved, removing the solar penalty. As expected, the emissions reduce as the collector area increases. Conversely, the emissions rise with the increase in storage volume, as shown on the right side in Figure 5.8, where the roof area is static at 155 m^2. If imposing a constraint of achieving a specific solar ratio, apart from the expected collector area, the storage volume will increase. To achieve the desired temperature inside the large storage volume, the tank has to be fully charged, prolonging the boiler working hours even where the set load does not demand it. In real applications, the temperature stratification of the storage attenuates this problem. It can be concluded that the heating solar ratio of 30% represents an uneconomic goal for the cold climate in Moscow, due to thermal losses, both from the solar collector and from the thermal storage tank.

The supply penalty exhibits small local peaks at certain parts of the domain, which represents a buffer area to the set of surely feasible solutions. This part of the system configurations in not necessarily unable to satisfy the demand, but requires further investigation. In

[i] The model imposes bounds to prevent temperatures that are lower than the expected return, and differentiates between low and high temperature heating.
[ii] The annuity calculation period in all examples is 20 years.
[iii] This is only to inform that different scaling of CO_2 emission values can be encountered in the graphical representations throughout the rest of section 5.4.

further sections it will be seen the supply penalty does not exhibit such behavior if the storage in not utilized.

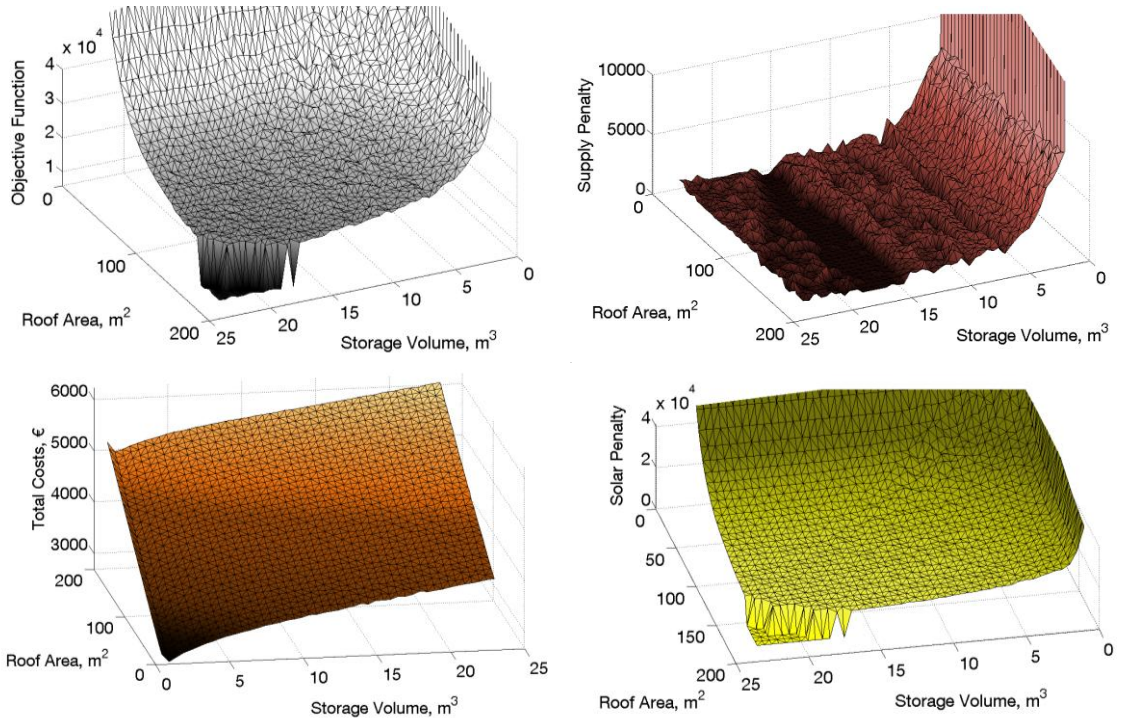

Figure 5.7 Objective function (total cost optimization), solar penalty and total costs for Moscow climate, "S" building, SR=30%, P= 30 kW, DR= 0.2, T= 60°C.

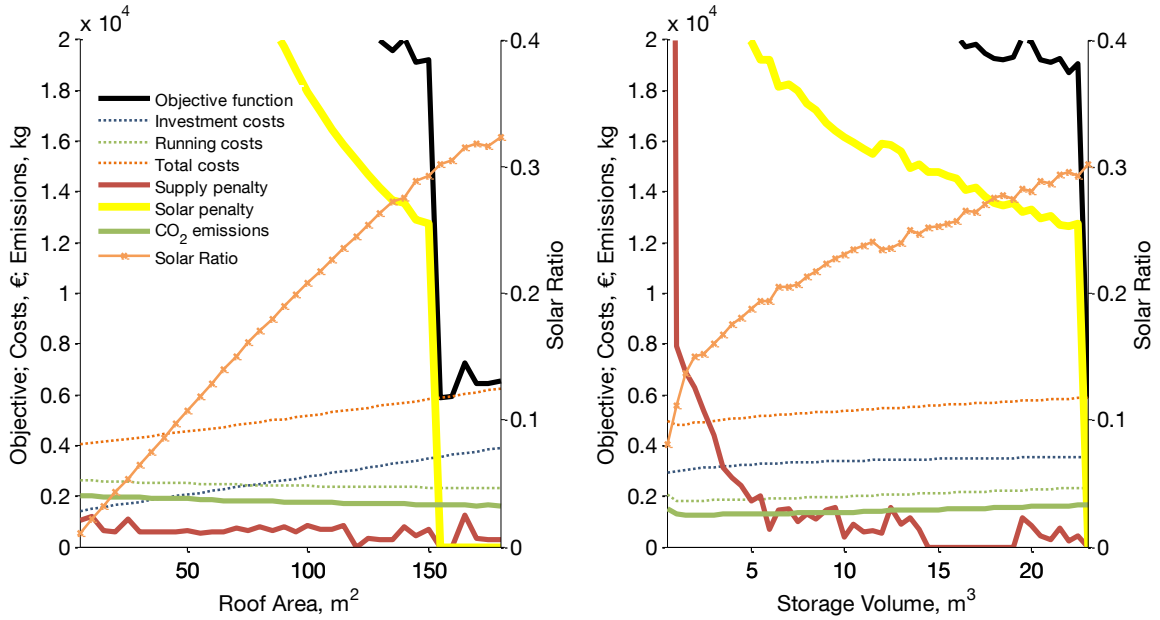

Figure 5.8 Total cost optimization, Moscow climate, "S" building, SR= 30%, P= 30 kW, DR= 0.2, T=60°C. *Left*: V=23 m^3. Emissions decrease with the collector area. *Right*: RA=155 m^2. Emissions increase if the boiler charges an oversized storage.

5.4.1.1 Optimization Result Analyses

Apart from comparing the two algorithms, Figure 5.9 and Figure 5.10 show an overview of optimization results for both climates and both building sizes. Clearly, the components are larger for the much colder Moscow climate and the cost therefore higher.

In general, if solar collectors are utilized due to the set solar ratio target, the boiler size is lower but storage volume increases. The inclination of storage cost is insignificant compared to the solar penalty. Consequently, the investment cost rises and the running cost becomes smaller. In the cases of an extreme increase in storage volume, the problem mentioned in the last section occurs, leading to an increase in running cost rather than a decrease. The same happens with emissions. The running cost comparison between configurations with and without a solar ratio constraint will show that the utilization of solar collectors for heating purposes is justified only for suitable climates.

As a reminder, the value of the supply penalty provides information of how severe is the underproduction, where it occurs. Conversely, the value of the “supply task” is introduced, visible in the lower graph in Figure 5.9, which indicates how large the overproduction is. Its absolute value can have different weighting for different SMs due to differences in models, since it is calculated by comparing the delivery to demand on the hour to hour basis. However, as long as that value is not lower and not much higher than 100%, the system has performed satisfactory in terms of supplying the demand. Lower values indicate comfort violation and higher values indicate overproduction and energy waste.

For all the results shown, the supply task has been satisfied. The only case that penalized the solar constraint is the “M” building in Moscow, with the objective to reach the solar ratio of 30%. Utilizing the provided maximal available roof area, the solar ratio of only 14% is achieved, and the penalty has forced an increase in storage volume, which prolonged the boiler operation hours causing the emissions to rise, for reasons explained in the previous section. For the Shanghai climate, where the solar gains are higher, the boiler power decrease with the increase in solar ratio is as expected, while emissions also decrease.

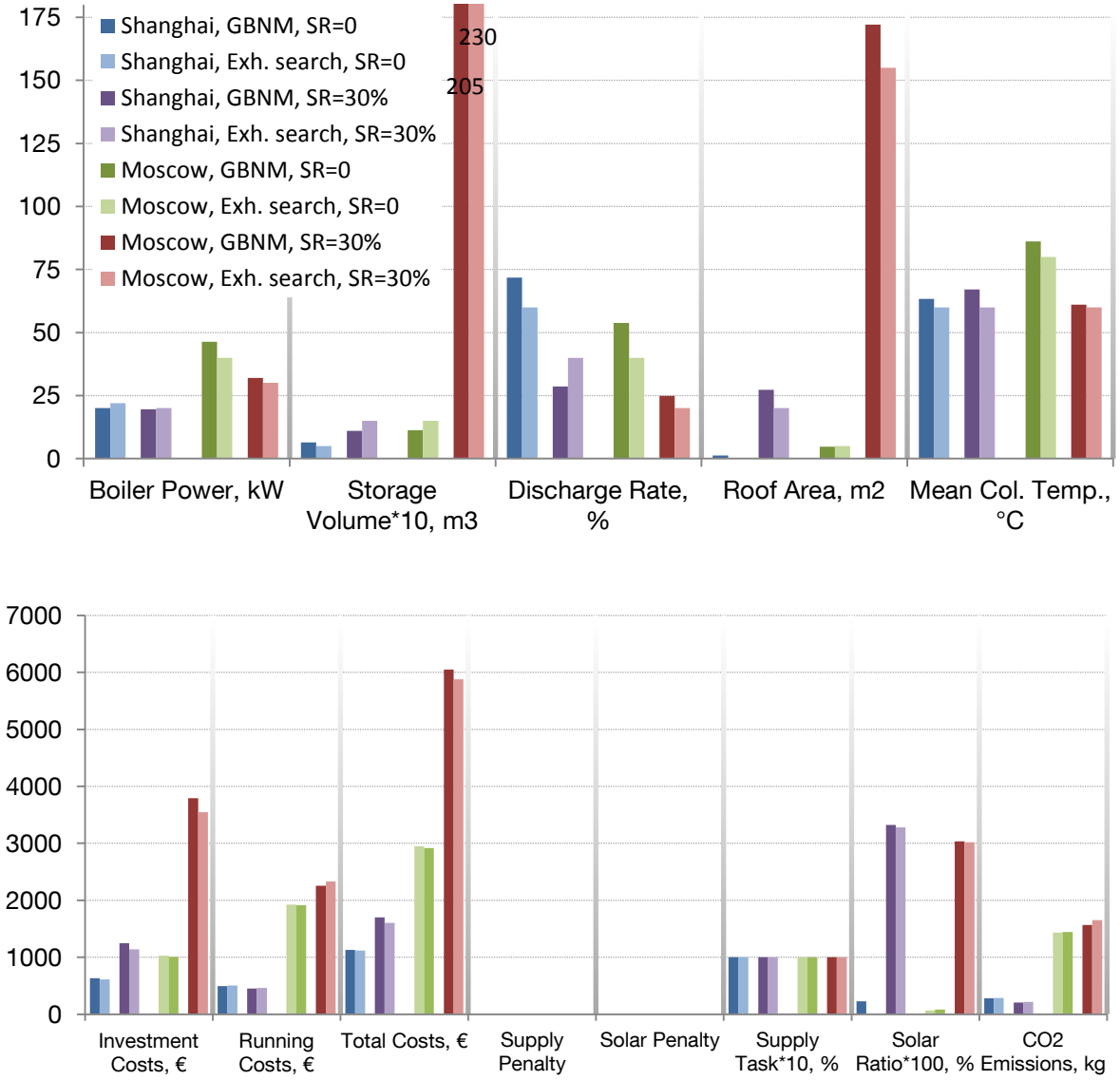

Figure 5.9 Total cost optimization results for building "S", both discrete and GBNM algorithms. Each variable's 2nd and 4th pair of bars have target SR of 30%.

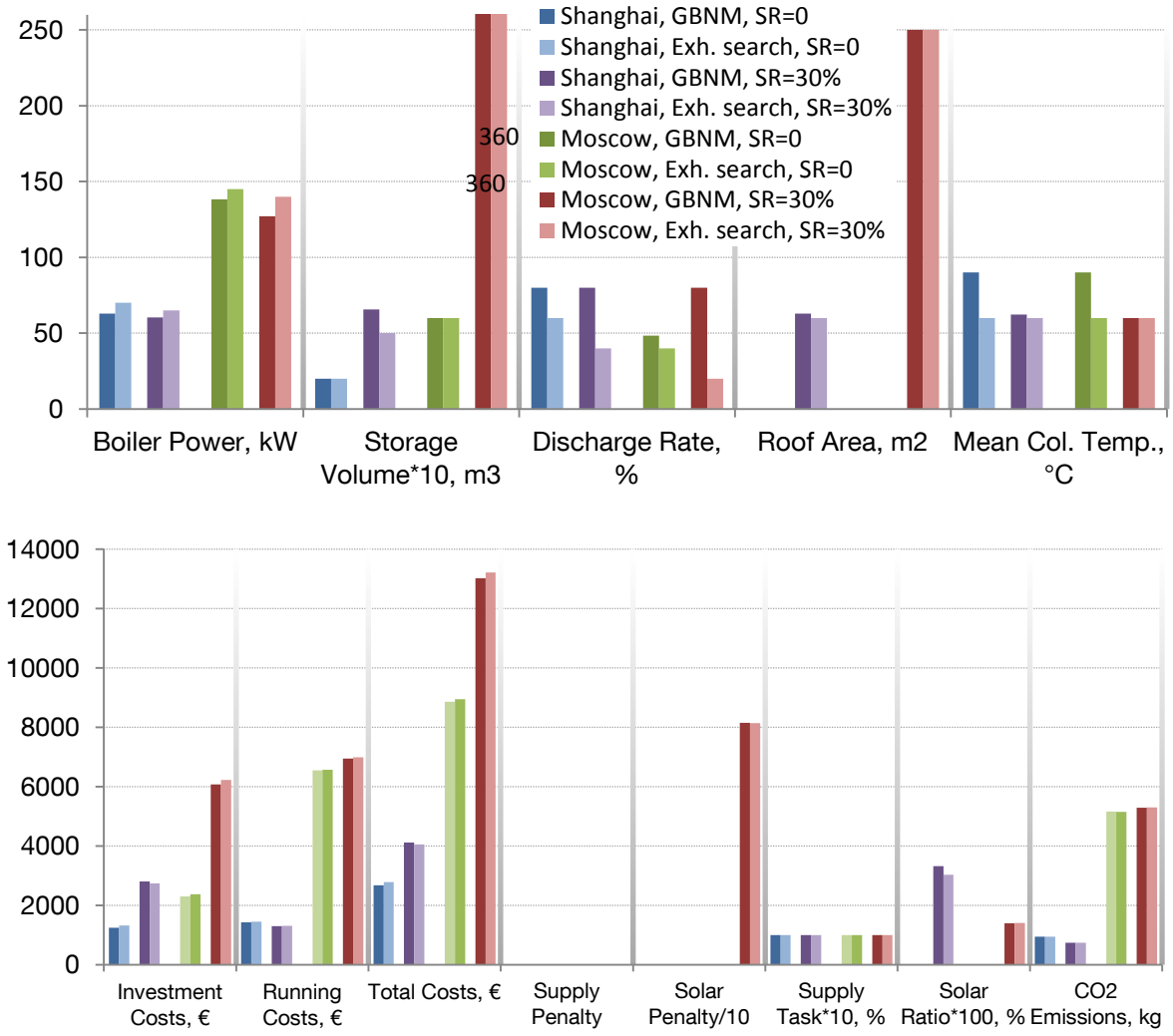

Figure 5.10 Total cost optimization results for building "M". In Moscow climate the solar ratio of 30% has not been satisfied.

As promised at the beginning of the section on SM1 optimization, one of the features presented in Figure 5.9 and Figure 5.10 is the comparison between the optima obtained using discrete parameters optimization and the GBNM continuous algorithm. This is done to examine the applicability of the GBNM algorithm. Firstly, it can be concluded that the differences in objective function values lie below 3%, confirming that minima near to the global minimum have been identified by the GBNM algorithm, encouraging further utilization. Further improvements can be expected through adjusting the parameters of the GBNM algorithm. Secondly, larger discrepancies in storage discharge rates, yielded by the two algorithms, need to be discussed. This parameter influences the performance of the system only where the maximal hourly storage discharge is too restricted. In other words, if the discharge rate values are very small, such as those shown in Figure 5.11, the supply penalty is activated. It is the same outcome where the storage volume is small, causing prolonged boiler operation and boiler staging. After the minimal satisfying discharge rate was reached, its further increase will not change the performance. Obviously, a real system will always operate with the lowest sufficient discharge rate, to minimize the pump size.

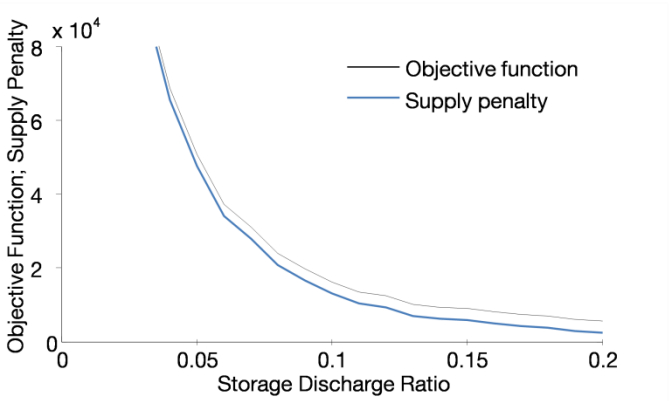

Figure 5.11 Systems with small storage discharge rates fail to satisfy the supply task. Moscow climate, "S" building, SR=0, P= 40 kW, V= 2 m^3, DR= 0.2, T= 60°C.

Thanks to the presented optimization procedure, the benefits of dedicating a certain surface area to solar collectors can be quantified. The large thermal storage tanks can often not be utilized due to the lack of space or possibility to mount them, which can be resolved by planning in advance. The biomass boilers are considered to have neutral carbon emissions and in order to implement them, the building space needs to be planned for accommodating the biomass fuel storage.

5.4.2 SM2: Condensing Boilers

This SM optimization example will be used to demonstrate how the type of the heating emission system influences the optimal design. The optimization parameters are:

- The condensing boiler design sizes.

Optimizations of two variations of SM2 have been performed, both utilizing two condensing boilers. The optimization parameters are the nominal boiler powers. According to Table 5.1, these two systems, CBo1 and CBo2, are identical in their minimal PLR and utilized fuel. The only difference is that CBo1 serves a radiator heating circuit, while CBo2 supplies panel heating (e.g. a floor heating system) and, therefore, operates with a lower return and supply temperature. This causes differences in boiler performance, which is defined by the two curves in Figure B 1. The consequent difference in optimal design is shown in the next section but before that, the optimization of CBo1 targeting total cost minimization is presented and analyzed.

Table 5.1 Data utilized for simulating systems CBo1 and CBo2.

SM	No. of boilers	Minimal PLR for both boilers, %	Fuel type for both boilers	Heating emission type
CBo1	2	30	Gas	Radiator
CBo2	2	30	Gas	Panel

Exhaustive search evaluates all boiler size combinations with a step of 2 kW revealing surfaces defined by objective, cost and penalty functions, which are shown in Figure 5.12. Functions are symmetric with respect to the line of equal boiler powers, since both boilers have identical performance characteristics. The supply penalty excludes those boiler combinations, which have an insufficient sum of design powers, in the relation to the demand. This penalty added to total costs, which increase with the growth in boiler powers, forms a dip in objective function, with two identical global minima formed at its ends. These minima are caused by lower investment cost when utilizing a single boiler. The graph in the lower right corner of Figure 5.12, illustrating the CO_2 emissions, indicates that the identified total cost optimum is not also the emission minimizing configuration. The lowest emissions while maintaining the demanded supply are achieved by utilizing one larger and one smaller boiler. This is confirmed by the result of CO_2 emission minimization, presented in the diagrams in the next section.

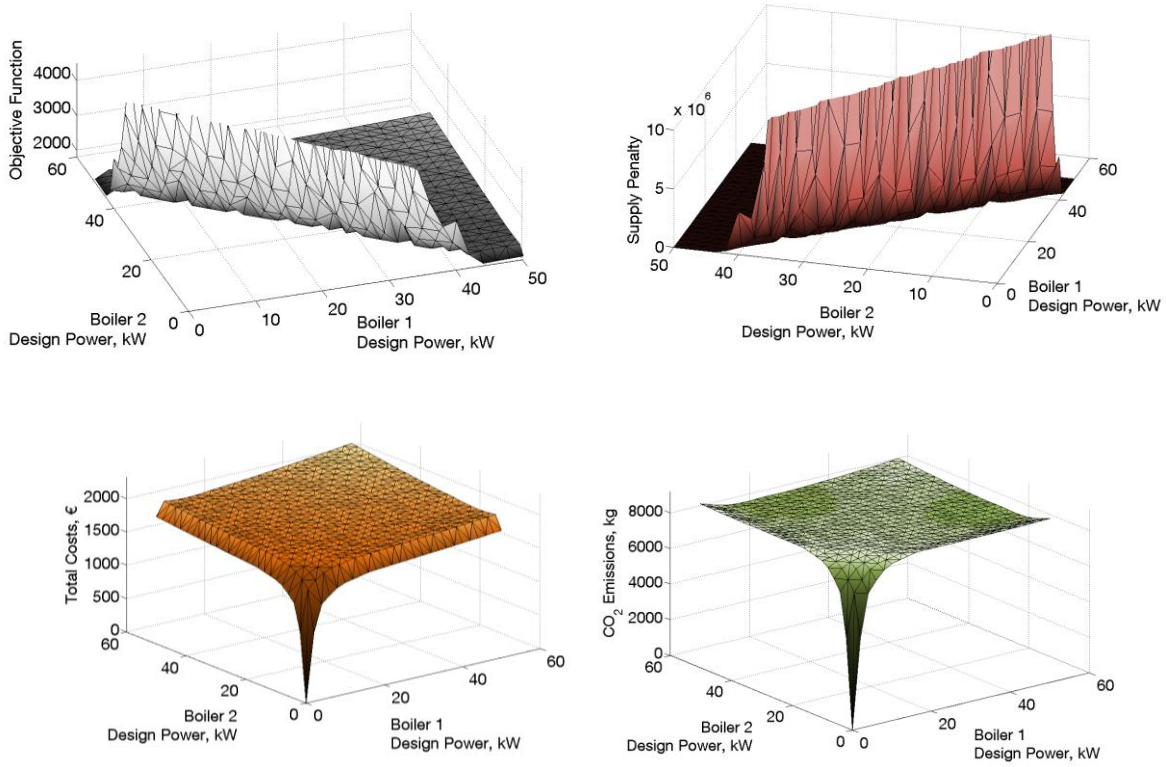

Figure 5.12 Surfaces representing objective function (*upper left*), supply penalty (*upper right*), total costs (*lower left*), and CO_2 emissions (*lower right*) obtained by exhaustive search in order to identify component sizes that minimize total costs. System: CBo1 (Table 5.1), Moscow, "S" building.

To obtain the graphs shown in Figure 5.13, yet another optimization parameter is set to be constant (total cost optimum value), compared to the three-dimensional plots.

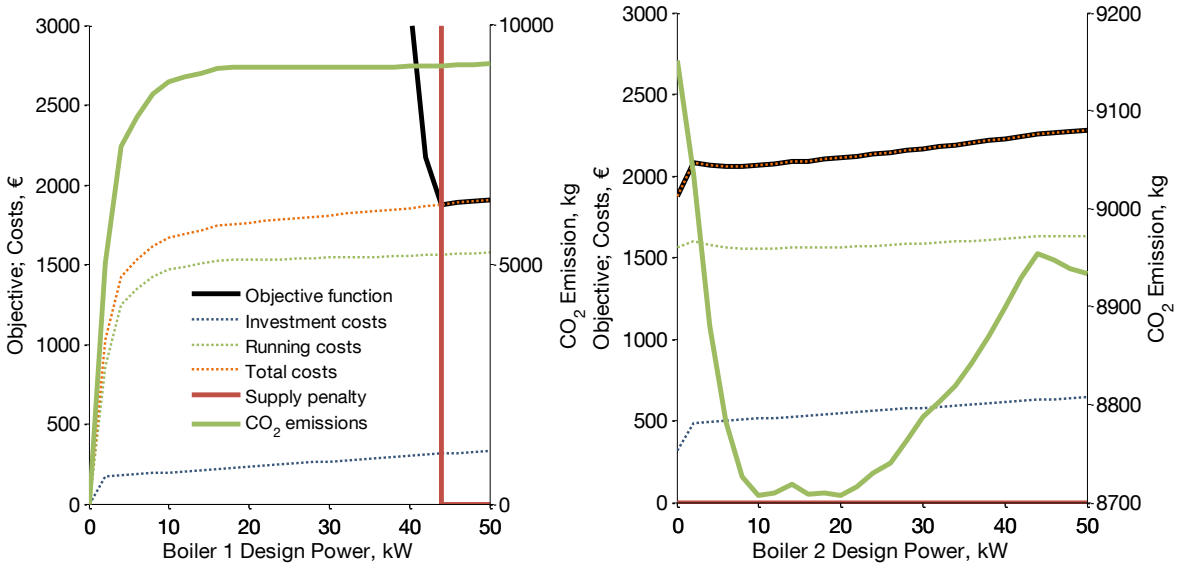

Figure 5.13 Sensitivity of optimization relevant variables to variations of one boiler size. The other boiler power stays fixed to its optimal value. *Left*: Boiler 2 design power = 0; *Right*: Boiler 1 design power = 44 kW. Total cost optimization; System: CBo1 (Table 5.1), Moscow, "S" building.

The left graph shows how the objective, costs and emissions develop while the design power of the first boiler changes from the 0 to 50 kW. The power of the second boiler stays at its optimum, which is 0 kW. According to the supply penalty curve, only a boiler with a design power larger than 44 kW will maintain the prescribed comfort at all times. Values above 44 kW would lead to total cost elevation. Therefore, this value is the optimum in the case of total cost optimization. The right side of the figure reveals the behavior of optimization relevant variables if the power of the first boiler is kept to its optimum, 44 kW, and the power of the second boiler is varied. As expected, investment cost increases monotonically with the power. On the other hand, CO_2 emission and fuel consumption have a minimum between 10 and 15 kW. This indicates the possibility to reduce the emissions by utilizing a second boiler, which is able to cover low demand more efficiently due to its small minimal power. Among other things, the following subsection provides more information on this.

5.4.2.1 Optimization Result Analyses

Results of the optimization of CBo1 and CBo2 are shown in Figure 5.14 and Figure 5.15. The exhaustive search method, with a step of 2 kW for both boilers was used. The optimization results for all four optimization goals are presented.

Total and investment cost minimization yield the same result for both radiator and panel heating. This result is a single 44 kW boiler. If minimizing the costs, the emission system related difference in boiler performance had no influence on the optimal boiler dimensions, since the peak demand remains the same. However, it did cause the difference in the running cost. The investment for an additional boiler increases the cost so significantly, that the related running cost decrease was not able to prevail and influence the optimization result.

If the cost is disregarded and the fuel consumption or emissions are minimized, a different image is obtained. Fuel consumption and emissions minimization yields identical results due to the absence of a further fuel type or source of energy. Both CBo1 and CBo2 are sized to have two boilers, one large and one smaller. It can be seen that boilers serving floor heating do not need to be as big as those for radiator heating. However, even in the case of the smaller boilers yielded by CBo2 optimization, their sums of powers in higher than the peak load and will not impair the supply quality. Namely, minimizing the emission and fuel consumption yields boilers somewhat larger than the peak load, which can be related to an increase in efficiency if operating in part load.

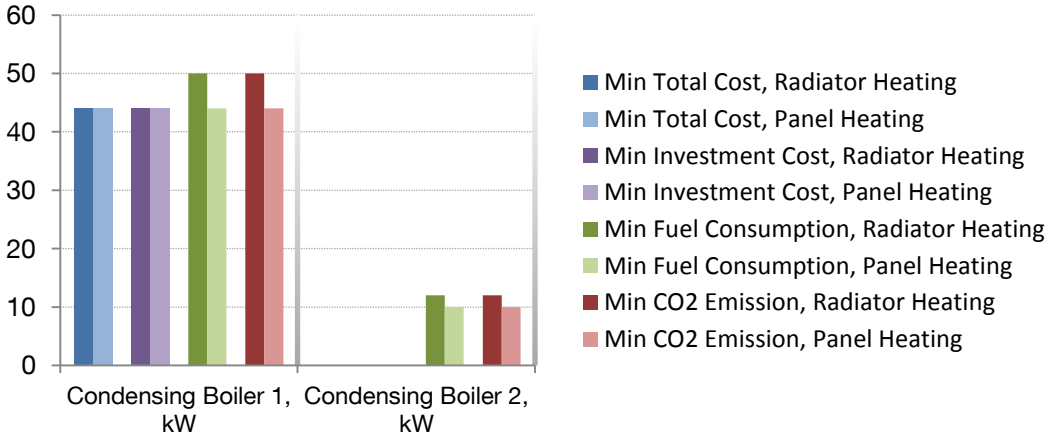

Figure 5.14 Component sizes. Exhaustive search optimization results for CBo1 and CBo2 (Table 5.1). If costs are minimized, a single boiler is recommended. To obtain an environmentally friendly performance an additional smaller boiler should be utilized. Moscow, "S" building.

The penalty function equals zero in all the observed cases. The supply task values higher than 100% (Figure 5.15) indicate the severity of the overproduction. Cost minimization recommends a system consisting of a single boiler, which causes overproduction and its supply task is significantly larger than 100%. This is a consequence of the rather large minimal power of a single boiler. The improvement of this is achieved in the case of fuel consumption and emissions minimization by choosing a smaller second boiler to take care of small loads.

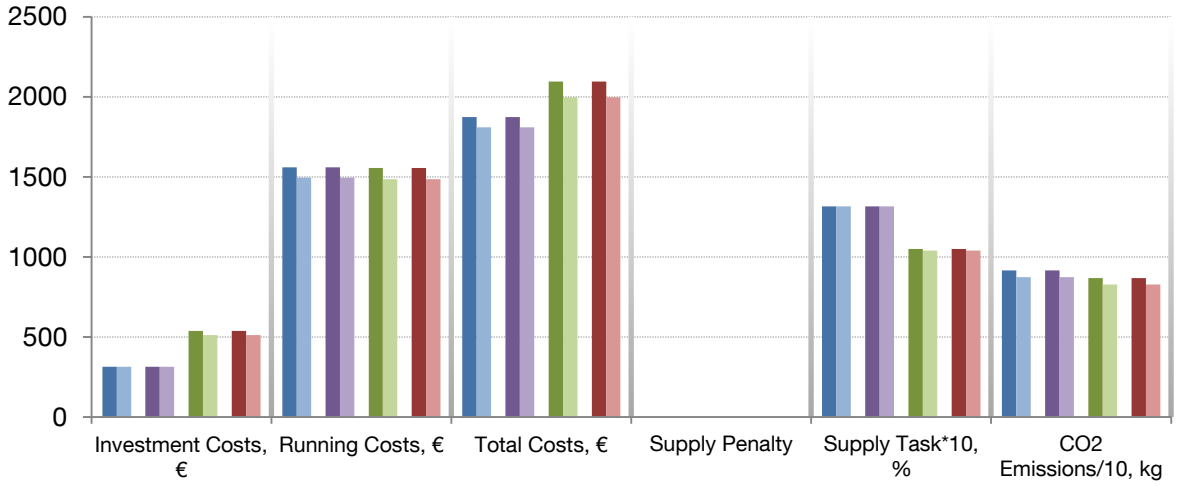

Figure 5.15 Costs, emissions and supply task fulfilment. Exhaustive search optimization results for CBo1 and CBo2 (Table 5.1). Supply task is satisfied, although also exceeded (overproduction) in case of saving on investment costs. Moscow, "S" building.

Finally, by performing such a simulation, an architect would be informed of benefits in case of panel heating utilization. This could influence the planning of the building interior in terms of omitting the radiators, preparing for floor heating, dimensioning a mechanical room for a plant of two condensing boilers, etc.

5.4.3 SM3: Thermal Storage, Solar Collectors and Condensing Boilers

A SM3, comprising of a thermal storage, solar collectors and two condensing boilers, has been optimized to supply an "S" building located in Moscow. The optimization parameters are:

- The condensing boiler design sizes;
- The storage tank volume;
- The storage tank discharge rate; and
- The roof area to be covered with solar collectors.

The average collector fluid temperature is kept at a constant value of 60°C.

The example shows how significantly the imposing the solar ratio target of 30% can influence the optimal design.

Before studying the results, the shapes of optimization related functions are illustrated using two- and three-dimensional analyses. The optimization with the goal to minimize the total costs using exhaustive search yields functions presented in Figure 5.16. In that figure, the storage discharge rate and condensing boiler powers are kept at their total cost optimum (DR=20%, CP1=45 kW, CP2=0 kW). Since evacuated tube solar collectors are utilized, it is possible to achieve the demanded solar ratio of 0.3, although only by covering an area larger than 150 m^2 with collectors, see Figure 5.16, the graph on the left. The illustrated solar penalty function also shows that, the bigger the solar collector area, the smaller

the minimal storage volume is for reaching the imposed solar ratio. On the right, the CO_2 emissions are illustrated. They drop with the increase in collector covered roof area and reach a minimum at storage volume of 9.5 m^3.

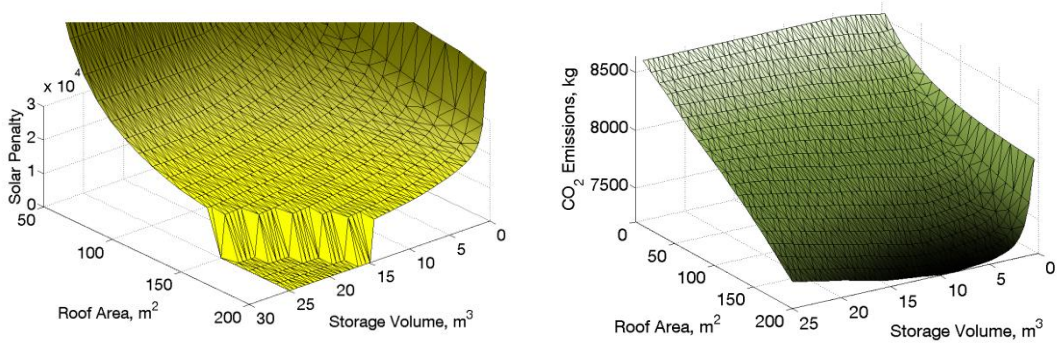

Figure 5.16 Surfaces represent solar penalty (*left*) and CO_2 emissions (*right*) obtained by exhaustive search in order to identify component sizes that minimize total costs. Solar ratio target: 30%. Constant values: CP1=45 kW, CP2=0 kW, DR=20% (total cost optimization - Figure 5.18). Moscow heating load, "S" building.

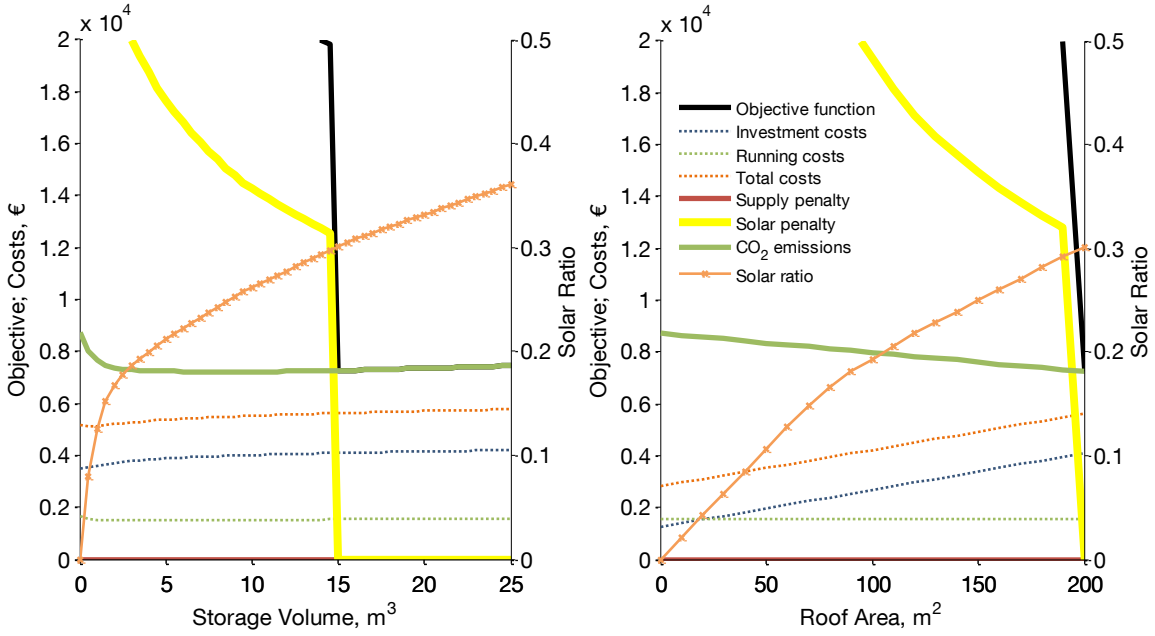

Figure 5.17 Sensitivity of optimization relevant variables to storage volume - *Left*: Roof area = 150 m^2 and roof area covered with tube solar collectors - *Right*: Storage volume = 25 m^3. Solar Ratio target: 30%. Constant values: CP1=35 kW, CP2=10 kW, DR=20% (total cost optimization - Figure 5.18). Moscow heating load, "S" building.

Two-dimensional analysis is provided in Figure 5.17. Storage thermal losses to the environment grow linearly with the storage volume, thus increasing both the dissipation of stored solar energy and condensing boiler working hours, needed in order to fully charge it. This causes a slight emission increase, despite of the increased solar energy utilization. As soon as the solar ratio of 30% is reached, the solar penalty is deactivated.

5.4.3.1 Optimization Result Analyses

A comparison of optimal component sizes and corresponding cost and penalty-related values for solar ratios of 0 and 30% is given in the charts illustrated in Figure 5.18 and Figure 5.19. Results for all four objectives are compared.

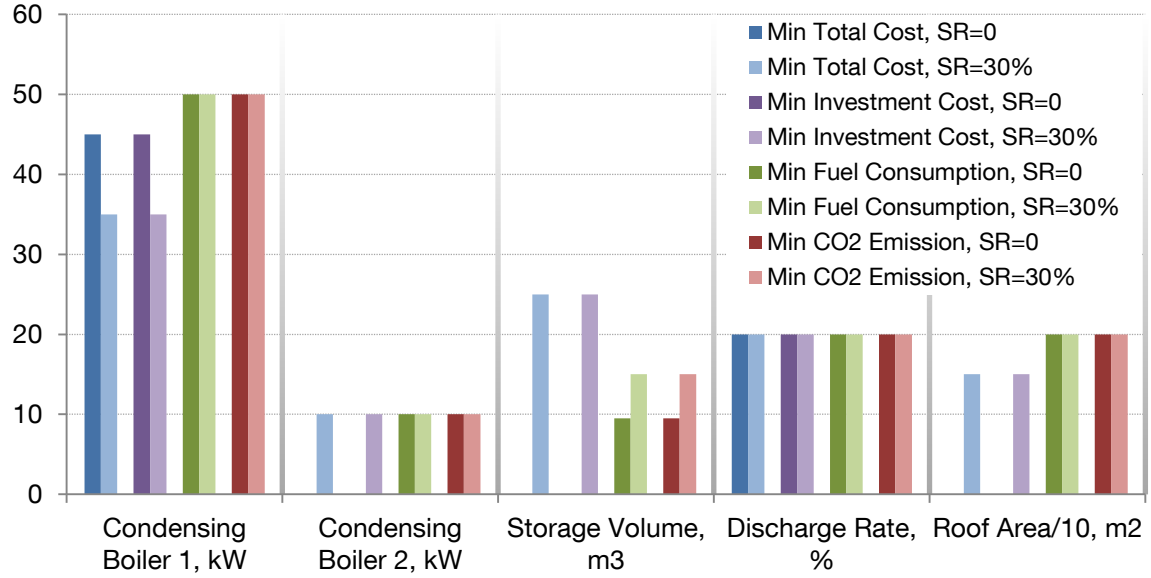

Figure 5.18 Optimal component sizes. Exhaustive search optimization results, Moscow heating load, "S" building. If a certain solar ratio is not imposed, only the emission and fuel consumption minimization will implement solar collectors.

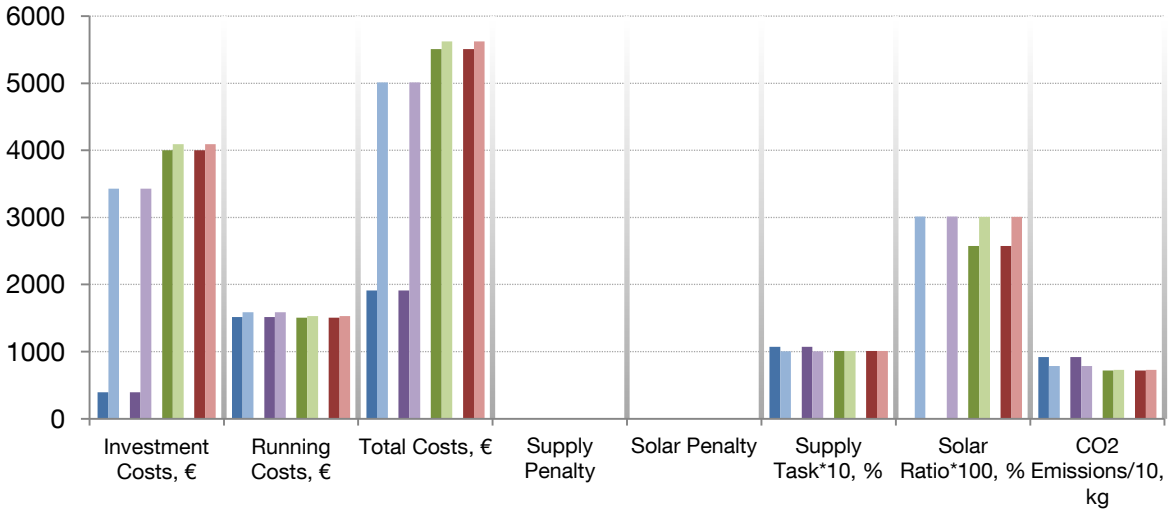

Figure 5.19 Costs, emissions and supply task fulfilment. Exhaustive search optimization results for Moscow heating load, "S" building. Minimal emissions yield maximal total cost. Systems that achieve a solar ratio of 30% have significantly higher costs.

According to both total and investment cost minimization with no requests in solar energy utilization, the system for the Moscow climate includes neither storage nor collectors, but two condensing boilers. On the other hand, fuel consumption and emission minimization always recommend investment in solar collectors and thermal storage tanks, and both

yielded the imposed maximal solar collector area of 200 m^3. The difference in the optimal result after a solar ratio target of 30% is added to each of these two goals is the increased optimal storage volume. Therefore it can be said that cost minimization suggests a large storage, while fuel consumption and emissions minimization choose to invest in more collector area and minimize overproduction. If optimizing the cost under the same solar ratio target, the optimum is reached at 150 m^2.

This example has the similar influence on the architectural decisions as the SM1. The space needed to mount the solar collectors is to be considered, including its distribution system. The lack of suitable space often limits the volume of the storage tank. The architect could even consider changing the shape of the building to provide more roof space to place the collectors. The idea is to run an additional optimization for the new roof area limit and evaluate the resulting effects.

5.4.4 SM4: On-Off Boiler, Thermal Storage and Condensing Boilers

This example shows what impact the choice of the optimization objective can have on the system configuration. The component dimensions to be optimized in SM4 are:

- The boiler design power;
- The condensing boiler design sizes;
- The storage tank volume; and
- The storage tank discharge rate.

Prior to analysing the optimization results, a short parameter analysis of the example for minimal carbon emissions is shown. SM4 was optimized for an “S” building in Moscow.

The area around the global minimum of CO_2 minimization objective is shown on the left of Figure 5.20. Emissions increase with the condensing boiler power due to the increase in minimal boiler power, which causes overproduction. Optimal storage volume is 1.5 m^3 and an increase in this has a negative effect on the objective, due to higher thermal losses and longer charging.

At the right side of Figure 5.20, all component sizes apart from storage volume are fixed at their emissions optimum. Interestingly, the initial value of supply penalty is 0 and increases for storage sizes smaller than 0.5 m3. As the storage volume increases further, the penalty decreases and reaches zero at 1.5 m3. The cause of this is the ability of the biomass boiler to cover the load by itself, due to its 50 kW size. However, it should be remembered that this is a single stage boiler. Such an operation would produce a large amount of CO2, since no matter how small the load is, without the storage, full load power is supplied. The supply task is not satisfied and the penalty is active until the storage volume reaches 0.5 m3. Small storage has a small discharge power even at higher DRs and often is not able to meet the load. At the same time the biomass boiler is not turned on to make up for the unmet load, since the control signals the storage is full. This causes insufficient supply, demonstrated by the drop in the supply task satisfaction curve and penalty activation. This is previously illustrated in 5.4.1, Figure 5.11. When the storage discharge power is suffi-

ciently high, the benefits of storage utilization are restored and emissions are much lower than without the storage.

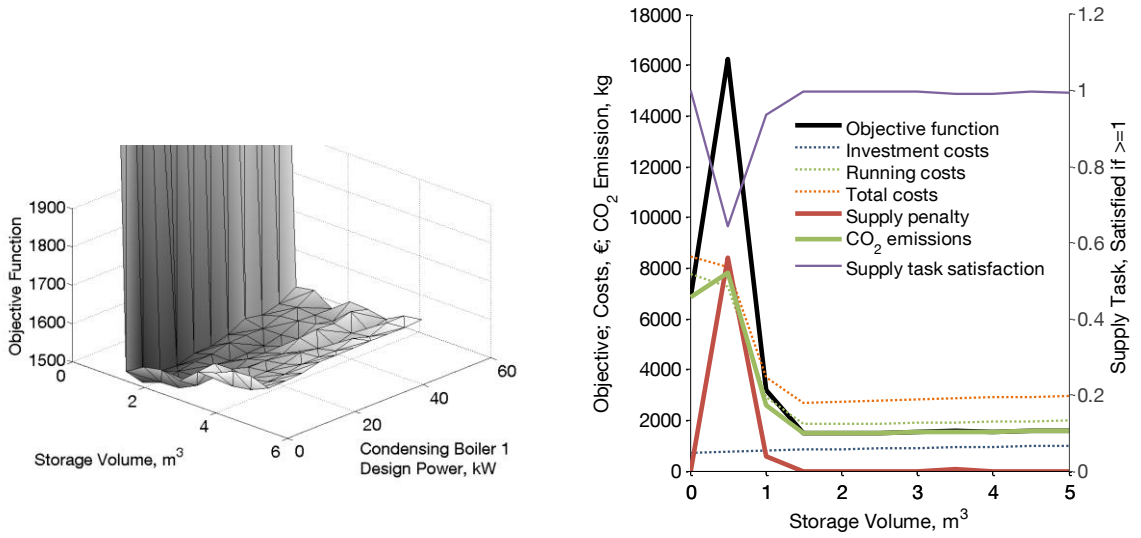

Figure 5.20 *Left*: Objective function - CO_2 emissions minimization. Constant values: P=50 kW, CP2=0 kW, DR=60% (minimal CO_2 emission - Figure 5.21). *Right:* Sensitivity to storage volume variation. Additional constant value: CP1=5 kW. Moscow heating load, "S" building.

5.4.4.1 Optimization Result Analyses

A single condensing boiler is the most economical solution from both the total and investment cost perspective, see Figure 5.21. The minimal amount of fuel, in units of energy, is consumed if the load can be allocated between the two condensing boilers. Only carbon emission reduction benefits from using the whole configuration, a biomass single stage boiler, storage and one condensing boiler. Due to the two energy sources burning two different fuels, the optimization yields different systems for consumption and emission minimization. To save fuel, one bigger and one smaller condensing boiler is recommended.

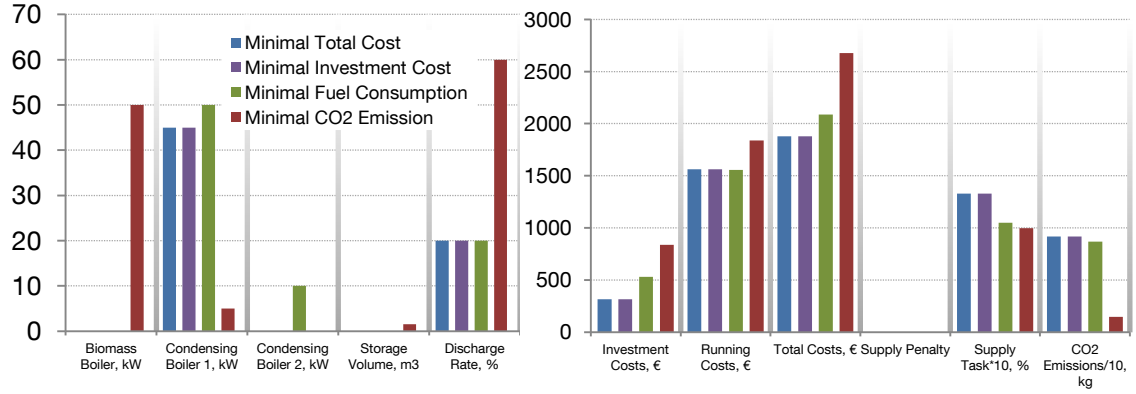

Figure 5.21 Exhaustive search optimization results for Moscow heating load, "S" building. Component sizes (*left*). Costs, emissions and supply task fulfilment (*right*).

Even though this SM does not include a solar collector of photovoltaic components which would influence the building façade, the design can still benefit from analysing it. Figure

5.21 has shown how different the system configurations can be as the optimization goal changes. If the designer has the objective to keep the cost as low as possible, he or she should simply provide space for a single condensing boiler. Hopefully more and more buildings will be built considering their carbon footprint. To reach this significantly lower carbon emission, the recommended system includes a pellet boiler with a storage tank, and a small condensing boiler to cover the peak loads. Such a configuration requires significantly more space compared to the one consisting of a single condensing boiler. Apart from that, consideration must be given to the space for a storage tank, pellet boiler and its fuel storage.

5.4.5 SM5: Two Stage Boiler and Condensing Boilers

Similar to the SM4 optimization, the optimal configuration of the SM5 depends strongly on the optimization goal. Sizes to be optimized are:

- The two stage boiler design power; and
- The condensing boiler design powers.

Again the carbon emission minimization allowed both boiler types, a biomass and two condensing boilers.

The left side of Figure 5.22 shows the shape of carbon emission function depending on the pellet boiler size and the size of one of the condensing boilers. In the figure, the second condensing boiler has a size of 6 kW. On its right, the graph is showing how simple the supply penalty is in case the thermal storage is not utilized. Since this second condensing boiler is rather small, the performance is penalized for all pellet boiler powers in case the power of the first condensing boiler stays very low. The cause is the control strategy not allowing the two stage boiler to turn on until its first or second stage power cannot be fully utilized.

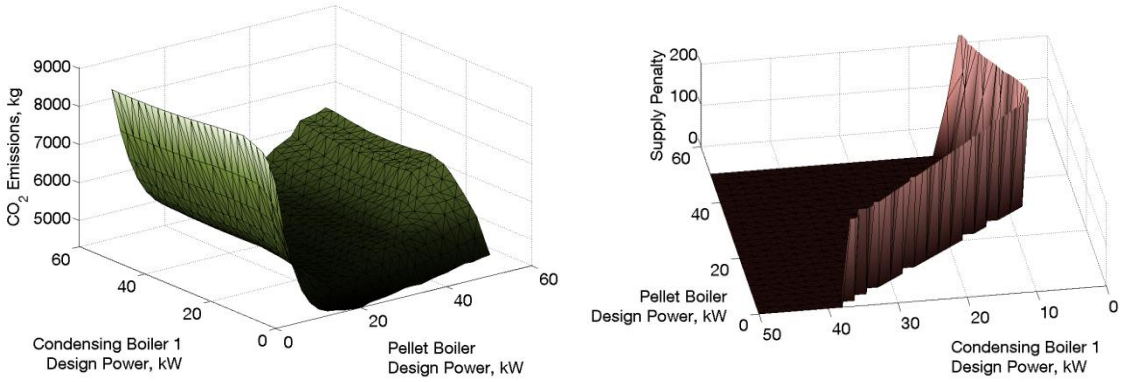

Figure 5.22 *Left*: Carbon emissions. *Right:* Supply penalty. Constant value: CP2=6 kW (CO_2 emission minimization - Figure 5.24). Moscow heating load, "S" building.

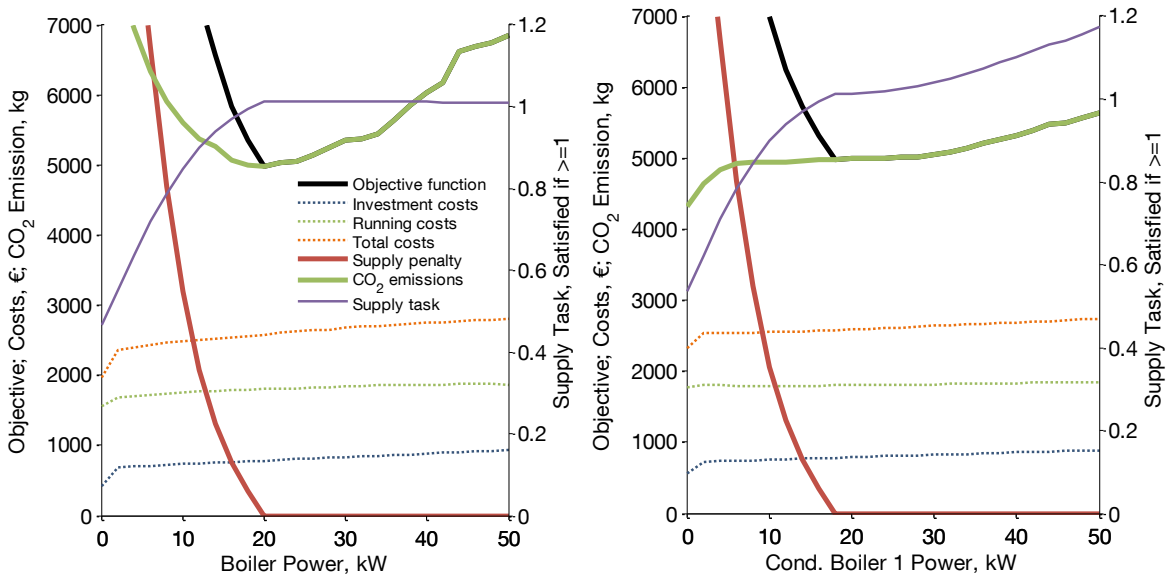

Figure 5.23 Sensitivity to condensing and pellet boiler power variation. Additional constant values are also carbon emission optima: *Left*: CP2=18 kW, *Right*: P=20 kW. Related to the previous figure.

The analysis continues with the Figure 5.23, where on the left only the influence of the pellet boiler size is presented. It can be noticed how the objective function coincides with the emissions once the supply penalty is deactivated. On the right, the pellet boiler has its optimal size of 20 kW, while the minimal emissions are achieved along with the penalty deactivation, at 18 kW.

5.4.5.1 Optimization Result Analyses

Exhaustive search optimization results for an “S” building in Moscow are given in Figure 5.24. Naturally, the load can also be satisfied by a single condensing boiler. This will cause slight overproduction (the supply task value is higher than 100%), but according to the cost minimization it is the best solution. Again, two condensing boilers achieve minimal fuel consumption. Emissions are the smallest if the base load is covered by the two-staged biomass boiler, due to low biomass fuel emissions, and two condensing boilers sized to have minimal overproduction.

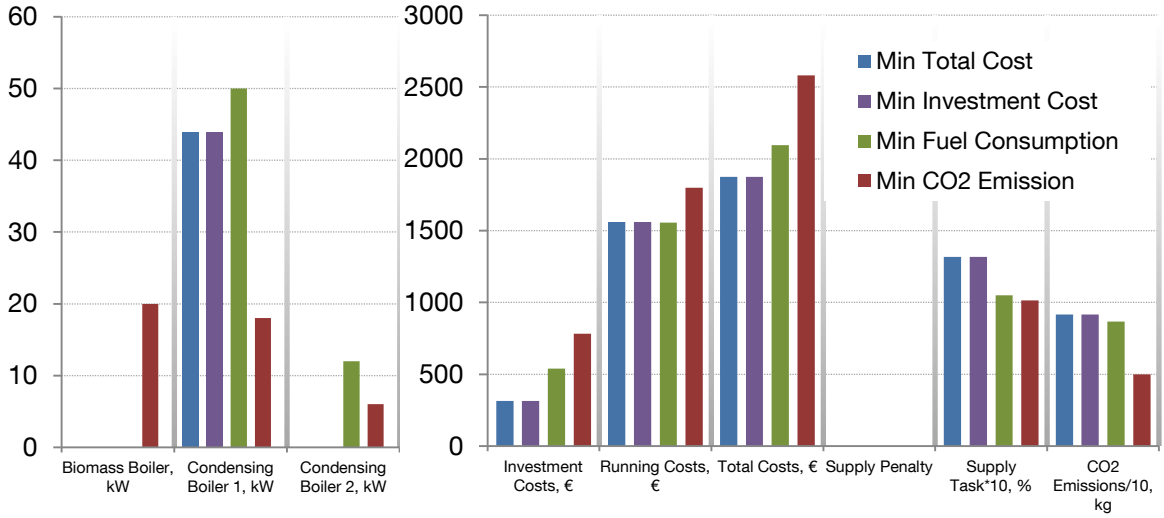

Figure 5.24 Exhaustive search optimization results for Moscow heating load, "S" building. Component sizes (*left*). Costs, emissions and supply task fulfilment (*right*).

The influence on architect decisions would be similar to the one described for SM4 at the end of the section 5.4.4.

5.4.6 SM6: Vacuum Compression Chillers

In this section, another aspect of the optimization model utilization is introduced. The optimizer automatically selects the number of chillers in a system unless it has already been explicitly stated by the user. The automatic minimal number of chillers in a system is based on the recommendations from ASHRAE Standard 90.1, [18] (table G3.1.3.7). The maximal number of chillers defined by the optimizer is the minimal increased in 1. Despite the fact that the same source recommends the usage of equally sized chillers, this restriction has not been implemented. Namely, the chiller efficiency can be increased by using unequal chiller sizes. Unequally sized chillers are able to achieve sustained performance close to full load operation, leading to increased annual chiller COP. This has been confirmed in [60] for air-cooled chillers.

The optimization parameters are:

- The chiller design capacities.

To investigate this issue, SM6, consisting of two chillers, has been optimized for a "B" building in Dubai. The cooling tower is autosized based on the chiller size. The optimization has been performed using the exhaustive search algorithm. The optimization time with two threads and a chiller size step of 20 kW was 278 s.

Figure 5.25 presents the optimization process. The left side illustrates total cost optimization objective function depending on the two chiller sizes. The optimization domain has been modified based on the imposed load in order to reduce the number of evaluations. As Chiller 1 capacity increases to deactivate the supply penalty, the valley of the solutions

capable of satisfying the demand is created. At Chiller 1 capacity of 400 kW a bend can be noticed, which is due to the preset chiller type change. Namely, if not stated otherwise, the model defines all chillers smaller than 400 kW as reciprocating, while the bigger chillers are centrifugal. Centrifugal chillers have higher COPs, which causes a drop in running cost after the 400 kW margin has been exceeded. The same can be seen at the right side of the figure, where Chiller 2 design capacity is kept to its optimum of 1040 kW. As soon as Chiller 1 capacity exceeds 400 kW, the penalty function becomes steeper and the running costs and the emissions decrease. Shortly afterwards, the penalty is deactivated and the optimum is achieved, at 420 kW.

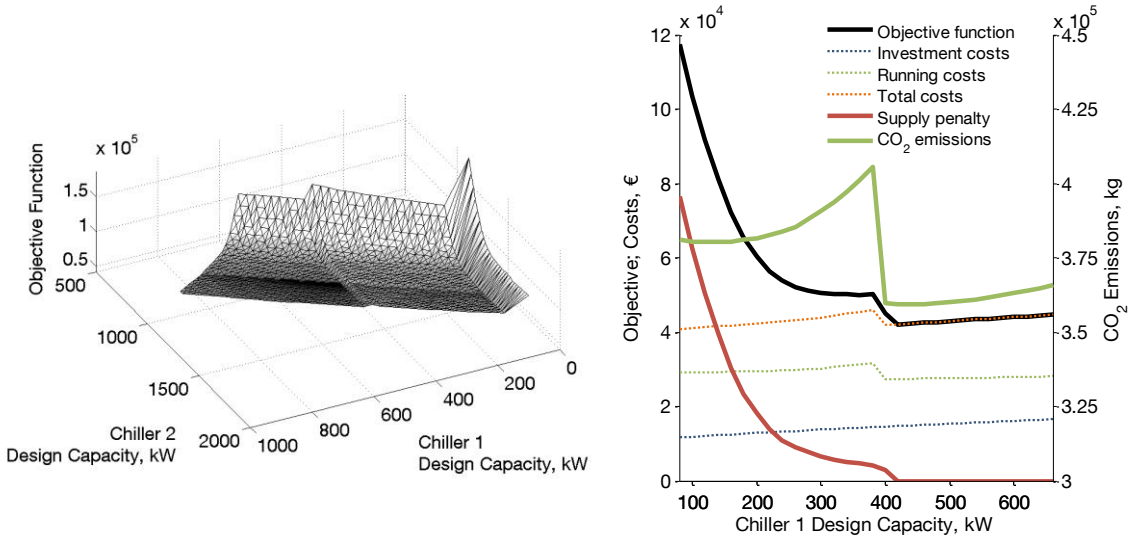

Figure 5.25 *Left:* Total cost minimization objective function related to chiller design capacities. *Right:* Chiller 2 design capacity is kept to its optimum, 1040 kW. Cost, emissions and penalty sensitivity to Chiller 1 design capacity. A "B" building in Dubai.

Evidently, the result of total cost optimization consists of unequally sized chillers. In the next section this result is compared to equally sized chillers, together with the other three optima obtained.

5.4.6.1 Optimally Versus Equally Sized Chillers

Figure 5.26 shows a comparison of chiller sizes, costs and emissions for each of the four optimal results, with the system consisting of equally sized chillers. The later configuration has been defined by the first smallest equal chiller sizes able to satisfy the load without activating the penalty. The upper part of the figure compares the obtained chiller design capacities of 730 kW to each of the optima. Total cost minimization yields chillers of 420 kW and 1040 kW. The difference in size is even bigger for investment cost minimization. Due to electrical power being the only utilized energy carrier in this SM, both CO_2 and power consumption minimization yield identical results. Their optimum is similar to total cost optimization, with 20 kW added to the smaller and subtracted from the bigger chiller sizes.

The lower part of the figure shows the costs, emissions and the quality of the supply. All configurations satisfy the demand. Equally sized chillers have slightly higher investment

cost compared to each of the optima. In return, only the investment cost optimum has higher running costs than the equally sized chillers, bringing these two configurations to the same total cost annuity. Data from Table B 5 were utilized for these calculations. The result may vary with other performance data.

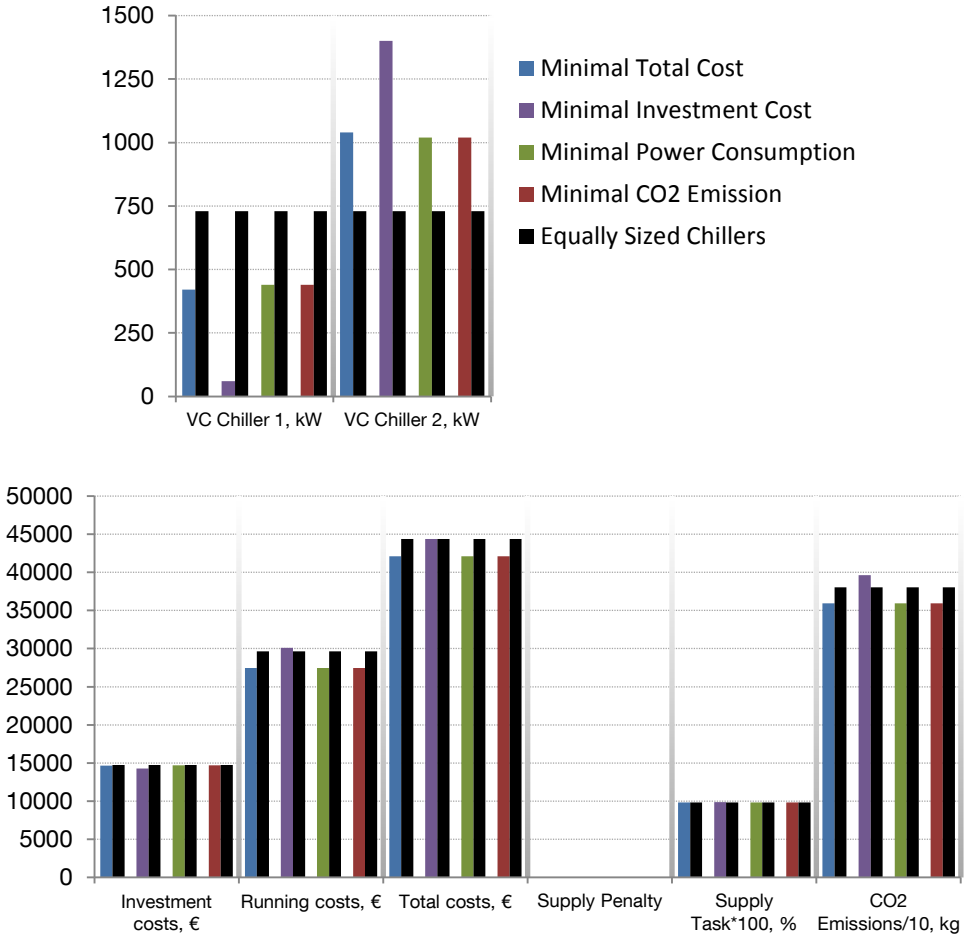

Figure 5.26 Exhaustive search optimization results vs. equally sized chillers. A "B" building in Dubai. Performance results for each of the four optima is compared to the performance of the equally sized chiller combination.

Table 5.2 shows annual COP and PLR values for both chillers of optimally (total cost) and equally sized configurations. Lower average PLR and COP for the equally sized chillers justify the higher running cost. To clarify, the configuration of 2 unequally sized chillers has three full load stages, whereas for the equally sized chillers the number of stages equals the number of chillers, in this case 2. Consequently, the number of timesteps where the load approaches one of the full load chiller stages is also higher and thus, so are the average PLR and COP. Optimal configuration contains a smaller chiller, at 420 kW which, with its minimal power, can cover a larger span of loads without overproducing, compared to a 730 kW chiller. The advantage with using equally sized chillers is that one can replace the other and continue the operation in case of failure. Additionally, the load could be distributed equally between such boilers (to yield identical number of operation hours) leading to identical replacement time. However, unequally sized boilers have lower cumulative operation hours, as shown in Table 5.2.

Table 5.2 Comparison of annual performance parameters for optimal (total cost minimization) and equally sized chiller SM6 configuration supplying a B building in Dubai.

	Chiller 1		Chiller 2	
	Optimal (420 kW)	Equal (730 kW)	Optimal (1040 kW)	Equal (730 kW)
COP	5.6	4.2	6	5.6
PLR	0.66	0.35	0.68	0.67
Operation Hours, h/a	1772	1101	2118	3502

Therefore it is recommendable to allow unequal chiller sizes. The dimensions of a mechanical room should be suitable to accommodate the chiller plant. The cooling tower is usually placed at the roof of the building. Commercial buildings often have mechanical rooms with AHUs at each floor.

5.4.7 SM7: Vacuum Compression Chillers and Photovoltaics

Section 5.2.1 described the supply penalty function. This section investigates how the increase in permitted number of undersupply timesteps, C_{SuP}, influences the optima. Before comparing the optima obtained using C_{SuP}=8 h and those with C_{SuP}=16 h, the optimization relevant variables are analyzed.

The building and the location from the last section have been used ("B" building in Dubai) to perform the optimization. Again the maximal number of chillers in the system was set to two. The maximal area dedicated to PV panels was set to 300 m^2 of both horizontal and optimally tilted surfaces (24°, facing south, Table 3.3). Although, within the model, there is a possibility to allow placing the PV panels on any of the vertical façades, those PV area values were set to zero. The optimization targets a solar ratio of 20%. The variables that are optimized in SM7 are:

- The chiller design capacities; and
- The PV panel area for each of the orientations.

The calculation lasted for 23 min with four threads.

Figure 5.27 presents the results of exhaustive search carbon emission optimization. Its upper left corner shows the surface formed by the objective function if Chiller 2 capacity and optimally tilted PV area are kept constant (960 kW and 300 m^2). Its value is obtained by the summation of the other three functions shown in the same figure. The upper right quarter of the figure shows the carbon emissions. Their value decreases monotonically with the increase in PV area. The same is visible in the right half of Figure 5.28. The emissions are rising with the increase in Chiller 1 capacity up to 400 kW, where the chiller type changes and the emissions drop. The same is displayed in Figure 5.28 on the left. After the sudden decrease at 400 kW, the emissions reach their minimum at 420 kW. With further increases in Chiller 1 capacity, its minimal PLR increases, as does the overproduction and therefore the emissions.

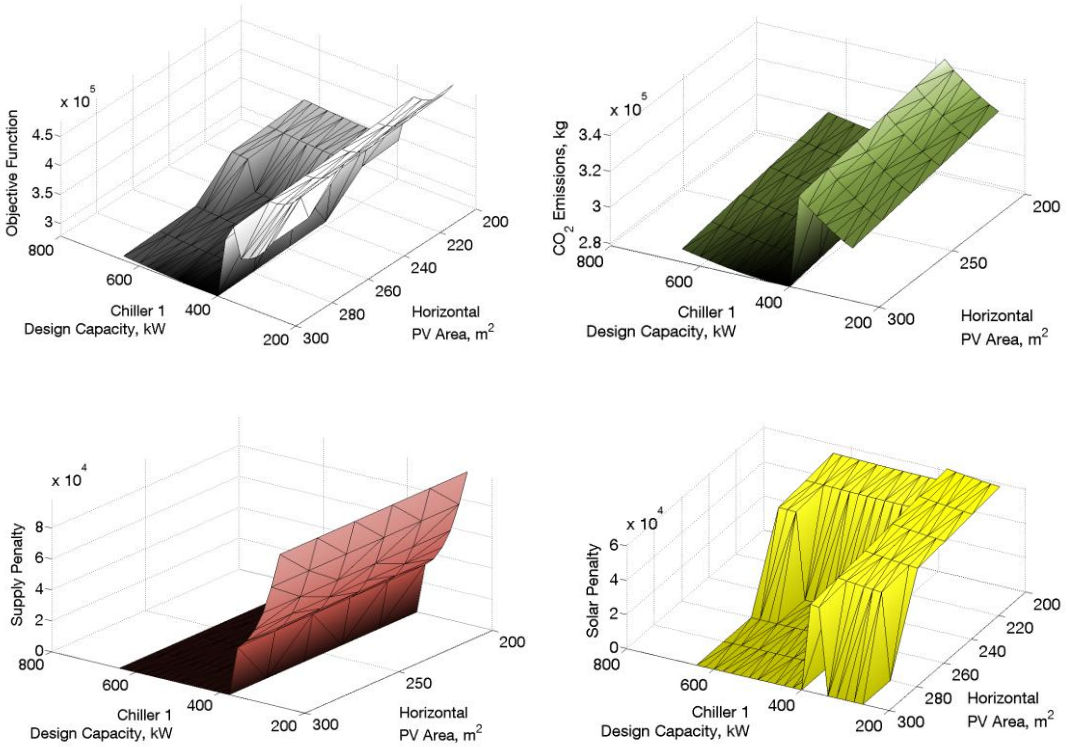

Figure 5.27 *Upper left:* Carbon emission minimization objective function is a sum of the remaining three illustrated functions. U*pper right:* Carbon emission depending on the chiller 1 capacity and horizontal PV area. *Lower left:* Supply penalty. *Lower right:* Solar penalty. A "B" building in Dubai, permitted number of undersupply timesteps is 16. Constants: Chiller 2 capacity equals 960 kW, Optimally tilted PV area is 300 m^2, no other PV surfaces (facing N, S, E, or W) allowed.

The lower left quadrant of Figure 5.27 presents the supply penalty, which depends on Chiller 1 capacity and is not influenced by changing the PV area. As the capacity increases to 380 kW, the penalty is deactivated, which is also easy to recognize at Figure 5.28 (left). The fourth component of the objective is the solar penalty shown in the lower right part of Figure 5.27. It ensures that the targeted solar ratio is achieved if it is feasible under the PV surface area limitations provided. Solar penalty is deactivated at 240 m^2 in the case of optimal chiller sizes and tilted PV area of 300 m^2, shown in the right side of Figure 5.28. The left side of the figure, where the horizontal PV area is constant and equals 300 m^2 (carbon emission optimum), shows that the solar penalty is deactivated for small Chiller 1 sizes, until the chiller reaches 340 kW. Namely, chillers that are too small are unable to satisfy the load. This yields smaller energy consumption and an increased solar ratio. However, the system performance is not satisfactory. As the chiller size increases, the consumption also increases and the supply penalty drops. The solar penalty is still active, since now the consumption is higher and covers the whole cumulative demand, which is a consequence of shifting the remaining load. It enables somewhat smaller components to deliver the demanded energy. After the 400 kW margin has been exceeded, the consumption drops, increasing the solar ratio to a permitted value higher than 0.2 and the penalty is finally deactivated.

Figure 5.28 shows how the investment costs grow with the increase in both component sizes. The running cost increase is interrupted at 400 kW, as expected. The total and investment cost optima are revealed in the next section.

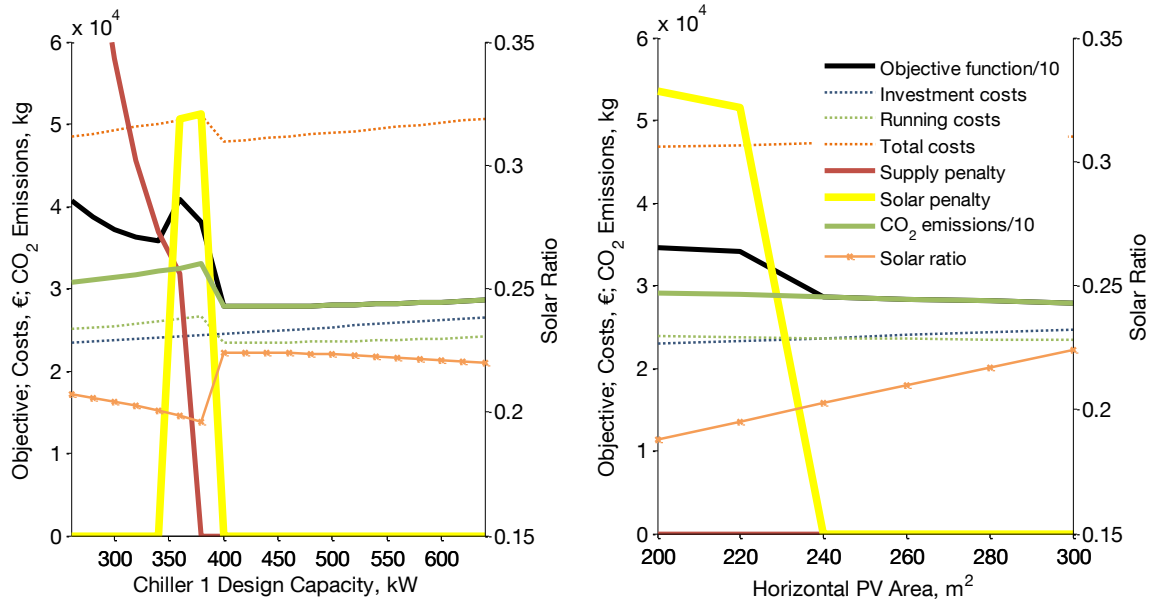

Figure 5.28 Refers to the same case as Figure 5.27. Additional constants (equal the minimal CO_2 optima): *Left:* Horizontal PV area is 300 m^2. *Right:* Chiller 1 design capacity is 420 kW.

5.4.7.1 Optimization Result Analyses

Figure 5.29 shows that if the permitted number of undersupply timesteps is increased, the optimal chiller design capacities are lower. For total cost optimization, the total chiller capacity in the case of 8 permitted hours is 130 kW higher than if 16 hours are permitted. Since the demand load profile remains the same, the lower design capacities lead to an increase in annual chiller PLR. In those 16 instances the undelivered energy, which is very small compared to the annual demand, was postponed and delivered during the timestep(s) that followed. This maintains energy balance. Consequently the PV areas required to achieve the targeted SR are identical for both observed cases.

If discussing the connection between the supply penalty and the building load, the increase in C_{SuP} would mean allowing more "hours of slight discomfort" in the building space. To quantify this dependence, the building and the system should be simulated together, with direct coupling. However, there is the possibility to use such a simplified formulation to obtain the first information on load postponing potential. This penalty function could be useful in the field of demand side management.

The building integrated PV (BIPV) are gaining popularity and their performance is accessed relatively easily during the planning phase. The earlier the architect receives quantification of the meaning of façade and roof mounted PV to a building's energy balance, the better.

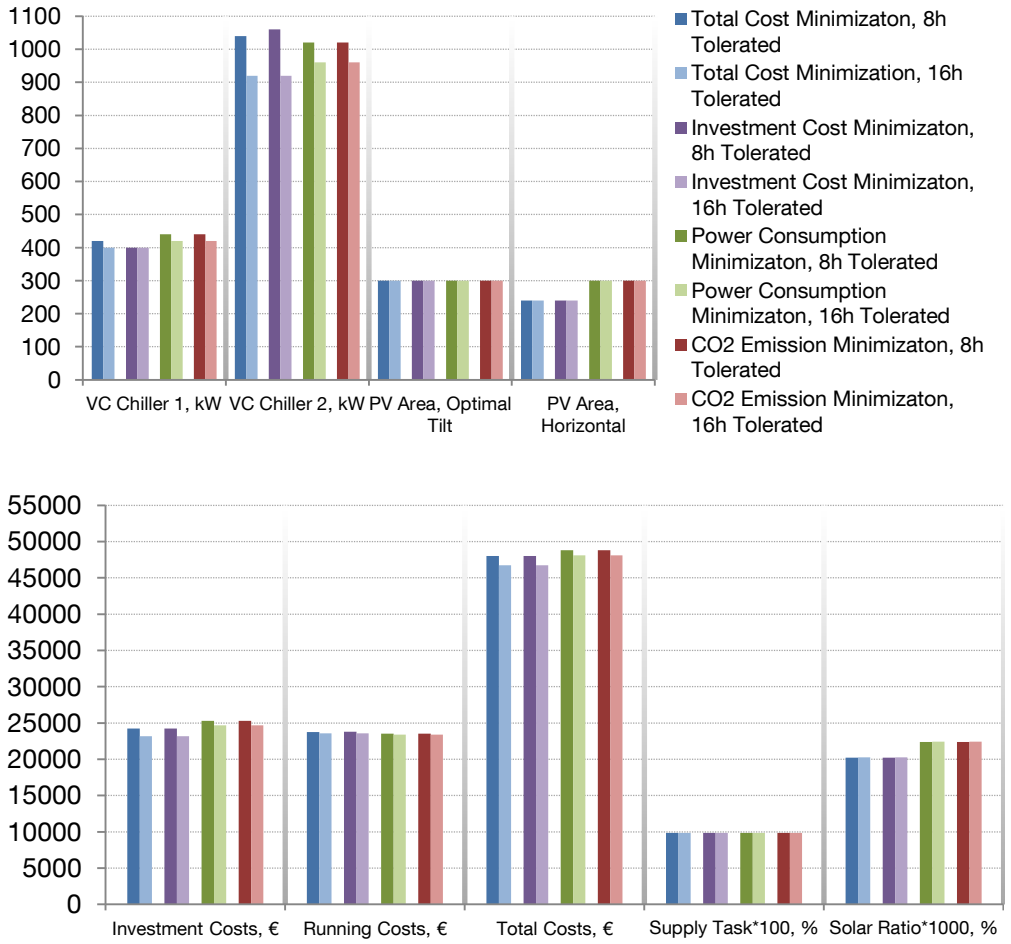

Figure 5.29 Exhaustive search optimization results for the all four optima. The difference between two SM7 with identical PV area limits and SR targets (0.2), one with C_{SuP} of 8 h (Figure 5.27 and Figure 5.28), the other of 16 h. A "B" building in Dubai.

5.5 Summary and Discussion

In this chapter, the optimization problem has been configured and suitable optimization algorithms described. Since the algorithms were able to solve the problem, as demonstrated through the optimization examples, the target of performing the primary HVAC optimization based on the system performance simulation, which relies on limited system and building configuration data, has been reached. The optimization goals were selected to suit the intentions of the potential users. Namely, each of the interested parties can identify its targets within the featured set of goals, for instance:

- For the investors – e.g. investment cost minimization;

- For the owners – e.g. total cost minimization, carbon emission minimization (concerning the building certification); and
- For the tenants – e.g. fuel consumption and carbon emission minimization.

The constraints were transformed into two penalty functions. The penalties enable two levels of result quantification – the first informs whether the constraint has been breached, while the second quantifies the violation. Therefore, formulating the constraints as penalties simplified the assessment of the quality of the results which cause slight constraint violations. The first penalty, the supply penalty, ensured the set load was met by the optimal system. Physically, this penalty deals with the inertia existing between the building and the system and offers further implementation potential in the field of the demand side management. It would be interesting to further investigate the causes of the "bumpy" behaviour of this penalty function; exhibited where the system contains thermal storage. The second one, the solar penalty, provided an additional optimization goal, which can be combined with any of the four objective functions, enabling multi-objective optimization. It forces the system to generate a desired solar ratio (a fraction of total energy fed to the building space originating from the solar source). For instance, even while targeting minimal investment, a certain solar ratio can still be requested. The assignment of scalar values to both penalties and to the objective function finalizes the simulator, see Figure 2.1.

Two optimization algorithms, the Global Bounded Nelder Mead (GBNM) and the exhaustive search, including its modifications, were proposed as solvers. Although both algorithms were able to solve the optimization problem, the exhaustive search (with adaptations in domain size and grid step) has performed more reliably and within a tolerable speed. This is due, firstly, to the number of optimization parameters in the treated problem being small and, secondly, since the exhaustive search steps are mutually independent, they can easily run in parallel. As long as the steps of the grid in all dimensions correspond to the differences between manufactured component sizes, it is recommended to utilize this method. However, the major advantage of the globalized bounded Nelder-Mead (GBNM) algorithm lies in its significantly lower sensitivity to the number of optimization variables. Still, to be certain, the global minimum has been identified by the GBNM, the permitted number of function evaluations and probabilistic restarts needs to be high, which prolongs the calculation time.

With this chapter, the flowchart from Figure 2.2 has been completed. In its last part, the presented optimization methods were used to demonstrate the SM dimensioning through optimization. An optimization example was given for each of the SMs, configured in chapter 3. The purpose of each example was primarily to evaluate several aspects and potentials of the overall model utilization. In addition, the examples have shown how this optimization can influence the early design. The next chapter of the thesis provides an example to further explain this aspect.

There is space for improving the optimization run time and the suitable optimization algorithms have also not been exhausted. Further zero order methods could be evaluated, or the problem reformulated in order to expand the selection of suitable algorithms. The quality of the optimization algorithm becomes even more significant if the generic system model, introduced in 3.4 is created, due to the increased number of optimization variables of such a model. As announced in the section mentioned, a generic model would allow a system to

be configured by the optimization procedure, based on the imposed goal and considering the climate and building load (building envelope and its utilization). An illustration of this is the SM4 optimization, the example from section 5.4.4. In this example, if minimal emissions were targeted, the full SM4 configuration was obtained, while the cost and fuel consumption minimization yielded a system that, in fact, equals SM2. A generic model would demand even lower engagement of the potential user, the architect, which has both advantages and disadvantages.

As for now, the architect needs to be informed on each of the SMs and decide himself which one to optimize. Nevertheless, some help is still provided to the user. This will be explained along with the proposed user interface, presented in the last chapter before conclusion.

6 PROBA Tool Prototype

Developing and configuring system models, defining the optimization problem and identifying its appropriate solution method are all necessary but not sufficient to enable their actual utilization during conceptual design. Many architects would prefer to face a user-friendly interface instead of using a command line. In answer to these requests a tool entitled PROBA is proposed. PROBA stands for primary system optimization for buildings targeting architects. It is a tool created by adding a wizard-style graphical user interface between the previously described model structure and the user. It provides the majority of the functionality of the developed model and provides it to a non-expert user. PROBA is compatible with the ClimateTool and the FassadenTool, [12]. This chapter describes the structure of the initial version of the user interface developed in MATLAB and shows an example of its utilization through a case study.

6.1 PROBA User Interface

Figure 6.1 presents the steps the user takes to utilize the tool. The three basic steps are:

- Simplified load and weather data input;
- Selection of an SM and proceeding with optimization or simulation; and
- Additional SM related input before running the calculation.

These and the other steps illustrated in Figure 6.1 are explained in this section. The procedure after selecting an SM is explained through a subsequent case study.

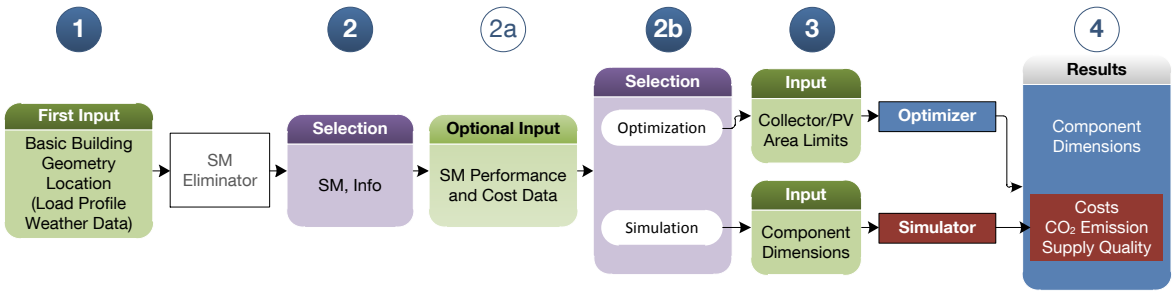

Figure 6.1 Basic information flow in the PROBA tool. Steps 1, 2, 2b and 3 are obligatory. Step 2a is optional.

1 First Input

To enable SM simulation and optimization, the user is required to provide the ideal building load and the weather data for the location. In general, any externally generated hourly load profile can be provided. Figure 6.2, on the left, shows a screenshot of the first user input window.

In the current version of the tool there are two possibilities to supply the building load to the simulation:

- Fast building geometry input is available for the 4 cities (Shanghai, Dubai, Bangalore and Moscow). Locations climatically similar to any of the cities can also use this fast input. Namely, for these locations, a database with single office ideal load profiles has been provided by Liedl [12]. Appendix A offers detailed description of the connection between the single office load profiles and their scaling to obtain the building load. The upper part of the screenshot shown in the left of the Figure 6.2 shows the basic building geometry input required after choosing the location.
- If the user has created the individual ideal building load prior to using the tool, this file can be loaded using the “Browse” button at the lower part of the window. The required file format is a text file, where the hourly load data should be placed in the second column, while the first one indicates the hour. This way of setting the load allows greater variety in building geometry.

2 SM Selection

After the user inputs the city and the geometry, or provides an external load data file, the SM Eliminator eliminates the SMs considered, unsuitable for such a load. Currently, heating systems are eliminated if the location requires only cooling, and vice versa.

The user makes the choice of the SM to be optimized. To support this selection, the user is provided with basic information on the system and its limitations, such as place requirement and environmental considerations. In the example illustrated in Figure 6.2, the cooling systems are not available, since the building is located in Moscow. In the next command the user selects the info button explaining the model consisting of a biomass boiler, thermal storage and solar collectors (SM1).

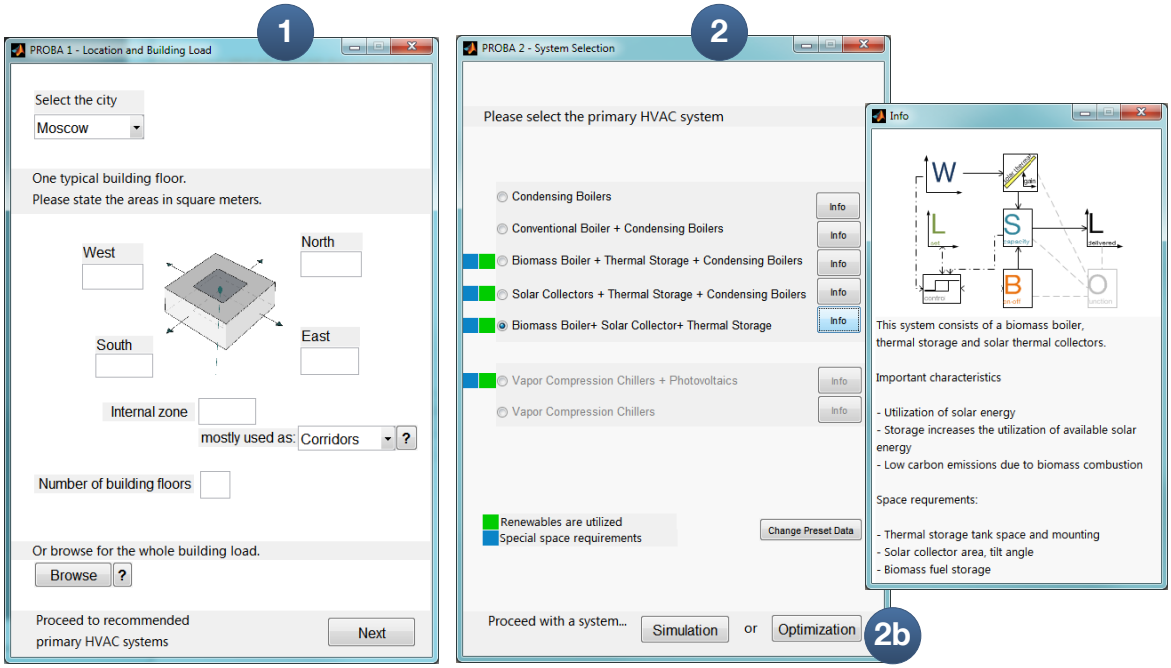

Figure 6.2 *Left*: First data input. *Middle*: SM selection. *Right*: SM information window.

2a Performance and cost data customization

For more demanding users, there is a possibility of editing the preset data, as illustrated in Figure 6.3. However, only a limited set of data is currently accessible. This principle could be extended to component price functions and performance data.

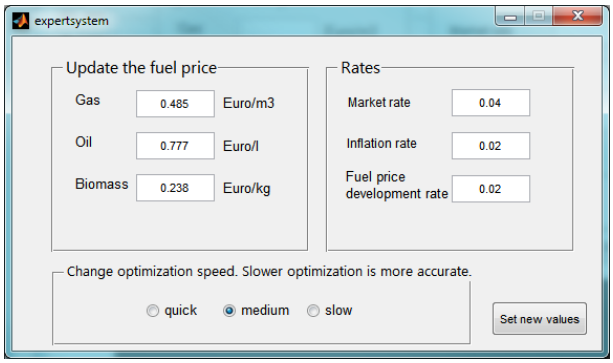

Figure 6.3 Optional user input – basic cost data customization.

After deciding on the system to evaluate, the process can be continued by running either the optimization or the simulation. To run the simulation, the user needs to provide the component dimensions. To run the optimization, only the models with solar collectors and PV panels require additional input, which consists of the available façade or roof area to mount the stated components. The description of the user interface continues from step 3 in the next section. It presents an example of the tool utilization for performing an optimization.

6.2 A Case Study

The following case study shows how a change in building geometry influences the primary HVAC component dimensions, costs, and emissions. As an example, a building with 6250 m^2 of office area is planned in Dubai. The designer has a goal to reach a solar ratio of 30%, while minimizing the total cost. First the initial design is presented and its primary HVAC optimized using PROBA. Since the initial design fails to reach the target, an alternative design is proposed and its optimization presented. Corrections are based on information on optimal PV tilt angles, section 3.2.6, and guidelines provided in Liedl [12].

The initial building has 10 floors, with more office area facing west and east (120 m^2 per building floor) than north and south (80 m^2). The internal zone has an area of 224 m^2 at each floor. The window area ratio is 50 %.

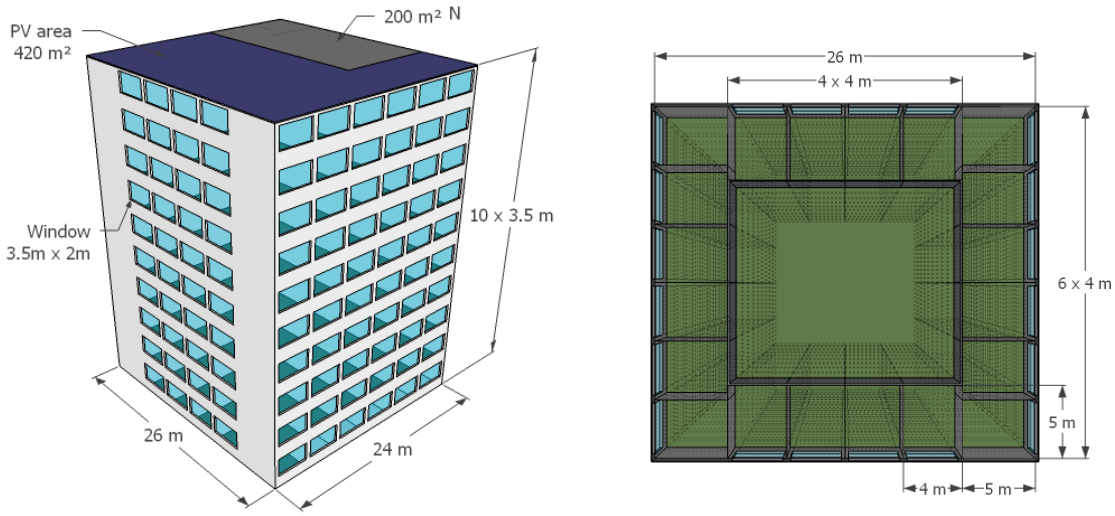

Figure 6.4 Initial design of a 10 floor building located in Dubai, 6250 m^2 of office area. Window area ratio is 50%.

After entering the building geometry into the PROBA 1, illustrated in Figure 6.5 on the left, the SM selector eliminates all the heating systems, since there is no heating demand in Dubai. One of the remaining available models has a green square next to it, indicating utilization of renewables. Thus, the SM7 featuring chillers and PVs is selected to be optimized.

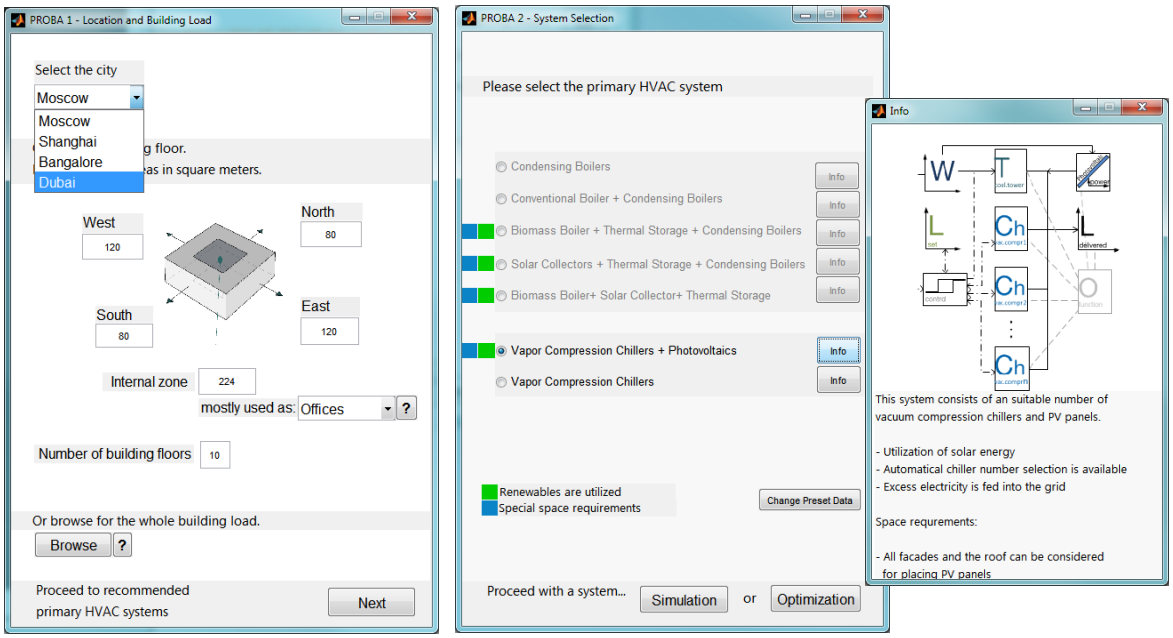

Figure 6.5 Selecting Dubai as a location, entering the building geometry. Selecting vapour compression chillers with PVs to condition the building, based on the information provided in "Info".

3 Final Input

The user is required to provide the PV area limits and target solar ratio, see Figure 6.6. The roof has a horizontal area of 624 m^2, of which 200 m^2 need to be left free for other utilizations, allowing 424 m^2 to be reserved for PV panels.

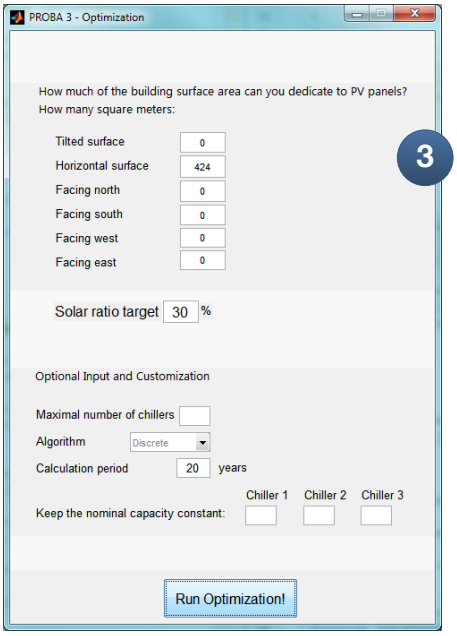

Figure 6.6 Final input before optimization: the targeted solar ratio and maximal façade and roof areas available for PV panels.

4 Results

After the optimization has completed, the window shown on the left side of Figure 6.7 opens automatically. It offers four sets of results to the user, each belonging to one of the objective functions explained in chapter 5. Since the user is interested in total cost minimization, after clicking the appropriate button, the results for the initial design are shown, as in the middle screenshot in Figure 6.7. The system achieved a solar ratio of 20% and has thus failed to achieve the target of 30%.

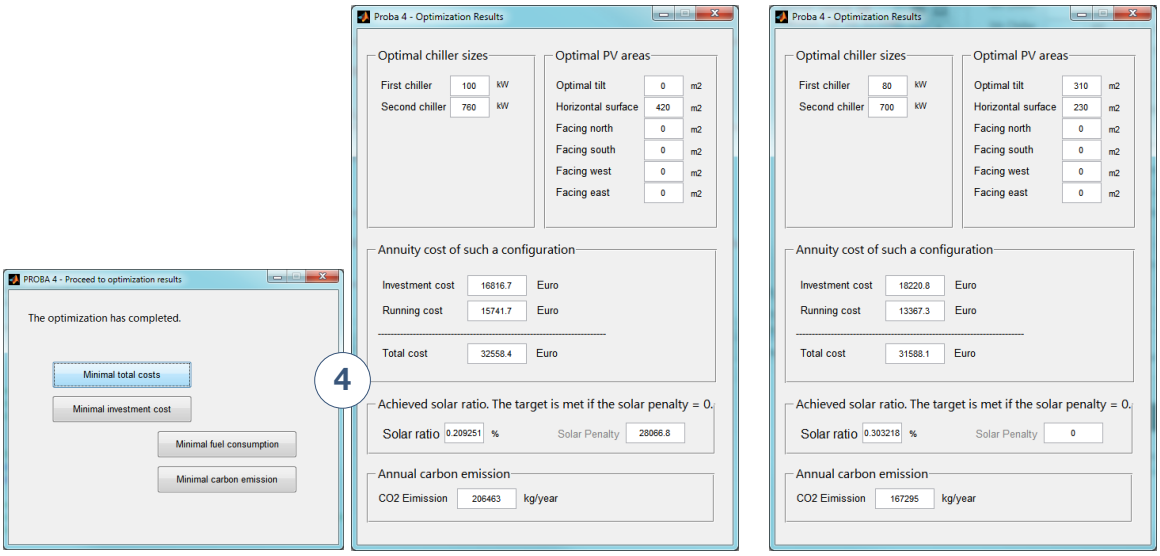

Figure 6.7 *Left*: Results for all objective functions are available – total cost minimization is selected and the results for the initial building can be viewed (*Middle*). *Right*: The results for the alternative design. With this new design the target has been reached.

An alternative design needs to be proposed in order to reach the specified target. The modifications in building design consist of:

- Increasing the roof area by reducing the number of building floors, which provides more area available for PV;
- Tilting the part of the roof at an optimal angle, Table 3.3. This in addition makes the south façade smaller than the north, leading to lower heat gains.
- [12], (page 179), states the west façade has the highest gains – the building is reoriented to reduce the office area facing west; and
- [12], (page 177), provides a diagram with the interaction between the natural lightning, the office length and the window area ratio. The new window area ratio of 30% has been selected, which provides 300 lux.

The proposed alternative design is illustrated in Figure 6.8. Figure 6.9 shows the new iteration of supplying the input to the first and third step of the PROBA interface.

After running the optimization, the result shown in the Figure 6.7 on the right is obtained. Here, the solar ratio target has been achieved. Furthermore, the total cost annuity has also decreased, due to the decrease in running costs being greater than the increase in the investment cost. As expected, significant carbon emission savings have been achieved.

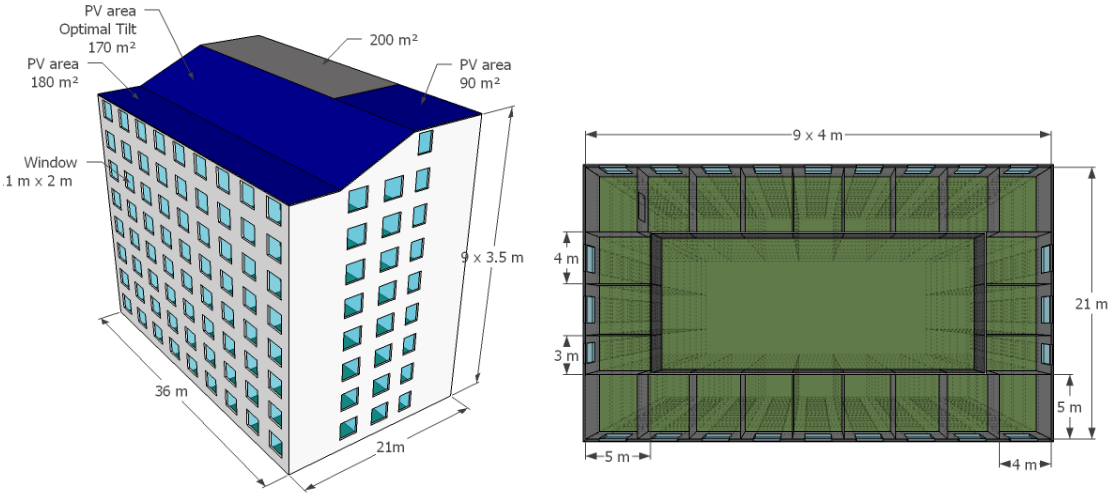

Figure 6.8 Alternative building design. The building surface area remained approximately the same. The number of building floors is decreased to 8 (9 towards the south). The south oriented roof tilt equals the optimal angle, Table 3.3.

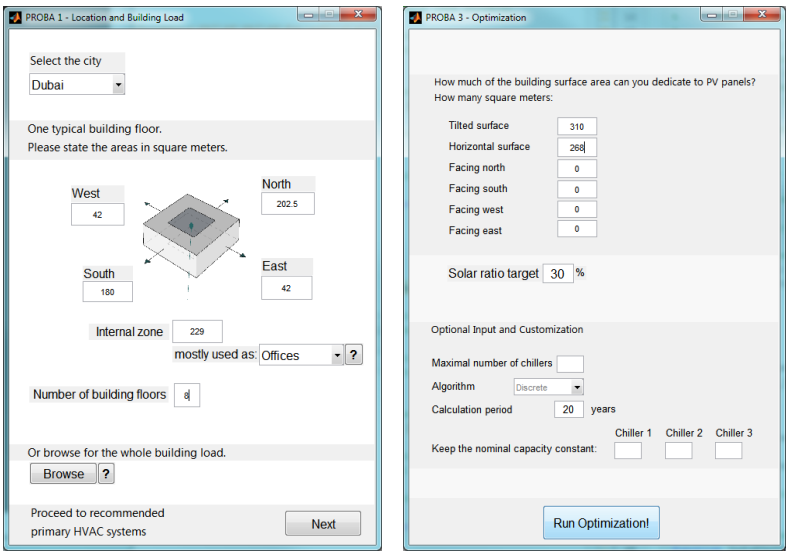

Figure 6.9 First and final input windows for the new building design. Its optimization results are given in Figure 6.7, along with the initial design results.

6.3 Summary and Discussion

As defined in the problem statement, in section 1.1, the goal was to provide a tool, which would help to foresee the influence of the preliminary building design decisions on the

primary HVAC configuration and related energy consumption. This was achieved through configuring a test version of a tool entitled PROBA, whose major characteristics are:

- It provides guidance in terms of user input and SM selection before running the optimization or the simulation; and
- It features developed models and optimization algorithms, which form the fundamental intelligence of the tool.

The user interface was created to simplify the utilization of the models developed. Each of the system models can be optimized and their results compared for a single or for several building designs. Where the building design remains unchanged, the user can simply compare the resulting costs and emissions for different SM configurations. Depending on the configuration of the SM, yielding the most suitable results, the interior or exterior building design may be influenced. Receiving basic information on these requirements, available in the information section of the tool, the architect can consider them in further design stages. In the example presented, a comparison of two alternative designs was performed. A set of transformation measures helped to reduce the demand (using FassadenTool, [12]) and increase the solar gains, enabling the new design to reach the targeted solar ratio, which failed when using the initial building design.

Further benefits could be drawn from connecting PROBA to planning tools developed by Liedl, [12]. Namely, if the database of the FassadenTool is directly accessible by the PROBA load input, a connection between the change in façade construction and the primary HVAC performance and configuration can be investigated more easily. However, this is currently available only for the four targeted cities. The ClimateTool is able to provide the second obligatory input – the weather data including the radiation on the tilted surface. This is available for locations worldwide. If both these connections exist, the PROBA input is defined. When it comes to the selection of the SM to be optimized, there are the two options to improve it:

- If a generic model, as mentioned in previous summaries (3.4, 4.4 and 5.5), is created, the user selection becomes redundant. The optimization configures the model automatically, based on the optimization goal; or
- Adding capabilities to the SM eliminator based on the mutual dependency between the meteorological data, such as air humidity, temperature, solar radiation, etc. and component characteristics.

In general, if continuing the development of such preliminary design tools, the thermal distribution system needs to be described more precisely, rather than using a coarse approximation. A series of test and improvements, both in terms of software development and in terms of applicability, are required to upgrade PROBA into a reliable tool.

7 Conclusion and Outlook

The decisions required during the conceptual building design have an important effect on the building energy performance (BEP). The consequences of these decisions are often overlooked and the extents of their influences disregarded. Therefore a more strategic approach to the interaction between the BEP and the conceptual building design has been investigated within the scope of the International Graduate School of Science and Engineering project “Buildings, User, Climate”.

The selection of feasible heating and cooling energy generation and storage systems and their components becomes increasingly limited as the building design progresses. This thesis investigated the relationship between the primary HVAC system and the conceptual building design. The goal was to provide a quantification of this interplay between the initial design decisions and the configuration, dimensions, consumption and emissions of the primary HVAC system. In order to achieve this, a tool enabling the following needed to be developed:

- The system design optimization, providing a configuration suitable to satisfy the thermal conditioning demand of provided building alternatives;
- The quantification of the fuel consumption and carbon emissions of the proposed system while conditioning the provided building; and
- The cost assessment, including both the investment and the energy consumption related costs on an annual basis.

The major challenges which mutually influenced the development of this tool, suitable for preliminary design utilization, can be categorized as follows:

- Proper assessment of the intermittent renewable energy sources (RES), thermal storage and component part load efficiencies requires a time domain system simulation;
- A large number of primary and secondary HVAC system characteristics and parameters are unknown during the conceptual building design; and
- The targeted users having a low level of expertise in the field of HVAC engineering.

Seven primary HVAC system models were configured, including components such as boilers, chillers and cooling towers, thermal storage, solar thermal collectors, and photovoltaic modules. A control strategy has been developed for each of the models and their yearly quasi-stationary simulation performed in hourly steps. Simulation performance has been evaluated using building conditioning demand and weather data for four cities situated in four different climates. The performance profiles obtained, yielded the information

necessary to calculate the energy consumption and related cost, and carbon emission. The annuity method has been employed to calculate the cost. The annual values of total and running cost, energy consumption and carbon emissions were used to form the four optimization goals. In the formulation of the optimization problem, the constraints were defined as two penalty functions. The first ensured the system satisfies the energy demand, while the second enabled obtaining a desired annual solar ratio. Two optimization algorithms, the global bounded Nelder Mead and the exhaustive search algorithm were implemented. Their purpose was to identify the system component dimensions that provide minimal costs, emissions or consumption while maintaining the quality of the supply on an hour to hour basis and, where specified, achieving the targeted annual solar ratio. Finally, a tool entitled PROBA has been designed and proposed by adding a user interface to the models. The major characteristic of the interface is its suitability for non-expert users. This is achieved by, firstly, reducing amount of input data by implementing preset values and, secondly, providing information support.

As a conclusion, the developed modeling and optimization method enables the following:

- Informing the designer of the suitable primary HVAC configuration, its size, costs, consumption and emissions very early in the building design process. The same information can be provided for each consecutive design variation, thus illuminating and quantifying the consequences that a certain design decision has on the primary HVAC performance, dimensions and configuration.

In that methodology, each of the listed challenges was treated as follows, respectively:

- The hourly annual system performance was used to identify the optimal design, as opposed to one stationary peak load condition. This also helped to avoid the component oversizing, increased the system efficiency, whilst decreasing the investment cost and carbon emission;
- The lack of input data was answered by using standard and approximated values, implemented as preset data. At the point of simulation, the demand on input data has been reduced by developing a load based simulation with a set of corrections and limitations, which prevent thermodynamical inconsistencies;
- Finally, a simple user interface has been developed, that simplifies model utilization. The combination of this interface and the model functionality yielded the PROBA tool. However, such a tool represents merely one of the possibilities to apply the developed models.

Apart from using the methodology during conceptual building design, further utilization potential of the models developed lies in the analysis of the existing systems. The simulation and optimization models could serve as support during planning the primary HVAC system improvements and refurbishments. Further implementation of the optimization procedure is possible in planning or analyzing the thermal conditioning supply on the scale of the block of buildings or even, the whole settlement. Minor adjustments and extensions (e.g. seasonal storage) would allow both the investigation of the centralized and decentralized energy supply design and performance. Namely, such problems take advantage of the hourly simulation, in terms of system dimensioning, the same way a single building does.

Two major tasks define the work necessary in order to enable the broader utilization of the overall model presented. The first task includes model validations and the consequent model adjustments. The second task requires a more precise assessment of the performance of the secondary systems at the level of preliminary design. Further work on the system model itself includes the integration of additional generation and storage components and follows the proposed use of a generic model. Adding all these improvements to the developed methodology would yield a sophisticated thermal conditioning generation plant design and analysis tool for the preliminary design of a single or of several buildings. The tool would be able to automatically both configure and size the primary HVAC system. However, the development of such a tool would require effort that severely exceeds the scope of a dissertation.

Providing architects with the developed tool represents an efficient and effective way to consider the primary HVAC during the preliminary design, without causing additional cost. It offers part of the knowledge of an HVAC engineer, without actually employing one. However, such a tool can never replace an engineer and there are added risks in terms of having a passive user incapable of judging the quality of the result. Nevertheless, if considered with care, the information provided by the tool is beneficial for the building energy performance. In addition, the use of this and similar tools heightens the awareness of architects regarding the significance of the building energy consumption and inspires further education in this field. As a consequence, the interest in interdisciplinary communication increases and creates an environment more readily prepared to accept and investigate the benefits brought by building information modeling.

Appendix A
Load and Weather Data

The essential input data required to utilize the proposed models are the weather data and the primary HVAC load profiles. The primary HVAC load assessment is explained in A 1, and includes presenting the loads used for calculating the examples throughout chapters 3 and 4. Annual profiles for solar radiation, wet and dry bulb temperature are the meteorological data required. The weather conditions at targeted locations are introduced in A 2.

A 1 Primary HVAC Load Data Assessment

If the thermodynamical conditions inside the building space, where the user comfort needs to be satisfied, differ from the ambience conditions, the heat and mass is transferred between the two. Assuming the conditions inside the building remain at a constant set value, an annual profile of this heat and humidity transfer can be obtained. Such a load is often called an "ideal load". Presuming the planned building geometry and materials are known, the ideal load can easily be calculated by building thermal simulation tools such as TRNSYS or EnergyPlus. If the emission system can meet such a load, the set point is maintained.

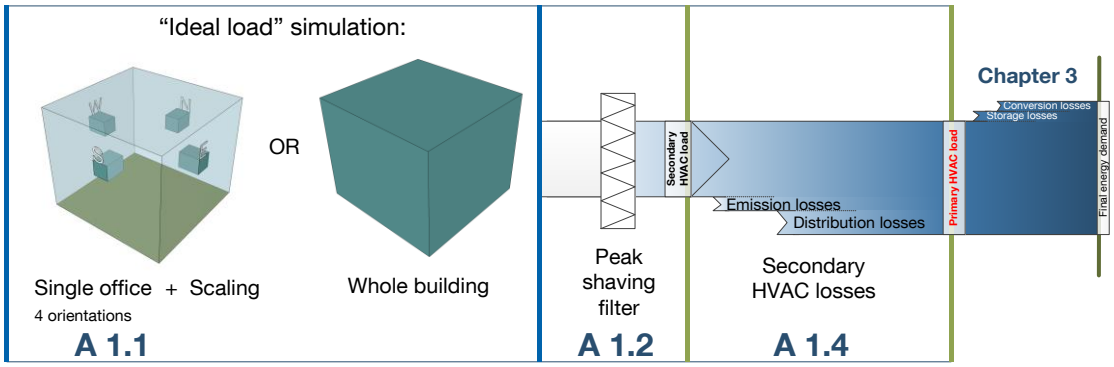

Figure A 1 From the ideal building load to the primary HVAC load. The first input in PROBA tool, the ideal load, is processed by peak shaving, adding distribution and emission losses to obtain the primary system demand profile used to simulate and optimize the SMs.

The load demanded as an input to the PROBA tool is in fact the ideal building load. Two approaches to ideal load assessment are utilized, see Figure A 1:

1) Constructing the whole building load by scaling the one zone single office simulation results provided in FassadenTool. The validation of this method is presented in A 1.1.
2) Whole building simulation yielding a cumulative building load.

Both methods are implemented in the PROBA tool.

The simulated ideal building loads can sometimes contain unrealistic peaks. In real systems such peaks could be avoided by a suitable control system. Such a control system is able to take advantage of the building storage mass and allow preheating/precooling of the building or to reset the temperature set point in case of an extremely cold/hot day. Therefore, before using an ideal load as an input to the primary system simulation, the peaks of the simulated load are shaved depending on their size and frequency – the calculation details are presented in section A 1.2. The load obtained by the peak shaving procedure is considered to be the secondary HVAC load.

To convert the secondary into the primary system load, it needs to be enlarged for the distribution and emission losses. Simplified loss coefficients have been used to account for these losses, see A 1.4.

A 1.1 Scalability of Single Office Load Profiles

In this section, scaled load profiles originating from a single office simulation are compared to results of whole building simulation. This benchmark, carried out for an office building in Shanghai, has confirmed that for an early cooling load estimation, it is indeed possible to simulate just one office for all necessary orientations and scale the result. The scaled result and the core zone loads are aggregated to obtain the secondary whole building load. The core zone is taken into consideration assuming constant internal loads per unit of area. The absolute value depends on the function of that space (e.g. staircase or office space).

A 1.1.1 Validation Approach

The Shanghai climate was chosen to investigate the described issue. Four single zone simulations of an office were performed, each for one cardinal direction. After choosing the appropriate building geometry, the office results were scaled and compared to the results of the building simulation. The corresponding building zone is compared to the appropriately scaled office with the same orientation. Since the single office simulation only accounts for the peripheral area of the building, a building model with and without heat exchange between the core zone and peripheral offices was investigated to assess the influence of building's core zone. The heat exchange through the roof and floor is similarly investigated.

The construction parameters for the single office façade are given in Table A 1. The same parameters have been used to simulate the whole building. The building has been chosen to have an elongated shape with six floors, as illustrated in Figure A 2. There is an array of 15 offices on each of the two opposite sides of one floor. Due to its shape, the building space is approximated by three zones.

Two basic building orientations are simulated. The first was the north/south, after which, the building was rotated for 90° to face the east/west orientation. Since the majority of the results presented here originate from the north/south orientation, the zones of the building

are referred to as North, South and Core zone. The comparison for the east/west orientation gave results similar to those from the north/south orientation. The Core zone represents the internal building zone without windows, positioned between the North and the South zones. Two thirds of its surface area is assumed to be conditioned.

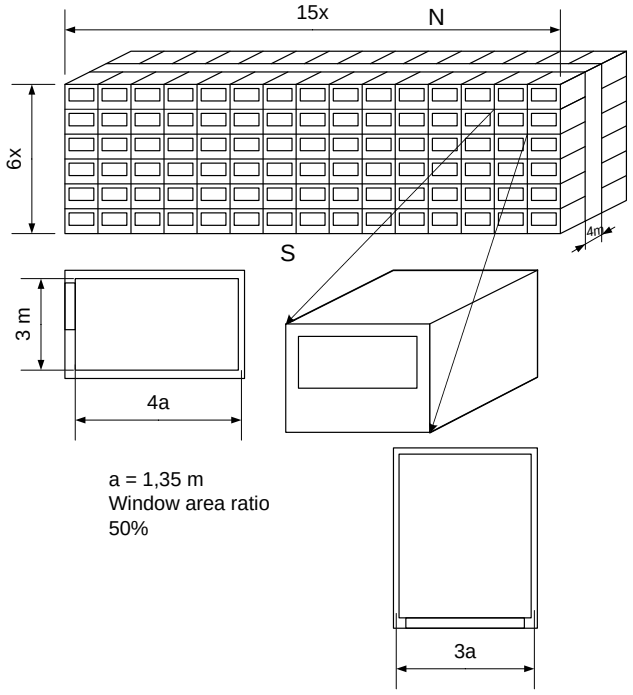

Figure A 2 Test building basic geometry scheme and office dimensions.

Table A 1 Test building envelope properties.

Wall	Layers	Thickness
Internal	Gypsum Mineral wool Gypsum	126 mm
External	Gypsum Wood Insulation Wood	133 mm
Ceiling/Floor	Carpet Screed Mineral wool Concrete Air Mineral wool	295 mm
Window	Interpane IPASOL natura 6634 6/16/4	

Internal gains used are represented in Table A 2. At the early design stages the precise function of a particular part of the building is unknown. Thus a constant internal gain of

50 W/m^2 inside the conditioned fraction of the Core zone is assumed. No shading was assumed in this test scenario.

Table A 2 Internal gains

Internal gains		Power	No. per office
North and South zone	Person	30 W radiation, 45 W convective	2
	PC	230 W	2
	Lights	5,77 W	1
Core zone	50 W/m^2 x 1000 m^2=50 kW		

To evaluate the comparison results, four variations of building simulation were implemented, see Figure A 3. A single office simulation is performed assuming no heat transfer through the internal walls. The first variation of the building simulation, "Building 1", takes heat exchanges between the zones into account, as well as those through the northern and southern external wall. All other walls, except those inside one zone, are considered to be adiabatical. "Building 2" is equivalent to the office simulation and allows the heat exchange only through the northern and southern external wall. The third version, "Building 3", is more realistic and adds heat exchange through the eastern and western walls of zones S and N to "Building 1". "Building 4" is the version closest to reality, keeping only vertical external walls of the core zone adiabatical. The four building simulation cases quantify the influence of the simplification grade.

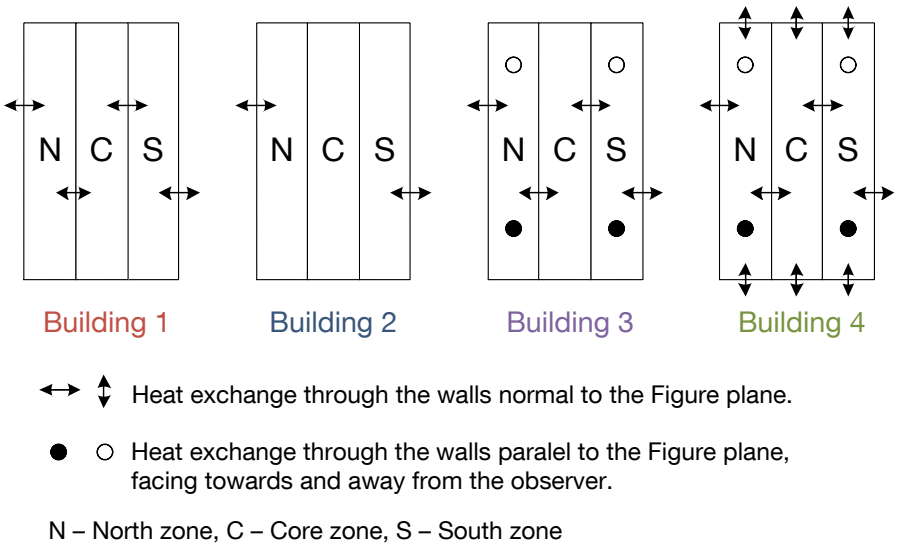

Figure A 3 Definition of four building simulation variations, starting from complete equivalence to office simulations (Building 2) to the option closest to reality (Building 4). N – North zone, C – Core zone, S – South zone.

In both building and office simulation a time schedule was introduced to control the conditioning operation. Heating, cooling and ventilation were operating between the office hours of 08:00 and 18:00. Infiltration was allowed from 00:00 to 24:00. One complete air change

per hour is assumed for the ventilation (1/h), 0.1 air change per hour for the infiltration ((0.1)/h).

Cooling loads are dominant in the Shanghai climate. The cooling and heating energy demand resulting from the single office simulation, as well as its sensible energy gains from ventilation and infiltration, are scaled to match the building size. These scaled office results are compared to the corresponding simulation results for the four building variations.

A 1.1.2 Load Comparisons

The results are compared and presented in hourly and monthly resolution.

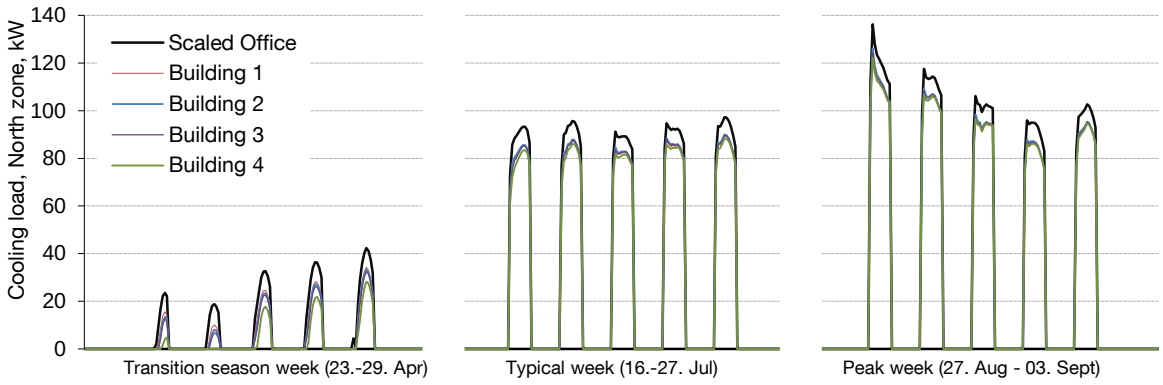

Figure A 4 Cooling load profile for North zone during three representative weeks within one year. The bigger the load the better the curves agree – absolute error remains similar.

The cooling load profiles of the building simulation show good agreement with the scaled office profile during the cooling season. During the transition season, the error is more significant, due to the influence of the Core zone.

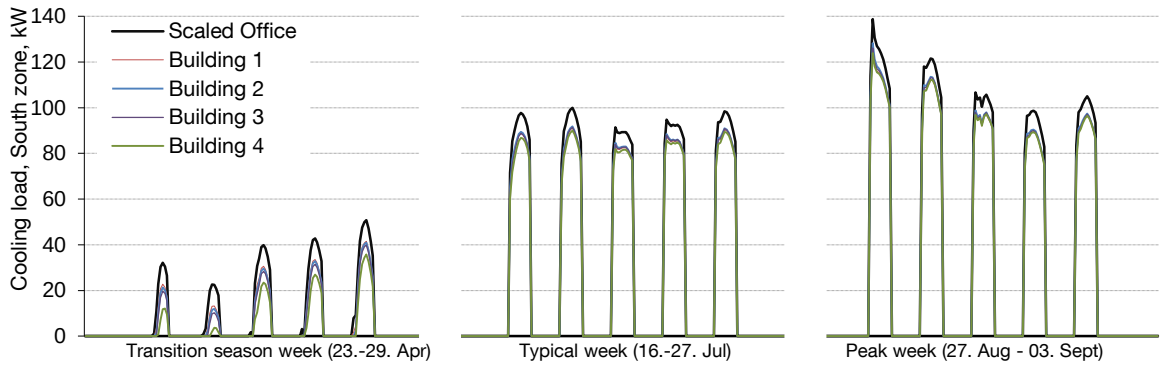

Figure A 5 Cooling load profile for South zone during three representative weeks within one year. The bigger the load the better the curves agree.

The version with the biggest relative error is Building 4 (see Figure A 6). It is important to notice the error is higher during the transition season, as shown in Figure A 5. Since in this

period the loads are small, this difference will not have a significant influence on the total energy consumption estimation and primary HVAC performance.

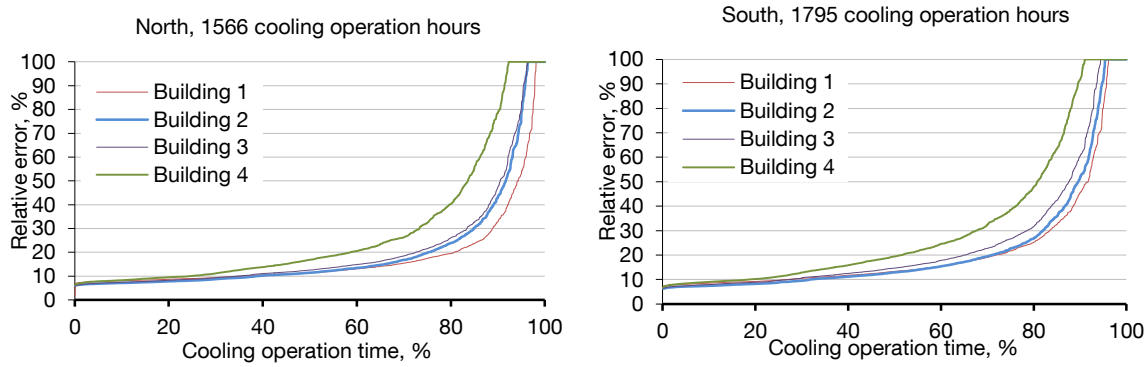

Figure A 6 Sorted relative error of building simulation versions compared to scaled room for North and South zone. Only the results during operation time are taken into account.

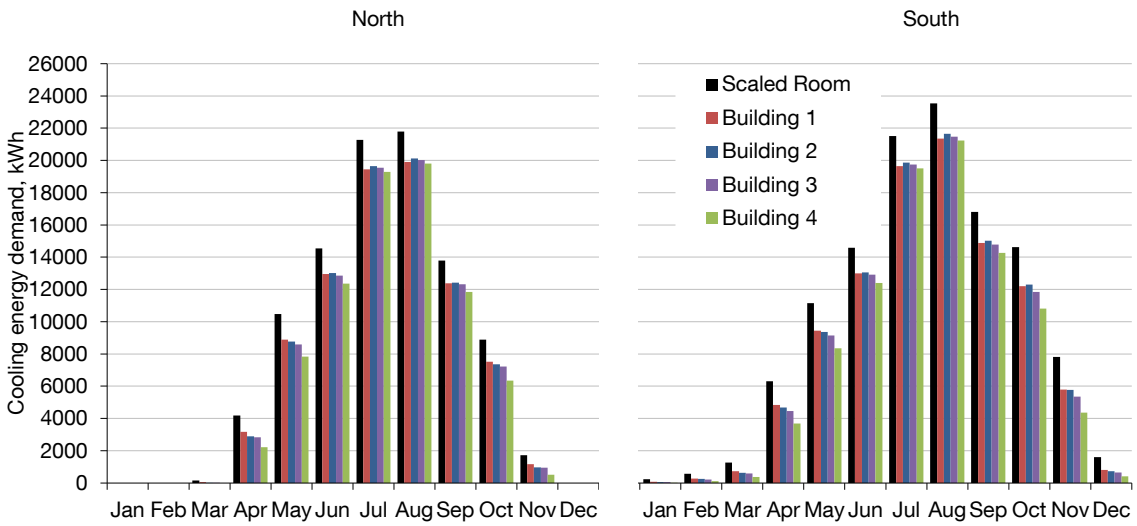

Figure A 7 Comparison of monthly cooling energy demands for North and South zone - scaled office vs. building simulations.

When it comes to monthly energy demand, shown in Figure A 7, the differences between the building options are insignificant, but the absolute error between the office and building simulation stays almost constant during the year.

The ventilation load comparisons show very good correspondence, which can be seen in Figure A 8 and Figure A 9.

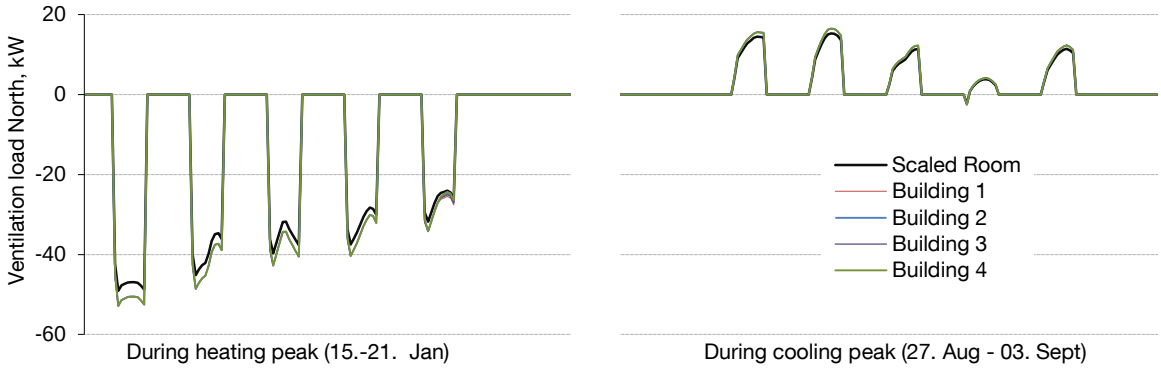

Figure A 8 Ventilation load profile for the North zone during heating and cooling peek weeks.

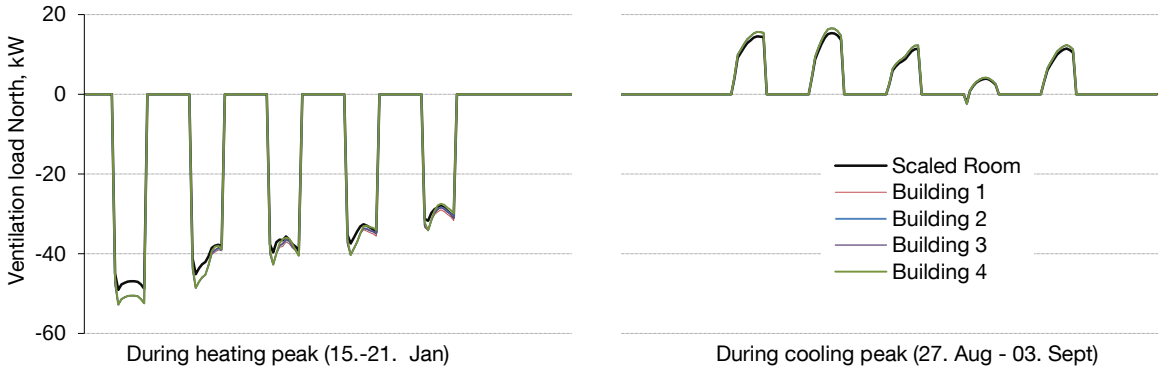

Figure A 9 Ventilation load profile for South zone during heating and cooling peek weeks.

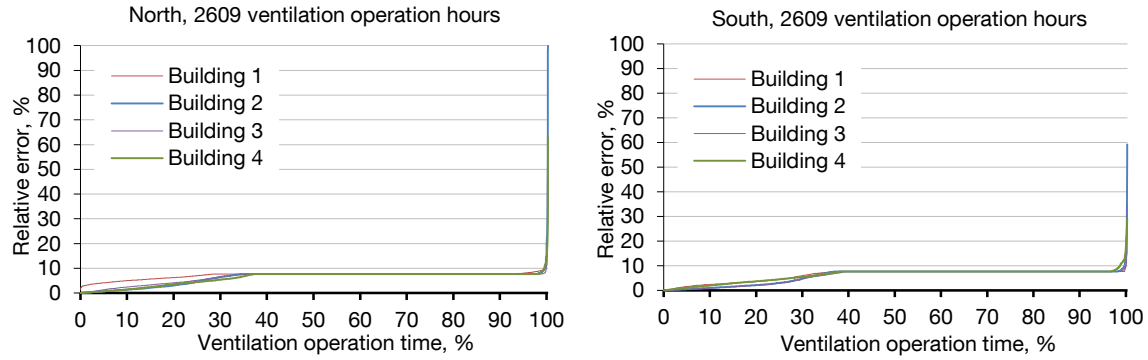

Figure A 10 Sorted relative error of building simulation versions compared to scaled room for North and South zone. Only the results during operation time are taken into account.

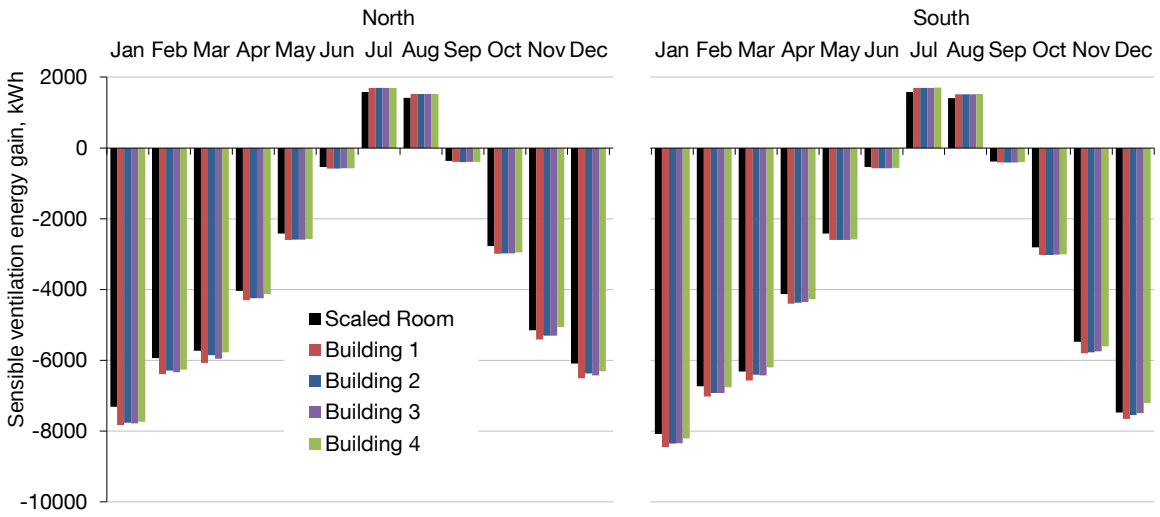

Figure A 11 Comparison of monthly ventilation energy gains for North and South zone- scaled office vs. building simulations.

The heating loads are relatively low and do not exceed 140 kW. The load profiles of the building follow the scaled room load profile. Similarly to the cooling transitions season, the relative errors are high during low loads (see Figure A 12). For Building 4, the relative error stays under 20% for only 10% of the operation time. However, such low loads are not significant for the level of detail required during the preliminary design.

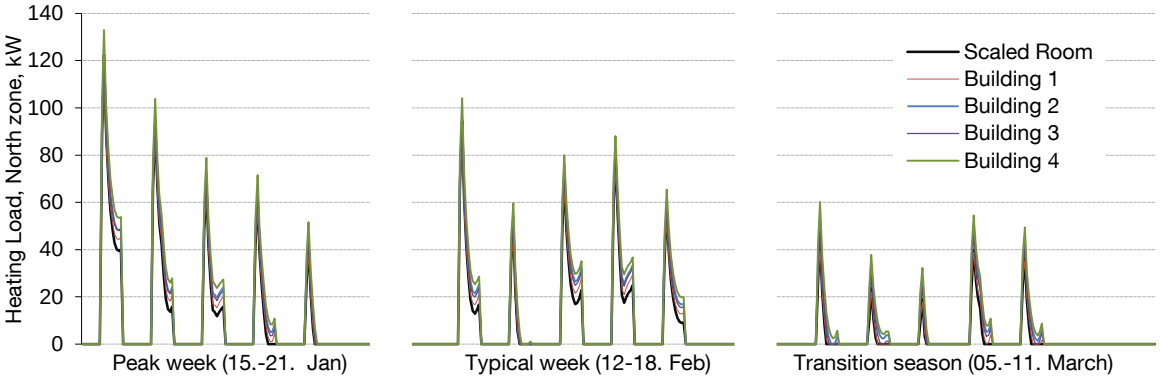

Figure A 12 Heating load profile for North zone during three representative weeks within one year.

Heating is not needed in the Core zone due to internal gains and heating the peripheral offices.

The infiltration for all the versions shows less than 10% error during 90% of the year.

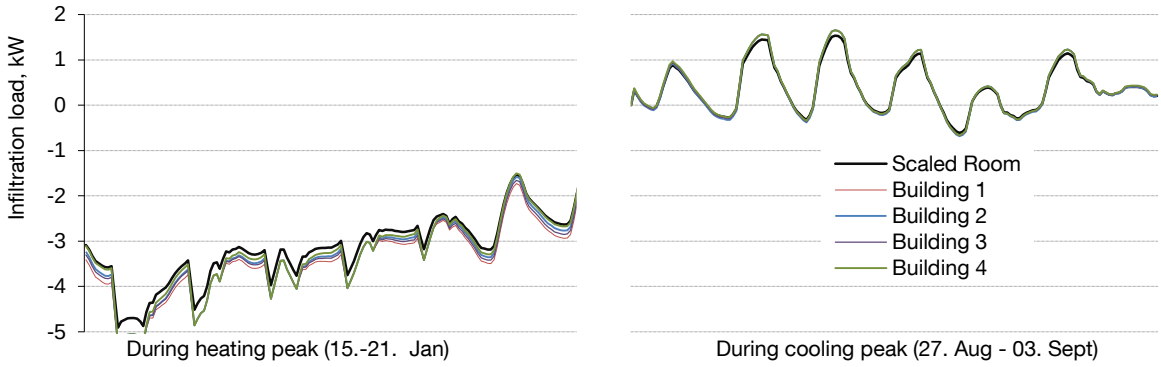

Figure A 13 Infiltration load profile for South zone during heating and cooling peek weeks.

A 1.1.3 Conclusion and Utilization

The results have shown that the suggested approach can be utilized to estimate the ideal loads of the whole building. Consequently, the method is implemented in order to utilize the data available in the FassadenTool, [12]. Namely, that tool provides the loads for a representative single office facing all four cardinal directions, for a variety of façade constructions. Scaling these loads according to the building geometry and adding an approximation of the internal building zone load yields an estimated secondary HVAC load profile. This approach ensures fast load assessment after making changes on the building size or shape without the need for additional simulations. The procedure is incorporated within the PROBA tool and allows fast analyses for the cities of Bangalore, Dubai, Moscow and Shanghai. A change in façade design featured in the FassadenTool, such as window area ratio or shadings, can quickly be projected onto the primary HVAC load in order to investigate how the change influences the primary system design.

A 1.2 Ideal Load Profile Preprocessing

An ideal load profile is calculated assuming an energy generation system of an infinite power. Due to this infinite power, it is possible for the ideal profile to have occasional high but short-lasting peaks. These peaks are not to be considered while dimensioning the primary HVAC. For that reason, before imposing a simulated load to an SM, these unrealistic peaks are shaved. The calculation procedure to be presented can be applied for an arbitrary load profile supplied. It can be either a primary or a secondary load, depending whether or not the emission and distribution losses have already been accounted for. Energy conservation is satisfied by reallocating the shaved energy.

Figure A 14 shows an ideal heating load profile for Shanghai obtained for 50% of window to external wall area ratio, assuming ideal heating. The building has three stories. On all stories, 100 m^2 face north and south and 40 m^2 face east and west. In the following section, this building is entitled the S building, and is referenced as such throughout the thesis. The core zone of the building is used as a staircase and hallway and thus has no heating de-

mand. The Shanghai climate results in a rather small heating demand of 6.15 kW/(m^2a) for the light façade configuration, as defined in [12].

The peak load, slightly above 25 kW, occurs only once. Additionally, peaks above 20 kW occur only 11 times. Therefore, utilizing a boiler with a design power of 20 kW would fail to provide comfort in no more than 11 non-consecutive hours throughout the year. The duration and relative size of these peaks is represented by a load duration curve, showing the load data in descending order, see Figure A 15. With slightly more than 1000 heating system operation hours, the insufficient supply utilizing the stated 20 kW boiler, would occur at around 1% of heating demand duration.

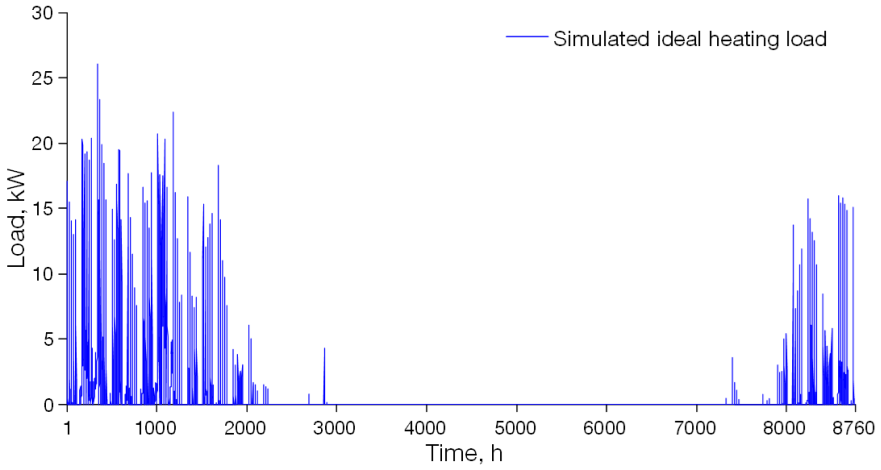

Figure A 14 Ideal heating load. Location: Shanghai. Building: 3 stories with 100 m^2 facing each north and south and 40 m^2 facing east and west, 50% window area ratio.

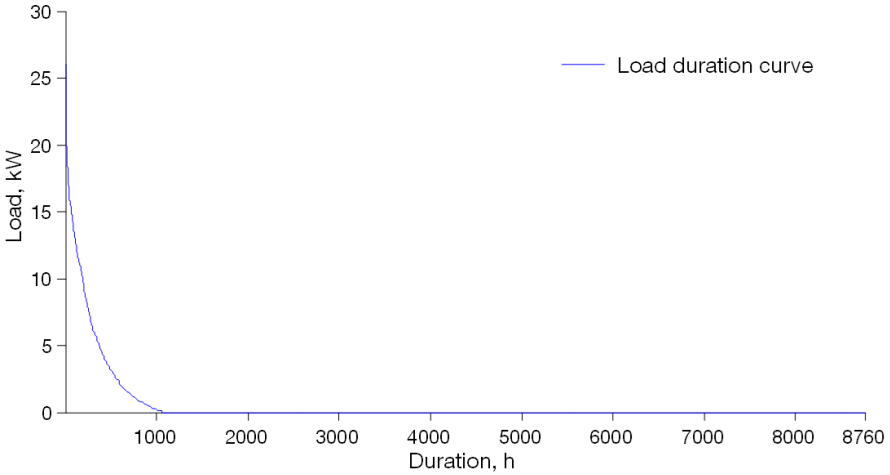

Figure A 15 Heating load duration curve.

To determine both how short lasting and how large a peak must be before beeing affected by the peak shaving, the negative first derivative of the duration curve, *LD'*, in hourly resolution is observed:

$$LD' = -\frac{\Delta LD}{\Delta D} \tag{A 1}$$

where *ΔLD* is the change of the simulated primary load duration curve during one timestep and *ΔD* is the duration of the timestep. This curve, see Figure A 16, illustrates the steepness of the duration curve.

The values of this derivative close to the origin are much higher than the mean first derivative of all positive *LD'* values $\overline{LD'}$. This is shown in Figure A 15. The next step consists of counting the instances where the following inequality is satisfied:

$$LD' > c \cdot \overline{LD'} \tag{A 2}$$

where c is a measure for the steepness of the peak. The heuristically selected c value is 4, yielding satisfying results in performed simulations. Steep peaks fulfill the latest equation and are thus shaved. The number of counted instances, D_{sh}, corresponds to the number of timesteps when the load is shaved. The maximal allowed load is defined by the intersection between a vertical line drawn through the number of counted instances and the load duration curve. Loads preceding this maximal allowed load at the load duration curve are shaved to the value of the maximal load, as shown in Figure A 17.

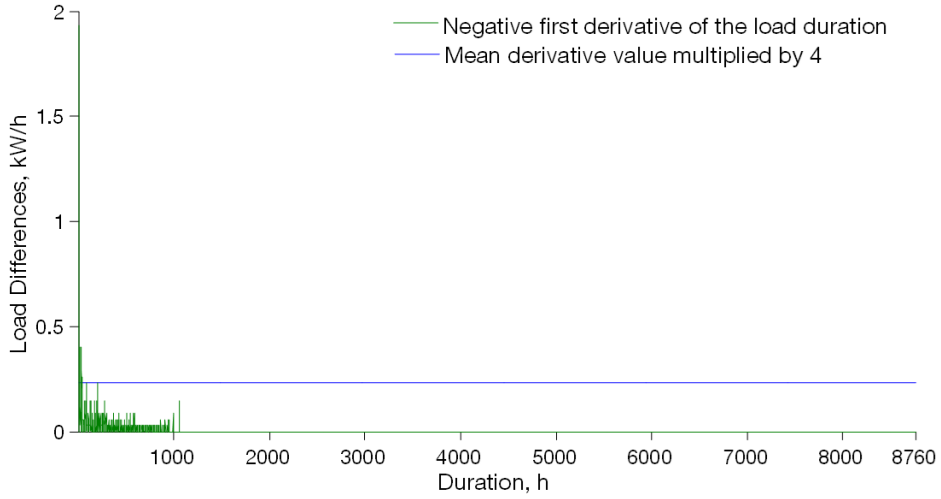

Figure A 16 Negative first derivative of the load duration curve.

In this process it is assumed that the largest first derivative values occur at the beginning of the duration curve. It is very unlikely that some of those very steep changes in load duration curve occur for smaller loads. Even if this does occur, it will only slightly increase the number of shaved instances without significantly influencing the quality of the shaved load.

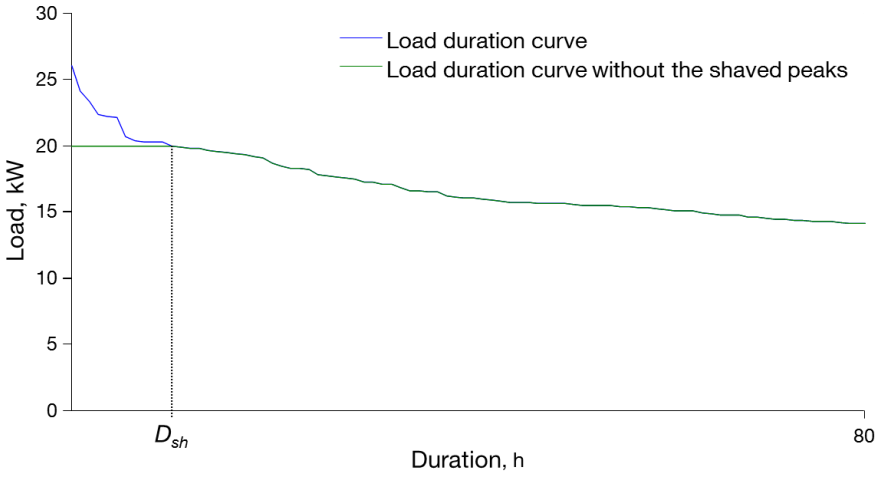

Figure A 17 Determining the maximal allowed hourly load. All larger loads are shaved to the value of the maximal load. D_{sh} is determined by counting instances satisfying, eq. (A 2).

Now the procedure of duration curve creation is reversed and the data is re-sorted by time, as shown in Figure A 18.

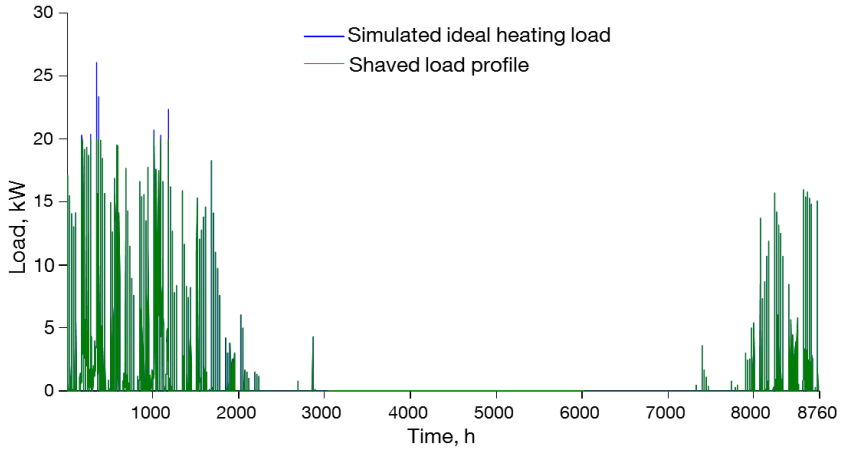

Figure A 18 Shaved load data sorted by time. Shaved peaks are clearly visible.

In order to maintain the energy balance, the shaved energy is reallocated to the following timesteps, again without exceeding the identified load maximum.

Due to the preferences of the supply penalty function explained in chapter 5, the value of the load preprocessing parameter c can be adapted to the values of the supply penalty function. If c is set to 0, there is no load preprocessing, which is also a legitimate approach for relevant problems.

A 1.3 Showcase Load Profiles

The load profiles utilized to calculate the examples presented in chapters 3 and 5 are given in the two tables bellow. They are obtained by applying the steps discussed in sections A 1.1 and A 1.2 on the ideal loads provided by FassadenTool. The actual façade construction is a reference case from [12] for each of the climates. Ideal heating and/or cooling is assumed, while maintaining the necessary air quality.

Three buildings sizes were selected:

- A small 3 stories building having an approximate floor area of 1000 m^2;
- A middle 6 stories building (3000 m^2); and
- A big 10 stories building (10000 m^2).

Table A 3 Heating load profiles used in chapters 3 and 5 to demonstrate model performance and optimization.

Gross Area, m^2	Location; Load Profile	
	Moscow; kW	Shanghai; kW
1000 (S for small)	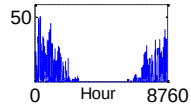	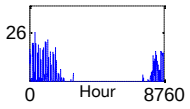
3000 (M for middle)	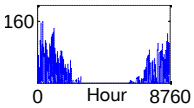	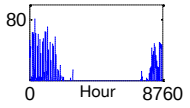

Table A 4 Cooling load profiles used in chapters 3 and 5 to demonstrate model performance and optimization.

Gross Area, m^2	Location; Load Profile		
	Bangalore; kW	Dubai; kW	Shanghai[i]; kW
1000 (S for small)	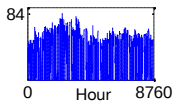	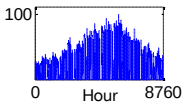	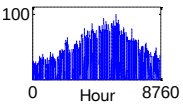
10000 (B for big)	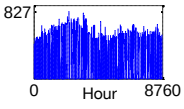	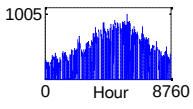	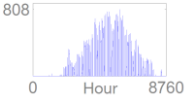

All buildings are shaped similar to the one in Figure A 2, with longer facades facing north and south. The Shanghai and Moscow locations are suitable to demonstrate heating generation systems. All cities apart from Moscow exhibit significant cooling demand and were thus used to demonstrate cooling systems.

[i] Cooling loads for Shanghai B Building have not been used within the example calculations provided in the thesis. However, it is interesting to compare them to loads of identical buildings at other locations.

Table A 5 Core zone internal loads

Type	Staircase	Offices
Load, W/m^2	0	50

The internal zone of the building is considered to be a non-conditioned staircase which has negligible internal gains. Another option provided within the PROBA tool is a an office usage of the internal zone (Table A 5).

Estimated distribution and emission losses are added to these profiles within the system simulation based on the selected SM.

A 1.4 Distribution and Emission Losses

The most desirable model of an HVAC system would include the building simulation, thermal distribution system (secondary HVAC – distribution and emission system, see Figure 1.1), and the energy generation and storage (primary HVAC). However, due to the complexity of these systems, they are still often investigated separately. The power consumed and thermal energy (and mass) lost while delivering the energy generated by the primary system cannot be disregarded. A significant saving potential of air distribution systems in California buildings is presented and investigated in [92]. In [93] the thermal distribution system consumption is compared to the commercial sector consumption in Germany. Relatively detailed losses and consumption calculation methods are available in VDI 2067 [66] and DIN EN 15316 [53].

The subject of losses and consumption in water and air distribution networks and emission systems for early design requires efforts that exceed the scope of this thesis. Therefore these losses have been accounted for through increasing the calculated secondary load for 10% to 30%, depending on the assumed distribution system and the peak load value. The value obtained is the set load for the primary system.

A 2 Weather Data

The weather data used throughout the thesis are Meteonorm [55] typical years. The locations used are Bangalore, Dubai, Shanghai and Moscow.

A detailed climate analysis for each of these cities, relevant for the building design and BEP, is provided in [12]. For each of the cities, the source provides the analysis the weather data and evaluates their influence at the façade design considering the urban layout. Hereafter, only a short overview of the weather characteristics focusing on data implemented throughout the theses is given. Therefore Figure A 19 shows the solar radiation

profiles, dry and wet bulb temperatures for the stated locations. Solar radiation data are used to assess the solar collector and PV gains. The cooling tower operation depends on the wet bulb temperature, thus influencing the chiller performance.

The **Bangalore** climate is tropical, with a rather narrow span of temperatures throughout the year. Total daily solar radiation also stays relatively constant, apart from its attenuation during the summer months, due to the wet season. Indoor comfort requires a cooling and dehumidifying system.

Dubai has a subtropical desert climate. Although the precipitation values are low, being so near to the coast, the city has very high air humidity during the summer. Cooling and dehumidification systems are required.

Shanghai lies in the humid subtropical climate zone. It has four seasons with hot and humid summers and mild winters. Most of its thermal comfort related energy demand is due to cooling and dehumidification, although buildings also require a heating system.

Moscow is positioned in a humid continental climate. Long and cold winters cause a high heating and humidification demand. Summers are warm, resulting in a cooling demand, but with good potential for passive cooling.

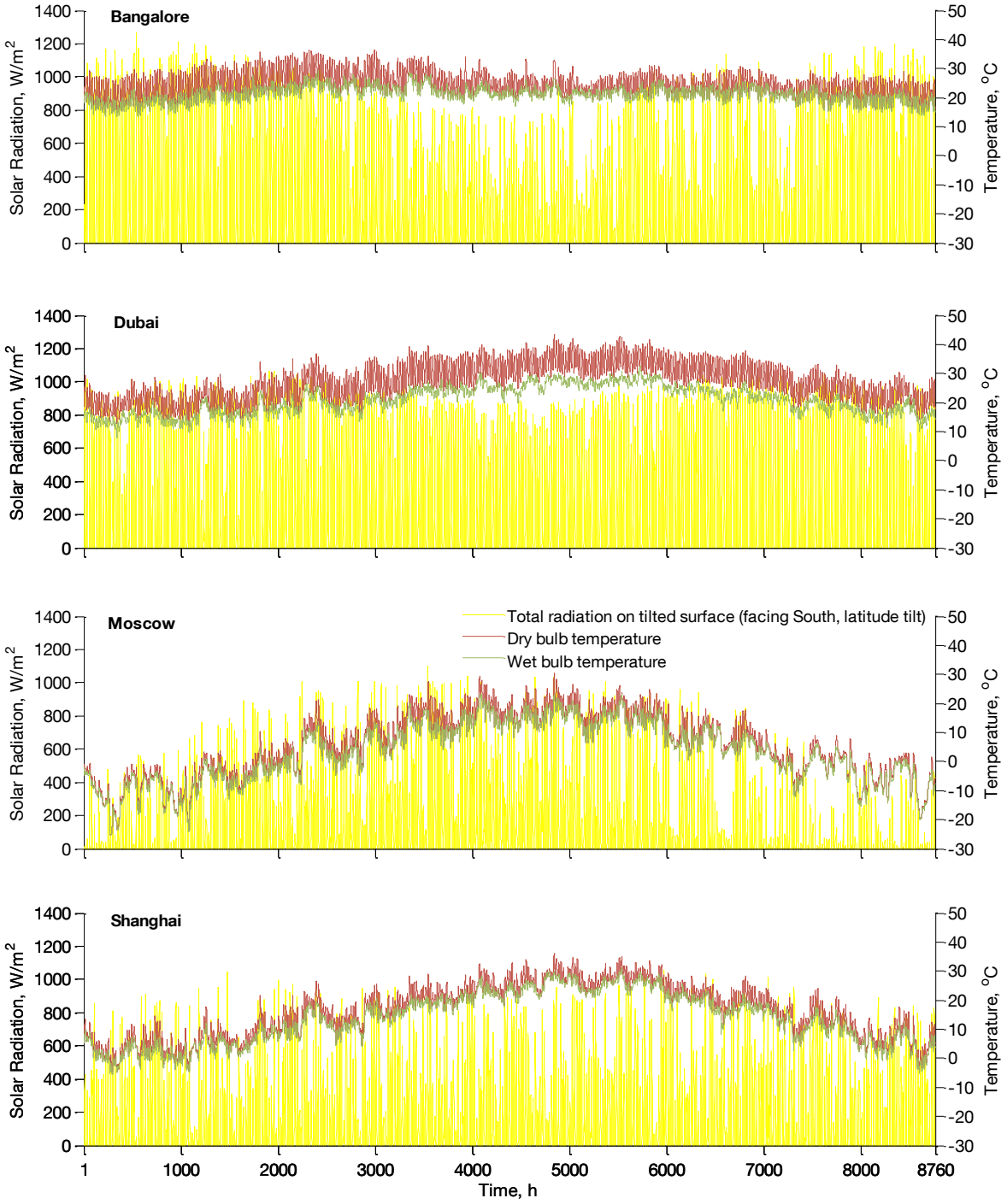

Figure A 19 An overview of SM relevant weather data for Bangalore, Dubai, Moscow and Shanghai.

Appendix B
Cost and Performance Data

B 1 Technical Data

Table B 1 Test rated collector properties (with respect to the absorber area), [48]

	Optical Eff., η_0	Loss coef. a_1 W/(m^{2}K)	Loss coef. a_2 W/(m^{2}K^2)	IAM at 50° incidence	Absorber/ Gross area, %	Test Flow/ Gross area, kg/(m^{2}h)
Flat plate	79.46	4.0363	0.0078	0.8522	89.82	71.36
Evac. tube	78.79	2.0933	0.0072	1.1417	59.65	50.69

Table B 2 Optimal tilt angles (annual and seasonal optima) and latitudes for additional cities.

		Flat Plate			Evacuated Tube		
	Location Latitude °N	Annual Optimum, °	Seasonal Optimum, °		Annual Optimum, °	Seasonal Optimum, °	
			Winter	Summer		Winter	Summer
Belgrade	45	36	60	24.5	35	56	22.5
Munich	48	39	63	28	37	60	25
Singapore	1	4	19	-4	7	22	-8

Table B 3 PV model parameters. Reference conditions are T_{ref}=25°C, I_{ref}=1000 W/m^2.

Ref. Eff. $\eta_{ref,pv}$	System factor f_{sys}	Temp. coef. β_{pv}, 1/°C	Vent. factor k_T, °C/(W/m^2)
0.14	0.78	-0.004	0.05

Table B 4 Data implemented in the thermal storage tank model

Emission type	Water density, kg/m^3	Water heat capacity, kJ/(kgK)	Assumed storage temp. difference, °C	Storage energy density, kWh/m^3	Storage thermal loss, kW/m^3
Radiator	1000	4.2	50	60	0.1
Panel			30	35	

Table B 5 DOE-2 Generic vacuum compression chillers: performance curves coefficients, reference performance, and reference and limit conditions [28]

Chiller Type	a_1	a_2	a_3	a_4	a_5	a_6
Centrifugal	0.257896	0.0389016	-0.00021708	0.0468684	-0.00094284	-0.00034344
Reciprocating	0.507883	0.145228	-0.00625644	-0.0011178	-0.0001296	-0.00028188
	b_1	b_2	b_3	b_4	b_5	b_6
Centrifugal	0.933884	-0.058212	0.00450036	0.00243	0.000486	-0.0012150
Reciprocating	1.03076	-0.103536	0.00710208	0.0093186	0.00031752	-0.00104328
	c_1	c_2	c_3	Ref. COP		
Centrifugal	0.222903	0.313387	0.463710	5.5		
Reciprocating	0.088065	1.137742	-0.225806	3.67		
	Temper.	Minimum	Reference	Maximum	Min. PLR	Max. PLR
Both types	$T_{chil,out}$, °C	5	6.67	10	0.1	1
	$T_{cool,in}$, °C	24	29.4	35		

Table B 6 Factors describing cooling tower and air cooled condenser electrical energy and cooling tower water consumption, (sources: [33], [38], [39], [40])

Sizing coefficient, $k_{el,ct}$	Turn off limit, $PLR_{min,ct}$	Blowdown, $p_{ct,wloss}$, %	Water flow ratio, k_{wc}, m^3/kWh	Air: El. energy cons. coefficient
0.0105	0.15	0.1	0.194	0.035+0.009

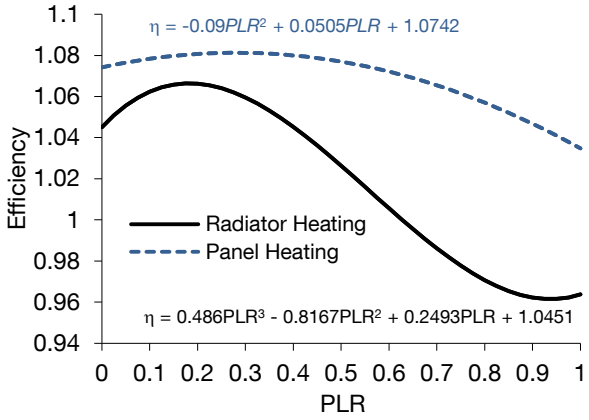

Figure B 1 Condensing boiler efficiency as a function of part load ratio (PLR) for two different supply and return temperatures (radiator-higher and panel-lower heating). Manufacturer data fit.

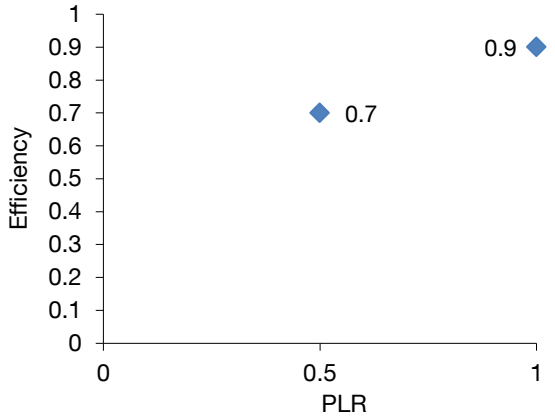

Figure B 2 Single and two stage boiler efficiencies. (PLR=1 and PLR=[0.5;1]).

B 2 Cost Related Data

Table B 7 Default values of various cost related data. Sources [66], [67], [76], heuristic data.

	R_p	T_{life}, years	f_{inst}	β_m	Rates
Pellet boiler	0.02	20	0.03	0.02	
Condensing boiler	0.02	20	0.03	0.02	
Solar collector	0	20	0.005	0.005	
Thermal storage	0.02	20	0.02	0.01	R=0.04 R_i=0.02
Photovoltaics	-0.1	15	0.03	0.015	
Vacuum compression chiller	0.02	23	0.02	0.01	
Cooling tower	0.02	20	0.02	0.01	

Table B 8 Fuel prices and emissions used for demonstration purposes.

	Pellet	Gas	Oil	Source
Price	0.238 €/kg	0.485 €/m^3	0.777 €/l	May 2011 in Germany
Emissions	0.04 kg/kWh	0.277 kg/kWh	0.33 kg/kWh	DIN EN 15603, [77]

Table B 9 Electrical energy related CO_2 emissions. PV feed-in tariffs.

City	PV Feed-in tariff, €ct/kWh	Source	Electricity CO_2 emission, g/kWh	Source
Bangalore	29.94	[78]	968	From electricity and heat generation countrywide, [81]
Dubai	-	[79]	842	
Moscow	-	(not found)	339	
Shanghai	11.64	[80]	745	

Table B 10 Water and electricity prices for four demonstration cities, currency converter [82] used.

City	Water prices			Source	Electrical energy prices			Source
Bangalore	kl/month	INR/kl	€ct/m^3	[83]	kWh/month	INR/kWh	€ct/kWh	[87]
	<10000	36	54.2		<100	2.9	4.4	
	10 - 20000	39	58.7		100 – 200	3.9	5.9	
	20 - 40000	44	66.2		200 – 300	4.6	6.9	
	40 - 60000	51	76.7		300 – 400	5.0	7.5	
	60 - 100000	57	85.6		>400	5.9	8.9	
	>100000	60	90.3					
Dubai	IG*/month	AED/IG	€ct/m^3	[84]	MWh/month	AED/kWh	€ct/kWh	[84]
	0 – 10000	0.035	155.9		<2	0.23	4.7	
	1000 – 20000	0.040	178.2		2 – 4	0.28	5.7	
	>20001	0.046	204.9		4 – 6	0.32	6.5	
					>6	0.38	7.7	
Moscow		RUB/m^3	€ct/m^3	[85]		RUB/kWh	€ct/kWh	[88]
	All consump.	26.1	60.1		All consump.	3.4	7.8	
Shanghai		CNY/m^3	€ct/m^3	[86]		CNY/kWh	€ct/kWh	[89]
	All consump.	2	23.3		All consump.	0.91	11.7	

*** IG-Imperial gallon**

Table B 11 Photovoltaic price

	Price, €/W_{pk}	Customer price, €/W_{pk}	Source
Multicrystalline Si	1.12	1.904	Price in Germany, Dec 2011, [90]

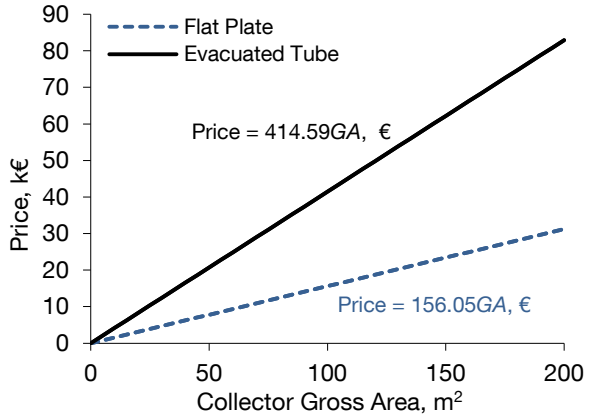

Figure B 3 Solar collector initial investment cost functions. Averaged manufacturer data from [48].

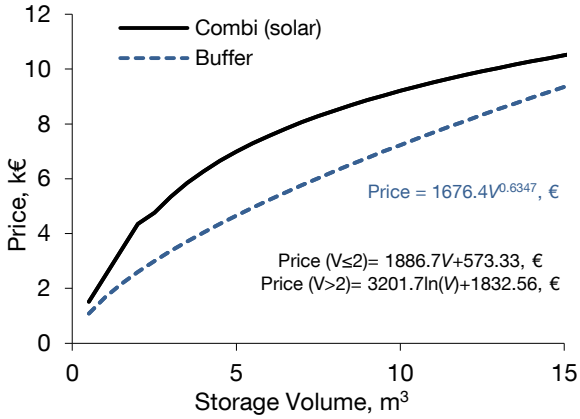

Figure B 4 Thermal storage initial investment cost functions, [40] and [91]. The combination storage tank is used in combination with solar collectors and buffer storage otherwise.

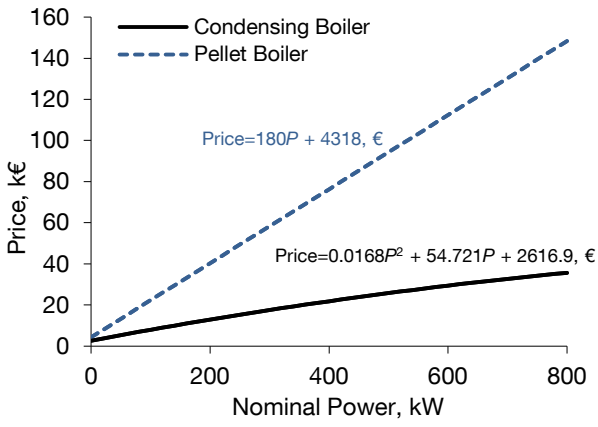

Figure B 5 Pellet and condensing boiler investment cost function. Manufacturer data fit.

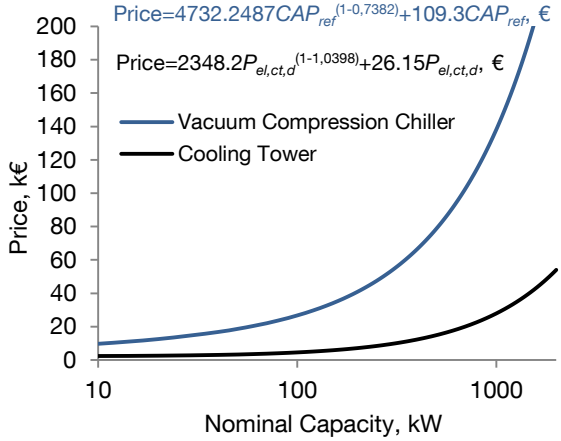

Figure B 6 Investment cost functions for vacuum compression chillers and cooling towers, data fit curves taken from [40].

List of References

[1] U.S. Energy Information Administration. Annual Energy Outlook 2011 With Projections to 2035. *Report DOE/EIA-0484*, Washington, DC, USA, 2011.

[2] Redaktionsgruppe „Energie für Deutschland“. Energie für Deutschland. *Weltenergierat – Deutschland e.V.* Berlin, Germany, 2010.

[3] U.S. Department of Energy, Office of Energy Efficiency and Renewable Energy. 2010 Buildings Energy Data Book. *D&R International, Ltd.*, Silver Spring, Maryland, USA, 2011.

[4] H. Kleeberger, P. Tzscheutschler, and B. Geiger. Erstellen der Anwendungsbilanz 2008 für den Sektor Gewerbe, Handel, Dienstleistungen (GHD). *Lehrstuhl für Energiewirtschaft und Anwendungstechnik, Technische Universität München*, Munich, 2008.

[5] Directive 2010/31/EU of the European Parliament and of the Council of 19 May 2010 on the energy performance of buildings. *Official Journal of the European Union L 153/13*, 2010.

[6] U.S. Energy Information Administration. Annual Energy Outlook 2010 With Projections to 2035. *Report DOE/EIA-0383*, Washington, DC, USA, 2010.

[7] RESET - Renewable Energy Sources Estimation Tool. *The Chartered Institution of Building Services Engineers London*, 2006. *Available at*: http://www.cibse.org/index.cfm?go=page.view&item=658. Last accessed: April 2012.

[8] J.A. Clarke. *Energy Simulation In Building Design*. Butterworth-Heinemann, Oxford, 2nd Edition, 2001. ISBN 9780750650823.

[9] V. Bazjanac. Virtual building environments (VBE)-applying information modeling to buildings. *In Proceedings of the 5th European Conference on Product and Process Modeling in the Building and Construction Industry*, Istanbul, Turkey, 2004.

[10] U.S. Department of Energy. Building Energy Software Tools Directory. *Available at:* http://apps1.eere.energy.gov/buildings/tools_directory/. Last accessed: March 2012.

[11] ASHRAE Handbook - Heating, Ventilating, and Air-Conditioning Systems and Equipment - HVAC System Analysis and 2067Selection. *American Society of Heating, Refrigerating and Air-Conditioning Engineers, Inc.*, Atlanta, USA, 2008.

[12] P. Liedl. Interaction Climate–Human–Building: Planning tools for office buildings in different climate zones in the context of room climate and energy with a detailed climate analysis. *PhD thesis, Technische Universität München*, Munich, 2011.

[13] M. Pfaffinger, P. Liedl, M. Egger, C. van Treeck, P. Tzscheutschler, M. Grahovac, E. Rank, G. Hausladen, and U. Wagner. Zusammenspiel zwischen Gebäuden, Nutzern, Klima und Energieeffizienz. *In Proceedings of BauSIM 2008*, Kassel, Germany, 2008.

[14] M. Trčka and J. Hensen. Overview of HVAC system simulation. *Automation in Construction*, 19(2):93–99, 2010.

[15] DIN V 18599:2007. Energetische Bewertung von Gebäuden. *Deutsches Institut für Normung e. V.*, 2007.

[16] Carrier. Hourly Analysis Program (HAP). *Available at:* http://www.docs.hvacpartners.com/idc/groups/public/documents/marketing/e20s-hap410fs.pdf. Last accessed: March 2012.

[17] Trane. TRACE™ 700 HVAC load design and analysis software. *Trane, CDS-SLB005-EN*, 2010.

[18] ANSI/ASHRAE/IESNA Standard 90.1. Energy Standard for Buildings Except Low-Rise Residential Buildings. *American Society of Heating, Refrigeration and Air-Conditioning Engineers Inc.*, Atlanta, GA, USA, 2007.

[19] Natural resources Canada. RETScreen. *Available at:* http://www.retscreen.net/. Last accessed: March 2012.

[20] F. Sakurai, T. Inooka, R. Yanagihara, E. Higashizawa, J. Hamane, T. Fujii, H. Nishihata, H. Hayashi, F. Arizumi, H. Ninomiya, K. Koike, and N. Shinohara. FACES (Forecasts of air-conditioning system's energy, environmental, and economical performance by simulation). *In Proceedings of Building Simulation 2007*, Beijing, China, 2007.

[21] T. Lambert, P. Gilman, and P. Lilienthal. Micropower system modeling with HOMER. *Integration of Alternative Sources of Energy*, John Wiley & Sons, Inc., 2006.

[22] E. Fabrizio. Modeling of multi-energy systems in Buildings. *PhD thesis, Politecnico di Torino*, Torino, Italy, 2008.

[23] M. Geidl. Integrated Modeling and Optimization of Multi-Carrier Energy Systems. *PhD thesis, ETH Zürich, No. 17141*, Zürich, Switzerland 2007.

[24] LBNL and James J. Hirsch & Associates. Overview of DOE-2.2. *University of California and James J. Hirsch*, Camarillo, CA, USA, 1998.

[25] James J. Hirsch & Associates. eQuest Introductory Tutorial version 3.63. *James J. Hirsch & Associates*, Camarillo, CA, USA, 2009.

[26] S. Attia, L. Beltrán, A. De Herde, and J. Hensen. "Architect Friendly": a comparison of ten different building performance simulation tools. *In Proceedings of Building Simulation 2009*, Glasgow, Scotland, 2009.

[27] TRNSYS (A Transient System Simulation Program) Documentation. *Solar Energy Laboratory, University of Wisconsin-Madison*, Madison, WI, USA, 2009.

[28] EnergyPlus Energy Simulation Software. *U.S. Department of Energy*. *Available at:* http://www.energyplus.gov/. Last accessed: March 2012.

[29] DesignBuilder Software Ltd. DesignBuilder. *Avbl. at:* http://www.designbuilder.co.uk. Last accessed: March 2012.

[30] M. Wetter. GenOpt – A Generic Optimization Program, User Manual Version 2.1.0. *Lawrence Berkeley National Laboratory*, Berkeley, CA, USA, 2008.

[31] MathWorks. MATLAB. *The MathWorks Inc.*, 1994-2012. *Available at*: http://www.mathworks.de/. Last accessed: March 2012.

[32] T.S. Lee and W.C. Lu. An evaluation of empirically-based models for predicting energy performance of vapor-compression water chillers. *Applied Energy*, 87(11):3486–3493, 2010.

[33] EnergyPlus Version 7.0 Documentation, Engineering Reference. *The Board of Trustees of the University of Illinois and the Regents of the University of California through the Ernest Orlando Lawrence Berkeley National Laboratory*. 2011.

[34] M. Hydeman and K.L. Gillespie. Tools and techniques to calibrate electric chiller component models. *ASHRAE Transactions*, 108(1): 733–741, 2002.

[35] M. Hydeman, P. Sreedharan, N. Webb, and S. Blanc. Development and testing of a reformulated regression-based electric chiller model. *ASHRAE Transactions*, 108(2): 1118–1127, 2002.

[36] G. Zweifel, V. Dorer, M. Koschenz, and A. Weber. Building Energy and System Simulation Programs: Model Development, coupling and integration. *In proceedings of Building Simulation 1995*, Madison, WI, USA, 1995.

[37] TESS Experts in Energy Modeling & Analyses. TESS Component Libraries, General Descriptions. *Thermal Energy System Specialists LLC*, Madison, WI, USA, 2008.

[38] M. Hydeman, S.T. Taylor, and D. Winiarski. Application of Component Models for Standards Development. *ASHRAE Transactions*, 108(1):742–750, 2001.

[39] Water conservation: Best practice guidelines for cooling towers in commercial buildings. *Sydney Water*, Sydney, Australia, 2008.

[40] M. Gebhardt, H. Kohl, and Th. Steinrötter. Ableitung von Kostenfunktionen für Komponenten der rationellen Energienutzung. *Institut für Energie- und Umwelttechnik e.V. (IUTA)*, Duisburg-Rheinhausen, 2002.

[41] M. Haller. Type 869 Boiler Model, Version 5.02. *Institut für Wärmetechnik, Technische Universität Graz*. Graz, Austria, 2009.

[42] V. I. Hanby. Modeling the performance of condensing boilers. *Journal of the Energy Institute* 80(4): 229-231, 2007.

[43] R.M. Lazzarin and L. Schibuola. Performance analysis of heating plants equipped with condensing boilers. *Journal of Heat Recovery Systems* 6(4): 269-276, 1986.

[44] U. Wehmhörner. Multikriterielle Regelung mit temperaturbasierter Speicherzustandsbestimmung für Mini-KWK-Anlagen. *PhD thesis, Technische Universität München*, Munich, 2012.

[45] J.A. Duffie and W.A. Beckman. *Solar Engineering of Thermal Processes*. John Wiley & Sons, Inc., New York (1991). ISBN 0471510564.

[46] ASHRAE Standard 93-77. Method of Testing to Determine the Thermal Performance of Solar Collectors. *American Society of Heating, Refrigeration and Air-Conditioning Engineers Inc.*, Atlanta, GA, USA, 1977.

[47] DIN EN 12975-2:2006. Thermische Solaranlagen und ihre Bauteile – Kollektoren – Teil 2: Prüfverfahren. *Deutsches Institut für Normung e. V.*, 2006.

[48] Official page of Institut für Solartechnik. Rapperswil, Switzerland. *Available at*: http://www.solarenergy.ch/. Last accessed: April 2012.

[49] E.G. Evseev and A.I. Kudish. The assessment of different models to predict the global solar radiation on a surface tilted to the south. *Solar Energy* 83(3):377-388, 2008.

[50] A. Mermoud and M. Villoz. User's Guide – PVsyst Contextual Help. *University of Geneva*, Geneva, Switzerland, 1994-2010. *Available at:* http://www.pvsyst.com/. Last accessed: April 2012.

[51] Renewable Energy Unit. PVGIS - Photovoltaic Geographical Information System. *Joint Research Centre, Institute for Energy European Commission*, Ispra, Italy. *Available at:* http://re.jrc.ec.europa.eu/pvgis/. Last accessed: April 2012.

[52] S. Attia and A. De Herde. Sizing Photovoltaic Systems during Early Design: A Decision Tool for Architects. *In proceedings of National Solar Conference - Solar 2010*, Phoenix, AZ, USA, 2010.

[53] DIN EN 15316:2009. Heizungsanlagen in Gebäuden - Verfahren zur Berechnung der Energieanforderungen und Nutzungsgrade der Anlagen. *Deutsches Institut für Normung e. V.*, 2009.

[54] D.E. Carlson, G. Lin, and G. Ganguly. Temperature dependence of amorphous silicon solar cell PV parameters. *In Conference Record of the Twenty-Eighth IEEE Photovoltaic Specialists Conference:* 707-712, Anchorage, AK, USA, 2000.

[55] Meteonorm – a comprehensive meteorological reference. *Available at*: http://meteonorm.com/. Last accessed: April 2012.

[56] R.K.L. Chan, E.W.M. Lee, and R.K.K. Yuen. An integrated model for the design of air-cooled chiller plants for commercial buildings. *Building and Environment*, 46(1):196-209, 2011.

[57] F. Bo, J. Xinqiao, and D. Zhimin. Optimal control strategies for multi-chiller system based on probability density distribution of cooling load ratio. *Energy and Buildings*, 43(10):2813-2821, 2011.

[58] L. Wen-Shing, C. Yi-Ting, and K. Yucheng. Optimal chiller loading by differential evolution algorithm for reducing energy consumption. *Energy and Buildings*, 43(2–3):599-604. 2011.

[59] D.J. Swider. A comparison of empirically based steady-state models for vapor-compression liquid chillers. *Applied thermal engineering*, 23(5):539–556, 2003.

[60] F.W. Yu and K.T. Chan. How chillers react to building loads. *ASHRAE Journal*, 46(8): 52-57, 2004.

[61] F.W. Yu and K.T. Chan. Part load performance of air-cooled centrifugal chillers with variable speed condenser fan control. *Building and Environment*, 42(11): 3816-3829, 2007.

[62] L. Blank and A. Tarquin. *Engineering Economy*. *McGraw Hill*, New York, 6th Edition, 2005. ISBN 0073203823.

[63] Y. Jaluria. *Design and optimization of thermal systems*. CRC Press, Boca Raton, 2008. ISBN 0849337534

[64] A. Bejan, G. Tsatsaronis, and M. J. Moran. *Thermal design and optimization*. Wiley-IEEE Press, New York, 1996. ISBN 0471584673

[65] VDI 6025. Betriebswirtschaftliche Berechnungen für Investitionsgüter und Anlagen, *Verein Deutscher Ingenieure, Beuth Verlag GmbH*, 1996.

[66] VDI 2067 Blatt 1. Wirtschaftlichkeit gebäudetechnischer Anlagen - Grundlagen und Kostenberechnung. *Verein Deutscher Ingenieure, Beuth Verlag GmbH*, 2010.

[67] DIN EN 15459:2008. Energy Efficiency for Buildings – Standard economic evaluation procedure for energy systems in buildings. *Deutsches Institut für Normung e. V.*, 2008.

[68] S. Sieniutycz and J. Jeżowski. *Energy Optimization in Process Systems*. Elsevier, Amsterdam, 2009. ISBN: 9780080914428.

[69] T.R. Nielsen. Optimization of buildings with respect to energy and indoor environment, *PhD thesis, Danmarks Tekniske Universitet*, Lyngby, Denmark, 2002. ISBN 8778770947.

[70] H. Roth. Modellentwicklung zur Kraftwerksparkoptimierung mit Hilfe von Evolutionsstrategien. *PhD thesis, Technische Universität München, IfE Schriftenreihe*, Munich, 2008. ISBN 9783933283535.

[71] P. Kuhn. Iteratives Modell zur Optimierung von Speicherausbau und -betrieb in einem Stromsystem mit zunehmend fluktuierender Erzeugung. *PhD thesis, Technische Universität München*, Munich, 2012.

[72] J. Dorfner. Development of a Simulation Tool for Renewable Hydrogen Supply of Fuel Cell Vehicles. *PhD thesis, Technische Universität München*, Munich, 2010.

[73] J.A. Nelder and R. Mead. A Simplex Method for Function Minimization. *The Computer Journal*, 7(4):308-313, 1965.

[74] F. Walters, L. Parker, S. Morgan, and S. Deming. *Sequential simplex optimization: a technique for improving quality and productivity in research, development, and manufacturing*. CRC Press, 1991. ISBN: 0849358949.

[75] M.A. Luersen, and R. Le Riche. Globalized Nelder-Mead method for engineering optimization. *Computers & structures*, 82(23–26):2251–2260, 2004.

[76] U.S. Department of Energy. Energy Cost Calculator for Air-Cooled Electric Chillers. *Available at*: http://www1.eere.energy.gov/femp/technologies/eep_ac_chillers_calc.html. Last accessed: April 2012.

[77] DIN EN 15603:2008. Energieeffizienz von Gebäuden- Gesamtenergiebedarf und Festlegung der Energiekennwerte. *Deutsches Institut für Normung e. V.*, 2008.

[78] India Environment Portal. *Available at*: http://www.indiaenvironmentportal.org.in. Accessed: September 2011.

[79] Technical Review, Middle East. Dubai announces freeze on electricity and water tariffs. *Available at:* http://www.technicalreviewmiddleeast.com/power-a-water/transmission/642-dubai-to-freeze-electricity-and-water-tariffs.html. Last accessed: April 2012.

[80] L. Hook. China unveils feed-in tariff for solar power. *Financial Times*, Beijing, China, 2011.

[81] IEA Statistics. CO2 Emissions from fuel combustion – Highlights (2010 Edition). *International Energy Agency*, Paris, France, 2010.

[82] XE Universal Currency Converter. *Available at:* http://www.xe.com/. Accessed: September 2011.

[83] Official page of Bangalore Water Supply and Sewerage Board. *Available at:* http://bwssb.org/?p=264. Accessed: September 2011.

[84] Government of Dubai, Dubai Electricity and Water Authority. Electricity and water tariffs. *Available at*: http://www.dewa.gov.ae/tariff/tariffdetails.aspx. Accessed: September 2011.

[85] Official page of Mosvodokanal. http://www.mosvodokanal.ru/index.php?do=cat&category=tari. Accessed: September 2011.

[86] Official page of Shanghai Municipal Waterworks South Co., Ltd. *Available at:* http://www.water-sh.com/. Acessed: September 2011.

[87] My Bengaluru. Bangalore Electricity Tariff Hike. *Available at*: http://www.mybengaluru.com/resources/2248-Bangalore-Electricity-Tariff-Hike.aspx. Accessed: September 2011.

[88] B. Sysoev. Energy Tariffs, Ways of Their Reducing Through Implementing Energy Saving Technologies in Production. Moscow, 2010. *Available at*: http://energonavigator.n4.biz/. Accessed: September 2011.

[89] China Electric Power Information Disclosure Network. *Available at*: http://www.12398.gov.cn/. Accessed: September 2011.

[90] Official page of pvXchange. *Available at*: http://www.pvxchange.com/. Accessed: September 2011.

[91] Haase-Wärmespeicher T400. Preisliste 2010. *Haase GFK-Technik GmbH*, Großröhrsdorf, 2010.

[92] R. Diamond, C. Wray, D. Dickerhoff, N. Matson, and D. Wang. Thermal distribution systems in commercial buildings. *Lawrence Berkeley National Laboratory Report, LBNL-51860*, Berkeley, CA, USA, 2003.

[93] A. Luibl. Energieverbrauch der Wärme und Kälteverteilung in Bürogebäuden. *Studienarbeit, Technische Universität München*, München, 2011.